Ingeniaritza Goi Eskola Teknikoa
Escuela Técnica Superior de Ingeniería
Bilbao

eman ta zabal zazu
Euskal Herriko Unibertsitatea
Universidad del País Vasco

EUSKAL HERRIKO UNIBERTSITATEA / UNIVERSIDAD DEL PAÍS VASCO
Escuela Técnica Superior de Ingeniería de Bilbao
Departamento de Ingeniería Química y del Medio Ambiente

Advanced reaction systems for hydrogen production

A dissertation Submitted to the University of the Basque Country
In partial fulfillments of the requirements for the degree of
Ph.D. in Chemical Engineering

By

Mr. Urko Izquierdo Ereño

Thesis Advisors:

Dr. Victoria Laura Barrio Cagigal
Prof. Dr. José Francisco Cambra Ibáñez

Bilbao 2014

Servicio Editorial de la Universidad del País Vasco (UPV/EHU) -
Euskal Herriko Unibertsitateko (UPV/EHU) Argitalpen Zerbitzua
- University of the Basque Country (UPV/EHU) Press
- ISBN: 978-84-9082-224-1

Nigan sinistu duzuen guztioi eta bereziki, baserriko erreginari.

Agradecimientos

Seguramente al acabar de escribir los siguientes párrafos, seguirán faltándome palabras de agradecimiento hacia muchas de las personas que han hecho posible y tanto me han ayudado a alcanzar esta meta, por lo que primeramente me gustaría empezar disculpándome por ello.

En mi humilde opinión, el ser Doctor no es únicamente los años de investigación. Ni siquiera los de la carrera. El llegar a ser Doctor es un reconocimiento a la trayectoria de nuestras vidas que está fuertemente arraigado a nuestra educación y a los valores que desde que nacimos nos han trasmitido. Por tanto, es obvio pensar en mi ama y en mi aita como las primeras personas a las que me gustaría dar las gracias. He sido un desastre en muchos ámbitos y el perfecto humano tropezando más de una vez en la misma piedra; y he sido, cómo no, aquella persona cabezona que aunque el blanco fuera blanco, me empeñaba en verlo muy oscuro. Ellos supieron transmitirme desde pequeño una serie de valores por los cuales hoy en día me siento orgulloso. Infinitamente agradecido por vuestra infinita paciencia. Esto me hace pensar en el futuro, ya que me gustaría que mis hijos pudieran decir lo orgullosos que están de sus padres, tal y como yo con estas líneas intento expresar. No me quiero olvidar de mi hermano Eneko, quien a día de hoy sigue contagiándome sus conceptos ingenieriles, ni de mi hermana Irune, quien también ha aportado muchos granitos de arena a esta Tesis. Muchas gracias a toda la familia, y en especial a mi tía Alicia.

Yo siempre he dicho que he tenido ama y aita en casa, y que además he tenido otra ama y otro aita en la universidad. Puede que suene exagerado, pero es así como lo siento. Laura, mi directora de Tesis, me ha demostrado muchas cosas tanto a nivel profesional como personal. Por una parte, ha sido realmente admirable saber que siempre estaba ahí. Que por muy ocupada que estuviera, siempre atendía las diferentes dudas que me surgían. Que si algo estaba mal, no pasaba nada, se empezaba de nuevo y se intentaban hacer las cosas lo mejor posible. En cuanto a la parte humana, me ha demostrado muchas cosas y otras muchas yo mismo he tenido la posibilidad de irlas aprendiendo con ella. No se me olvidan las innumerables vueltas que dio por mí, especialmente cuando estuve en Alemania. De todos modos, sin duda alguna todo lo mencionado anteriormente queda relegado a un segundo plano por su actitud mostrada en mis peores momentos; las cosas a veces salen bien o salen mal, pero yo tengo la sensación de que siempre opto a un nivel superior, el de "muy mal". Esa es la mejor manera de describir mi corta experiencia en el mundo laboral cuando formé parte de la empresa Bionor Berantevilla. Nunca se me olvidará la preocupación continua de Laura por mi salud en aquella época, y menos aún la oportunidad que me fue otorgada para volver a la Universidad y poder acabar satisfactoriamente la Tesis. No soy un hombre de palabras bonitas, pero puedes estar segura de que esto no se me va a olvidar nunca. Las personas demuestran como son en este tipo de situaciones; y tú Laura, me lo demostraste. Gracias.

Siendo Laura mi ama, mi aita en la universidad siempre ha sido Pedro. Fue el primer profesor que conocí. Una referencia, un modelo a seguir. Además de profesor, mi relación con Pedro fue continua a través de la asociación IAESTE Euskadi como nexo en común; él como profesor tutor de la asociación y yo como Secretario General durante el periodo de tres años. Por lo tanto, fueron muchas las veces en las cuales tuvimos que coincidir, y Pedro, como siempre, impresionante. Ha sido una persona que me ha tratado muy bien y me ha mostrado siempre su preocupación tanto en el ámbito profesional como en el personal. Mi Tesis doctoral ha sido en gran parte gracias a Pedro ya que fue él quien me dio la posibilidad de poder trabajar con Laura. Además, a lo largo de mi doctorado ha estado siempre dispuesto a ayudarme mediante consejos, ánimos, correcciones, sugerencias etc. Es otra de las personas de la que continuamente aprendes, y él siempre ha tenido la puerta abierta para ello.

Y cómo no, José Cambra, "el mago". La persona que ha hecho posible que vuelva a creer en mi sueño de ser profesor. Esto suena a señal del destino, porque es un sueño que tenía desde pequeño, y al que ya había renunciado. José es otra de las personas fáciles de admirar por la gran capacidad de trabajo, profesionalidad y sobre todo por su amplia visión de las cosas. Persona con la que siempre aprendes algo nuevo, y a la que admiras de tal manera que tomas como modelo a seguir. Más aún, porque todo lo descrito anteriormente viene acompañado de una actitud siempre positiva y una amabilidad impresionante, ambas dignas de ser contagiadas. La verdad es que leyendo los párrafos anteriores, me siento una persona afortunada. ¡Seguiremos echando risas a cuenta de los txupitos de agua!

No me quiero olvidar de la gente que ha trabajado conmigo. Ahora me refiero a aquellas personas que año tras año han estado desarrollando su proyecto fin de carrera conmigo. Esta Tesis es fruto del trabajo que hemos llevado juntos a cabo, y de las horas que hemos invertido todos en ello. Me enorgullece poder decir que he trabajado con mucha gente y que toda esta gente ha trabajado muy bien conmigo. Muchas gracias a tod@s. Siempre se han llevado de la mejor manera posible tanto los buenos como los malos momentos. Mikel Moja, mi primer compañero con el cual pasé momentos difíciles ya que los dos éramos nuevos e inexpertos en el área de catálisis y la persona con la cual llevé a cabo los primeros ensayos con microreactores. Nerea Lago, Impresionante en el trabajo. Constancia, esfuerzo, empeño y no rendirse. Nunca se me va a olvidar lo bien que trabajamos juntos y lo mucho que has aportado a esta Tesis. Kepa Bizkarra, Nirekin eta ni gabe esperimentu gehien burutu dituen pertsona. Denbora gutxien dedikatu diodanari (Alemanian eginiko egonaldiagatik) eta hala ere, sortatu zaizkion oztopo guztiak gainditu izan dituena. Pertsonarik konstanteena zentzu askotan eta gaur egun oso harro sentitzen naizenaz. Mila esker berriz ere Kepa. Judit Otazua. Oso pertsona langilea ere. Beharbada laborategian usain txarrak (H_2S) gehien sufritu behar izan dituena. Oso koadrila polita izan genuen pasa den urtean katalisi laborategian. Oso emaitza onak eta interesgarriak atera ziren berarekin, besteekin bezala, ondo eginiko lanaren ondorioz. Mila esker zuri ere. También he trabajado directamente con gente de la cual he aprendido

mucho y que aunque el trabajo llevado a cabo no ha sido incluido en esta Tesis, les estoy muy agradecido: David, Laura y Nemanja. A todos ellos mila esker, gracias or thank you very much! I would not like to forget about the colleagues in Mainz, Germany. Specially acknowledge Prof. Dr. Kolb and Dr. Pennemann for their acceptance at IMM. To Martin, who is a very good friend and better engineer. To Stefan, for teaching me handling their lab scale set ups. Thanks to Berta, Steffen, Sascha, Athanassios and Ralf, especially for Ralf, the keeper of the catalysts.

Todo esto tampoco hubiera sido posible sin la impresionante paciencia de Jesús. ¿Cuántas horas habremos pasado delante del Autosorb?. Siempre tendré en mente la respuesta a mi pregunta de "¿Tienes un momento?". Muchas gracias Jesús; además de un momento, siempre has tenido una sonrisa para mí. Otra de las personas que se tiene el cielo ganado es Mari Feli. Siempre, y cuando digo siempre, es siempre, impresionante. Desde el principio hasta el final. Te admiro por lo bien que piensas y razonas las cosas, así como por lo bien que las explicas y lo bien que las ejecutas. ¡Gracias!. Y sigo con Belén, otra de las personas que demuestra día tras día la profesionalidad de nuestro departamento. Además, ahora que últimamente estoy teniendo ocasión de trabajar más directamente con ella, me reitero en lo dicho. Siempre me he sentido muy apoyado y respaldado por ti. ¡Muchísimas gracias!

¡Esthertxuuuuu, que iba a ser yo sin tí! ¡Eres muy grande y sin duda has sido la mejor compañera! Gracias por todo. Rubixeeee, tú también sabes lo mucho que te admiro y no sólo por lo mucho y bien que trabajáis en pirólisis. ¡¡Sin duda, el vuestro es el mejor despacho!!

Finalmente me gustaría agradecer y hacer mención al resto de compañeros de estos últimos años. A aquellos que se han comportado como verdaderos compañeros, ayudando, trabajando, mirando hacia adelante, haciendo frente a las dificultades que surgían día a día, invirtiendo tiempo por mejorar las cosas y a los que de un modo u otro han querido formar parte y mejorar el grupo de investigación SuPrEn. Hemos pasado muy buenos momentos. Gora DIQMA!! Y cómo no, me gustaría agradecer también la presencia de las personas que me han ayudado a ser más fuerte. Rectificar es de sabios.

Finalmente, mil gracias a Nerea. Por escucharme, y por demostrarme que lo más importante es quererse. Por enseñarme y no dejarme olvidar las cosas bonitas de esta vida. Por Jazz. Por el día a día. Por poder imaginar un futuro juntos.

Amurrio, Diciembre 2013.

Table of contents

Resumen

La presente Tesis Doctoral tuvo su inicio en Marzo de 2010 gracias a la obtención de la beca perteneciente al programa de "*Formación de Personal de investigación*" impulsado por la Universidad del País Vasco / Euskal Herriko Unibertsitatea (UPV/EHU). Esta Tesis ha sido desarrollada prácticamente en su totalidad en el Departamento de Ingeniería Química y del Medio Ambiente de la Escuela Técnica Superior de Ingeniería de Bilbao, como miembro del grupo de investigación Sustainable Process Engineering (SuPrEn). Además, esta Tesis incluye el trabajo realizado durante el periodo de seis meses de estancia pre-doctoral en el centro Institut für Mikrotechnik Mainz GmbH, IMM, de Alemania.

El trabajo llevado a cabo durante los cuatro años se centra en la **obtención de hidrógeno**, vector energético limpio y combustible del futuro, a partir de diversas materias primas. Sin embargo, el mayor aporte de esta Tesis a la comunidad científica viene dado por la utilización de los sistemas de reacción denominados microrreactores para la producción de hidrógeno. Este tipo de sistemas están siendo hoy en día objeto de estudio ya que son una solución viable a la producción de hidrógeno de manera descentralizada y porque además, presentan varias ventajas en comparación con los métodos actuales de producción de hidrógeno. Asimismo, la comparación entre sistemas de reacción convencionales y los **microrreactores**, también ha sido objeto de estudio en la presente Tesis. De igual modo, para los procesos de reformado estudiados, se han desarrollado varios **sistemas catalíticos** que han mostrado altas actividades en cuanto a conversión de reactivos se refiere, gran selectividad a hidrógeno y muy buena estabilidad en cuanto a operación y durabilidad se refiere.

Inicialmente, se empleó **metano** y **gas natural** como fuentes de alimentación no renovables, llevando a cabo una comparativa de los dos sistemas de reacción previamente mencionados. Sin embargo, otro de los objetivos de la presente Tesis ha sido el uso de fuentes de alimentación renovables, ya que uno de los grandes retos de la comunidad científica recae en la obtención de un producto limpio, el hidrógeno, a partir de recursos renovables. De este modo, la mayor parte del trabajo se basa en el estudio de la producción de hidrógeno a partir de **biogás**. Este gas, procedente de la descomposición anaerobia de la materia orgánica, como puede ser la biomasa, se compone prácticamente de metano y dióxido de carbono. De esta forma, convirtiendo estos dos gases a hidrógeno, los beneficios económicos, ambientales y sociales alcanzables serían de gran relevancia dado que los dos contribuyen en gran medida al denominado efecto invernadero. Además de con biogás, también se han llevado a cabo ensayos de actividad catalítica con **etilenglicol**, recurso renovable mayoritario procedente de la conversión catalítica de la celulosa.

Acorde a cada una de las materias primas a tratar se prepararon diferentes formulaciones catalíticas, con el objetivo de conocer el efecto de los diferentes soportes a utilizar, de sus modificaciones, de las cargas metálicas y cómo no, de las concentraciones de las propias especies metálicas presentes en los catalizadores. Con el objeto de poder interpretar los resultados obtenidos con los catalizadores utilizados en cada apartado, se llevó a cabo una exhaustiva caracterización de los mismos antes y después de haber sido probados en los ensayos de actividad catalítica, así como un estudio de la correlación entre las propiedades superficiales medidas mediante caracterización y los resultados de actividad catalítica.

Para poder detallar de manera satisfactoria toda la información recabada a lo largo de los cuatro años de investigación, esta Tesis ha sido dividida en 6 capítulos independientes, los cuales se resumen a continuación:

En el **Capítulo 1**, se justifica la necesidad de llevar a cabo este trabajo de investigación, mediante el cual se busca un cambio en el sistema energético actual basado en el petróleo. Sin duda, la creciente demanda energética existente y el agotamiento de los recursos fósiles hacen necesario la búsqueda de alternativas para poder mantener la calidad de vida actual. Además, en este apartado introductorio también se detalla el estado del arte en cuanto a los métodos de producción de hidrógeno se refiere, los reactores existentes y los catalizadores más comúnmente empleados.

En el apartado siguiente, el **Capítulo 2**, se detalla el propósito establecido para el desarrollo de esta Tesis. Además de la producción de hidrógeno mediante sistemas de reacción convencionales y su comparación con los sistemas de reacción avanzados denominados microrreactores, el uso de diferentes fuentes de alimentación y tipos de catalizadores, también han sido metas a alcanzar en esta Tesis. Por otra parte no hay que olvidar que el propósito impulsado por la Universidad de País Vasco / Euskal Herriko Unibertsitatea, es el de formar a personas como futuros investigadores, siendo éste un objetivo alcanzado a medida que se ha desarrollado la Tesis Doctoral.

El **Capítulo 3,** es el primero de los apartados correspondientes a la actividad experimental llevada a cabo. En él se detallan los ensayos realizados con metano y gas natural como reactivos para la obtención de hidrógeno. Además, en esta sección se hace una comparación de los dos sistemas de reacción empleados habiendo sido llevados a cabo los ensayos a iguales velocidades espaciales. Para el desarrollo de los correspondientes ensayos de actividad catalítica se prepararon cuatro catalizadores diferentes, basados en alúmina y magnesia con especies metálicas nobles (Pt y Pd) y no nobles (Ni).

A lo largo de este capítulo se detalla la metodología empleada a la hora de preparar, impregnar y acondicionar los microrreactores, así como la llevada a cabo para preparar los reactores de lecho fijo empleados. También se describe el equipamiento utilizado para realizar los ensayos de reacción, así como para la identificación y cuantificación de los productos obtenidos en reacción.

Entre los resultados obtenidos cabe destacar la gran estabilidad mostrada por los microrreactores y la alta actividad medida en operación para el catalizador de Ni/MgO tanto en el reformado de metano como en el de gas natural. En cuanto al catalizador de Ni/Al_2O_3, también se midieron altas conversiones de metano; sin embargo, sufrió una desactivación severa cuando fue utilizado para la producción de hidrógeno a partir de gas natural. En cuanto a los catalizadores basados en metales nobles y soportados sobre alúmina, éstos no mostraron actividad alguna posiblemente debido a la deposición de coque, que fue detectado por SEM.

El **Capítulo 4,** se compone de tres secciones en función de los catalizadores empleados para el reformado de biogás, que se detallan a continuación:

Sección 4.3: Estudio de los diferentes tipos de reformado de biogás con catalizadores basados en γ-Al_2O_3

En este apartado se prepararon 4 catalizadores basados en alúmina cuyos soportes fueron modificados con CeO_2, ZrO_2 o una mezcla de ambos. A uno de los catalizadores se le añadió una pequeña cantidad de Rh con el objetivo de estudiar su influencia. Además, se utilizó también un catalizador basado en MgO y otro comercial basado en alúmina con el propósito de poder comparar los resultados obtenidos. En cuanto a los procesos, cuatro fueron objeto de estudio utilizando el reactor de lecho fijo: reformado seco (dry reforming, DR), reformado de biogás con vapor de agua (biogas steam reforming, BSR), reformado oxidativo de biogás (biogas oxidative reforming, BOR) y tri-reformado (tri-reforming, TR). En ellos se probaron los catalizadores anteriormente mencionados para ratios crecientes de vapor de agua/carbono (S/C), O_2/CH_4 o ambos conjuntamente en el caso del proceso de tri-reformado. Una vez establecidos los parámetros de operación óptimos mediante el reactor de lecho fijo, los tres sistemas catalíticos que obtuvieron los mejores resultados se impregnaron y ensayaron en los microrreactores. De este modo, se pudo llevar a cabo una interesante comparación entre ambos sistemas de reacción. Asimismo, los sistemas catalíticos se caracterizaron antes y después de los ensayos realizados.

Entre los resultados obtenidos, cabe destacar las altas conversiones alcanzadas por todos los catalizadores, cercanas a las calculadas por el equilibrio termodinámico. En el proceso de DR, el catalizador Rh-Ni/Ce-Al_2O_3 fue el que alcanzó el mayor rendimiento a hidrógeno. En cuanto al proceso de BSR, las mejores condiciones de operación

fueron medidas para el ratio S/C=1.0 y para el catalizador Ni/Ce-Al_2O_3. El ratio óptimo de O_2/CH_4 para lograr una mayor conversión de reactivos fue de 0.25 para el catalizador Ni/Ce-Zr-Al_2O_3, que fue el que mejores resultados obtuvo. En cuanto al proceso de TR, nuevamente el catalizador Rh-Ni/Ce-Al_2O_3 obtuvo los mejores resultados operando con ratios de S/C=1.0 y O_2/CH_4=0.25. Por lo tanto, éstos fueron los tres catalizadores seleccionados para ser impregnados en los microrreactores y probados bajo diferentes condiciones experimentales en los procesos de BOR y TR.

Aunque la operación con microrreactores fue llevada a cabo a velocidades espaciales considerablemente superiores, un orden de magnitud superior en comparación con los reactores de lecho fijo, se obtuvieron conversiones y rendimientos muy similares a los medidos en los sistemas de reacción convencional. La comparativa entre ambos sistemas de reacción se llevó a cabo a través de los parámetros Turnover Frequency (TOF) y Hydrogen Productivity (PROD). Los resultados muestran que mediante el uso de microrreactores se obtienen actividades catalíticas superiores hasta en un orden de magnitud. El catalizador más activo fue el Ni/Ce-Al_2O_3 debido a su baja dispersión metálica medida mediante quimisorción de hidrógeno y mayores valores de TOF y PROD alcanzados.

Sección 4.4: Reformado de biogás con catalizadores basados en zeolitas L

En este apartado se muestra el procedimiento llevado a cabo para la síntesis de distintas zeolitas tipo L que fueron posteriormente utilizadas como soporte para preparar nuevos catalizadores. El interés de la propia síntesis recae en la posibilidad de dar forma y tamaños diferentes a las zeolitas. De manera similar que en el apartado anterior, se llevaron a cabo nuevos ensayos con estos sistemas catalíticos basados en zeolitas para establecer las mejores condiciones de operación. Además, estos catalizadores también fueron caracterizados antes y después de los ensayos realizados.

Para los catalizadores preparados basados en zeolitas se alcanzaron elevadas conversiones de metano y dióxido de carbono. Los resultados obtenidos evidencian el mejor comportamiento de los catalizadores bimetálicos. En cuanto a la diferente morfología del soporte se refiere, los catalizadores basados en la zeolita disco fueron los mejores operando en BSR con un ratio S/C=1.0. Por el contrario, los catalizadores basados en la zeolita con forma de cilindros (30–60 nm) fueron los más apropiados para operar en procesos de BOR a O_2/CH_4=0.25 y de TR. Finalmente, los catalizadores basados en la zeolita con forma de cilindros (1–3 μm) fueron los que obtuvieron en comparación los peores resultados de actividad.

Sección 4.5: Reformado de biogás con catalizadores basados en Zeolitas LTL dopadas con Na^+ y Cs^+

En este último apartado correspondiente al Capítulo 4, se describe el procedimiento de síntesis llevado a cabo para preparar unas nuevas zeolitas. A diferencia de las zeolitas L utilizadas en el apartado anterior, en el proceso de síntesis se utilizaron óxidos que contenían Na y Cs con el objetivo de dopar las zeolitas con estas especies. Además, el uso de ondas micro-ondas permitió mejorar y disminuir el tiempo de síntesis requerido en la sección anterior. Haciendo uso de este tipo de soportes, se prepararon catalizadores bimetálicos de Ni y Rh que fueron posteriormente probados en los procesos de reformado seco y reformado oxidativo.

Los resultados obtenidos mostraron una actividad superior de los catalizadores cuyos soportes no fueron modificados, Rh-Ni/D and Rh-Ni/N, aunque la diferencia no fue muy notable. Además, se observó que la modificación del soporte con estos óxidos afectó en mayor medida a las zeolitas con geometría de disco. Realizando una comparativa entre estos catalizadores y los usados en el apartado 4.4, se concluyó que a igualdad de resultados obtenidos en BOR, los preparados en este último apartado resultaron ser menos activos para el proceso de DR.

Capítulo 5: Reformado con vapor de agua y reformado oxidativo de etilenglicol

Este capítulo detalla el trabajo realizado en el Institut für Mikrotechnik Mainz GmbH, IMM, lugar en donde todos los ensayos fueron llevados a cabo con microrreactores.

Sección 5.3: Catalizadores xRh-cm y xRh-np para el reformado de etilenglicol

En este apartado, se comparan los resultados de actividad obtenidos por los catalizadores basados en α-Al_2O_3 para una misma carga metálica, pero habiendo sido preparados a través de dos métodos diferentes. El objetivo principal fue el de obtener partículas metálicas de tamaño nanómetrico. Asimismo, en esta sección se describe también la metodología llevada a cabo para la preparación e impregnación de los catalizadores en los microrreactores, las técnicas analíticas y equipamiento utilizado para el desarrollo de los ensayos de actividad catalítica, y para la determinación y cuantificación de las especies creadas en reacción. En cuanto a los procesos de reformado estudiados, primeramente se llevaron a cabo ensayos de reformado de etilenglicol con vapor de agua a diferentes temperaturas y velocidades espaciales, y a continuación, se llevaron a cabo los correspondientes ensayos de reformado oxidativo de etilenglicol a una única temperatura y diferentes velocidades espaciales.

Los resultados de actividad obtenidos muestran un comportamiento significativamente superior para los catalizadores preparados mediante el método convencional de impregnación. Aun así, se detectó la presencia de sub-productos como acetaldehído, etano y etileno para la mayoría de los catalizadores, tanto añadiendo oxígeno como si no. Los mejores resultados de actividad para el proceso de reformado de etilenglicol en estas condiciones se obtuvieron para el catalizador 2.5Rh-cm.

Sección 5.4: Modificación del catalizador 2.5Rh-cm con CeO_2 y La_2O_3 para el reformado de etilenglicol

Una vez interpretados los resultados tanto de actividad catalítica como los correspondientes a la caracterización de los catalizadores empleados en la sección anterior, se seleccionó el mejor catalizador y se modificó el soporte con CeO_2 y La_2O_3, con el objetivo de mejorar aún más su rendimiento y disminuir la formación de sub-productos. Por lo tanto, en este apartado se muestran los resultados obtenidos con estos catalizadores bajo las mismas condiciones, con el objetivo de poder ser comparados. Además, para el catalizador 2.5Rh.cm con el que se alcanzaron los mejores resultados, en cuanto a sus propiedades físico-químicas y sus resultados de actividad catalítica se refiere, se llevó a cabo un ensayo de estabilidad permaneciendo en funcionamiento estable durante más de 115 horas. Cabe destacar que en todos los casos se logró reducir de manera muy significativa la formación de sub-productos, detectada en el aparado anterior.

Capítulo 6: Conclusiones

Este es el último capítulo de la Tesis Doctoral, y en él se detallan las conclusiones más relevantes fruto del trabajo experimental llevado a cabo, y de acuerdo con los objetivos establecidos para la generación de hidrógeno a partir de recursos fósiles y renovables.

Summary

This PhD work started in March 2010 with the support of the University of the Basque Country (UPV/EHU) under the program named "*Formación de Personal Investigador*" at the Chemical and Environmental Engineering Department in the Faculty of Engineering of Bilbao. The major part of the Thesis work was carried out in the mentioned department, as a member of the Sustainable Process Engineering (SuPrEn) research group. In addition, this PhD Thesis includes the research work developed during a period of 6 months at the Institut für Mikrotechnik Mainz GmbH, IMM, in Germany. During the four years of the Thesis, conventional and microreactor systems were tested for several feedstocks –renewable and non-renewable, gases and liquids– through several reforming processes in order to produce hydrogen. For this purpose, new catalytic formulations which showed high activity, selectivity and stability were design. As a consequence, the PhD work performed allowed the publication of seven scientific articles in peer-reviewed journals. This PhD Thesis is divided into the following six chapters described below.

The opportunity of this work is established on the basis of the transition period needed for moving from a petroleum based energy system to a renewable based new one. Consequently, the present global energy scenario was detailed in **Chapter 1,** and the role of hydrogen as a real alternative in the future energy system was justified based on several outlooks. Therefore, renewable and non-renewable hydrogen production routes were presented, explaining the corresponding benefits and drawbacks. Then, the raw materials used in this Thesis work were described and the most important issues regarding the processes and the characteristics of the catalytic formulations were explained. The introduction chapter finishes by introducing the concepts of decentralized production and process intensification with the use of microreactors. In addition, a small description of these innovative reaction systems and the benefits that entailed their use were also mentioned.

In **Chapter 2** the main objectives of this Thesis work are summarized. The development of advanced reaction systems for hydrogen rich mixtures production is the main objective. In addition, the use and comparison between two different reaction systems, (fixed bed reactor (FBR) and microreactor), the processing of renewable raw materials, the development of new, active, selective and stable catalytic formulations, and the optimization of the operating conditions were also established as additional partial objectives.

Methane and natural gas (NG) steam reforming experimental results obtained when operated with microreactor and FBR systems are presented in **Chapter 3**. For these experiments nickel-based (Ni/Al_2O_3 and Ni/MgO) and noble metal-based (Pd/Al_2O_3 and Pt/Al_2O_3) catalysts were prepared by wet impregnation and their catalytic activity was measured at several temperatures, from 973 to 1073 K, different S/C ratios, from 1.0 to 2.0, and atmospheric pressure. The Weight

Hourly Space Velocity (WHSV) was maintained constant in order to compare the catalytic activity in both reaction systems. The results obtained showed a better performance of the catalysts operating in microreactors. The Ni/MgO catalyst reached the highest hydrogen production yield at 1073 K and steam-to-carbon ratio (S/C) of 1.5 under Steam methane Reforming (SMR) conditions. In addition, this catalyst also showed good activity and stability under NG reforming at S/C=1.0 and 2.0. The Ni/Al_2O_3 catalyst also showed high activity and good stability and it was the catalyst reaching the highest methane conversion (72.9 %) and H_{2out}/CH_{4in} ratio (2.4) under SMR conditions at 1073 K and S/C=1.0. However, this catalyst suffered from deactivation when it was tested under NG reforming conditions. Regarding the activity measurements carried out with the noble metal-based catalysts in the microreactor systems, they suffered a very quick deactivation, probably because of the effects attributed to carbon deposition, which was detected by Scanning Electron Microscope (SEM). When the FBR was used no catalytic activity was measured with the catalysts under investigation, probably because they were operated at the same WHSV than the microreactors and these WHSVs were too high for FBR system.

In **Chapter 4** biogas reforming processes were studied. This chapter starts with an introduction explaining the properties of the biogas and the main production routes. Then, the experimental procedure carried out is detailed giving concrete information about the experimental set-up, defining the parameters measured, specifying the characteristics of the reactors used and describing the characterization techniques utilized. Each following section describes the results obtained from activity testing with the different catalysts prepared, which is subsequently summarized:

Section 4.3: Biogas reforming processes using γ-Al_2O_3 based catalysts

The activity results obtained by several Ni-based catalysts and a bimetallic Rh-Ni catalyst supported on magnesia or alumina modified with oxides like CeO_2 and ZrO_2 are presented in this section. In addition, an alumina-based commercial catalyst was tested in order to compare the activity results measured. Four different biogas reforming processes were studied using a FBR: dry reforming (DR), biogas steam reforming (BSR), biogas oxidative reforming (BOR) and tri-reforming (TR). For the BSR process different steam to carbon ratios (S/C) from 1.0 to 3.0, were tested. In the case of BOR process the oxygen-to-methane (O_2/CH_4) ratio was varied from 0.125 to 0.50. Finally, for TR processes different S/C ratios from 1.0 to 3.0, and O_2/CH_4 ratios of 0.25 and 0.50 were studied. Then, the catalysts which achieved high activity and stability were impregnated in a microreactor to explore the viability of process intensification. The operation with microreactors was carried out under the best experimental conditions measured in the FBR. In addition, the physicochemical characterization of the fresh and spent catalysts was carried out by Inductively Coupled Plasma Atomic Emission Spectroscopy (ICP-AES), N_2 physisorption, H_2 chemisorption, Temperature

Programmed Reduction (TPR), SEM, X-ray Photoelectron Spectroscopy (XPS) and X-ray powder Diffraction (XRD).

Operating with the FBR, conversions close to the ones predicted by thermodynamic calculations were obtained by most of the catalysts tested. The Rh-Ni/Ce-Al_2O_3 catalyst obtained the highest hydrogen production yield in DR. In BSR process, the Ni/Ce-Al_2O_3 catalyst achieved the best activity results operating at S/C=1.0. In the case of BOR process, the Ni/Ce-Zr-Al_2O_3 catalyst showed the highest reactants conversion values operating at O_2/CH_4=0.25. Finally, in the TR process the Rh-Ni/Ce-Al_2O_3 catalyst obtained the best results operating at S/C=1.0 and O_2/CH_4=0.25. Therefore, these three catalysts were selected to be coated onto microchannels in order to test its performance under BOR and TR processes conditions.

Although the operation using microreactors was carried out under considerably higher WHSV, similar conversions and yields as the ones measured in FBR were measured. Furthermore, attending to other measurements like Turnover Frequency (TOF) and Hydrogen Productivity (PROD), the values calculated for the catalysts tested in microreactors were one order of magnitude higher. Thus, due to the low dispersion degree measured by H_2-chemisorption, the Ni/Ce-Al_2O_3 catalyst reached the highest TOF and PROD values.

Section 4.4: Biogas reforming processes using Zeolites L based catalysts

In this section three type of L zeolites, with different morphology and size, were synthesized and used as catalyst support. Then, for each type of L zeolite three nickel monometallic and their homologous Rh-Ni bimetallic catalysts were prepared by the wetness impregnation method. These catalysts were tested using the FBR under DR process and different conditions of BSR (S/C ratio of 1.0 and 2.0), BOR (O_2/CH_4 ratio of 0.25 and 0.50) and TR processes (at S/C=1.0 and O_2/CH_4=0.25). The characterization of these catalysts was also carried out by using the same techniques mentioned in the previous section.

Very high methane and carbon dioxide conversion values were measured for almost all the catalysts under investigation. The experimental results evidenced the better catalytic behavior of the bimetallic catalysts as compared to the monometallic ones. Comparing the catalysts behavior with regards to their morphology, for the BSR process the Disc catalysts were the most active ones at the lowest S/C ratio tested. On the contrary, the Cylindrical (30–60 nm) catalysts were more active under BOR conditions at O_2/CH_4=0.25 and TR processes. By the contrary, the Cylindrical (1–3 μm) catalysts showed the worst activity results for both processes.

Section 4.5: Biogas reforming processes using Na+ and Cs+ doped Zeolites LTL based catalysts

A method for the synthesis of Linde Type L (LTL) zeolite under microwave-assisted hydrothermal conditions and its behavior as a support for heterogeneously catalyzed hydrogen production is described in this section. Then, rhodium and nickel-based bimetallic catalysts were prepared in order to be tested by DR process and BOR process at O_2/CH_4=0.25. Moreover, the characterization of the catalysts under investigation was also carried out.

Higher activities were achieved by the catalysts prepared from the non-doped zeolites, Rh-Ni/D and Rh-Ni/N, as compared to the ones supported on Na^+ and Cs^+ exchanged supports. However, the differences between them were not very significant. In addition, the Na^+ and Cs^+ incorporation affected mainly to the Disc catalysts. Comparing the results obtained by these catalysts with the ones studied in the section 4.4, in general worst results were achieved under DR conditions and almost the same results when operated under BOR conditions.

In **Chapter 5** the ethylene glycol (EG) as feed for syngas production by steam reforming (SR) and oxidative steam reforming (OSR) was studied by using microchannel reactors. The product composition was determined at a S/C of 4.0, reaction temperatures between 625°C and 725°C, atmospheric pressure and Volume Hourly Space Velocities (VHSV) between 100 and 300 NL/(g_{cat}h). This work was divided in two sections. The first one corresponds to the introduction of the main and most promising EG production routes. Then, the new experimental procedure is detailed and the information about the experimental set-up and the measured parameters is described. The characterization was carried out using the same techniques as for the previous chapter. Then, the next sections correspond to the catalytic activity and catalysts characterization results.

Section 5.3: xRh-cm and xRh-np catalysts for ethylene glycol reforming

Initially, catalysts with different rhodium loading, from 1.0 to 5.0 wt. %, and supported on α-Al_2O_3 were prepared by two different preparation methods (conventional impregnation and separate nanoparticle synthesis). Then, the catalysts were compared regarding their measured activity and selectivity, as well as the characterization results obtained before and after the activity tests carried out. The samples prepared by a conventional impregnation method showed generally higher activity compared to catalysts prepared from Rh nanoparticles. By-product formation of species such as acetaldehyde, ethane and ethylene was detected, regardless if oxygen was added to the feed or not. Among the catalysts tested, the 2.5Rh-cm catalyst was considered the best one.

Section 5.4: 2.5Rh-cm catalyst support modification with CeO_2 and La_2O_3

In this part of the Chapter 5, the catalyst showing the best performance in the previous section, the 2.5Rh-Al_2O_3 catalyst, was selected in order to be improved. Therefore, new Rh based catalysts were designed using α-Al_2O_3 and being modified this support with different contents of CeO_2 or La_2O_3 oxides.

All the catalysts containing additives showed complete conversion and selectivities close to the equilibrium in both SR and OSR processes. In addition, for these catalysts the concentrations measured for the C_2H_4, CH_4, CH_3CHO and C_2H_6 by-products were very low. Finally, the 2.5Rh-20Ce catalyst was selected according to its catalytic activity and characterization results in order to run a stability test, which lasted more than 115 hours under stable operation.

The last chapter, **Chapter 6**, summarizes the main conclusions achieved throughout this Thesis work. Although very high reactant conversions and rich hydrogen mixtures were obtained using a fixed bed reaction system, the use of microreactors improves the key issues, heat and mass transfer limitations, through which the reforming reactions are intensified. Therefore, they seem to be a very interesting and promising alternative for process intensification and decentralized production for remote application.

List of acronyms

In order of appearance

FBR	Fixed Bed Reactor
NG	Natural Gas
WHSV	Weight Hourly Space Velocity
S/C	Steam-to-Carbon ratio
SMR	Steam methane Reforming
SEM	Scanning Electron Microscope
DR	Dry Reforming
BSBR	Biogas Steam Reforming
BOR	Biogas Oxidative Reforming
TR	Tri-Reforming
O_2/CH_4	Oxygen-to-Methane ratio
ICP-AES	Inductively Coupled Plasma Atomic Emission Spectroscopy
TPR	Temperature Programmed Reduction
XPS	X-ray Photoelectron Spectroscopy
XRD	X-ray powder Diffraction
TOF	Turnover frequency
PROD	Hydrogen productivity
LTL zeolite	Linde Type L zeolite
EG	Ethylene Glycol
SR	Steam Reforming
OSR	Oxidative Steam Reforming
VHSV	Volume Hourly Space Velocity
IEO2013	International Energy Outlook 2013
OECD	Organization for Economic Cooperation and Development
GHG	Greenhouse Gases
Mtoe	Million Tons
Mha	Million hectares
AEBIOM	European Biomass Association
r-WGS	Reversible Water Gas-Shift
IMM	Institut für Mikrotechnik Mainz
WGS	Water Gas-Shift
HPLC	High Performance Liquid Chromatography
GC	Gas Chromatograph
FID	Flame Ionization Detector
TCD	Thermal Conductivity Detector
HP	High Performance

X	Conversion
S	Selectivity
CSi	Silicon carbide
i.d.	Internal diameter
EDX	Energy Dispersive X-Ray Spectroscopy
µ-GC	Micro Gas Chromatograph
N_i	Molar flow of *i*
w_{cat}	Catalyst weight in each reactor system
wt_{Me}	Elemental weight given by ICP-AES
D_{Me}	Metal dispersion for the catalyst
Pm_{Me}	Metal molecular weight
BET	Brunauer-Emmett-Teller
BJH	Barrett-Joyner-Halenda
TPR	Temperature programmed reduction
TEM	Transmission electron microscope
CPO	Catalytic Partial Oxidation
PTFE	Polytetrafluoroethylene
KOH	Potassium Hydroxide
DLS	Dynamic Light Scattering
PDF	Powder Diffraction File
LTL	Linde Type L zeolite
N	Nano
D	Disc
APR	Aqueous Phase Reforming
SR	Steam reforming
PVP	Polyvinylpyrrolidone
PVA	Polyvinyl Alcohol
LMFC	Liquid Mass Flow Controller
MS	Mass Spectrometer
SA	Surface Area
PV	Pore Volume
PR	Pore size Radius
BE	Binding Energy
AC	Atomic Concentration
AR	Atomic Ratio

CHAPTER 1

INTRODUCTION

Table of contents

List of figures

List of tables

Today's society, particularly Europe and USA, has accommodated on an extremely high standard of living, including consumption habits which are highly energy dependent. In addition, the so-called emerging countries aspire to achieve the same social status. This thesis would not exist if the consumptions habits and transportation requirements would be sustainable, but unfortunately this is not the case. Additionally, in spite of being aware of the non-sustainable worldwide situation, the emerging countries are growing by following the same way. Therefore, this situation could become even worse taking into account that the world's largest population belongs to non-developing countries.

This skeptical introduction is derived from the critical scenario achieved. More than 150 years have been needed to study, understand, establish and develop the technology required for the use of petroleum and its different by-products. The technology developed has been used in order to achieve the above mentioned standard of living, mainly dependent on petroleum derived products. Thus, the petroleum has become so important that controls the economy of the world´s richest countries and has become the reason for many conflicts in all over the world.

Being aware of this, the scientific community is trying to look for new alternatives that apart from being able to replace the petroleum, be also environmentally attractive in order to ensure a sustainable production and guarantee a safe distribution and use. In this sense, hydrogen seems to be a very good candidate because it is a clean fuel and it can be produced from different sources, renewable and non-renewable. Furthermore, hydrogen can also be used for electricity production through fuel cells, and the electricity generated be used to move cars. This alternative is real and possible and that is why this PhD Thesis has been focused on different hydrogen production routes.

1.1 Global energy scenario

The projections given in the International Energy Outlook 2013 (IEO2013 [1]) estimated in a 56 % the world energy consumption growth between 2010 and 2040. Attending to the use of petroleum and other liquid fuels, an increase from 87 million barrels per day in 2010 to 97 million barrels per day in 2020 and 115 million barrels per day in 2040 is expected. The mentioned growth in liquid fuels use is mostly attributed to the transportation and industrial sectors. In particular, around the 63 % of the forecasted liquid fuel demand increase is expected to be used by the transportation sector from 2010 to 2040. The remainder is attributed mostly to the industrial sector, and particularly to the consumption of the chemical industries that will continue consuming large quantities of petroleum according to the IEO2013 predictions [1].

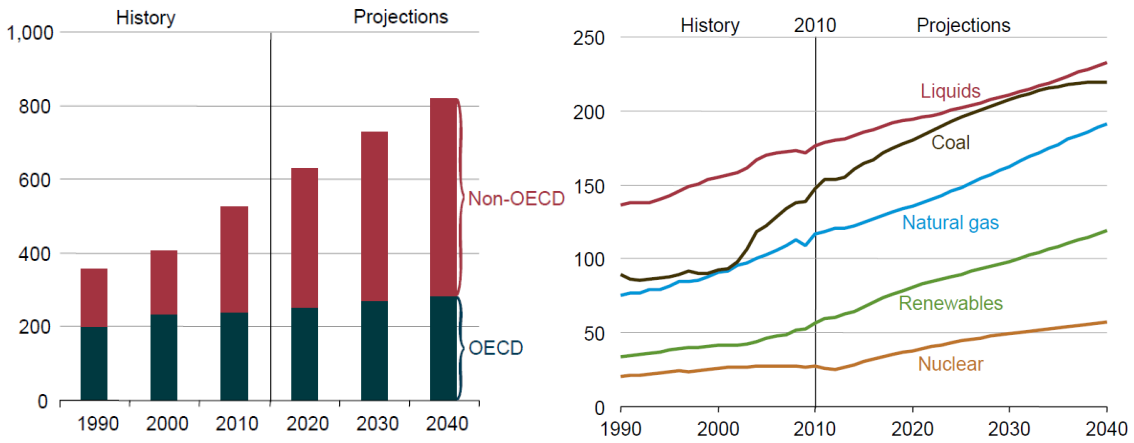

Figure 1: *Left: World energy consumption, 1990-2040 (quadrillion Btu). Right: World energy consumption by fuel type, 1990-2040 (quadrillion Btu)* [1].

In this projection, the energy consumption was separated between the countries that are part of the Organization for Economic Cooperation and Development (OECD) and the ones which are not[1]. Then, a modest increase is expected in the countries that are part of the OECD, being the major part of the growth, around the 85% of the primary energy use during that period, attributed to the non-OECD countries.

Another interesting point of view, also taken into account in the IEO2013 report, regards to the energy related carbon dioxide emissions. In this study it is affirmed that the combustion of liquid fuels, natural gas and coal contributed to the most of the anthropogenic greenhouse gases emissions (GHG). This fact relates directly the energy consumption and the global climate change. According to the mentioned above, the predicted energy consumption growth would lead into a GHG emission increase. Therefore, the estimations for the world energy-related

[1] *OECD member countries as of September 1, 2012, are the United States, Canada, Mexico, Austria, Belgium, Chile, Czech Republic, Denmark, Estonia, Finland, France, Germany, Greece, Hungary, Iceland, Ireland, Israel, Italy, Luxembourg, the Netherlands, Norway, Poland, Portugal, Slovakia, Slovenia, Spain, Sweden, Switzerland, Turkey, the United Kingdom, Japan, South Korea, Australia, and New Zealand. For statistical reporting purposes, Israel is included in OECD Europe.*

carbon dioxide emissions, without assuming the global climate change debate, were quantified in an increase from 31.2 billion metric tons in 2010 to 36.4 billion metric tons in 2020 and 45.5 billion metric tons in 2040. Logically, as the major part of the energy related consumption until 2040 is attributed to the non-OECD countries, the higher growth in emissions is consequently assigned to this group of nations. Therefore, the IEO2013 establish the total non-OECD carbon dioxide emissions around 31.6 billion metric tons in 2040, or 69 % of the world total.

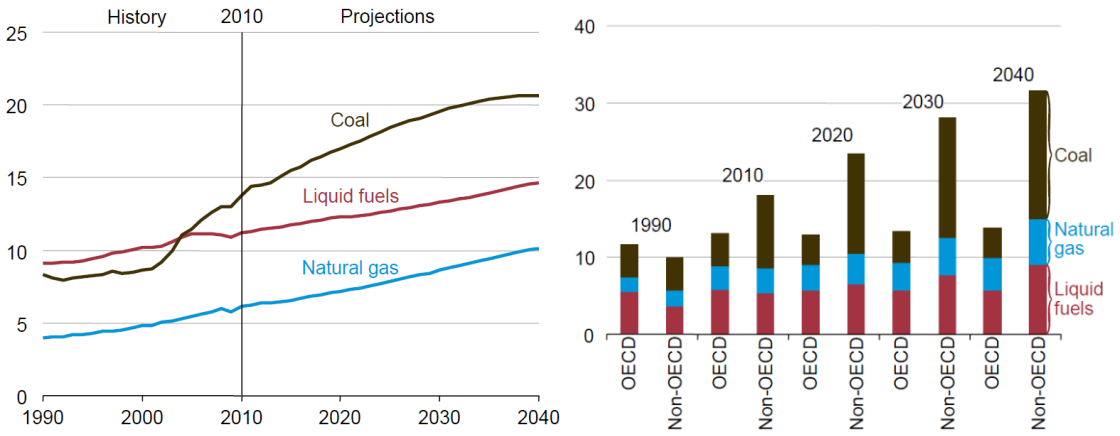

Figure 2: *World energy-related carbon dioxide emissions by fuel type, 1990-2040 (billion metric tons). OECD and non-OECD energy-related carbon dioxide emissions by fuel type, 1990-2040 (billion metric tons)* [1].

The scenario described by the IEO2013 predicts a situation in which the energy-related carbon dioxide emissions will follow reaching new maximums instead of remaining constant or decrease. In addition, the significant increase on the energy demand and the consequent carbon dioxide emissions that mainly corresponds to the non-OECD countries should concern even more about the real and urgent necessity to development a new energy system in order to be applied for at least try to stop the increasing tendency. Besides, the technological transference to the developing countries seemed to be necessary in order to try to decrease the impact of the predictions, not only the ones regarding the energy consumption, but also the ones that affect to the GHG emissions, because they are directly related.

If the governments showed a real concern about the situation described above, drastic changes would be implemented in order to avoid it. Unfortunately, the decrease of the investments for research and development of new techniques as well as for looking new energy alternatives makes even more difficult the energy system transition needed. Anyway, it is evident that a transition is required because of the known carbon based fuels depletion and the environmental problems entailed from their use. In this sense, the scientific community has focused the attention on hydrogen and the possibility of the application of this known green energy vector and clean fuel into diverse areas.

1.2 Hydrogen; a green energy vector, the fuel of the future

The interest for hydrogen is gaining interest and extensive research is being carried out to search new and competitive techniques for its production. Hydrogen can be viewed as a sustainable energy carrier for, at least, two reasons. The first one corresponds to the way of production because among many others, it can be obtained from renewable raw materials such as water, biomass or biogas. The second regards to the green fuel nature, because when it is combusted or oxidized, it generates water as the only by-product; no particles, no non-combusted products, and no CO or CO_2 emissions are produced. Its combustion reaction is described as follows:

$$H_2 + 1/2\ O_2 \rightarrow H_2O \qquad (1)$$

Hydrogen does not exist in a free state in nature due to its highly reactive character, so unfortunately, it must be produced or obtained from other primary energy sources. However, in spite of being always combined with other elements, it is the most abundant element available in natural sources like hydrocarbon (non-renewable), water and biomass [2] which are the major feedstock for hydrogen production [3] (renewable). Therefore, the hydrogen must be produced for its utilization, and the production can be based on renewable or non-renewable primary energy sources.

In this context, a new concept named as “hydrogen economy” has been created; this concept involves everything around the use of hydrogen. The hydrogen economy is based on four stages: production, storage, distribution and end-use [4-6]. Every stage of hydrogen economy can be studied and analyzed separately, and many factors can be considered as key issues, but without any doubt, the development of the hydrogen economy is strongly dependent on the production step. Hence, the main challenge is to find out the most efficient, cost-effective, sustainable and green production route [7,8].

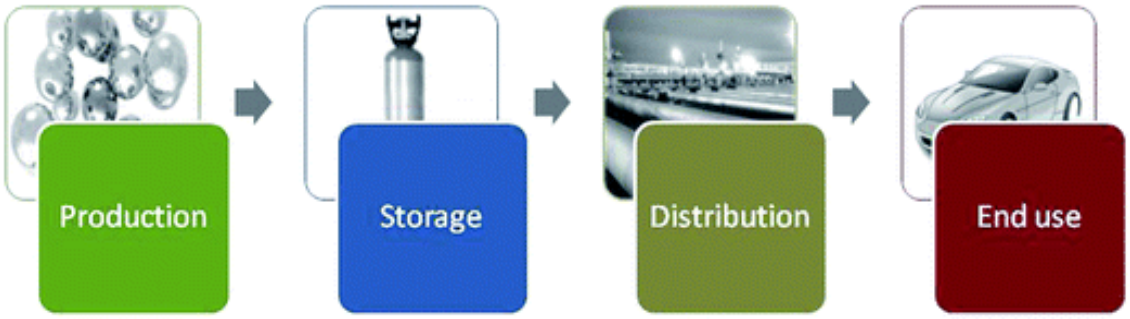

Figure 3: *Hydrogen economy stages* [9].

Different chemical processes are necessary for the production of hydrogen, and all those processes require an energy input. Depending on the process and the energy input required, the hydrogen production methods can be classified intro three major categories: thermochemical, electrochemical and biological [10]. Besides, depending on the departing primary energy, the hydrogen produced could be considered renewable or not. Then, if renewable sources are used and processed through the application of green routes, the production of green hydrogen can be properly carried out. This hydrogen production would be the ideal one. However, the production from fossil fuels seems to be the starting point in order to facilitate the transition to the green hydrogen economy. Anyhow, improvements on the existing processing techniques and new production routes are being investigated in order to achieve an efficient and economically viable production. In addition to these issues, safety, distribution, availability and the possible applications should be considered, which are out of the aim of this thesis, but mandatory for a real use of this green energy vector and clean fuel.

1.3 Main hydrogen production routes

In the next section the most common hydrogen production routes are described. The distinction between them depends on the nature of the primary energy used, so that a classification by renewable and non-renewable hydrogen production routes has been selected for the corresponding description.

1.3.1 Non-renewable hydrogen production

In Figure 4 the main non-renewable hydrogen production routes are shown. At present, they represent the 96% of the total hydrogen produced. The main raw material to produce non-renewable hydrogen is natural gas. Around 48 % of the production comes from the steam methane reforming (SMR) process. The 30 % is obtained in refineries from petroleum fractions, and approximately 18 % is produced from coal gasification [11,12]. Finally, the contribution from water electrolysis covers the rest 4 % of the hydrogen produced. The low contribution of the electrolysis route is due to the economic drawback regarding the much higher operating costs than the thermochemical routes.

According to that reasons and attending to the predictions, as long as natural gas remains at moderate prices, the SMR will be the technology chosen for massive hydrogen production [13]. However, owe to the depletion of petroleum and the consequent political divergences that this effect can provoke, an increase of the petroleum price is expected. Therefore, a real alternative for the carbon based energy system replacement is needed.

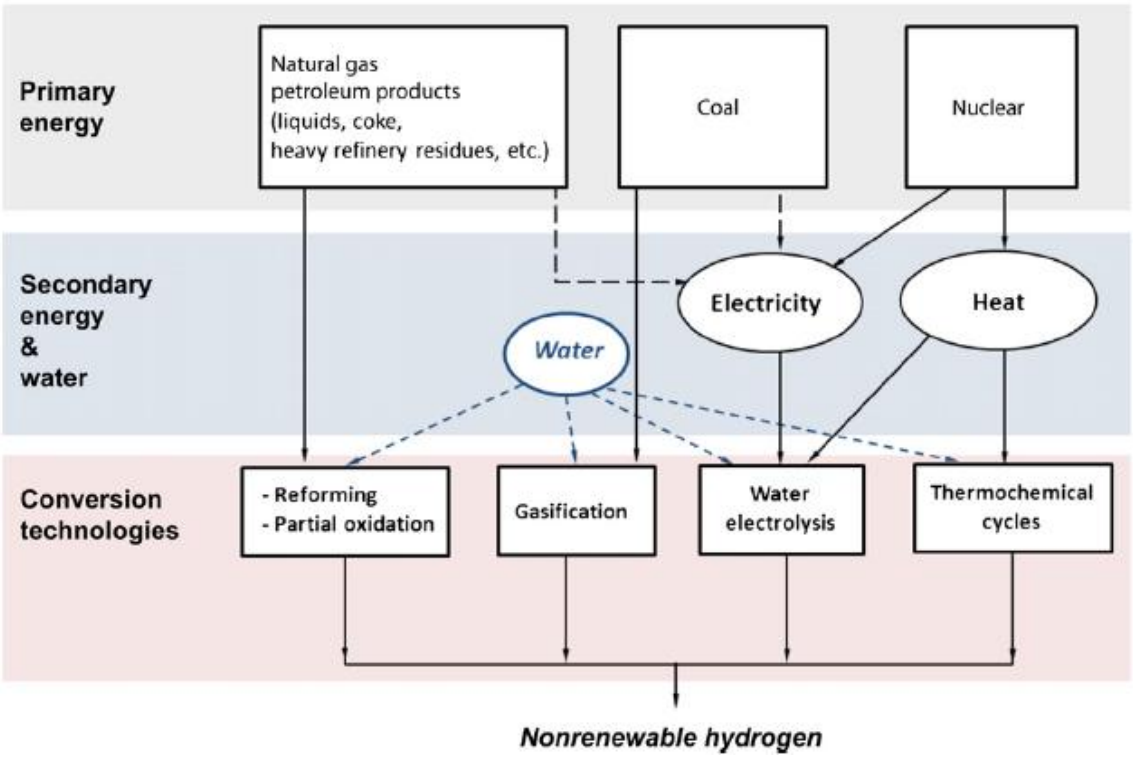

Figure 4: *Main non-renewable hydrogen production routes* [14].

1.3.1.1 Methane and natural gas reforming for hydrogen production

Natural gas is mainly composed of methane (CH_4) some ethane (C_2H_6), propane (C_3H_8) and butane (C_4H_{10}) and impurities such as CO_2, H_2S, and N_2. Depending on its origin the composition can slightly vary, as it is indicating in the following table:

Table 1: *Natural gas standard composition* [15].

	CH_4	C_2-C_3-C_4	CO_2	O_2	N_2	H_2S	He, Ne, Xe
Composition (Vol.%)	70-90	0-20	0-8	0-0.2	0-5	0-5	Traces

The reforming of natural gas, or methane, for a large hydrogen production is nowadays the most promising route due to its abundance, easy supply and low price [16,17]. Steam reforming technology is the oldest and the most feasible route to convert CH_4 into H_2 [18]. It consists on an endothermic reaction between H_2O and CH_4 that typically proceeds over a nickel based catalysts: this process produces syngas in a H_2/CO ratio of 3. Due to the endothermic nature of the reaction, it is favored at high temperature and low pressure, so that the reformer operates at temperatures between 1073 and 1373 K. When this process is carried out, the coke formation is one of the problems to take into account, and in order to avoid it, an excess of steam is usually introduced to the reformer [19,20]. Then, steam to carbon (S/C) ratios of 2.5 or 3.0 are commonly used and the heat required for the process is generally supplied by burning natural gas [21].

Today, the catalysts used under steam reforming conditions must meet at least the next requirements:

- High activity: This makes the process more efficient because higher production of the desired product is ensured.
- Reasonable period of life: A catalyst that can work under stable operation during a long period of time will require less maintenance work.
- High thermal stability: Due to the high operation temperatures required for running the steam reforming process.

In addition to those properties, good heat transfer, low pressure drop and excellent mechanical strength are also desired [22]. In general, the metals corresponding to the group VIII of the periodic table are considered active for the SMR process, especially nickel. Although other metals that belong to this group are also active, certain drawbacks have been noticed. For example, it is known that iron is rapidly oxidized and cobalt cannot resist the steam partial pressure. On the other hand, the noble metals (rhodium, ruthenium, platinum and palladium) are very active for reforming reactions but also too expensive for commercial operation [22].

The support of the catalysts is another issue to take into account. It plays a very important role in the catalyst behavior and an inadequate selection can strongly affect the catalyst, and as a consequence, the process. The supports for industrial applications are normally based on ceramic oxides or oxides which are previously stabilized by hydraulic cement. Therefore, the supports based on α -alumina, magnesia, calcium aluminates or magnesium aluminates are the most commonly used ones [23-29].

As commented before, one of the effects that can strongly affect to the activity and stability of the catalyst is the surface coke deposition because it can block the pores and the active metal sites of the catalyst, resulting in the catalyst failure [30-32]. In order to avoid this undesirable effect, there are some coke resistant oxides as the cerium oxide, CeO_2. When CeO_2 is used as a promoter to a metal, a coke-resistant behavior has been noticed [31-33]. This approach leads to the development of advanced reforming catalysts with better coking resistances and reforming performances [34].

1.3.2 Renewable hydrogen production

In Figure 5 the main renewable hydrogen production routes are shown. The primary energies obtained from solar, wind, hydroelectric, geothermal or wave energy are appropriate for electricity generation, but in general, they are considered expensive for hydrogen production [35]. Several reviews of the previously mentioned hydrogen production technologies can be found in [10,36-40]. Although the economics of the processes studied are out of the approach of this thesis, it is assumed that 1 kg of hydrogen has approximately the same energy of 1 gallon

(3.78 L) of gasoline [35] in order to compare the energy of hydrogen with the gasoline, which is at present the most used fuel.

Considering the economical aspects, at present, the most interesting routes are based on biomass transformation. In particular, the gasification process is the most studied one because of the expected low prices of hydrogen production ($1.44-2.83/kg) [11,35]. In addition, reforming and partial oxidation are also very attractive routes under investigation.

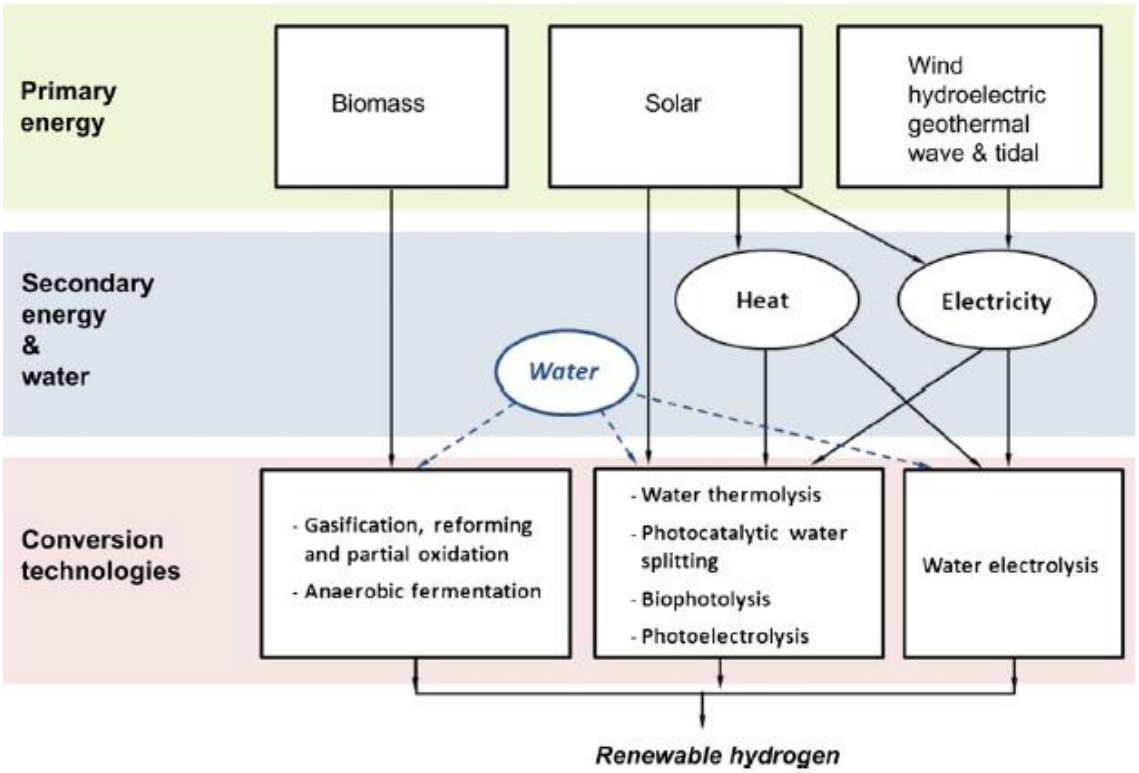

Figure 5: *Main renewable hydrogen production routes* [14].

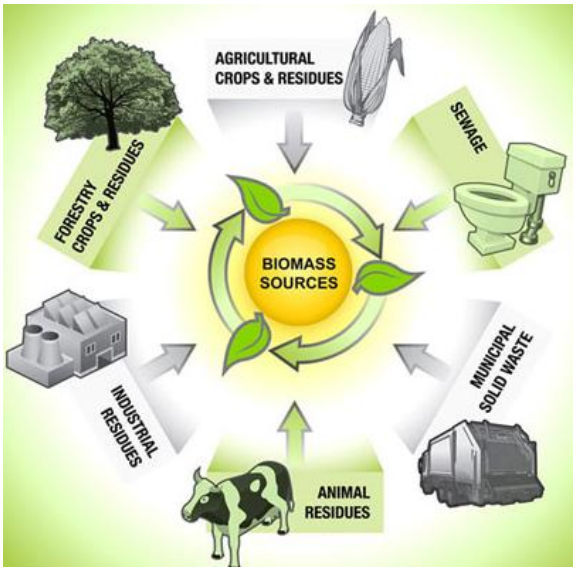

Figure 6: *Possible biomass sources* [41].

Apart from the alternatives mentioned in the previously described figures, there are other interesting and promising hydrogen production routes which are also considered renewable. Departing from biomass as a raw material, many different by-products can be obtained depending on the treatment carried out and on the type of biomass processed. Therefore, among many others, two different products obtained from biomass were used as a raw material for hydrogen production in this Thesis. One of them is the biogas (from anaerobic digestion of the biomass) and the other one ethylene glycol (indirectly from the catalytic conversion of the cellulose).

1.3.2.1 Biogas reforming processes for hydrogen production

The biogas is formed by biological anaerobic degradation of organic wastes (including biomass) and it contains high amounts of methane and carbon dioxide (around 60 and 40 vol.% respectively). Therefore, there is an enormous interest in using this natural source in the possible reforming processes to produce hydrogen or syngas. This is another example of a renewable hydrogen source, meeting the sustainability criteria favorably [9].

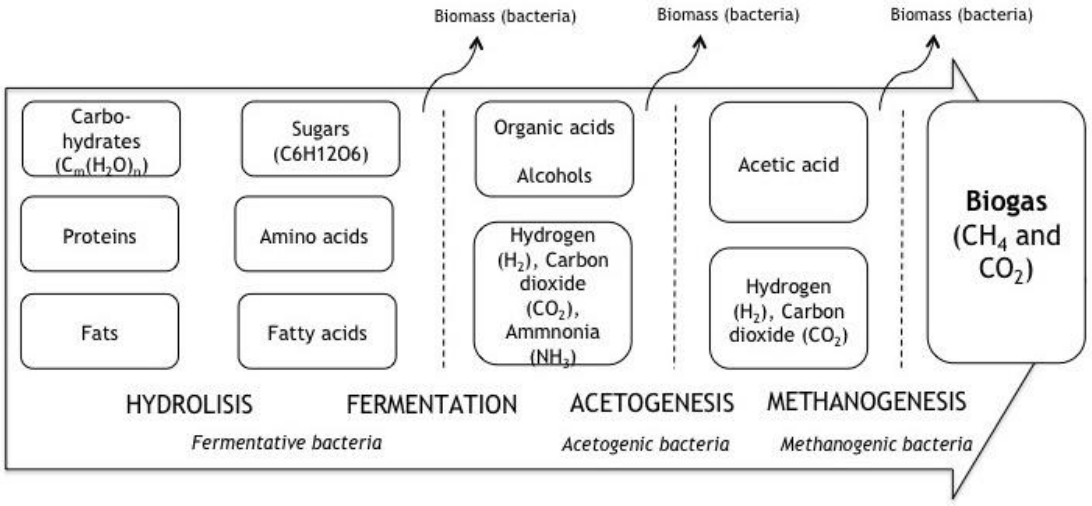

Figure 7: *Anaerobic digestion process of complex organic molecules, proteins and fats for biogas production. Source: D. Spuhler (2010).*

As the global concern about the use of renewable energies has increased during the last years, the world markets for biogas has increased in parallel by developing modern biogas technologies and competitive national biogas markets. This has been possible because of an intensive research and the development of programs complemented by governmental and public support. Many biogas plants have been created during the last years. Germany, Austria, Denmark and Sweden are considered the European biogas sector forerunners with the largest number of modern biogas plants. This technology has also been implemented in other parts of the world by the installation of an important number of biogas plants. In China, it is estimated that up to 18 million rural household biogas digesters were operating in 2006, and the total Chinese biogas potential is estimated to be of 145 billion cubic meters, while in India approximately 5 million small-scale biogas plants are currently in operation [42].

Introduction

As shown in Figure 6, many different biomass resources are available which can give us an idea of the existing global potential for biogas production. It has been reported that this potential was estimated by various experts and regardless the results of their estimations, the overall conclusion was always that only a very small part of this potential is being used today. This means that there is a real possibility to increase the present production of biogas significantly. The conclusion is supported by the European Biomass Association (AEBIOM) estimating that the European production of biomass based energy can be increased from the 72 million tons (Mtoe) in 2004 to 220 Mtoe in 2020. In addition, the AEBIOM focused on the agriculture as the sector with the largest potential for the biomass originated from biogas production. Then, up to 20 to 40 million hectares (Mha) of land can be used for energy production in the European Union without affecting the European food supply [42].

The bridge that links biogas and hydrogen covers all the possible reforming processes, through which the biogas can be easily and effectively converted into hydrogen rich mixtures. The characteristics of those processes are much more deeply described in Chapter 4 of this thesis. In general, as they are endothermic reactions, they are favoured at high temperatures and low pressures. As an introduction, the processes involved are the following:

- Dry reforming (DR): The reaction between methane and carbon dioxide for the production of syngas with low CO/H_2 ratios [43].
- Biogas steam reforming (BSR): The presence of water promotes the SMR reaction apart from the mentioned DR.
- Biogas oxidative reforming (BOR): The addition of oxygen promotes the catalytic partial oxidation of the methane, which is exothermic and decrease the overall endothermicity of the process.
- Tri-reforming: It consists on the simultaneous introduction of oxygen and water to the feed stream, which increases the stability of the DR reaction by providing another oxidant to remove carbonaceous species on the catalyst surface.

It has been reported that the manipulation of steam to carbon and oxygen to carbon ratios in methane reforming allows controlling the H_2/CO product ratio [44,45]. This is especially useful for Fischer-Tropsch applications in which the process is dependent on the H_2/CO feed ratio. Additionally, higher steam to carbon ratios promotes the reversible water gas shift (r-WGS) reaction.

Once again, one of the most challenging issues regards to the catalytic formulations used. For industrial applications, the interest lies on the development of commercially viable catalysts that will make biogas reforming a successful process. Several studies carried out for DR process compared Ni-based commercial catalysts with a noble-metal based ones, concluding that the noble-metal based catalysts achieved higher stabilities, superior CH_4 and CO_2 conversions and higher selectivity to H_2 and CO [46,47]. In addition, the support always plays an important role

not being merely a spectator in the reforming process. Therefore, apart from the own support, several investigations centered on the support modification by adding certain amounts of cerium or zirconium oxides. For example, the addition of 3% CeO_2 to alumina support improve significantly the activity and stability of the dry reforming over Ni and Ni-Rh catalyst [48]. This effect has been attributed to the smaller particle size found on samples prepared with CeO_2. In general, smaller particle size translates to higher surface area and more active sites available for reaction. More properties that are attributed to the CeO_2 will be described in the corresponding chapters of this PhD Thesis.

1.3.2.2 Ethylene glycol reforming processes for hydrogen production

Following with the different uses and applications of biomass, as shown in Figure 6, the forestry crops and residues, lignocellulosic biomass, entailed the most abundant biomass on earth and is widely available in agricultural waste. However, the nature of this type of biomass, the compact and crystalline structure of the cellulose, makes difficult to be biologically degraded being a significant challenge to convert efficiently and selectively the cellulose into valuable chemicals. Nevertheless, among the possible routes [49-54], the catalytic conversion of lignocelluloses with heterogeneous catalysts is a very attractive route. Several studies demonstrated that this process has unique advantages like good selectivity for target products, reusability of catalysts, mild reaction conditions, and environmental friendliness [52-54]. It has been reported that cellulose can be converted into polyols with high selectivity over transition metal carbide and phosphide catalysts [55-59]. For the one-step conversion of cellulose, there are two types of desired products, sugar alcohols and ethylene glycol (EG).

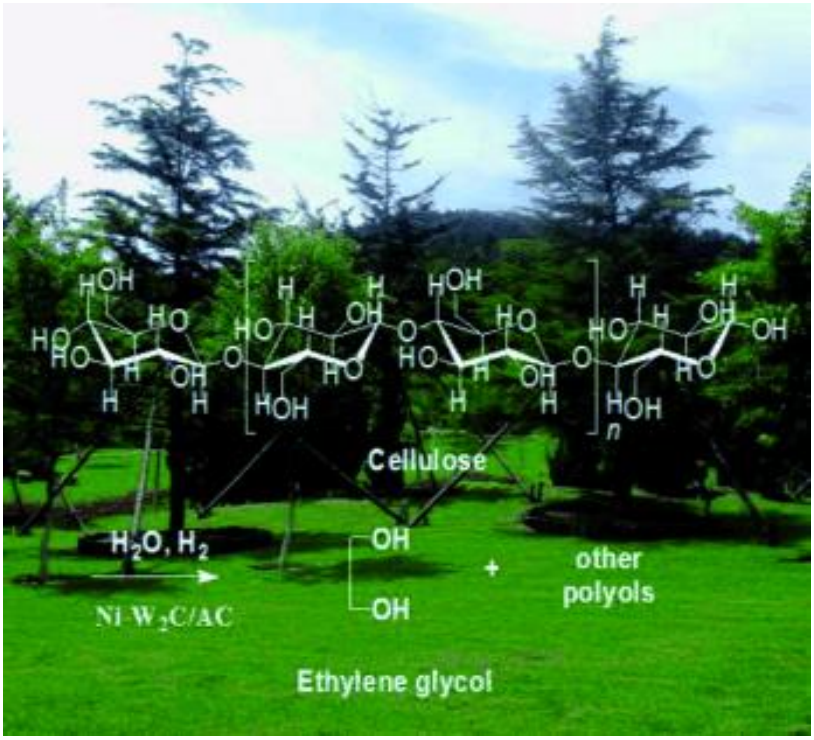

Figure 8: *Graphical scheme of cellulose conversion into ethylene glycol* [55].

Paying attention to the selective conversion of cellulose to EG, this process has been widely studied over various catalyst systems. In particular, over tungsten carbide (W_2C) supported on activated carbon and mesoporous carbon and nickel-promoted tungsten carbide catalysts, the highest ethylene glycol (EG) yield was obtained, 75 wt.% [57]. In addition, Ni-W bimetallic catalysts were successfully employed instead of Ni-W_2C because the Ni-W bimetallic catalysts also exhibited high activity and selectivity [58].

1.4 Decentralized hydrogen production through process intensification

Process intensification can be defined as “The improvement of yields and selectivities by using novel reactions or running reactions at more extreme parameters”. This concept has been attributed to microreactors due to their potential to reach those targets in the field of energy technology, wherever compact and decentralized solutions are required. Therefore, it can be said that the concept of process intensification and the use of microreactors have created the new filed known as microprocess engineering. The objective of microprocess engineering is not only to miniaturize production plants, but also to increase yields and selectivities of chemical reactions, thus reducing the cost of chemical production. This goal can be achieved by either using chemical reactions that cannot be conducted in larger volume, or by running chemical reactions at parameters (temperatures, pressures, concentrations) that are inaccessible in larger volume due to safety constraints [60].

The concept of decentralization tries to avoid the large scale production by using a portable system for remote production. As the natural gas pipelines are perfectly distributed throughout Europe in order to enable the distribution of this gas almost everywhere, this pipelines can be used for the distribution of other fuels. In a near future, if the natural gas is replaced by other type of fuels, as biogas for example, with the use of the natural gas grid, the transformation of those bio-fuels to hydrogen could be possible. Therefore, the use of the microreactors is the first step for the hydrogen decentralized production. This system would require a subsequent purification step, which could consist in an integrated hydrogen selective membrane, for the separation of hydrogen.

1.4.1 Microreactors

The distinction of “micro” is given to systems which one of their dimensions at least is in the scale of microns. This type of system was the result of the research at the Institut für Mikrotechnik Mainz (IMM), being the first ones fabricating a microreactor system based on metals [61]. The microreactors used in this thesis were supplied by IMM and they consist on two platelets carrying 14 channels each with 500 µm width and 250 µm depth introduced by wet chemical etching using an aqueous iron chloride solution [62].

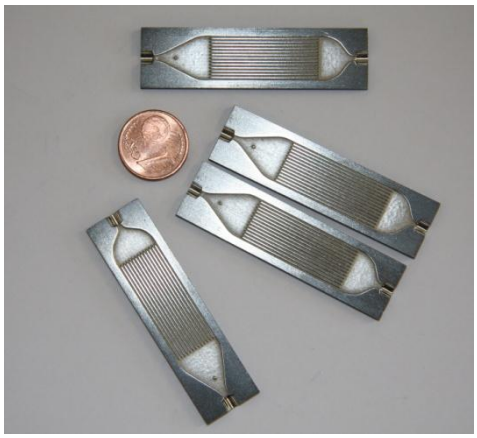

Figure 9: *Microreactors.*

In addition, there are other types of microreactors available, made of different materials which are not appropriate or adequate for the reactions studied: FOTURAN Glass [63], wafer-grade silicon [64] and Plastics [65]. As a consequence of the microreactors technology application, devices as micro-evaporators or micro-heat-exchangers have also been developed in order to run satisfactorily the different type of reactions allowed by this technology.

The use of microreactors provides several benefits, mainly because of their high heat and mass transfer capacities and perceived safety advantages [66,67]. Due to the heat and mass transfer optimization, these systems allow better utilization of the catalysts, but consequently more active catalysts are required which compensate their lower mass available per reactor volume. At the same time, the price of the catalyst is less compared to e.g. fixed bed reactor technology owing to the improved utilization [60]. Due to the small size of the flow channels, extremely high surface to volume ratios can be obtained, allowing excellent heat transfer properties. As a consequence, hotspots in exothermic reactions can be avoided because of the maintenance of uniform temperatures throughout the reactor [68,69]. This is corroborated due to the excellent temperature control allowed by these systems which are also more compact. The extensive fields in which microreactor technology is being applied can be found in [60].

1.5 References

[1] E.I.A., International energy outlook 2013, U. S. Energy Information Administration. (2013).

[2] J.A. Turner, Sustainable hydrogen production, Science. 305 (2004) 972.

[3] Hydrogen production, U.S. Department of Energy (DOE) Hydrogen Program, Available from www. hydrogen. energy. gov. (2006).

[4] A. Midilli, M. Ay, I. Dincer, M.A. Rosen, On hydrogen and hydrogen energy strategies: I: current status and needs, Renew Sust Energ Rev. 9 (2005) 255.

[5] S.S. Penner, Steps toward the hydrogen economy, Energy. 31 (2006) 33.

[6] G. Marbán, T. Valdés-Solís, Towards the hydrogen economy? Int J Hydrogen Energy. 32 (2007) 1625.

[7] T. Schlögl, The role of chemistry in the energy challenge, Chem Sus Chem. 3 (2010) 209.

[8] P.T. Anastas, Meeting the challenges to sustainability through green chemistry, Green Chem. 5 (2003) G29.

[9] U.B. Demirci, P. Miele, Overview of the relative greenness of the main hydrogen production processes. Journal of Cleaner Production. 52 (2013) 1.

[10] R. Chaubey, S. Sahu, O.O. James, S. Maity, A review on development of industrial processes and emerging techniques for production of hydrogen from renewable and sustainable sources, Renew Sust Energ Rev. 23 (2013) 443.

[11] M. Ball, W. Weindorf, U. Bünger, Hydrogen Production. In The Hydrogen Economy. Opportunities and Challenges. in: M. Ball, M. Wietschel (Eds.), , 2009, pp. 277.

[12] N. Armaroli, V. Balzani, The Hydrogen Issue, Chem Sus Chem. 4 (2011) 21.

[13] R.M. Navarro, M.A. Peña, J.L.G. Fierro, Hydrogen Production Reactions from Carbon Feedstocks: Fossil Fuels and Biomass, Chem Rev. 107 (2007) 3952.

[14]L.M. Gandía, G. Arzamendi, P.M. Diéguez, Renewable Hydrogen Energy: An overview, Renewable Hydrogen Technologies. (2013) 1.

[15] Siti Energy Limited. Available from http://www.sitienergy.com/background.htm.

[16] T. Zhang, M.D. Amiridis, Hydrogen production via the direct cracking of methane over silica-supported nickel catalysts, Applied Catalysis A: General. 167 (1998) 161.

[17] T. Koerts, M.J.A.G. Deelen, R.A.V. Santen, Hydrocarbon formation from methane by a low-temperature two-step reaction sequence, J Catalysis. 138 (1992) 101.

[18] T. Riis, E. Hagen, P. Vie, Ø. Ulleberg, Hydrogen production-gaps and priorities, IEA Hydrogen Implementing Agreement. (2006).

[19] Y. Matsumura, T. Nakamori, Steam reforming of methane over nickel catalysts at low reaction temperature, Appl Catal A Gen. 258 (2004) 107.

[20] J.R. Rostrup-Nielsen, J. Sehested, J.K. Nørskov, Hydrogen and synthesis gas by steam and CO_2 reforming, Adv Catal. 47 (2002) 65.

[21] S.D. Angeli, State-of-the-art catalysts for CH_4 steam reforming at low temperature, Int J Hydrogen Energy. http://dx.doi.org/10.1016/j.ijhydene.2013.12.001 (2013).

[22] S. Lee, Methane and its derivatives, New York: M. Dekker. (1997).

[23] A. Arpornwichanop, M. Wasuleewan, Y. Patcharavorachot, S. Assabumrungrat, Investigation of a dual-bed autothermal reforming of methane for hydrogen production, Chemical Engineering Transaction. 25 (2011) 929.

[24] S. Baek, J. Bae, J.Y. Cheon, K. Jun, K. Lee, Combined steam and carbon dioxide reforming of methane on Ni/$MgAl_2O_4$: effect of CeO_2 promoter to catalytic performance, Catalysis letters. 141 (2011) 224.

[25] N. De-Miguel, J. Manzanedo, P.L. Arias, Active and stable Ni-MgO catalyst coated on a metal monolith for methane steam reforming under low steam-to-carbon ratios, Chem Eng Technol. 35 (2012) 2195.

[26] Y. Jung, W. Yoon, Y. Rhee, Y. Seo, The surfactant-assisted Ni-Al_2O_3 catalyst prepared by a homogeneous precipitation method for CH_4 steam reforming, Int J Hydrogen Energy. 37 (2012) 9340.

[27] Y. Seo, Y. Jung, W. Yoon, I. Jang, T. Lee, The effect of Ni content on a highly active Ni-Al_2O_3 catalyst prepared by the homogeneous precipitation method, Int J Hydrogen Energy. 36 (2011) 94.

[28] I.H. Son, S.J. Lee, A. Soon, H. Roh, H. Lee, Steam treatment on Ni/γ-Al_2O_3 for enhanced carbon resistance in combined steam and carbon dioxide reforming of methane, App Catal B-Environmental. 134-135 (2013) 103.

[29] Y. Zhao, Y. Lü, L. Chang, W. Bao, Effects of MgO and CaO on properties of Ni/γ-Al_2O_3 catalyst for the reforming of methane and steam, J Fuel Chem Technol. 38 (2010) 218.

[30] J. Xu, M. Saeys, Improving the coking resistance of Ni-based catalysts by promotion with subsurface boron, J Catal. 242 (2006) 217.

[31] Y.F. Yu-Yao, J.T. Kummer, Low-concentration supported precious metal catalysts prepared by thermal transport, J Catal. 106 (1987) 307.

[32] Y. Zhang, S. Anderson, M. Muhammed, Nanophase catalytic oxides: I. Synthesis of doped cerium oxides as oxygen storage promoters, Appl Catal B Environ. 6 (1995) 325.

[33] N. Laosiripojana, W. Sutthisripok, S. Assabumrungrat, Synthesis gas production from dry reforming of methane over CeO_2 doped Ni/Al_2O_3: Influence of the doping ceria on the resistance toward carbon formation, Chem Eng J. 112 (2005) 13.

[34] A.P. Ferreira, D. Zanchet, J.C.S. Araujo, J.W.C. Liberatori, E.F. Souza-Aguiar, B.F. Noronha, J.M.C. Bueno, The effects of CeO_2 on the activity and stability of Pt supported catalysts for methane reforming, as addressed by *in situ* temperature resolved XAFS and TEM analysis, J Catal. 263 (2009) 335.

[35] J.R. Bartels, M.B. Pate, N.K. Olson, An Economic Survey of Hydrogen Production from Conventional and Alternative Energy Sources, Int. J. Hydrogen Energy. 35 (2010) 8371.

[36] C. Agrafiotis, H. Storch, M. Roeb, C. Sattler, Solar thermal reforming of methane feedstocks for hydrogen and syngas production-A review, Renew Sust Energ Rev. 29 (2014) 656.

[37] S.K. Ngoh, D. Njomo, An overview of hydrogen gas production from solar energy, Renew Sust Energ Rev. 16 (2012) 6782.

[38] M. Wang, Z. Wang, X. Gong, Z. Guo, The intensification technologies to water electrolysis for hydrogen production - A review, Renew Sust Energ Rev. 29 (2014) 573.

[39] G. Gahleitner, Hydrogen from renewable electricity: An international review of power-to-gas pilot plants for stationary applications, Int J Hydrogen Energy. 38 (2013) 2039.

[40] J. Udomsirichakorn, P.A. Salam, Review of hydrogen-enriched gas production from steam gasification of biomass: The prospect of CaO-based chemical looping gasification, Renew Sust Energ Rev. 30 (2014) 565.

[41] Production of energy from human, animal and bio-degradable waste. Available from http://abhishekbiogas.blogspot.com.es/2012/09/intoduction.html,.

[42] T. Al-Seadi, D. Rutz, H. Prassl, M. Köttner, T. Finsterwalder, S. Volk, R. Janssen, Biogas Handbook, ISBN 978-87-992962-0-0 ed., , Denmark, 2008.

[43] M. Rezaei, S.M. Alavi, S. Sahebdelfar, Z. Yan, Syngas production by methane reforming with carbon dioxide on noble metal catalysts, J Nat Gas Chem. 15 (2006) 327.

[44] L. Pino, A. Vita, F. Cipitì, M. Laganà, V. Recupero, Hydrogen production by methane tri-reforming process over Ni–ceria catalysts: Effect of La-doping, Appl Catal B: Environ. 104 (2011) 64.

[45] S. Araki, N. Hino, T. Mori, S. Hikazudani, Autothermal reforming of biogas over a monolithic catalyst, J Nat Gas Chem. 19 (2010) 477.

[46] N. Muradov, F. Smith, Thermocatalytic conversion of landfill gas and biogas to alternative transportation fuels, Energy Fuels. 22 (2008) 2053.

[47] B. Nematollahi, M. Rezaei, M. Khajenoori, Combined dry reforming and partial oxidation of methane to synthesis gas on noble metal catalysts, Int J Hydrogen Energy. 36 (2011) 2969.

[48] M. Ocsachoque, F. Pompeo, G. Gonzalez, Rh–Ni/CeO_2–Al_2O_3catalysts for methane dry reforming, Catal Today. 172 (2011) 226.

[49] L.R. Lynd, J.H. Cushman, R.J. Nichols, C.E. Wyman, Fuel ethanol from cellulosic biomass, Science. 251 (1991) 1318.

[50] G.P. Philippidis, T.K. Smith, C.E. Wyman, Study of the enzymatic hydrolysis of cellulose for production of fuel ethanol by the simultaneous saccharification and fermentation process, Biotechnol Bioeng. 41 (1993) 846.

[51] D. Mohan, C.U. Pittman, P.H. Steele, Pyrolysis of Wood/Biomass for Bio- oil: A Critical Review, Energy Fuels. 20 (2006) 848.

[52] A. Fukuoka, P.L. Dhepe, Catalytic Conversion of Cellulose into Sugar Alcohols, Angew Chem, Int Ed. 45 (2006) 5161.

[53] N. Yan, C. Zhao, C. Luo, P.J. Dyson, H.C. Liu, Y. Kou, One-step Conversion of Cellobiose to C-6-Alcohols using a Ruthenium Nanocluster Catalyst, J Am Chem Soc. 128 (2006) 8714.

[54] C. Luo, S.A. Wang, H.C. Liu, Cellulose conversion into polyols catalyzed by reversibly formed acids and supported ruthenium clusters in hot water, Angew Chem, Int Ed. 46 (2007) 7636.

[55] N. Ji, T. Zhang, M.Y. Zheng, A.Q. Wang, H. Wang, X.D. Wang, J.G. Chen, Direct catalytic conversion of cellulose into ethylene glycol using nickel-promoted tungsten carbide catalysts, Angew Chem, Int Ed. 47 (2008) 8510.

[56] N. Ji, T. Zhang, M.Y. Zheng, A.Q. Wang, H. Wang, X.D. Wang, Y.Y. Shu, A.L. Stottlemyer, J.G.G. Chen, Catalytic conversion of cellulose into ethylene glycol over supported carbide catalysts. Catal Today. 147 (2009) 77.

[57] Y.H. Zhang, A.Q. Wang, T. Zhang, New 3D meso-porous carbon replicated from commercial silica as a catalyst support for direct conversion of cellulose into ethylene glycol, Chem Commun. 46 (2010) 862.

[58] M.Y. Zheng, A.Q. Wang, N. Ji, J.F. Pang, X.D. Wang, T. Zhang, Transition metal-tungsten bimetallic catalysts for the conversion of cellulose into ethylene glycol, Chem Sus Chem. 3 (2010) 63.

[59] L.N. Ding, A.Q. Wang, M.Y. Zheng, T. Zhang, Selective transformation of cellulose into sorbitol by using a bifunctional nickel phosphide catalyst, Chem Sus Chem. 3 (2010) 818.

[60] G. Kolb, Review: Microstructured reactors for distributed and renewable production of fuels and electrical energy, Chem Eng Process. 65 (2013) 1.

[61] P.L. Mills, D.J. Quiram, J.F. Ryley, Microreactor technology and process miniaturization for catalytic reactions - A perspective on recent developments and emerging technologies, Chem Eng Sci. 62 (2007) 6992.

[62] H. Pennemann, V. Hessel, G. Kolb, H. Löwe, R. Zapf, Partial oxidation of propane using micro structured reactors, Chem Eng J. 135 (2008) S66.

[63] Mikroglas, 2007. Mikroglas Chemtech GmbH, Microreactor Technology. Mainz, Germany. www.mikroglas.com.

[64] K.F. Jensen , Microreaction engineering - is smaller better? Chem Eng Sci. 56 (2001.) 293.

[65] M. Heckele, W.K. Schomburg, Review on micro molding of thermoplastic polymers. Journal of Micromechanics and Microengineering, 14 (2004) 1.

[66] W. Ehrfeld, V. Hessel, H. Lowe, Microreactors: New Technology for Modern Chemistry, Wiley-VCH, Weinheim. (2002).

[67] K. Jahnisch, V. Hessel, H. Lowe, M. Baerns, Chemistry in microstructured reactors, Angew. Chem. Int. Ed. 43 (2004) 406.

[68] J. Yue, G. Chen, Q. Yuan, L. Luo, Y. Gontier, Hydrodynamics and mass transfer characteristics in gas–liquid flow through a rectangular microchannel, Chem Eng Sci. 62 (2007) 2096.

[69] W. Ratchananusorn, D. Semyonov, D. Gudarzi, E. Kolehmainen, I. Turunen, Hydrodynamics and mass transfer studies on a plate microreactor, Chem Eng Process. 50 (2011) 1186.

CHAPTER 2

Objectives and approach

Apart from its technological and academic objectives, this Thesis also faces out the environmental problems associated to the production of hydrogen from renewable sources. On one hand, hydrogen is considered a clean energy vector and one of the fuels of the future, so that its production can be considered sustainable. On the other hand, if the production of hydrogen comes from the processing of renewable sources, apart from being sustainable, it could also be considered green.

The main objective of this Thesis work is the hydrogen production through advanced reaction systems using both fixed bed reactor and the microreactor reaction systems. The hydrogen production will be based on renewable, biogas and ethylene glycol, and non-renewable, methane and natural gas, feedstocks. The processes intensification will be studied through the use of microreactors which will also allow the comparison between both reaction systems. Besides, new catalytic systems will be designed in order to optimize reforming processes and their possible intensification.

In order to achieve satisfactorily the goal of this PhD Thesis the following partial objectives, according to the different feedstocks studied, have to be accomplished.

1. **Methane and natural gas reforming processes.** Catalysts preparation will be the first step to carry out. Therefore, Al_2O_3 and MgO-based Ni catalysts as well as Al_2O_3-based Pd and Pt catalysts will be synthesized by wetness impregnation method. Then, the corresponding suspensions will be prepared in order to coat the catalysts into the microreactor systems. Next, catalytic experiments will be performed studying the most influencing operating parameters, temperature and S/C ratio, for both methane and natural gas reforming processes, in order to compare the performances of the different catalysts. Afterwards experiments at the same space velocity will be carried out studying also the same process variable in a fixed bed reactor. Thus, a comparison of the performance of both reaction systems will also be possible to carry out.

2. **Biogas reforming processes.** This study will be separated in three different sections according to the nature of the catalytic formulations to be designed.

   Initially, γ-Al_2O_3-based catalysts will be prepared by modifying the support using CeO_2 and ZrO_2 oxides. Regarding the active metal, a small amount of a noble metal will be incorporated to the previous catalyst showing the best performance. Thus, the influence of the modifiers and metal addition will be investigated. Furthermore, a MgO-based nickel catalyst and a commercial catalyst will also be tested for comparison purposes. Then, different reforming processes using biogas will be studied: Biogas dry reforming, steam reforming, oxidative reforming and tri-reforming. Besides, the influence of the process

variables, steam-to-carbon ratio, oxygen-to-methane ratio and their possible combinations, will be investigated at 800ºC and atmospheric pressure. The aim of this partial objective will be the specification of the optimum operating conditions that allow reaching the highest hydrogen yield and reactants conversions as well as the most appropriate synthesis gas ratio. In addition, this study and the corresponding characterization results will permit the selection of the best catalysts in order to be tested in the microreactor system and study the possible processes intensification. Then, the catalytic systems selected will be coated in the microreactors and also in this case, process variables optimization will be carried out. This will allow the comparison between the reaction systems when operating under different biogas reforming processes.

Next, zeolites with different morphology and sizes as catalyst support based on Ni and Rh-Ni metals for the study of the biogas reforming processes will be carried out in the fixed bed reactor. A similar process variables optimization, influence of steam-to-carbon ratio, oxygen-to-methane ratio and their combination, will be performed by the operation of the processes described above. Then, the study of the influence of the zeolites morphology and size, the noble metal addition and the processes variables optimization will be carried out.

Afterwards, Ni-Rh bimetallic catalysts will be prepared using zeolites with different morphology. These zeolites will also be doped with Na^+ and Cs^+. These catalytic systems will be tested under dry and biogas oxidative reforming processes at O_2/CH_4 ratio of 0.25 in the fixed bed reactor. The influence of the zeolites morphology and the Na^+ and Cs^+ addition to the support will be studied.

3. **Ethylene glycol reforming processes.** Catalysts with different noble metal loadings supported on α-Al_2O_3 will be designed by two different preparation methods. Then, the α-Al_2O_3 support will be modified with CeO_2 and La_2O_3 oxides in order to improve the catalytic activity, stability and to reduce by-product formation. In addition, processes variables optimization, temperature and space velocity, will be studied. Then, at a constant temperature, the influence of oxygen addition at different space velocities will also be studied. Based on the activity and characterization results, the best catalyst will be selected in order to test its stability in a long term activity test.

CHAPTER 3

Methane and natural gas reforming

A published article:

Title: Hydrogen production from methane and natural gas steam reforming in conventional and microreactor reaction systems

Authors: U. Izquierdo[1], V.L. Barrio[1], J.F. Cambra[1], J. Requies[1], M.B. Güemez[1], P.L. Arias[1], G. Kolb[2], R. Zapf[2], A.M. Gutiérrez[3], J.R. Arraibi[3]

[1] *Dept. of Chemical and Environmental Engineering, School of Engineering, University of the Basque Country UPV/EHU, c/ Alameda Urquijo s/n 48013, Bilbao, Spain*

[2] *Institut fur Mikrotechnik Mainz GmbH, IMM, Carl-Zeiss-Str. 18-20, 55129 Mainz, Germany*

[3] *Edp Naturgas Energía, c/ General Concha, 20, 48010 Bilbao, Spain*

Journal: International Journal of Hydrogen Energy

Year: 2012

Table of contents

List of figures

List of tables

3.1 Introduction

Europe needs a clean, safe and reliable energy supply that can ensure a high and sustainable quality of life. Natural gas, as a global energy source, has been gaining widespread use in recent years as a result of high oil prices, the need for energy diversification and supply security and the growing global awareness of environmental issues. These are also the reasons for considering hydrogen as a future energy vector [1-5]. In this context, the production of hydrogen from fossil fuels could allow a smooth transition between fossil to renewable energy systems. In addition, hydrogen can be used to produce electricity in fuel cells, which can significantly contribute to meet the targets of European public policy for energy security, air quality, GHG reduction and industrial competitiveness [6].

The main characteristic of hydrogen gas is that it is a clean energy vector: it releases the chemical energy stored in the H-H bond when combined with oxygen, producing only water vapor as reaction product. Thus, the attractiveness of hydrogen has led to increase the interest for this gas among companies, scientists and policy makers. Hydrogen is commonly produced by means of SMR, although it is also produced by steam reforming of naphtha, heavy oil fractions, methanol or coal. The SMR technology is very well known and it is the one commonly used in industry. The process involves several catalytic steps: S-removal, pre-reforming, reforming, high and low temperature water gas-shift (WGS) reactions, methanation and NO_x removal. The most important reactions are the following:

SMR:	$CH_4 + H_2O \rightarrow CO + 3H_2$	(ΔH^o = 206 kJ/mol)	(1)
WGS:	$CO + H_2O \rightarrow CO_2 + H_2$	(ΔH^o = - 41 kJ/mol)	(2)

While the cost of natural gas and other fossil fuels remains at a moderate level, the SMR will be the technology chosen for large scale of synthesis gas and hydrogen production. However, the miniaturization of this process is still a technological challenge [7,8]. Apart from this, it is necessary to increase the efficiency for remote or off-shore applications. Process intensification could be a way for it, in order to obtain hydrogen from fossil fuels or biomass. The need of distributed and portable power generation systems is clear nowadays [9,10].

The aim of this work is the study of hydrogen production by steam methane reforming using microreactors. These advanced reaction systems can be used for hydrogen decentralized production from NG. Thus, these system include microreactors and active, selective, stable and/or cheap catalytic formulations. Indeed, process intensification would allow better heat transfer which plays a key role in this process [11-13].

Different catalysts for methane steam reforming have been studied, especially Ni-based catalyst and noble metal-based catalysts like ruthenium, rhodium and platinum, amongst others [14,15].

Although the noble metal-based catalysts present high activity, their high cost limits their industrial application. The much lower cost of Ni-catalysts make them good candidates for methane reforming reactions. In this work, both noble and non-noble metals were studied in order to compare their performance.

3.2 Experimental

3.2.1 Activity measurements

Methane and natural gas steam reforming reactions were carried out to test all the catalysts. For the SMR experiments, a standard feed mixture consisted of CH_4:H_2O:N_2 = 1:1:1.88 (molar ratio) was fed into both reaction systems at atmospheric pressure. In addition, tests at S/C ratio of 1.5 and 2.0 were also carried out in order to obtain higher conversions and minimize the coke formation. The temperature was varied between 973 K and 1073 K, raising for 50 K after each previous experiment. In the case of the NG steam reforming experiments, a synthetic NG with the following composition was used: 87 % methane, 8 % ethane, 2 % propane, 0.5 % butane, 2 % nitrogen and 0.5 % carbon dioxide (vol.). With the objective of comparing the results the same volume of methane was feed in both tested feeds. All the experimental conditions were analyzed and simulated before the operation in the laboratory using Aspen Plus commercial software for the process analysis [16,17].

A bench-scale Microactivity plant (PID Eng&Tech), was used for activity tests (see Figure 1). The feed mixture gases flows were adjusted by electronic controllers and a High Performance Liquid Chromatography (HPLC) Gilson liquid pump was used for the deionized water injection. Both reactors were electrically heated in a furnace. The effluent stream was cooled down with a partial condenser. The condensed water was collected and weighted, and the gas phase was analysed by a Gas Chromatograph (GC 6890 N) equipped with Flame Ionization Detector (FID) and Thermal Conductivity Detector (TCD). Two columns, High Performance (HP) Plot Q and HP Molsieve, were used in a series/bypass arrangement for the complete separation of hydrogen, carbon monoxide, carbon dioxide, nitrogen, methane, ethane, propane and butane.

Before running the activity tests, each catalyst was reduced at 1073 K, using 360 NmL/min of a 3:1 = N_2:H_2 mixture, during 4 h for all the reaction systems. The measured parameters were defined as:

Methane conversion: $X_{CH4}\,(\%) = (V_{CH4}^{in} - V_{CH4}^{out}) / V_{CH4}^{in}$

Ethane conversion: $X_{C2H6}\,(\%) = (V_{C2H6}^{in} - V_{C2H6}^{out}) / V_{C2H6}^{in}$

Propane conversion: $X_{C3H8}\,(\%) = (V_{C3H8}^{in} - V_{C3H8}^{out}) / V_{C3H8}^{in}$

Butane conversion: $X_{C4H10}\,(\%) = (V_{C4H10}^{in} - V_{C4H10}^{out}) / V_{C4H10}^{in}$

H_2out/CH_4in (molar ratio) $= V_{H2}^{out} / V_{CH4}^{in}$

CO selectivity: $S_{CO}\,(\%) = V_{CO}^{out} / (V_{CO}^{out} + V_{CO2}^{out})$

Where: V_i^{in} corresponds to the volumetric flow-rate of reactant *i* (NmL/min).

V_i^{out} corresponds to the volumetric flow-rate of product *i* (NmL/min).

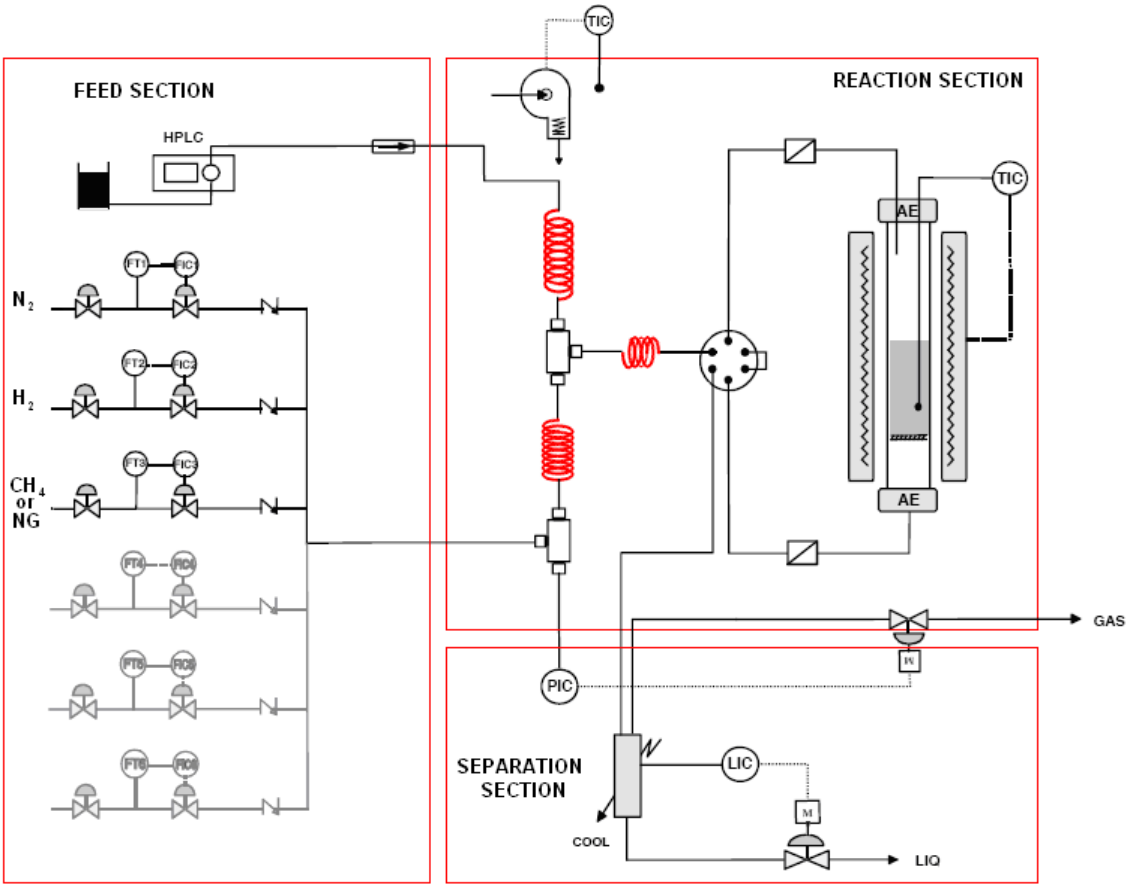

Figure 1: *Scheme of the Microactivity plant.*

3.3 Reactors

As two types of reactors were studied, the catalysts, prepared by wet impregnation, were deposited on them by two different methods. For the microreactors, the catalysts were washcoated into the microchannels and for the fixed bed reactors they were introduced in the catalytic bed diluted with silicon carbide (CSi).

3.3.1 The microreactor

The next procedure was carried out for the deposition of the micro-nanoparticles on the reactors microchannels [18,19] (see microreactor properties in section "4.2.2.2 Microreactor preparation"):

- Catalyst preparation: An IKA mill was used for the reduction of the catalysts particle size. Once powdered the catalysts were sieved with a 75 µm sieve.

- Microreactor preparation: The microreactors were introduced in an ultrasonic bath with isopropanol during 10 minutes for channel cleaning. After drying, they were calcined at 1273 K during four hours.
- Catalyst impregnation: A liquid phase suspension which ensures a perfect adhesion between catalysts and microchannels was prepared for the impregnation. Catalysts were manually impregnated filling microchannels with suspension and removing the excess.
- Conditioning of catalyst and microreactor: After impregnation, the catalysts were calcined at 1073 K during two hours under oxidative conditions. Finally, the platelets were welded and the microreactors conditioned for using them in the activity tests.

Through this process the two Ni-based catalysts (over MgO and calcium modified Al_2O_3) and two noble metal based catalysts (Pd and Pt over Al_2O_3) were impregnated. Different pictures of the above mentioned steps are shown in Figure 2.

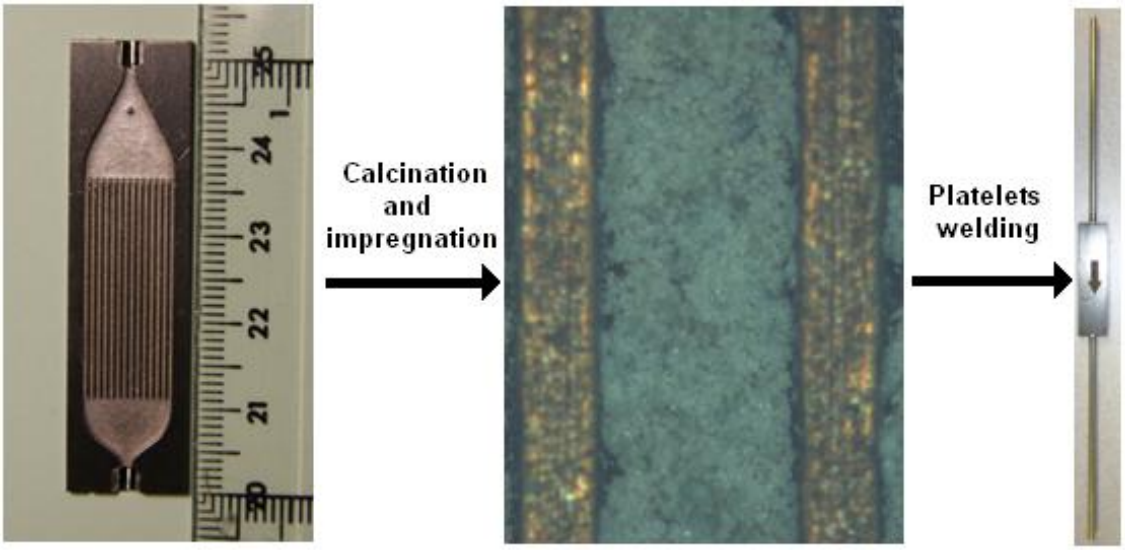

Figure 2: *The microreactor preparation process.*

3.3.2 Fixed bed reactor

As a traditional reactor system a stainless-steel fixed bed reactor (1.15 cm i.d. and 30 cm length) was used. As commented before, the same amount of catalyst than in the microreactors was used in the fixed bed reactor systems.

The reactor was filled with inert CSi particles (1.0 - 1.5 mm diameter particle size), from the bottom until the thermocouple was reached. Then, the needed catalyst amount (0.42-0.50 mm diameter particle size) was diluted with CSi at 1:9 w/w (0.5-1.0 mm diameter particle size) in order to avoid temperature gradients in the bed. Finally, the reactor was totally filled with another bed of the same CSi particles and closed. This higher size was used in order to separate satisfactorily CSi and tested catalysts after activity experiments.

Using the same feed flow and the same weight of catalyst, the WHSV values were kept equal in both reaction systems. In Table 1 the nominal and the experimental metal contents, as measured by (ICP-AES), the catalysts amount used and the WHSV values for the SMR and NG steam reforming are compiled. As it can be noticed, there are some differences between the WHSV values used; for Pt/Al_2O_3 catalyst, as the catalyst amount impregnated was higher the WHSV decreased one order of magnitude. In addition, for the SMR and NG steam reforming experiments the WHSV values changed. As the methane feed flow remained equal in both cases, and NG contained other compounds, the feed flow was slightly higher for the NG steam reforming increasing the WHSV.

Table 1: *Nominal and experimental chemical composition of calcined catalysts, weight used of catalyst in all the reaction systems and WHSV values for SMR and NG steam reforming experiments at different S/C ratios.*

Catalysts	Nominal (wt.%)	Real (wt.%)	Weight (g)	SMR			NG steam reforming	
				S/C=1.0	S/C=1.5	S/C=2.0	S/C=1.0	S/C=2.0
Ni/MgO	20 (Ni)	17.02 (Ni)	0.01889	1534.3	1693.1	1851.9	1614.2	1931.8
Ni/Al_2O_3	Commercial		0.02367	1224.4	1351.3	1477.9	1288.2	1541.7
Pd/Al_2O_3	1.0 (Pd)	0.31 (Pd)	0.01247	2324.1	2564.7	2805.3	2445.2	2926.4
Pt/Al_2O_3	1.0 (Pt)	0.79 (Pt)	0.14352	201.9	222.8	243.7	212.5	254.3

*Commercial catalysts composition: 18 wt% of NiO.

3.4 Results and discussion

All the activity tests started after the system was stabilized and lasted 480 minutes. All catalysts were tested at the same conditions and the same analysis procedure was carried out for all of them. All the reported measurements values in the tables correspond to the mean of the last two analyses.

3.4.1 Calcined catalysts chemical composition

The ICP-AES instrument, model 2000-DV (Perkin Elmer) was used for the determination of the metallic elements in the catalysts. The catalysts were properly dissolved using a digester and thereafter analyzed by ICP-AES instrument. A solution that consisted of HCl, HNO_3 and HF was used for Ni, Ca, Pt and Pd solution before their quantification. These results were summarized in Table 1. In general, the experimental contents measured for all the catalytic systems were slightly lower than the nominal ones.

3.4.2 Microreactor reaction systems

3.4.2.1 Microreactor 1: Ni/MgO catalyst

Experiments at different temperatures confirmed that as SMR reaction is endothermic, the lowest activity was measured at the lowest temperature, 973 K, (about 35 % of methane conversion, see Figure 3). Increasing the reaction temperature higher methane conversion was reached. During these experiments no significant deactivation of the catalyst was observed during the time on stream.

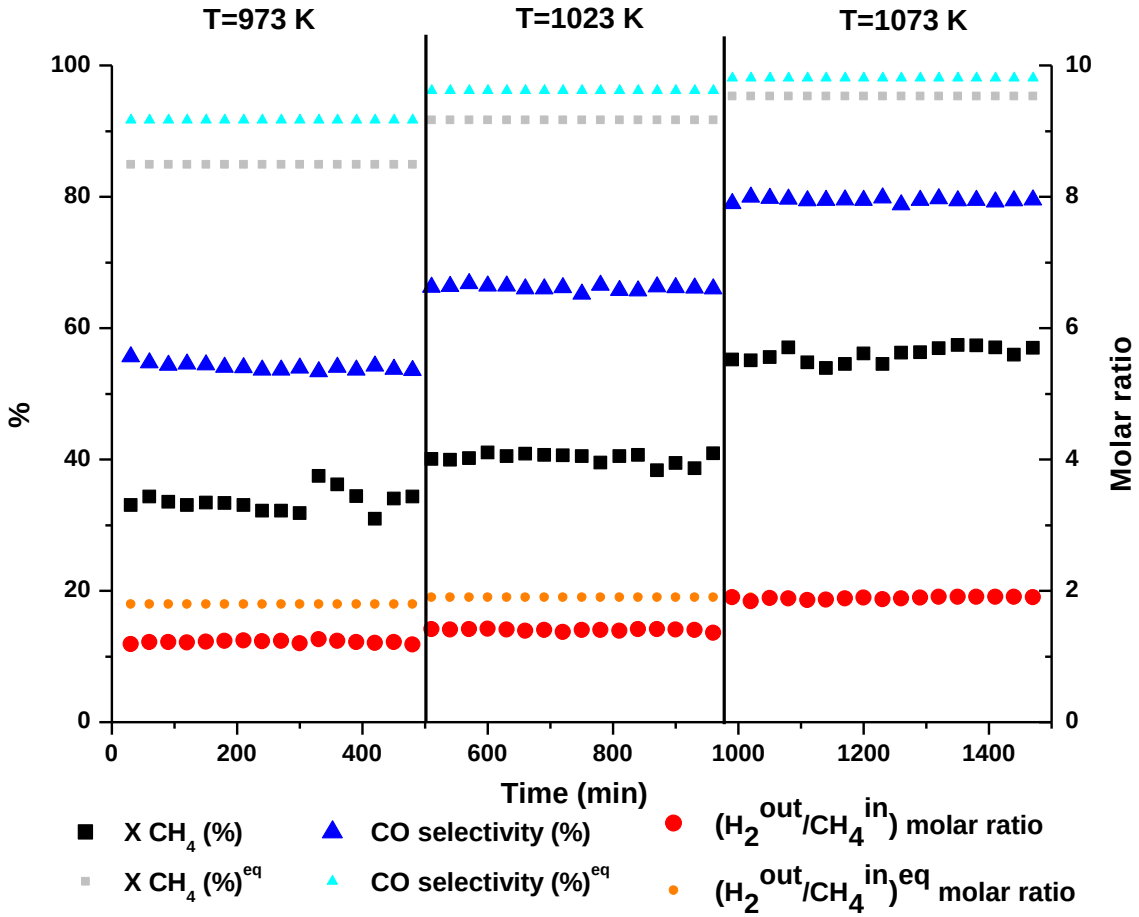

Figure 3: *SMR activity test results for Ni/MgO catalyst at S/C=1.0 and different temperatures.*

Results of the activity tests at 1073 K and different S/C ratios are shown in the Figure 4 for the Ni/MgO catalyst. The S/C ratio of 1.0 corresponds to the stoichiometric feed for the SMR reaction. Experiments in which more water was added than the required for this stoichiometric reaction were carried out at S/C=1.5 and 2.0.

For the experiments with Ni/MgO catalyst at 1073 K and S/C ratio of 1.0, the methane conversion was about 55.0%. When the S/C ratio was increased from 1.0 to 1.5 methane conversions grew to 60.5% increasing also the hydrogen yield. In the case of increasing the S/C ratio from 1.5 to 2.0 methane conversion remained with similar values for the first hours and

after that, the methane conversion lowered to 54.0%. In these first hours, the CO selectivity decreased from 71% to 59% and also the hydrogen yield. As methane conversion did not change, this effect could be explained through the promotion of the WGS reaction. For these experiments, significant deactivation of the catalysts was not observed.

As a summary, it could be affirm that increasing the S/C ratio, from 1.0 to 1.5, the conversion and hydrogen yield improved, as expected. Nevertheless, for the highest ratio, S/C=2.0, the activity did not improve.

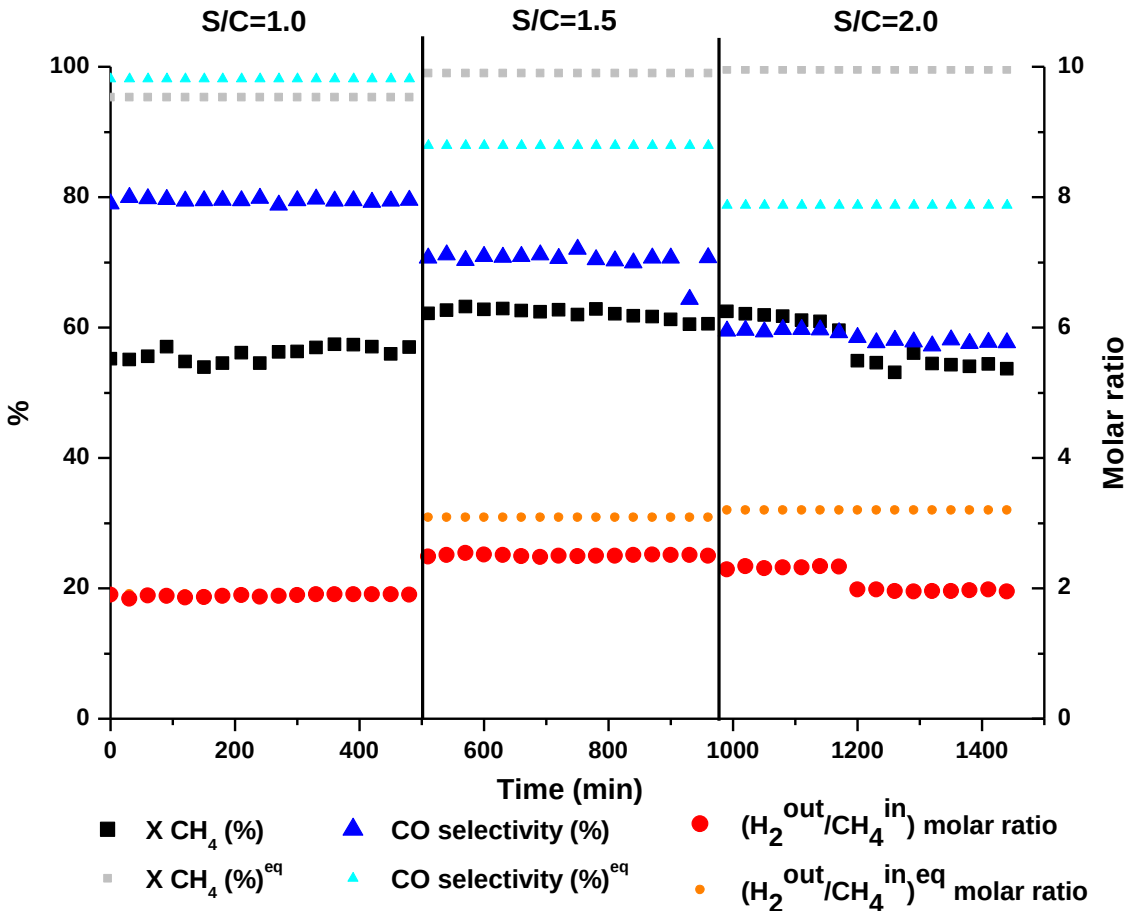

Figure 4: *SMR activity test results for Ni/MgO catalyst at 1073 K and different S/C ratios.*

Natural gas steam reforming activity tests were also carried out using the Ni/MgO catalyst. As it can be observed in Figure 5, the measured conversion for hydrocarbons was higher than for methane. The conversion of this latter remained almost constant when the S/C ratio was increased up to 2.0, but it was lower for ethane, propane and butane. However, hydrogen generation remained constant because of WGS reaction. Also in these experiments the catalyst did not suffer deactivation.

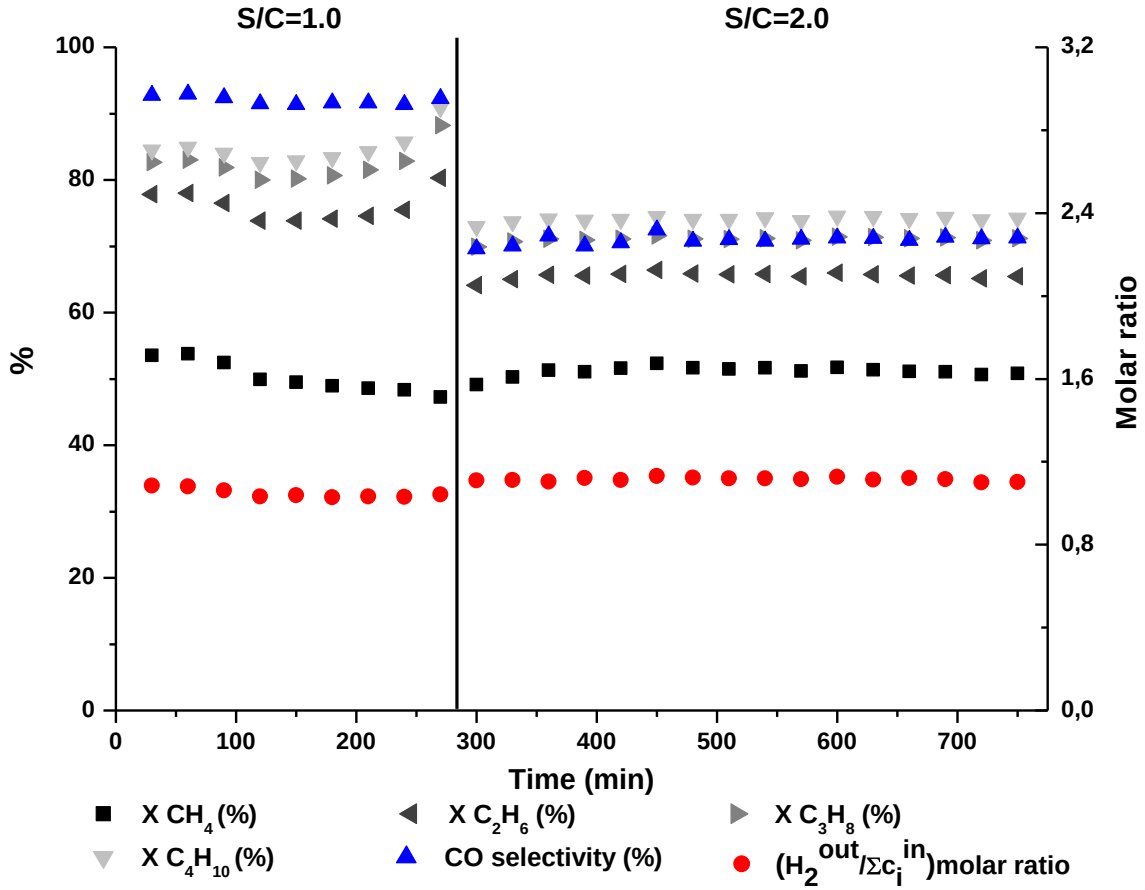

Figure 5: *NG steam reforming activity results for Ni/MgO catalyst at 1073 K and different S/C ratios.*

3.4.2.2 Microreactor 2: Ni/Al_2O_3 catalyst

Activity results for Ni/Al_2O_3 catalyst at S/C=1.0 and different temperatures are presented in Table 2. As it could be expected, all the measured parameters increased with reaction temperature. Activity results at different S/C ratios are also gathered in the same table. When the S/C ratio was increased, from 1.0 to 1.5, less methane was converted and less hydrogen was therefore produced. In addition, increasing the S/C ratio up to 2.0, no significant catalytic improvements were measured.

Table 2: *SMR activity results for Ni/Al_2O_3 catalyst at S/C 1.0 and different temperatures and at the temperature of 1073 K and different S/C ratios.*

Ni/Al_2O_3	Temperature (K)			S/C ratio	
	973	1023	1073	1.5	2.0
X_{CH4} (%)	30.7 (79.5)	46.3 (80.9)	72.9 (89.1)	62.5 (99.0)	62.50 (99.6)
H_{2out}/CH_{4in}	1.0 (2.5)	1.6 (2.7)	2.4 (2.8)	2.0 (3.1)	2.05 (3.2)
S_{CO} (%)	59.4 (91.6)	76.5 (96.0)	88.8 (98.0)	74.3 (88.0)	69.63 (78.8)

Note: Values in parentheses are equilibrium values.

In Figure 6, the quick deactivation suffered for this catalyst during the first 4 hours when NG was used in steam reforming experiments is observed. As for the Ni/MgO catalyst, the conversion of methane was lower than for the rest of hydrocarbons.

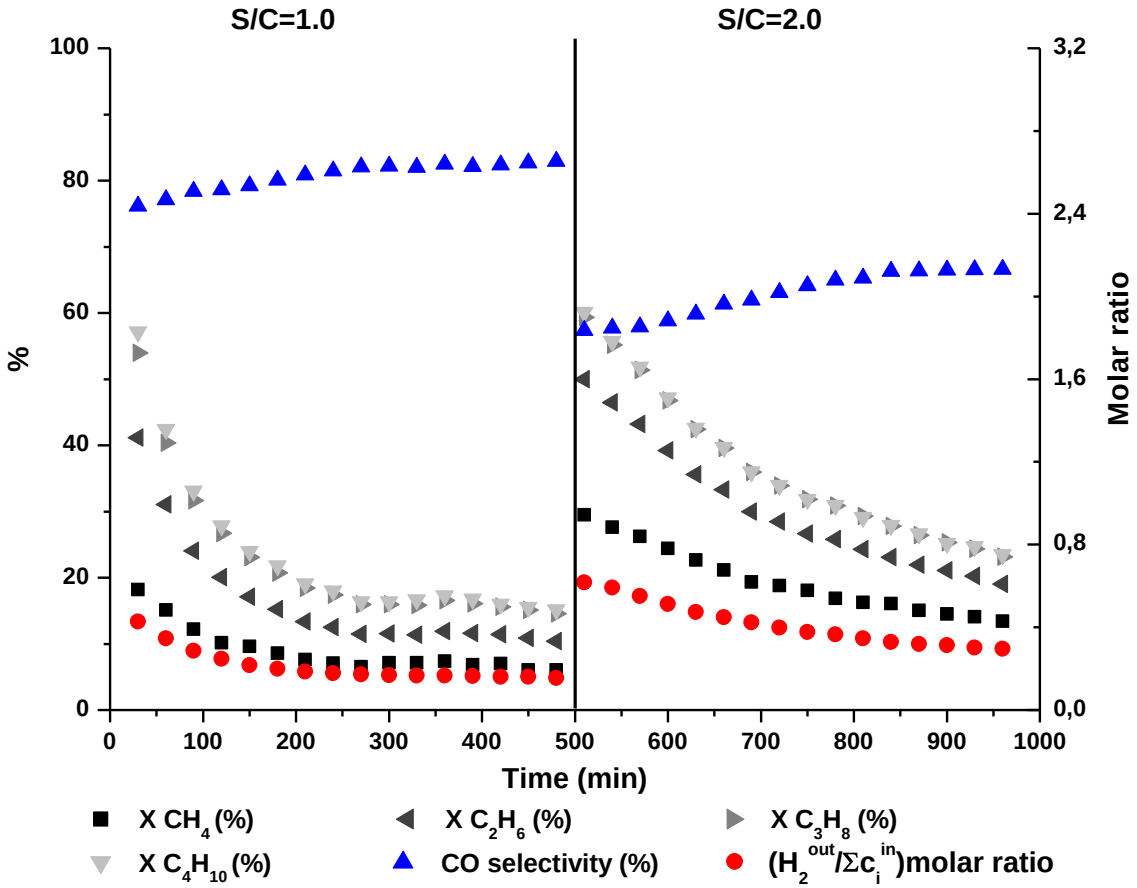

Figure 6: *NG steam reforming activity results for Ni/Al_2O_3 catalyst at 1073 K and different S/C ratios.*

This effect could be attributed to the high molecular weight hydrocarbons present in the natural gas. This fact and the high operating temperatures could contribute to the carbon generation and the consequent deactivation of the catalyst. In addition, due to the apparently carbon free surface presented by this catalyst (see Figure 7), this effect could also be attributed to the possible cracking process suffered by the higher hydrocarbons which could increase the quantity of methane present in the atmosphere and hence reduce methane conversion.

3.4.2.3 Microreactor 3&4: Pd and Pt/Al_2O_3 catalysts

For Pd/Al_2O_3 and Pt/Al_2O_3 catalysts, methane and NG steam reforming activity tests were also carried out at 1073 K and S/C=1.0. Unfortunately, no significant methane conversion (under 5%) was measured. For the other hydrocarbons less than 5 % of conversion was also reached, which means that those catalysts were rapidly deactivated and as a consequence, the hydrogen production was really low.

3.4.3 Fixed bed reactor reaction systems

Finally, a fixed bed reaction system at the same WHSV values was used for activity tests. For all catalysts and all experimental conditions really low conversions were achieved; for every S/C ratios the achieved methane conversion was under 5%. The results of conversion for NG steam reforming were also insignificant, only hydrocarbons like propane and butane reached high conversions.

3.4.4 Characterization by scanning electron microscope

The structure formed on the microchannels was characterized with an electronic microscope. SEM micrographs of tested catalysts were obtained using a JEOL JSM-7000-F scanning electron microscope, equipped with a Schottky field emission cathode. Composition was studied by combination of backscattered electron imaging and Energy Dispersive X-Ray Spectroscopy (EDX) using an Oxford Instruments Inca Energy 350 spectrometer installed in the same microscope.

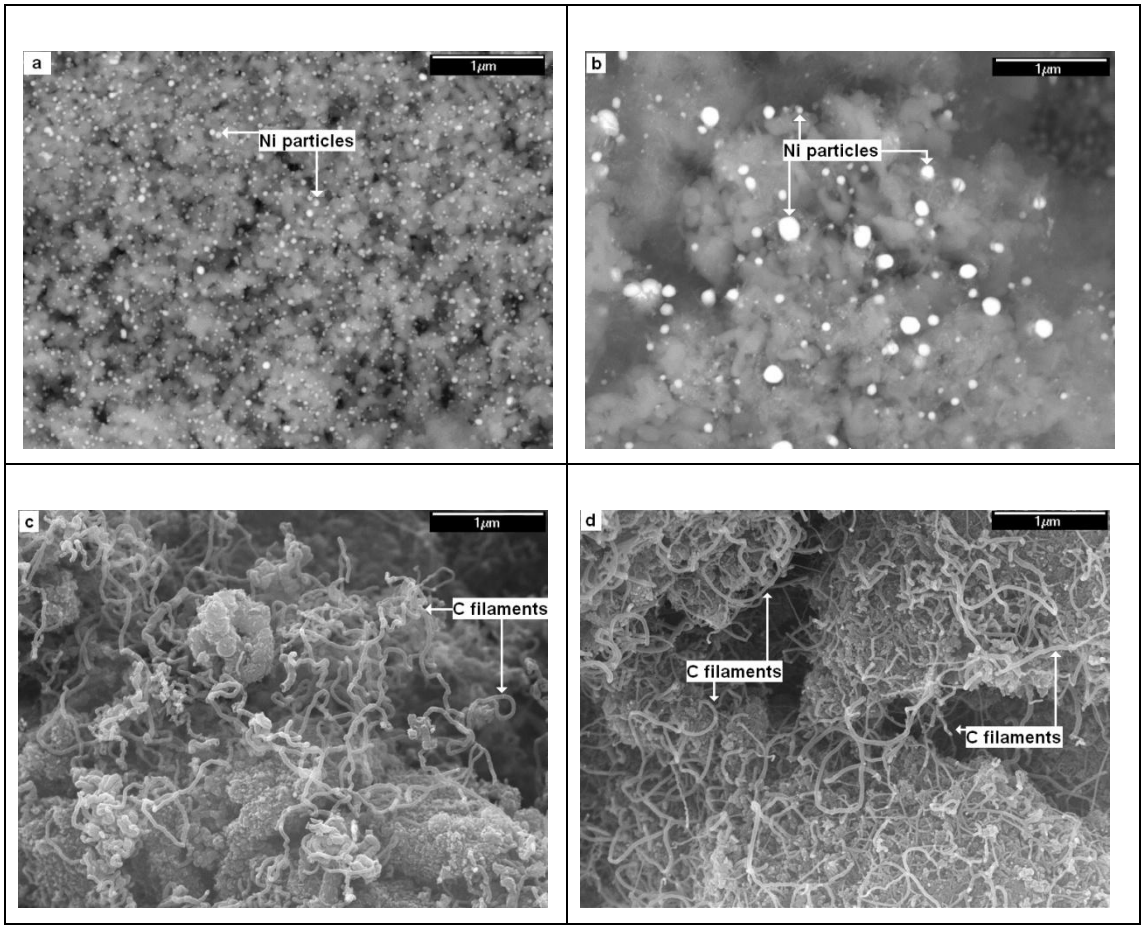

Figure 7: *Surface SEM backscattered micrographs for Ni/MgO (a) and Ni/Al_2O_3 catalysts (b) and morphology micrographs for Pd/Al_2O_3 (c) and Pt/Al_2O_3 catalysts (d).*

Comparing the behavior of the different impregnated catalysts, a homogeneous distribution and small particle size was reached for the Ni/MgO and Ni/Al_2O_3 catalysts. For these two catalysts (see Figures 7a and 7b, respectively) evidence of a uniform nickel particles distribution can be observed as well as the catalytic surface which is free of carbon. The presence of Ni particles in the catalytic surface of these two micrographs was confirmed by backscattered electron imaging. Moreover, in the case of Ni/MgO catalyst, a smallest particle size (15-60 nm) was measured [20] if compared with the Ni/Al_2O_3. In addition, for the Ni/MgO catalyst deactivation by sintering was not measured as the original particle size was 28.5 nm (measured by XRD [21]).

For Pd/Al_2O_3 and Pt/Al_2O_3 catalysts, SEM images were taken from secondary electron detectors in order to study surface morphology. In both catalysts (Figures 7c and 7d respectively) carbon filaments growth can be observed on Pd/Al_2O_3 and Pt/Al_2O_3 surfaces [22-24]. Therefore, the low activity measured for both noble metals catalysts can be attributed to the carbon filaments growth covering the catalytic surface.

3.5 Conclusions

Hydrogen production from methane and natural gas steam reforming process was studied by two different reaction systems at the same conditions.

Higher methane (or natural gas) conversion was reached at higher temperatures but it does not improve significantly operating at higher steam to carbon ratios. In the case of the Ni/Al_2O_3 catalyst, high methane and natural gas conversions were obtained despite of its quick deactivation. On the contrary, Ni/MgO catalyst did not suffer apparent deactivation and it reached the highest hydrogen production yield at the temperature of 1073 K and the S/C of 1.5 for steam methane reforming reaction. In this case, the water gas shift reaction was also promoted. For Pd/Al_2O_3 and Pt/Al_2O_3 catalysts, the obtained low catalytic activity might be due to the bad impregnation and the carbon filaments growth.

For all the catalysts, lower conversion was reached in a fixed bed reactor at the same weight hourly space velocity. Thus, higher hydrocarbons conversions and higher hydrogen yields were achieved in the microreactors.

As a result, decentralized hydrogen production from natural gas steam reforming through process intensification seems to be a promising technology. In a near future, these systems could be used together with other renewable feeds, such as biogas and bioalcohols, for the production syngas or hydrogen rich mixtures.

3.6 References

[1] F. Orecchini, The era of energy vectors, Int J Hydrogen Energy. 31 (2006) 1951.

[2] M. Momirlan, T.N. Veziroglu, The properties of hydrogen as fuel tomorrow in sustainable energy system for a cleaner planet, Int J Hydrogen Energy. 30 (2005) 795.

[3] H. Turton, L. Barreto, Long-term security of energy supply and climate change, Energ Policy. 34 (2006) 2232.

[4] M. Ball, M. Wietschel, The future of hydrogen – opportunities and challenges, Int J Hydrogen Energy. 34 (2009) 615.

[5] M. Momirlan, T. Veziroglu, Recent directions of world hydrogen production, Renew Sust Energ Rev. 3 (1999) 219.

[6] R. Bleischwitz, N. Bader, Policies for the transition towards a hydrogen economy: the EU case, Energ Policy. 38 (2010) 5388.

[7] D.A. Castelo Branco, A.S. Szklo, R. Schaeffer, CO_{2e} emissions abatement costs of reducing natural gas flaring in Brazil by investing in offshore GTL plants producing premium diesel, J Energy. 35 (2010) 158.

[8] Y. Men, G. Kolb, R. Zapf, H. Pennemann, V. Hessel, Total combustion of propane in a catalytic microchannel combustor, Chem Eng Res Des. 87 (2009) 91.

[9] M. O'Connell, G. Kolb, R. Zapf, Y. Men, V. Hessel, Bimetallic catalysts for the catalytic combustion of methane using microreactor technology, Catal Today. 144 (2009) 306.

[10] X. Zhai, S. Ding, Y. Cheng, Y. Jin, Y. Cheng, CFD simulation with detailed chemistry of steam reforming of methane for hydrogen production in an integrated micro-reactor, Int J Hydrogen Energy. 35 (2010) 5383.

[11] G. Kolb, V. Hessel, Micro-structured reactors for gas phase reactions, Chem Eng J. 98 (2004) 1.

[12] E.R. Delsman, B.J.P.F. Laarhoven, M.H.J.M. De Croon, G.J. Kramer, J.C. Schouten, Comparison between Conventional Fixed-Bed and Microreactor Technology for a Portable Hydrogen Production Case, Chem Eng Res Des. 83 (2005) 1063.

[13] T. Conant, A. Karim, A. Datye, Coating of steam reforming catalysts in non-porous multi-channeled microreactors, Catal Today. 125 (2007) 11.

[14] X. Zhai, S. Ding, Z. Liu, Y. Jin, Y. Cheng, Catalytic performance of Ni catalysts for steam reforming of methane at high space velocity, Int J Hydrogen Energy. 36 (2011) 482.

[15] E. Acha, J. Requies, V.L. Barrio, J.F. Cambra, M.B. Güemez, P.L. Arias, Water effect in hydrogen production from methane, Int J Hydrogen Energy. 35 (2010) 11525.

[16] J. Thormann, P. Pfeifer, K. Schubert, U. Kunz, Reforming of diesel fuel in a micro reactor for APU systems, Chem Eng J. 135 (2008) S74.

[17] J. Huang, J. Weinstein, R.S. Besser, Particle loading in a catalyst-trap microreactor: Experiment vs. simulation, Chem Eng J. 155 (2009) 388.

[18] V. Hessel, H. Löwe, A. Müller, G. Kolb, Chemical Micro Process Engineering, 1st ed ed., KGaA, Weinheim, 2005.

[19] G. Germani, A. Stefanescu, Y. Schuurman, A.C. Van Veen, Preparation and characterization of porous alumina-based catalyst coatings in microchannels, Chem Eng Sci. 62 (2007) 5084.

[20] L. Zhang, X. Wang, B. Tan, U.S. Ozkan, Effect of preparation method on structural characteristics and propane steam reforming performance of Ni-Al_2O_3 catalysts, J Mol Catal. 297 (2009) 26.

[21] J. Requies, M.A. Cabrero, V.L. Barrio, M.B. Güemez, J.F. Cambra, P.L. Arias, Partial oxidation of methane to syngas over Ni/MgO and Ni/La_2O_3 catalysts, Appl Catal A Gen. 298 (2005) 214.

[22] A.M. Pashaa, A. Shafiekhanib, M.A. Vesaghia, Hot filament CVD of Fe-Cr catalyst for thermal CVD carbon nanotube growth from liquid petroleum gas, Appl Surf Sci. 256 (2009) 1365.

[23] M. García-Diéguez, E. Finocchio, M.A. Larrubia, L. Alemany, Characterization of alumina-supported Pt, Ni and PtNi alloy catalysts for the dry reforming of methane, J Catal. 274 (2010) 11.

[24] M. García-Diéguez, I.S. Pieta, M.C. Herrera, M.A. Larrubia, L.J. Alemany, Nanostructured Pt- and Ni-based catalysts for CO_2-reforming of methane, J Catal. 270 (2010) 136.

CHAPTER 4

Biogas reforming processes

Published articles:

Title: Biogas steam and oxidative reforming processes for synthesis gas and hydrogen production in conventional and microreactor reaction systems

Authors: U. Izquierdo, V.L. Barrio, N. Lago, J. Requies, J.F. Cambra, M.B. Güemez, P.L. Arias

Title: Tri-reforming: a new biogas process for synthesis gas and hydrogen production

Authors: U. Izquierdo, V.L. Barrio, J. Requies, J.F. Cambra, M.B. Güemez, P.L. Arias

Title: Ni and Rh-Ni catalysts supported on Zeolites L for hydrogen and syngas production by biogas reforming processes

Authors: U. Izquierdo, V.L. Barrio, K. Bizkarra, A.M. Gutierrez, J.R. Arraibi, L. Gartzia-Rivero, J. Bañuelos, I. Lopez-Arbeloa, J.F. Cambra

Title: Microwave synthesis of LTL zeolite with tunable size and morphology: an optimal support for metal-catalyzed hydrogen production from biogas reforming processes

Authors: L. Gartzia-Rivero, J. Bañuelos, U. Izquierdo, V.L. Barrio, K. Bizkarra, J.F. Cambra, I. López-Arbeloa

Table of contents

List of figures

List of tables

4.1 Introduction

It is time for hydrogen and this opportunity should be seized by doing improvements and innovations in the existing technologies as well as for developing new ones [1]. At present, hydrogen is mostly produced by steam reforming of the fossil fuels. However, due to their depletion, the development of new processes or the modification of the existing ones, but based on renewable energy sources, is required [2-4]. The needs of an energy transition and hydrogen characteristics as a clean energy vector, derived in different efforts regarding to the development of new economical and competitive processes as an alternative to the existing ones.

In this work the comparison between microreactors, advanced reaction systems, and conventional fixed bed reactors was studied being both used for synthesis gas and hydrogen production. The microreactors provide several benefits if compared with a conventional reaction systems. The high surface area/volume relationship, which is around two orders of magnitudes higher, is one of the most interesting properties that allow the possibility to increase the WHSV of the catalytic reactions. These systems, apart from improving heat and mass transfer resistances, are also able to reach higher selectivity in the desired products [5-7].

Apart from facing out the miniaturization of the processes using microreactors, in this chapter different biogas reforming processes were studied for hydrogen and synthesis gas production: dry reforming, biogas steam reforming, biogas oxidative reforming and try-reforming. The biogas is considered a carbon dioxide-neutral biofuel and if used as transport fuel instead of fossil fuels, apart from reducing green house gases, hydrocarbons, carbon monoxide and particles emissions are also reduced [8-10]. Using the biogas as feed of the mentioned reforming processes, two of the most important GHG, carbon dioxide and methane, are consumed [4] and the low syngas ratio obtained is appropriate for gasoline, gasoil, kerosene, aldehydes and alcohols production [11].

Biogas is commonly produced from biomass anaerobic digestion [6,7] and its composition varied depending on the type of biomass: 55–70 CH_4, 27–44 CO_2, <1 H_2 and <3 H_2S as well as traces of NH_3 (vol.%) [8]. Therefore, CH_4:CO_2 ratio will be always higher than 1.0 regardless of the biomass precedence which can lead into a carbon deposition on the catalytic surface. In addition, another issue that can strongly affect to the biogas reforming processes and catalysts regards to the presence of sulphur compounds that could inhibit the chemisorption of small molecules (H_2, CO, NO, C_2H_4, etc.) and lead to deactivation of the catalysts effectiveness [12]. In addition, as nitrogen compounds are basic, their presence might poison the acid sites of catalysts. As a consequence, due to the poisoning effect of S and N compounds, the utilization of the biogas in any catalytic reforming process would require a previous purification stage [10].

In order to study the performance of the different processes described above, a model biogas was used in all the experiments. In Section 4.3 a thorough study of the influence of the reaction conditions, described below, were studied using a Ni/MgO and different γ-Al_2O_3 supported catalysts at atmospheric pressure and 1073 K. When operating under DR conditions with the fixed bed reactor, the selection of the best catalysts was carried out. However, as the rest of the studied processes are influenced by the S/C or O_2/CH_4 ratios, the most appropriate S/C ratio for BSR process; O_2/CH_4 ratio for BOR; and S/C and O_2/CH_4 ratios for TR process were established operating with the fixed bed reactor. Additionally, the existing differences between the catalysts tested at the different experimental conditions were also studied according to the fresh and tested characterization results obtained and the catalytic activity measured.

Once the best catalysts and operation conditions were chosen, the intensification of BOR and TR processes was studied using microreactors. In order to compare the results obtained, the same reactant feed flow was fed in all experiments for each reactor system. Therefore, reactor performances at very different WHSV (high for microreactors and low for fixed bed reactor due to the different catalysts amount used) were compared.

In the Sections 4.4 and 4.5 three different zeolite supports were tested. Zeolites offer high surface areas, specific micropores structures, and affinity to CO_2, and therefore they are good candidates for catalyzing the biogas reforming reactions under investigation. The differences between the zeolites tested in both sections lies in the synthesis method. Therefore, in section 4.5, zeolites were prepared by microwave-assisted hydrothermal synthesis and Na^+ and Cs^+ metals were used to adjust the acidity inside the channels. Therefore, the influence of those modifiers on the activity was also studied.

4.2 Experimental procedure

4.2.1 Activity measurements

For all the experiments a model biogas consisting of 60% CH_4 and 40% CO_2 (vol.) was fed [8,13,14] which corresponds to the WHSV of 75 h^{-1} for DR experiments. Tests were carried out at 1073 K and atmospheric pressure. For BSR process, experiments with S/C ratios from 1.0 to 3.0 were performed. In the case of BOR process, O_2/CH_4 ratios from 0.125 to 0.50 were tested. For TR process, operating at O_2/CH_4 ratios of 0.25 and 0.50, S/C increasing ratios from 1.0 to 3.0 were studied. Depending on the oxygen flow, nitrogen was also fed in order to simulate an air stream. Once the experiments were carried out in a fixed bed reactor system, the most stable and active catalysts were chosen to be tested in the microreactors at the same conditions. Using these innovative systems and operating with them at the same temperature, pressure and reactants flow, an increase in the WHSV is expected due to the needed lower catalysts amount.

A bench-scale Microactivity plant (PID Eng&Tech), was used for activity tests. The fed mixture gases flows were adjusted by electronic controllers and a HPLC-Gilson liquid pump was used for the desionizated water injection. Both, fixed bed and microreactors were electrically heated in a furnace (see also Figure 1 of Chapter 3).

Figure 1: *The experimental facility used for experiments.*

The effluent stream was cooled down with a partial condenser. The condensed water was collected and weighted, and the gas phase was online analyzed by a micro Gas Chromatograph (μ-GC) equipped with a TCD detector. Three columns, Molsieve 5 Å PLOT, CP-Sil 5 CB and Poraplot Q, were used in a series arrangement for the complete separation of hydrogen, carbon monoxide, carbon dioxide, nitrogen, oxygen and methane.

Before running the activity tests, each catalyst was reduced at 1073 K, using 350 NmL/min of a 3:1 N_2:H_2 mixture, during 4 h for all the reaction systems. The activity tests lasted 90 minutes and started after the process was stabilized. The measured parameters were defined as:

Methane conversion: $X_{CH4}\ (\%) = (V_{CH4}^{in} - V_{CH4}^{out}) / V_{CH4}^{in} \cdot 100$

Carbon dioxide conversion: $X_{CO2}\ (\%) = (V_{CO2}^{in} - V_{CO2}^{out}) / V_{CO2}^{in} \cdot 100$

Hydrogen yield: $H_2\ \text{yield}\ (\%) = V_{H2}^{out} / (2 \cdot V_{CH4}^{in} + V_{H2O}^{in}) \cdot 100$

$(H_2/CO)^{out}$ molar ratio $(H_2/CO)^{out} = (V_{H2} / V_{CO})^{out}$

Where: V_i^{in} corresponds to the volumetric flow-rate of reactant *i* (NmL/min).
V_i^{out} corresponds to the volumetric flow-rate of product *i* (NmL/min).

The turnover frequency (moles of converted methane per mole of active metal and second), and catalyst hydrogen productivity (moles of hydrogen produced per mole of active metal and second) was defined as the velocity of the reaction measured at the catalytic surface [15-17] which truly reflects the activity level of available catalytically active sites on surface. In the present work, each exposed Ni metal atom on the surface is considered as an active site for methane or carbon dioxide conversion. For the Rh–Ni bimetallic catalyst, the number of surface Rh metal atoms was also taken into account. Due to the possible carbon dioxide consumption through DR or r-WGS reactions or to its production through WGS reaction the TOF value was not calculated for this compound.

CH_4 Turnover Frequency: $TOF_{CH4}\ (s^{-1}) = X_{CH4} \cdot N_{CH4}^{in} / (w_{cat} \cdot wt_{Me} \cdot D_{Me} / Pm_{Me})$

H_2 catalyst productivity: $PROD_{H2}\ (s^{-1}) = N_{H2}^{out} / (w_{cat} \cdot wt_{Me} \cdot D_{Me}) / Pm_{Me})$

Where: N_i corresponds to the molar flow of *i* (methane or hydrogen) in mol/s.
w_{cat} is the catalyst weight in each reactor system.
wt_{Me} is the elemental weight given by ICP-AES.
D_{Me} is the metal dispersion for the catalyst.
Pm_{Me} is the metal molecular weight.

4.2.2 Reactors

4.2.2.1 Fixed bed reactor preparation

As a conventional reactor system, a 316-L stainless-steel fixed bed reactor (4.57 mm i.d. and 30 cm length) was initially used in order to establish the most appropriates S/C and O_2/CH_4 ratios because the preparation of this type of reactor is faster and their use cheaper.

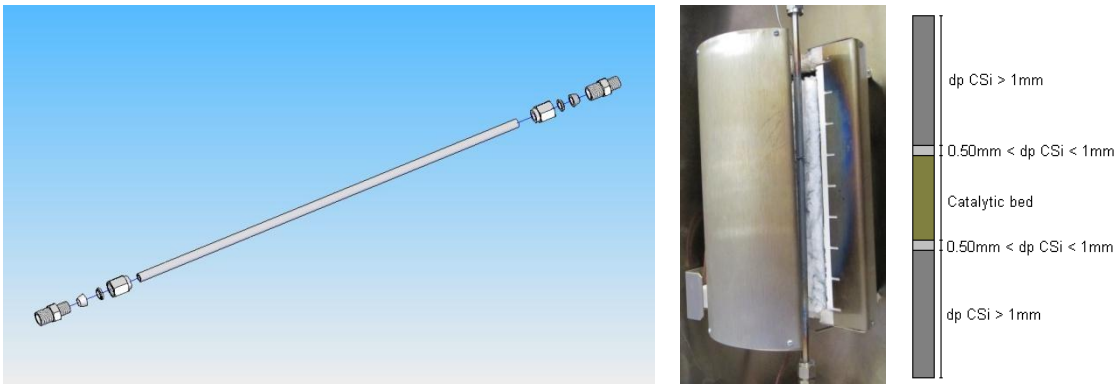

Figure 2: *Fixed bed reactor (left) and catalytic bed location in the microactivity plant (right).*

The same catalyst amount, 340 mg, (0.42-0.50 mm diameter particle size) was used in all fixed bed reactor tests. It was diluted with inert CSi at 1:4.5 w/w (0.5-1.0 mm diameter particle size), in order to avoid temperature gradients in the bed. The diluted catalyst bed was placed in the middle of the reactor and then it was totally filled with another bed of higher diameter CSi particles. This higher size was used in order to separate satisfactorily CSi and tested catalysts after activity experiments. Using 340 mg of catalyst, activity tests for biogas DR, BOR, BSR and TR processes were carried out at the following WHSV:

Table 1: *Calculated WHSV for the studied processes and conditions operating in a fixed bed reactor system.*

O_2/CH_4	WHSV in BOR (h^{-1})	S/C	WHSV in BSR (h^{-1})	WHSV in TR (h^{-1})	
				O_2/CH_4=0.25	O_2/CH_4=0.50
0.125	103	**1.0**	105	161	218
0.25	131	**2.0**	134	191	248
0.50	188	**3.0**	164	221	277

4.2.2.2 Microreactor preparation

The microreactors were made of stainless steel with the following composition: 53.22% Fe, 24.21% Cr, 19.09% Ni, 1.97% Si, 1.43% Mn, 0.05% C, 0.02% Pb and 0.001% S (wt.). The impregnated catalyst particle size must be small enough to be fixed and deposited on the channels as well as, to reduce the internal mass-transfer resistance. The external mass-transfer resistance was checked using Mears criteria [18]. All the experimental conditions were analyzed and simulated before the experiments in the laboratory [19,20].

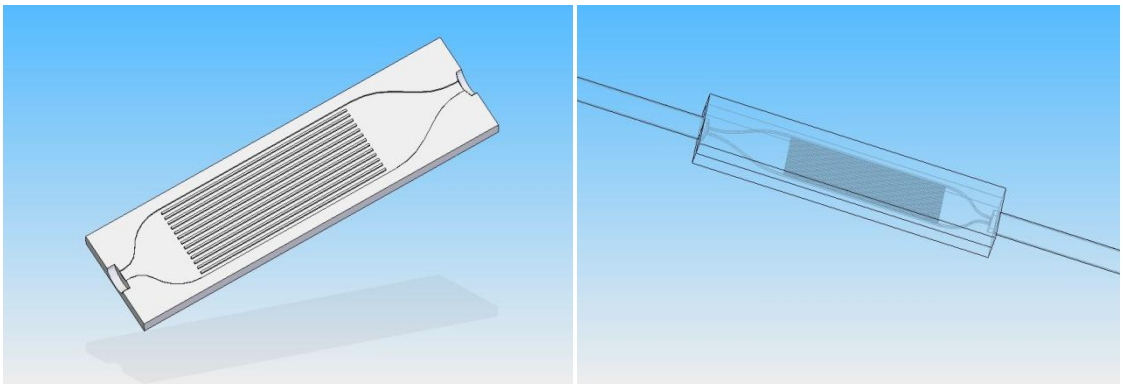

Figure 3: *Detail of the microchannels of the microreactors.*

The succeeding procedure was followed for the deposition of the micro-nano-particles on the reactors microchannels [21]:

- Catalysts preparation: An IKA mill was used for catalyst particle size reduction. Once powdered, catalysts were sieved and the 37–50 μm mesh fraction was used for the catalytic measurement.
- Microreactors preparation: The microreactors were placed in an ultrasonic bath with isopropanol during 10 min for channel cleaning. After drying, they were calcined at 1073 K during four hours.
- Catalysts impregnation: A liquid phase suspension which ensured a perfect adhesion between catalyst and microchannels was prepared for the impregnation. Catalysts were manually impregnated filling microchannels with the suspension and removing the excess. Through this method there is no possibility to previously know the amount of impregnated catalyst.
- Conditioning of catalysts and microreactor: After impregnation, the catalysts were calcined at 1073 K during two hours under oxidative conditions. Then, the platelets were weighted to know the exact amount of the impregnated catalyst (see Table 2). Finally, the platelets were welded and the microreactors conditioned for using them in the activity tests.

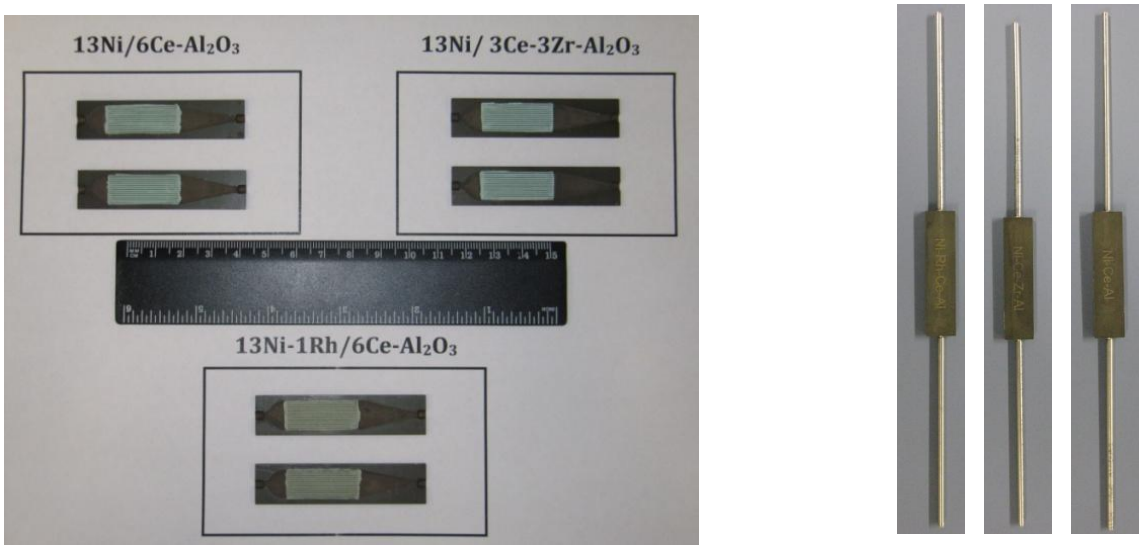

Figure 4: *Microreactors after catalysts calcinations and after welding of the platelets.*

The microreactors were only used with the best catalysts at the most favourable conditions determined with the fixed bed reactor systems. Thus, they were used under BOR conditions at O_2/CH_4 ratio of 0.25 as well as for TR conditions at O_2/CH_4=0.25 and 0.50 for S/C of 1.0. Then, the calculated WHSV when operating with microreactors were the followings:

Table 2: *Calculated WHSV according to the catalysts amount used for the studied processes and operating conditions in a microreactor system.*

WHSV (h^{-1})	**Ni/Ce-Al_2O_3**	**Ni/Ce-Zr-Al_2O_3**	**Rh-Ni/Ce-Al_2O_3**
Catalyst amount (g)	0.0262	0.0291	0.0240
BOR at O_2/CH_4=0.25	1710	1540	1867
TR at O_2/CH_4=0.25-S/C=1.0	2097	1888	2290
TR at O_2/CH_4=0.50-S/C=1.0	2483	2235	2710

4.2.3 Catalysts characterization techniques

All the catalysts were characterized before and after the experiments in order to obtain as much information about their physic-chemical properties as possible. Therefore, some of the characterization techniques were also used once the catalysts were tested with the intention to get valuable information for the discussion section.

4.2.3.1 Inductively coupled plasma atomic emission spectroscopy, ICP-AES

An inductively coupled plasma atomic emission spectroscopy instrument, model 2000-DV (Perkin Elmer), was used for determining the metallic elements in the catalysts. A solution that consisted of HCl:HNO_3:HF = 3:3:2 was prepared to properly disintegrate the amount of 100 mg of catalyst. In addition, a digester was used for the total catalysts disaggregation because the presence of some particles could affect the measurements results as well as obstruct the equipment.

4.2.3.2 Catalysts textural properties

The textural properties, Brunauer-Emmett-Teller (BET) surface area, pore volume and radius of the calcined and outgassed (at 473 K for 24 h) catalysts were evaluated by means of N_2 adsorption-desorption isotherms obtained at 77 K using an Autosorb 1C-TCD. Amounts of around 100 mg of catalysts were used in the measurements to ensure the minimum surface area required by the equipment, 10 m^2. With regard to the obtained results, pore volume was estimated by the Barrett-Joyner-Halenda (BJH) method for the Cumulative Desorption Pore Volume, and in the case of the radius, the BJH Desorption Dv(r) method was used.

4.2.3.3 Temperature programmed reduction, TPR

Through temperature programmed reduction, TPR, the reducible species formed during calcination step of the catalysts, and the reduction temperature were determined. The measurements were carried out using an Autosorb 1C-TCD apparatus, equipped with a thermal conductivity detector. A continuous flow of 5% H_2/Ar (40 NmL/min) was passed over 500 mg of calcined catalyst powder. The temperature was increased from room temperature to 1273 K at a rate of 10 K/min. The sample was previously outgassed at 573 K during 30 minutes.

4.2.3.4 Scanning electron microscope, SEM

SEM micrographs of fresh reduced catalysts and used catalysts were obtained using a JEOL JSM-7000-F scanning electron microscope equipped with a Schottky field emission cathode. Surface composition was studied by combination of backscattered electron imaging and Energy Dispersive X-Ray Spectroscopy using an Oxford Instruments Inca Energy 350 spectrometer installed in the same microscope. Images were also taken from secondary electron detectors in order to study surface morphology. These micrographs provide information about the dispersion of the particles in the catalytic surface as well as, the particle size distributions.

4.2.3.5 Transmission electron microscope, TEM

Transmission electron micrographs were acquired on a Philips CM 200 transmission electron microscope (TEM) at an acceleration voltage of 200 kV with a LaB_6 filament. Typically, a small amount of sample was suspended in pure ethanol, sonicated and dispersed over a Cu grid with a carbon coated cellulose acetate-butyrate holey film. TEM images were recorded using a 4k x 4k TVIPS CCD camera at different magnifications.

4.2.3.6 Hydrogen chemisorption

Nickel and rhodium-nickel dispersion was measured by H_2-pulse chemisorption at 313 K in the Autosorb 1C-TCD unit. Prior to pulse chemisorption experiment, all samples were reduced under pure H_2 flow (40 NmL/min) during 2 h at 1073 K. To calculate metal dispersion, adsorption stoichiometry of H/Ni = 2 was assumed.

4.2.3.7 X-ray powder diffraction, XRD

The X-ray powder diffraction, XRD, patterns were collected with a PHILIPS X'PERT PRO automatic diffractometer operating at 40 kV and 40 mA, in theta-theta configuration, secondary monochromator with Cu-Kα radiation (λ = 1.5418 Å) and a PIXcel solid state detector. The samples were mounted on a zero background silicon wafer fixed in a generic sample holder. Data were collected from 10 to 80° 2θ (step size = 0.026 and time per step = 625 s) at RT. A fixed divergence and antiscattering slit giving a constant volume of sample illumination were used.

4.2.3.8 X-ray photoelectron spectroscopy, XPS

XPS technique was used to evaluate the surface characteristics (oxidation state of the species formed, interactions, atomic ratios, etc) of the samples. The measurements were carried out with a VG Escalab 200R spectrometer equipped with a hemispherical electron analyser and an Al Ka1 (h = 1486.6 eV) 120 W X-ray source. The powdered samples were deposited on a stainless steel sample holder, placed in the pre-treatment chamber and degassed at 573 K. The base pressure of the spectrometer was typically 10^{-9} torr. The spectra were collected at pass energy of 20 eV, which is typical of high resolution conditions. Both fresh and used catalysts were analysed with this technique.

4.3 Biogas reforming processes using γ-Al_2O_3 based catalysts

Published papers:

Title: Biogas steam and oxidative reforming processes for synthesis gas and hydrogen production in conventional and microreactor reaction systems

Authors: U. Izquierdo, V.L. Barrio, N. Lago, J. Requies, J.F. Cambra, M.B. Güemez, P.L. Arias

Journal: International Journal of Hydrogen Energy

Year: 2012

Title: Tri-reforming: a new biogas process for synthesis gas and hydrogen production

Authors: U. Izquierdo, V.L. Barrio, J. Requies, J.F. Cambra, M.B. Güemez, P.L. Arias

Journal: International Journal of Hydrogen Energy

Year: 2013

4.3.1 Introduction

Using a biogas stream for hydrogen production DR reaction is apparently the simplest studied reaction which consisted on the reforming of CH_4 with CO_2. This reaction requires high energy application as it is very endothermic. Through biogas DR process, synthesis gas with low CO/H_2 ratios can be obtained which can be preferentially used for the production of liquid hydrocarbons. The most important reactions are the following:

DR: $CH_4 + CO_2 \leftrightarrow 2\ CO + 2\ H_2$ ($\Delta H^0 = 247$ kJ/mol) (1)

r-WGS: $CO_2 + H_2 \leftrightarrow CO + H_2O$ ($\Delta H^0 = 41$ kJ/mol) (2)

Due to r-WGS reaction, CO_2 conversions always will be higher than methane conversions. However, the required energy consumption and carbon formation at high temperature on the catalyst surface are the main disadvantages of this process [22,25-27].

In the case of BSR process, apart from the mentioned DR reaction, steam methane reforming reaction, SMR, also occurs during the process. The SMR reaction produce three H_2 moles per CH_4 and H_2O mole fed, and the presence of water reduces the possibility of carbon generation on the catalysts surface. In addition, WGS reaction can also occur, which contributes producing higher H_2 amounts. The most important reactions are the following:

SMR: $CH_4 + H_2O \leftrightarrow CO + 3\ H_2$ ($\Delta H^0 = 206$ kJ/mol) (3)

WGS: $CO + H_2O \leftrightarrow CO_2 + H_2$ ($\Delta H^0 = -41$ kJ/mol) (4)

The main advantage of the BOR process is the exothermicity of the catalytic partial oxidation of methane reaction (CPO) since it leads to a significant reduction of the operation cost. When exothermic CPO is combined with endothermic DR reaction the hot spots produced in the CPO reaction can be significantly reduced in the catalytic bed being possible to reach a thermoneutral process by controlling the $CH_4/CO_2/O_2$ ratios. Moreover, the presence of oxygen and nitrogen (simulating air) at high temperatures could avoid the carbon deposition in the catalyst [28]. For this process the presence of water was reported so that r-WGS reaction it is also necessary to be taken into account.

CPO: $CH_4 + 1/2\ O_2 \rightarrow CO + 2\ H_2$ ($\Delta H^0 = -36$ kJ/mol) (5)

In the case of TR process, water, oxygen and nitrogen were fed into the system. The most important reactions are (1), (3), (4) and (5). Therefore, according to the equilibrium, higher CO/H_2 synthesis gas ratios were expected to be obtained, and softer operation conditions were required. Through this process appropriate synthesis gas composition for the Fischer-Tropsch synthesis can be also obtained [23].

Theoretically, the main disadvantages mentioned for the DR can be avoided by TR process increasing the hydrogen production per mole of CH_4 through the SMR reaction. Besides that, the possible carbon generation on the catalyst surface is also reduced because of the water presence. In addition, WGS reaction also occurs contributing to produce higher H_2 yields. Furthermore, the addition of O_2 at high temperatures through CPO avoids carbon deposition on the catalyst surface and reduces significantly the energy requirements. It is even possible to reach a thermoneutral operation conditions by controlling the $CH_4/CO_2/O_2$ ratios [28].

New catalytic systems were designed in order to avoid the carbon deposition in DR process, as well as, to reach the highest conversions in all the processes studied. From an economical point of view, Ni based catalyst are the most used ones in reforming processes instead of precious metals based catalysts, but a small noble metal addition, as Rh, Pt or Pd can improve the catalyst stability and reducibility [29-31]. Regarding to the support modifiers it has been reported that small additions of rare-earth oxides as CeO_2 and ZrO_2 get better properties of Ni catalyst supported on alumina and avoid their deactivation. Small ZrO_2 additions improve the coke resistance of Ni catalysts and a small CeO_2 content favours the coke gasification and WGS activity [32-34]. Therefore, Ni-based catalysts and a bimetallic Rh-Ni catalyst were prepared supported on magnesia and modified alumina with CeO_2 and ZrO_2 oxides.

4.3.2 Al_2O_3 based catalyst preparation for DR, BSR, BOR and TR

Ni and Rh-Ni catalysts were prepared supported on magnesia (BET surface area 27.1 $m^2\ g^{-1}$, pore volume 0.16 $cm^3\ g^{-1}$ [35]) and alumina (BET surface area 255 $m^2\ g^{-1}$, pore volume 1.14 $cm^3\ g^{-1}$; Alfa Aesar) modified with oxides like CeO_2 and ZrO_2 as promoters, by wetness impregnation. First, modified alumina supports were prepared using the alumina, cerium (III) nitrate hexahydrate (99.5%; Alfa Aesar) and Zirconium (IV) oxynitrate hydrate (99.99%; Sigma Aldrich). An aqueous solution consisted of 10 mL of water per gram of support was used to dissolve promoters. The amounts of CeO_2 and ZrO_2 salts precursors were calculated in order to achieve a nominal content of 6% Ce and 8% Zr for the cerium- and zirconium-doped γ-Al_2O_3 supports, and 3% Ce and 4% Zr for the cerium-zirconium-doped γ-Al_2O_3 support. After wetness impregnation, all supports were dried at 373 K and calcined at 1073 K during 1 h and 4 h, respectively.

Thereafter, the Ni was incorporated to these supports by impregnation with Nickel (II) nitrate hexahydrate (99.99%; Sigma Aldrich) aqueous solution. The amounts of Ni salt precursor dissolved were calculated to achieve an intended load of 13% Ni for γ-Al_2O_3 based supports and 20% Ni for the MgO support. For the bimetallic catalyst a Rhodium (III) nitrate hydrate (~ 36% as rhodium; Sigma Aldrich) aqueous solution was used to achieve an intended load of 1% of Rh. Then, the catalysts were dried and calcined as it has been indicated before. The activity of a commercial catalyst was tested (ICI group; Katalco, 57-5 series) for comparison purposes.

4.3.3 Al_2O_3 based fresh catalysts characterization results

The prepared catalysts were characterized by the following techniques: ICP-AES, N_2 adsorption-desorption isotherms, TPR, H_2-pulse chemisorptions, XRD, XPS and SEM.

4.3.3.1 Chemical composition, ICP-AES, and textural properties, BET

The catalysts chemical compositions, which were determined by ICP-AES, are shown in Table 3. It was necessary to develop two different methodologies for catalyst disgregation. In the first one, a solution that consisted of HCl, HNO_3 and HF was used for Ni, Rh, Zr and Ca quantification. With this method it was not possible to detect any Ce, due to CeF_2 precipitate formation. For Ce quantification, a solution that consisted of H_2O_2 and HNO_3 was used [36]. After preparing the corresponding solutions, the catalysts were properly disgregated using a digester and thereafter analyzed by ICP-AES instrument.

As it can be observed, the metal compositions of most of the tested catalysts are slightly lower than their nominal ones. In the case of the Ce content, for both, Ni/Ce-Al_2O_3 and Rh-Ni/Ce-Al_2O_3 catalysts, is significantly lower than the expected one. With regard to the commercial catalyst, Ca and Ni were only measured even though other species could be present.

Table 3: *Calcined catalysts textural properties and chemical composition.*

Catalyst	Surface area (m^2/g)	Pore volume (cm^3/g)	Average Pore size (Å)	Nominal / ICP measured (wt%)
Ce-Al Support	195.0	0.76	150.1	-
Zr-Al Support	180.3	0.67	143.9	-
Ce-Zr-Al Support	191.7	0.74	150.7	-
Commercial	21.6	0.09	169.5	12.4 (Ni) 0.4 (Ca)
Ni/MgO	25.6	0.13	200.0	20.0/17.2 (Ni)
Ni/Ce-Al_2O_3	163.3	0.59	143.7	13.0/10.8 (Ni) 6.0/3.3 (Ce)
Ni/Zr-Al_2O_3	166.6	0.62	146.3	13.0/11.4 (Ni) 8.0/5.5 (Zr)
Ni/Ce-Zr-Al_2O_3	151.0	0.60	153.2	13.0/10.6 (Ni) 3.0/2.7 (Ce) 4.0/3.6 (Zr)
Rh-Ni/Ce-Al_2O_3	156.8	0.60	150.1	13.0/10.0 (Ni) 1.0/0.9 (Rh) 6.0/3.6 (Ce)

The textural properties of fresh calcined catalysts are also outlined in Table 3. Commercial and Ni/MgO catalysts presented the lowest surface area and pore volume. With regards to the pore size, Ni/MgO catalyst showed the largest value as compared to the Al_2O_3 containing catalysts. Regarding the prepared supports, as it should be expected, the more modifier is added, the lower surface area was measured. CeO_2 modified γ-Al_2O_3 support reached the highest surface area. Using ZrO_2 as promoter, instead of CeO_2, all textural parameter's values decreased. Finally, when the two promoters were used simultaneously, similar results as for CeO_2 promoted ones were measured.

4.3.3.2 Temperature-programmed reduction, TPR

Figure 5 shows all TPR profiles of fresh calcined supports and catalysts. Ni/MgO catalyst showed almost no reduction, and its main reduction peak appeared at 858 K [37]. Regarding the commercial catalyst, four different reduction peaks were detected being the biggest one at 1048 K. For the rest of the monometallic and bimetallic catalysts, the main reduction peaks appeared in the range 900 K to 1200 K.

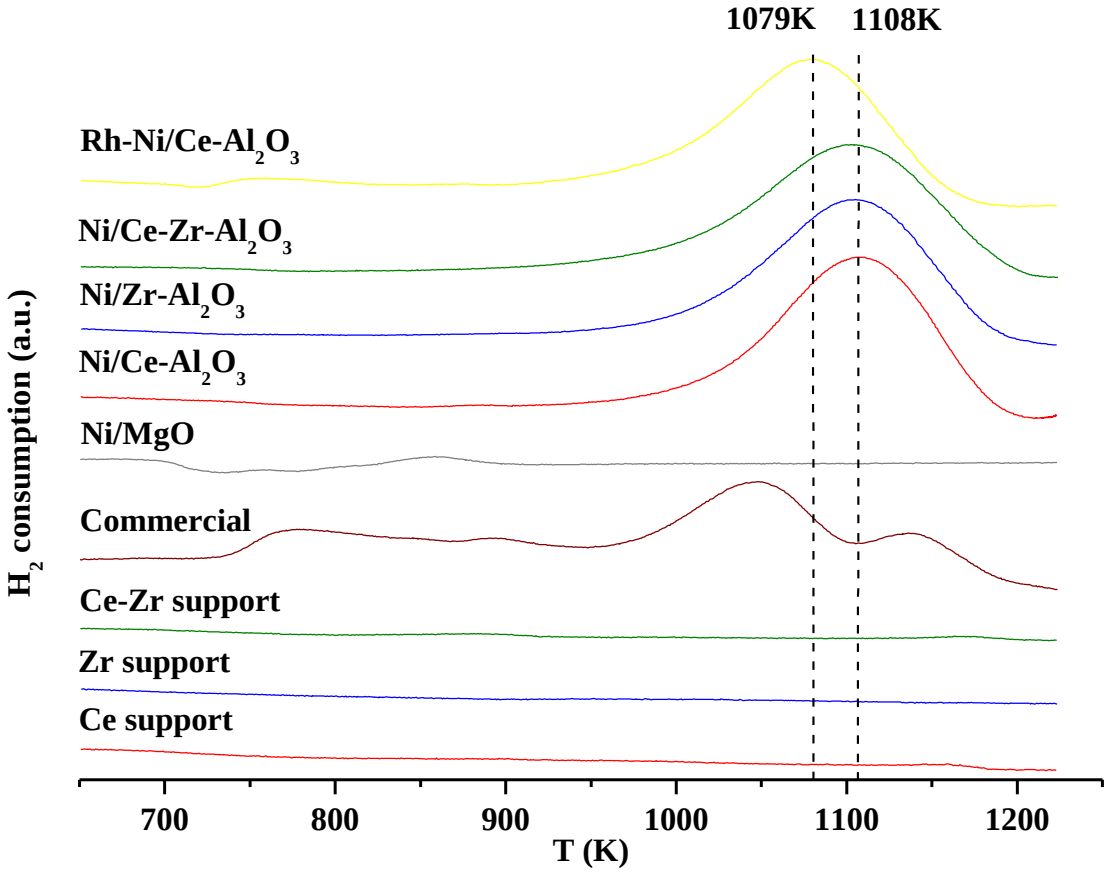

Figure 5: *TPR profiles of fresh calcined catalysts and supports.*

Different reduction peaks were observed for the promoted supports. For Ce-Zr-Al_2O_3, Ce-Al_2O_3 and Zr-Al_2O_3 supports contributions were measured at 690 K, 880 K, 1000 K and 1170 K. For all of them very small peaks were observed. If calcined catalysts and calcined supports profiles are compared, much lower H_2 consumption was detected.

The main peaks of Ni/Zr-Al_2O_3, Ni/Ce-Zr-Al_2O_3 and Ni/Ce-Al_2O_3 catalysts appeared at 1103 K, 1105 K and 1108 K respectively. Thus, this is a possible indication of Ce reduction taking place at higher temperatures than Zr reduction. If Ni/Ce-Al_2O_3 and Rh-Ni/Ce-Al_2O_3 catalysts are compared, lower reduction temperature was needed for the last one (1079 K). This could be related to the “spill over” effect which improved the nickel reducibility [27].

According to the literature, these broad peaks can be attributed to the contribution of three different species. The peaks around 950 K are attributed to the reduction of NiO-Al species with weak interaction with alumina support, while the reduction peaks reported at higher temperatures are related to the reduction of highly dispersed non-stoichiometric amorphous nickel aluminate spinels at around 1050 K and to a diluted $NiAl_2O_4$-like phase at 1100 K, respectively [13,37]. The quantitative TPR data after deconvolutions are summarized in Table 4.

Table 4: *Calcined catalysts quantitative TPR data.*

Catalyst	NiO-Al	Surface $NiAl_2O_4$	$NiAl_2O_4$ [b]
$Ni/Ce\text{-}Al_2O_3$	985 K - 10.6% [a]	1056 K - 23.2%	1114 K - 66.1%
$Ni/Zr\text{-}Al_2O_3$	947 K - 6.3%	1055 K - 20.4%	1114 K - 73.2%
$Ni/Ce\text{-}Zr\text{-}Al_2O_3$	976 K - 10.2% [a]	1051 K - 22.7%	1110 K - 67.1%
$Rh\text{-}Ni/Ce\text{-}Al_2O_3$	914 K - 7.9% [a]	1024 K - 26.2%	1086 K - 63.9%

[a] Includes ceria reduction.

[b] Includes ceria and partial surface zirconium reduction.

In Figure 6, deconvolution of the TPR profile for $Rh\text{-}Ni/Ce\text{-}Al_2O_3$ catalyst is shown. For this catalyst, the main peaks correspond to three different species that appeared at 914 K, 1024 K and 1086 K. Moreover, a small peak in $Rh\text{-}Ni/Ce\text{-}Al_2O_3$ catalyst profile was observed at 770 K which could be attributed to the Rh reduction [38].

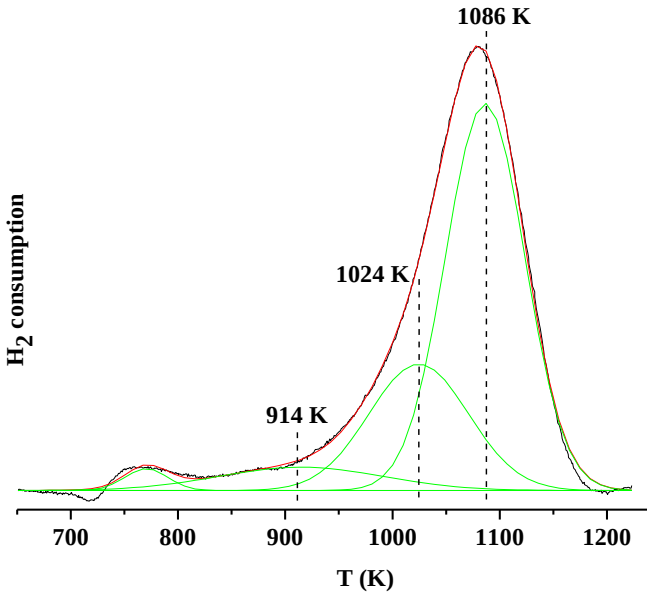

Figure 6: *Deconvolution of the TPR profile for the $Rh\text{-}Ni/Ce\text{-}Al_2O_3$ catalyst.*

4.3.3.3 Calcined catalysts SEM micrographs

SEM micrographs of calcined catalysts were taken in order to analyze their composition, catalytic surface, and particles size distributions. The results of the microscopy study are summarized in Figures 7 and 8 combining backscattered electron imaging and EDX.

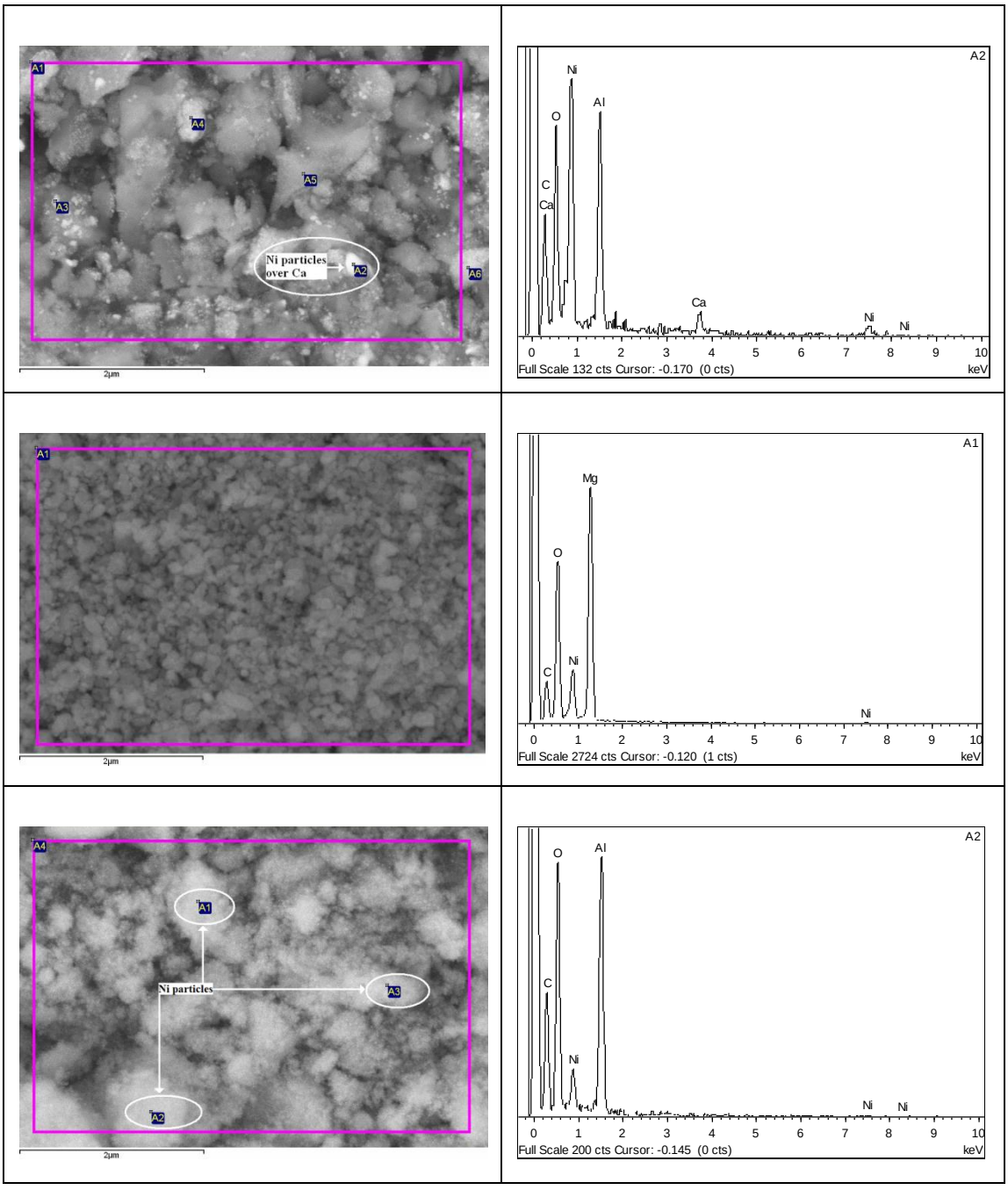

Figure 7: *Commercial, Ni/MgO and Ni/Ce-Al_2O_3 calcined catalysts SEM micrograph (left) and the analyzed composition by EDX (right).*

In Figure 7, the commercial calcined catalyst SEM picture and EDX spectrum can be observed. The EDX analysis confirms the presence of Ni, Ca and Al in the selected area (A2) as well as in all analyzed regions. Some Ni aggregates can be observed with sizes in the range between 10-250 nm but not individual Ni particle size can be estimated. Therefore, the composition determined by ICP-AES was confirmed by the EDX analysis, being Ni, Ca and Al_2O_3 the major components of the catalysts. Ni/MgO calcined catalyst SEM picture and EDX spectrum are shown also in this figure. EDX analysis confirms the presence of Ni and Mg in the analyzed A1 area. Smaller aggregates size distribution than for the commercial catalyst was measured. Also

in the same figure the Ni/Ce-Al_2O_3 calcined catalyst SEM picture and EDX spectrum are reported. EDX analysis confirms the presence of Ni and Al in the selected area (A2) as well as in all analyzed region. In this area Ce was not detected. Regarding the aggregates size, particles smaller than 100 nm were detected.

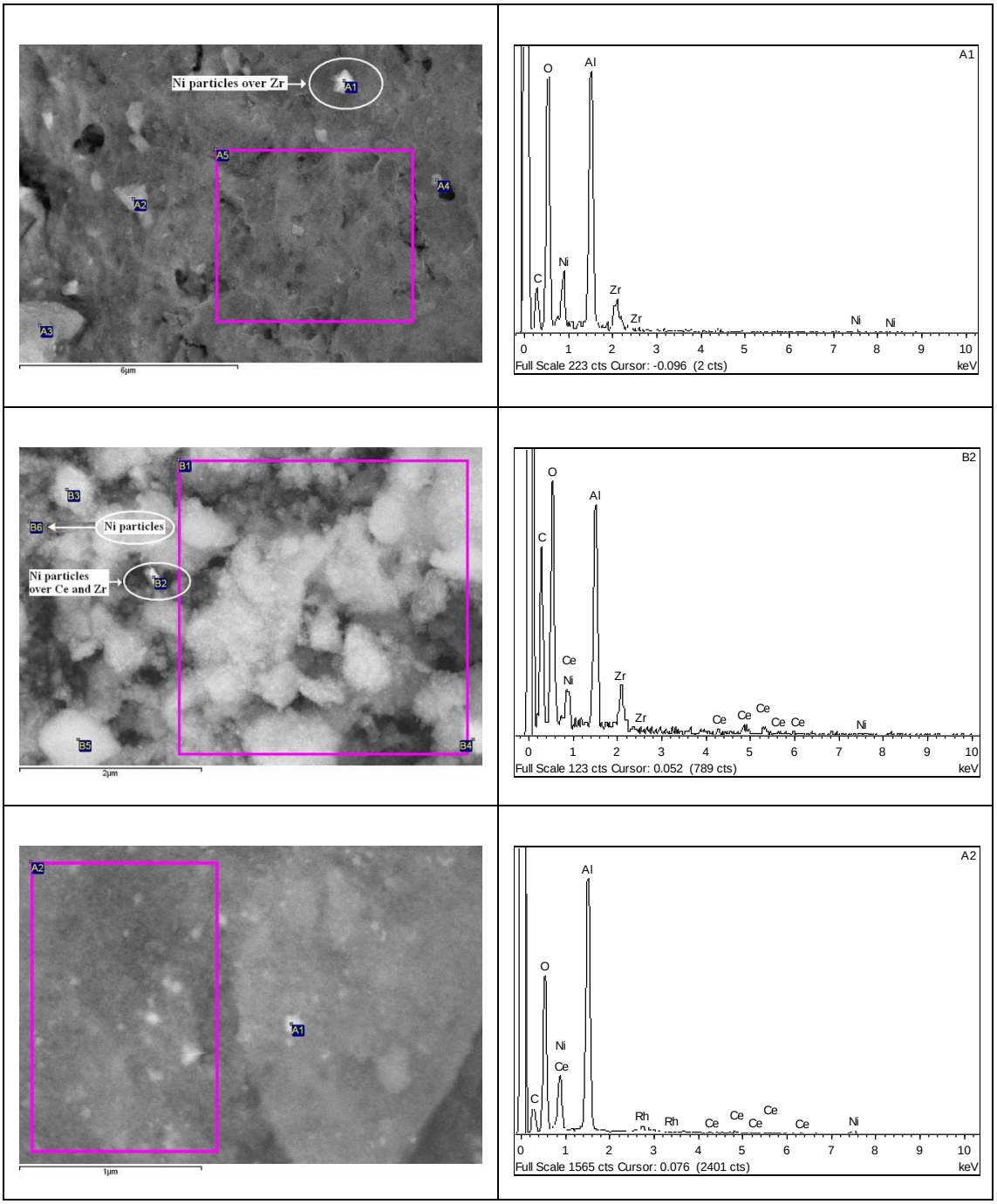

Figure 8: *Ni/Zr-Al_2O_3, Ni/Ce-Zr-Al_2O_3 and Rh-Ni/Ce-Al_2O_3 calcined catalyst SEM micrograph (left) and the analyzed composition by EDX (right).*

Ni/Zr-Al_2O_3 calcined catalyst SEM picture and EDX spectrum are shown in Figure 8. For this catalyst Ni, Zr and Al were detected in the selected area (A1) as well as in the analyzed region (A5). As it can be observed, bigger aggregates size than for the rest of analyzed catalysts was

measured, in the range of 2 µm – 100 nm. In this figure, the Ni/Ce-Zr-Al_2O_3 calcined catalyst SEM picture and EDX spectrum are also reported. For this catalyst Ni, Ce, Zr and Al were detected in most of the analyzed regions. In addition, a big difference in the aggregates size distribution was also observed. The aggregates were measured in the range between 1 µm – 10 nm. Finally, also in Figure 8 the last calcined catalyst, Rh-Ni/Ce-Al_2O_3, SEM picture and EDX spectrum are shown. For this catalyst, aggregates size distribution smaller than 100 nm was measured, and Rh, Ni, Ce and Al were detected. For this catalyst, uniform dispersion of Rh and Ni aggregates can be observed.

4.3.3.4 H_2 pulse chemisorption

Table 5 summarizes the amounts of exposed nickel atoms in the reduced catalysts, which were determined by pulsed-H_2 chemisorption. The analyzed catalysts were the ones used in the microreactors. For these catalytic systems, the metal dispersion degree of the catalysts was relatively low, as it is typically observed for high Ni content catalysts [27]. In the case of Rh-Ni/Ce-Al_2O_3 catalyst, the highest values of active metal surface area, dispersion degree and crystal sizes were measured.

Table 5: *Reduced catalysts hydrogen chemisorption results. Ni crystalline particles average size measured by XRD.*

Catalyst	Metal Surface area (m^2/g)	Dispersion (%)	Ni Crystallite size (nm)	Ni Crystallite size (nm) XRD
Ni/Ce-Al_2O_3	5.57	6.43	16	8
Ni/Ce-Zr-Al_2O_3	5.13	7.28	14	7
Rh-Ni/Ce- Al_2O_3	7.99	11.59	88	5

4.3.3.5 X-ray powder diffraction, XRD, patterns

XRD measurements were performed in order to obtain the crystallite average size of Ni, ceria and zirconium phases through the application of Scherrer equation. Applying this equation to the best defined Ni^0 reflections (43.26º for the Ni/MgO catalyst and around 52º for the rest of the catalysts) the Niº average crystallites sizes were calculated and summarized in the previous Table 5. Highest Niº crystallites were measured for the commercial (23 nm) and Ni/MgO (46 nm) catalyst. For comparison purposes, and due to the high peaks observed for the Ni/MgO and commercial catalysts, only the XRD profiles of the rest catalysts are shown in Figure 9.

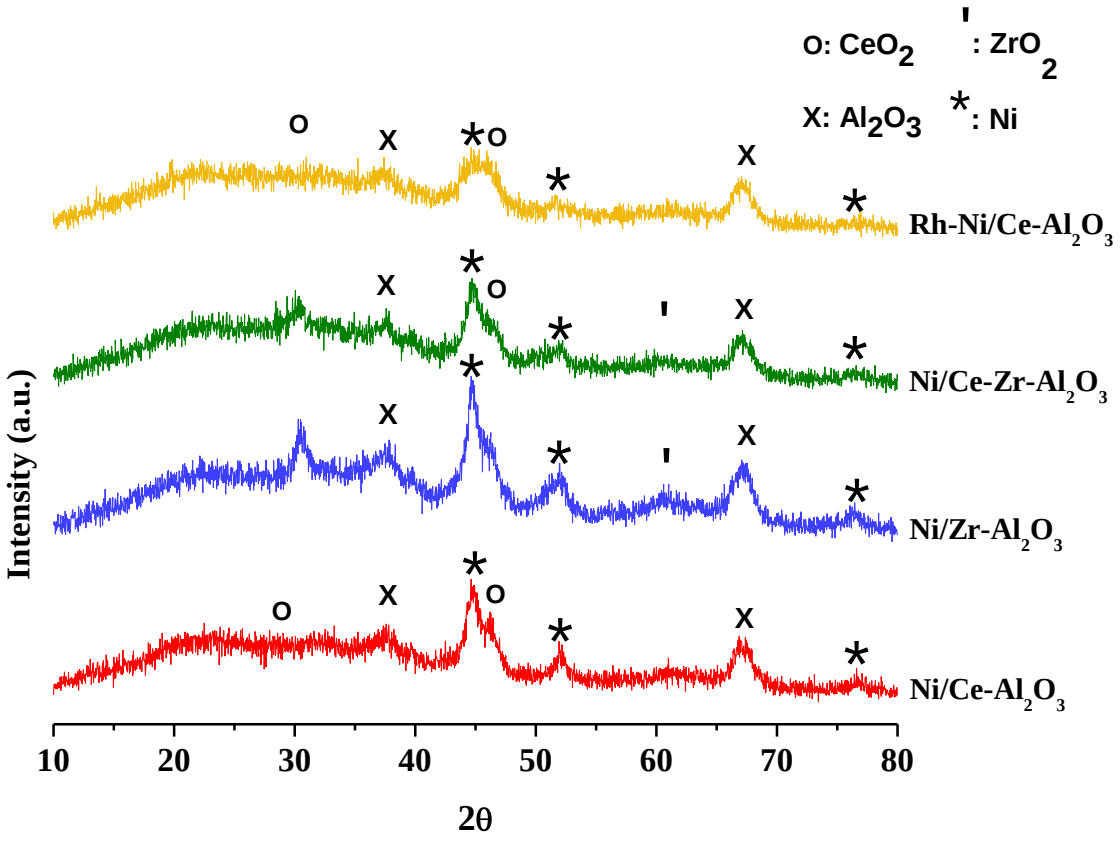

Figure 9: *XRD patterns for reduced catalysts: (*) Ni⁰, (x) CeO_2, and (') ZrO_2.*

Taking into account that the XRD technique presents limitations when crystalline particles size are below than 2-4 nm [39], CeO_2 characteristic reflections were not measured. This fact can be due to the good dispersion of the CeO_2 particles or due to the overlap with Ni high intensity reflections [40]. In the case of ZrO_2 particles, crystallite particles of 9 nm for the Ni/Zr-Al_2O_3 catalyst and of 11 nm for the Ni/Ce-Zr-Al_2O_3 catalyst were measured. According to the literature, the peaks that correspond to these measurements can be attributed to the mixture of tetragonal, monoclinic and cubic structures [32]. For both catalysts, Ni⁰ crystallites of 7 nm were measured.

4.3.3.6 X-ray photoelectron spectroscopy, XPS, studies

The XPS study reveals the oxidation state of the formed species and the surface atomic ratios. The Commercial catalyst was the one showing more reduced metal phases, and in contrast, the reduction level of Ni/MgO catalyst was lower as the TPR analyses suggested. The rest of alumina supported catalysts suffer almost the same reduction level. Taking into account the reduction rates and comparing these results with the TPR analysis, it can be said that the Ni of the diluted $NiAl_2O_4$ phase is the one which was not totally reduced. Moreover, the Rh-Ni/Ce-Al_2O_3 catalyst suffered the highest reduction level but it was lower than the predicted one by the TPR analyses. This effect can be related with the higher metal crystallite size measured by the hydrogen pulse chemisorption technique which can difficult the reduction of the Ni and Rh particles.

Attending to the binding energies, if the Ni/Zr-Al_2O_3 catalyst spectrum is compared with the spectrum of the rest of catalysts, a difference of 2 eV in the binging energies of Ni $2p_{3/2}$, Zr $3d_{5/2}$ and Al 2p can be observed. According to the literature the typically assigned binding energies for the analyzed species are: Al^{3+}=74.5 eV, $NiAl_2O_3$=256.5 eV, Ni^0=252.0 eV, Ce^{4+}=881.0 eV and Zr^{4+}=182 eV [15,32,41], which are in good agreement with the ones detected for the rest of catalysts.

Comparing the measured surface atomic ratios with the determined ones using ICP-AES, Ni surface dispersion was improved in the commercial, Ni/MgO and Ni/Zr-Al_2O_3 catalysts. However for the cerium doped catalysts, the increase of Ce surface dispersion decreased the Ni and Rh surface dispersion. In the case of zirconium doped catalysts the Zr dispersion decreased.

Table 6: *Reduced catalysts binding energies of Al 2p, Mg 2p, Ni $2p_{3/2}$, Ce $3d_{5/2}$, Zr $3d_{5/2}$ and Rh $3d_{5/2}$ core levels, Ni^0 and Rh^0 proportion (%, in parenthesis) and surface atomic ratios.*

Catalyst	Al/Mg 2p	Ni $2p_{3/2}$ (eV)		Ce $3d_{5/2}$	Zr $3d_{5/2}$	Rh$3d_{5/2}$ (eV)		Ni/Al	Ni/Mg	Ce/Al	Zr/Al	Rh/Al
	(eV)	Ni^{2+}	Ni^0	(eV)	(eV)	Rh^{3+}	Rh^0					
Commercial	74.0	855.2 (46.0)	852.4 (54.0)	-	-	-	-	0.233 0.129[a]	-	-	-	-
Ni/MgO	49.0	854.7 (95.8)	852.5 (4.2)	-	-	-	-	-	0.236 0.151[a]	-	-	-
Ni/Ce-Al_2O_3	74.3	855.9 (44.9)	853.5 (55.1)	881.9	-	-	-	0.072 0.114[a]	-	0.072 0.017[a]	-	-
Ni/Zr- Al_2O_3	76.3	857.8 (41.3)	855.6 (58.7)	-	184.1	-	-	0.163 0.127[a]	-	-	0.021 0.035[a]	-
Ni/Ce-Zr- Al_2O_3	74.5	855.7 (51.6)	853.5 (42.4)	881.8	182.2	-	-	0.057 0.117[a]	-	0.057 0.014[a]	0.010 0.086[a]	-
Rh-Ni/Ce- Al_2O_3	74.0	856.5 (38.5)	854.0 (61.5)	881.7	-	312.0 (38.1)	307.5 (61.9)	0.089 0.105[a]	-	0.089 0.018[a]	-	0.008 0.014[a]

[a] Surface atomic ratio determined from chemical composition (ICP-AES).

4.3.4 Results from activity testing for fixed bed reactors

All the activity tests started after the system stabilized and lasted 90 minutes. The reported measurements values correspond to the mean of the last two analyses. All catalysts were tested at the same conditions (1073 K and atmospheric pressure) and the same analysis procedure for the products obtained was also carried out for all of them (using the μ-GC).

4.3.4.1 DR activity results

In Figure 10 results from activity tests when operating in a fixed bed reactor under dry reforming conditions are presented.

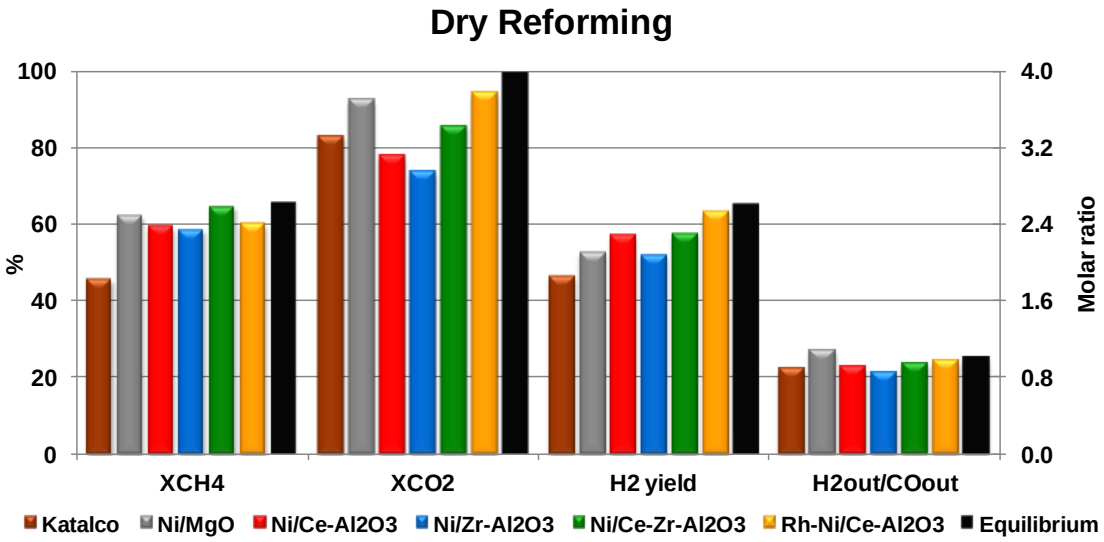

Figure 10: *DR activity results in the fixed bed reactor system.*

The commercial catalyst was the one which showed the worst results (conversion of CH_4=45.6% and conversion of CO_2 =83.0%) operating under DR conditions. Ni/MgO catalyst achieved the highest methane conversion (62.2%) but using a Rh-Ni/Ce-Al_2O_3 the highest carbon dioxide conversion (94.4%) were obtained, and as a result the highest hydrogen yields (63.3%). The high selectivity of Ni/MgO catalyst for r-WGS reaction could be the main reason for its low hydrogen yield (52.6%). As it was commented before, this is an undesirable effect because r-WGS reaction reduces the hydrogen yield and as a consequence, also the ratio H_2/CO. For the bimetallic catalyst, the values obtained were very close to the equilibrium ones. Carbon filaments were detected by SEM in all the catalysts samples after the DR activity tests (see Figure 20).

4.3.4.2 BOR activity results

The experimental results operating with fixed bed reactor under BOR conditions at O_2/CH_4=0.25 for all the catalysts under investigation are compiled in Figure 11.

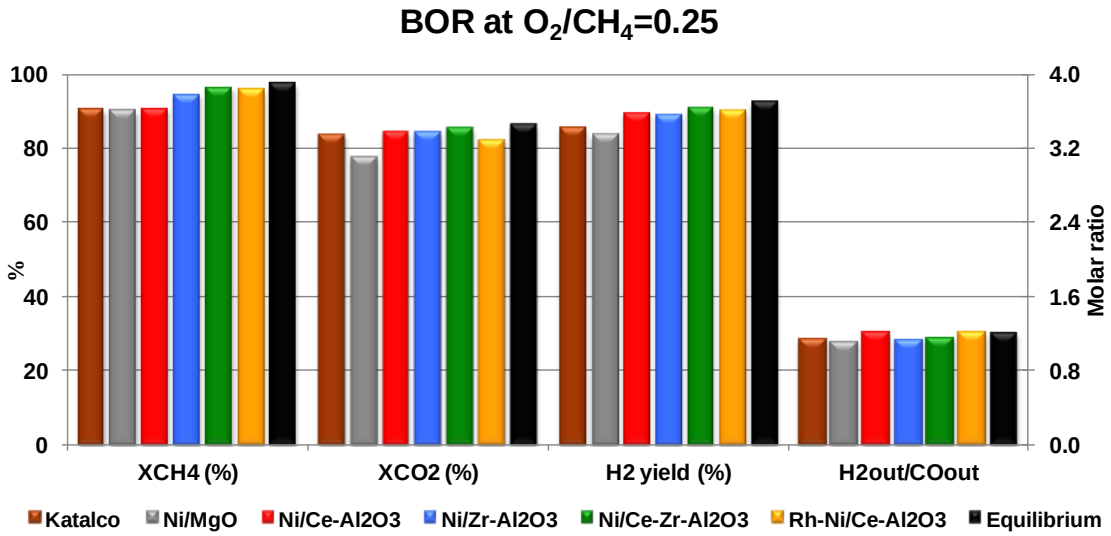

Figure 11: *BOR activity results in the fixed bed reactor system at O_2/CH_4=0.25.*

This figure shows that methane and carbon dioxide equilibrium conversion was almost reached by all tested catalysts. In addition, hydrogen yield was higher than 80% for all catalysts under investigation. The highest values of conversion and hydrogen yield were achieved for Rh-Ni/Ce-Al_2O_3 and Ni/Ce-Zr-Al_2O_3 catalysts.

Table 7: *BOR activity results in the fixed bed reactor system at different O_2/CH_4 ratios.*

Catalyst	O_2/CH_4=0.125				O_2/CH_4=0.25				O_2/CH_4=0.50			
	X_{CH4}	X_{CO2}	H_2 yield	H_2/CO	X_{CH4}	X_{CO2}	H_2 yield	H_2/CO	X_{CH4}	X_{CO2}	H_2 yield	H_2/CO
Commercial	-	-	-	-	90.4	83.7	85.6	1.1	98.0	52.3	83.4	1.2
Ni/MgO	76.2	92.0	78.4	1.1	89.9	77.5	83.4	1.1	96.2	47.5	81.2	1.2
Ni/Ce-Al_2O_3	76.5	92.7	82.3	1.2	90.4	84.3	89.4	1.2	97.4	46.6	80.7	1.2
Ni/Zr-Al_2O_3	84.4	95.1	84.7	1.1	94.4	84.2	89.1	1.1	97.5	50.4	81.1	1.2
Ni/Ce-Zr-Al_2O_3	87.4	96.6	87.6	1.1	96.3	85.4	90.9	1.2	98.1	48.8	80.9	1.2
Rh-Ni/Ce-Al_2O_3	84.6	94.6	86.5	1.2	95.7	82.0	90.2	1.2	97.6	50.0	82.6	1.2
Equilibrium	**87.1**	**96.6**	**85.9**	**1.1**	**97.3**	**86.1**	**92.2**	**1.2**	**99.7**	**52.6**	**82.0**	**1.2**

In these experiments, operating at higher ratios (O_2/CH_4=0.50) catalytic partial oxidation of methane was promoted, decreasing carbon dioxide conversion and consequently, the hydrogen yield. By the contrary, DR reaction mainly occurred using lower ratios (O_2/CH_4=0.125) which decreased methane conversion and consequently, also the hydrogen yield. In this case, as very low O_2 concentrations were used, once it was consumed through CPO reaction, the rest of methane reacts with the CO_2. Anyway, H_2^{out}/CO^{out} molar ratio remained more or less constant (see Table 7 or Figure 12) in both cases. Considering both environmental and production benefits, the O_2/CH_4 ratio of 0.25 seems to be the most interesting one.

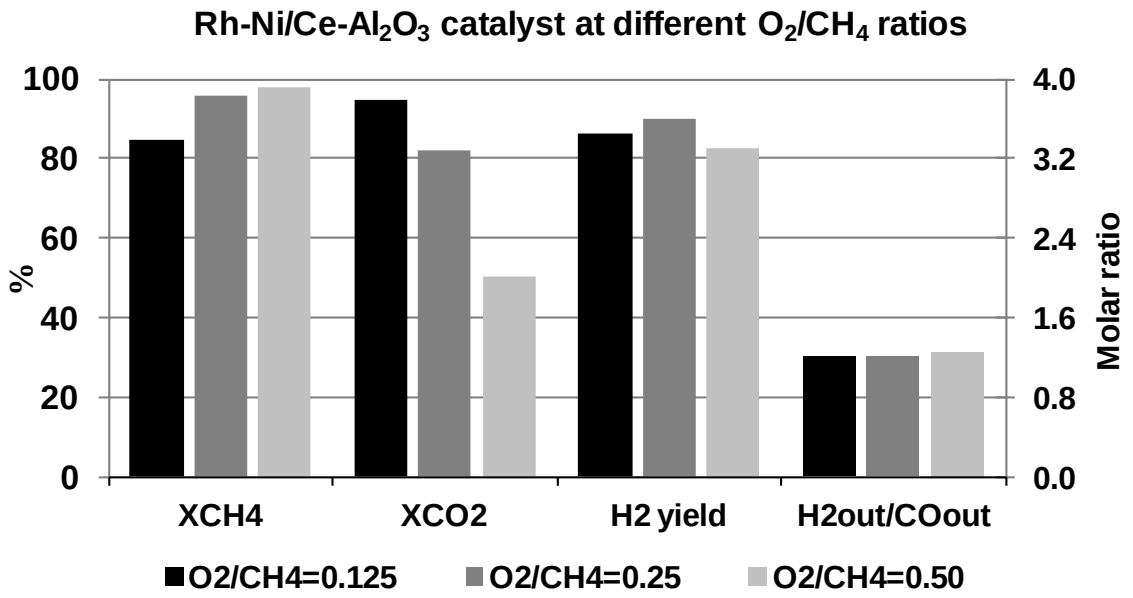

Figure 12: *BOR activity results obtained by the Rh-Ni/Ce-Al_2O_3 catalyst operating in the fixed bed reaction system at different O_2/CH_4 ratios.*

4.3.4.3 BSR activity results

The experimental results operating with fixed bed reactor under BSR conditions at S/C=1.0 for all the catalysts under investigation are compiled in Figure 13.

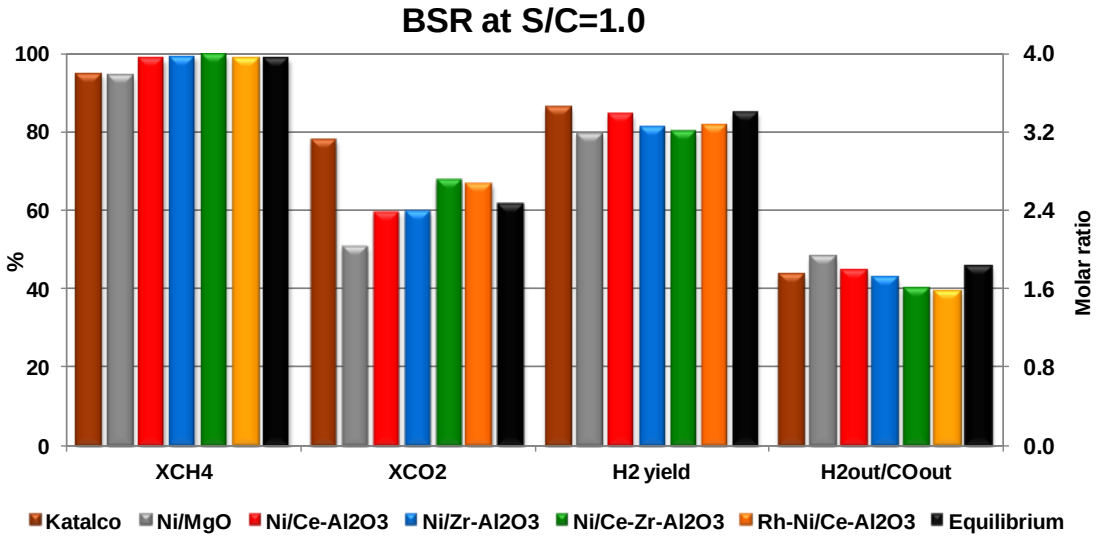

Figure 13: *BSR activity results in the fixed bed reactor system at S/C=1.0.*

All the catalytic activity results obtained after the operation under BSR conditions at different S/C ratios are presented in Table 8. For this processes methane and carbon dioxide conversions were very close to the equilibrium calculation values and in some cases, higher than the predicted ones by the equilibrium calculations. For these experiments, the highest methane and CO_2 conversion values were reached by Rh-Ni/Ce-Al_2O_3 and Ni/Ce-Zr-Al_2O_3

catalysts. In the case of the hydrogen yield and H_2^{out}/CO^{out} molar ratio, the measured values are slightly lower for these two catalysts. This effect might be due to their selectivity for the DR reaction, which produces 1 mole H_2 less and 1 mole CO more per mole of CH_4 than the SMR reaction.

Table 8: *BSR activity results in the fixed bed reaction system at different S/C ratios.*

Catalyst	S/C=1.0				S/C=2.0				S/C=3.0			
	X_{CH4}	X_{CO2}	H_2 yield	H_2/CO	X_{CH4}	X_{CO2}	H_2 yield	H_2/CO	X_{CH4}	X_{CO2}	H_2 yield	H_2/CO
Commercial	94.7	77.9	86.2	1.7	98.9	33.0	72.7	2.5	98.8	8.9	57.3	2.5
Ni/MgO	94.3	50.8	79.4	1.9	98.8	28.7	69.3	2.3	98.6	-1.0	58.3	2.9
Ni/Ce-Al_2O_3	98.6	59.5	84.3	1.8	99.8	27.3	67.2	2.3	98.9	4.5	58.2	2.8
Ni/Zr-Al_2O_3	99.1	59.8	81.3	1.7	98.8	31.6	67.1	2.2	98.7	-10.6	55.1	3.0
Ni/Ce-Zr-Al_2O_3	99.5	67.7	80.0	1.6	99.6	40.4	68.1	2.2	99.5	17.5	56.5	2.5
Rh-Ni/Ce-Al_2O_3	98.4	66.6	81.4	1.6	99.6	11.3	65.2	2.1	99.6	16.5	59.7	2.6
Equilibrium	**98.5**	**61.7**	**84.8**	**1.8**	**99.6**	**23.3**	**70.8**	**2.5**	**99.8**	**-3.7**	**60.4**	**3.1**

Increasing the S/C parameter, methane conversion remained constant but lower carbon dioxide conversions were measured (see Figure 14). This effect contributed to the reduction of the hydrogen yield. However, H_2^{out}/CO^{out} molar ratio increased through the WGS reaction. As a result, the effect of adding water affected negatively to the DR reaction by promoting the WGS reaction. For this process the highest carbon dioxide conversions and hydrogen yields were reached at the ratio of S/C=1.0.

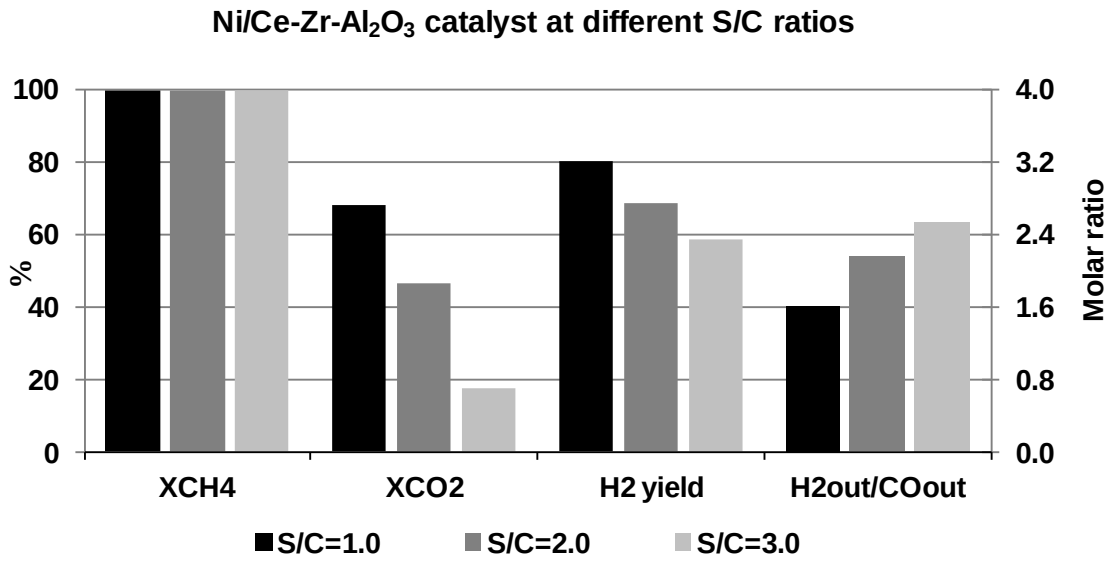

Figure 14: *BSR activity results obtained by the Ni/Ce-Zr-Al_2O_3 catalyst operating in the fixed bed reaction system at different S/C ratios.*

4.3.4.4 TR activity results

After replacing the catalysts, new experiments were carried out for TR process in the fixed bed reactor. TR activity results for all the catalysts under investigation operating at O_2/CH_4=0.25 and S/C=1.0 in a fixed bed reactor system are presented in Figure 15.

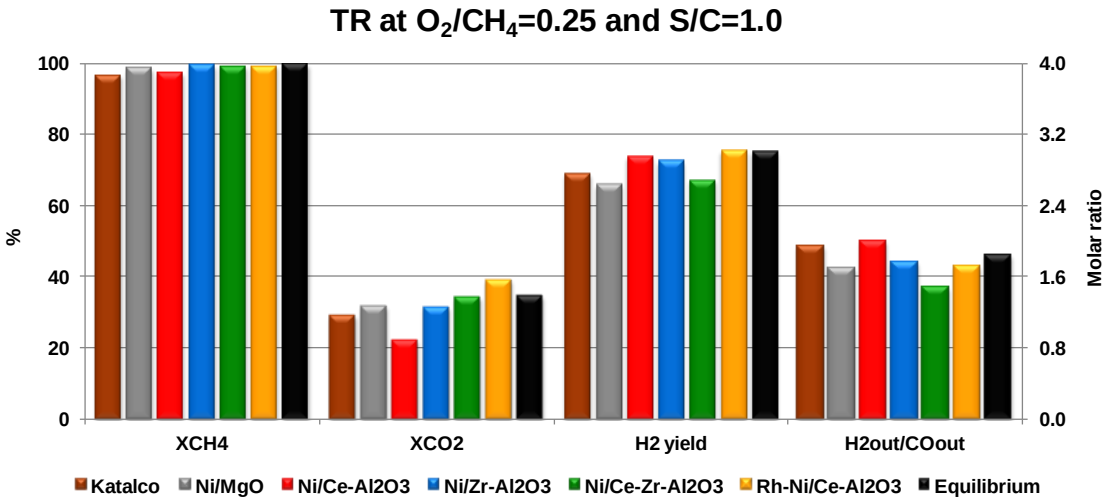

Figure 15: *TR activity results in the fixed bed reactor system at O_2/CH_4=0.25 and S/C=1.0.*

Table 9: *Catalytic activity results for TR experiments in a fixed bed system.*

TR O_2/CH_4=0.25	S/C=1.0				S/C=2.0				S/C=3.0			
	X_{CH4}	X_{CO2}	H_2 yield	H_2/CO	X_{CH4}	X_{CO2}	H_2 yield	H_2/CO	X_{CH4}	X_{CO2}	H_2 yield	H_2/CO
Commercial	96.4	29.2	68.8	1.9	98.6	1.1	54.5	2.3	98.9	-15.4	45.6	3.0
Ni/MgO	98.6	31.9	65.9	1.7	96.6	-8.6	56.4	2.1	95.2	-38.8	49.8	3.2
Ni/Ce-Al_2O_3	97.2	22.3	73.7	2.0	98.9	-12.9	61.2	2.6	99.5	-33.7	53.6	3.4
Ni/Zr-Al_2O_3	99.3	31.6	72.4	1.8	99.5	6.7	58.8	2.3	99.5	-26.5	50.7	2.9
Ni/Ce-Zr-Al_2O_3	99.0	34.4	67.1	1.5	99.4	**14.4**	60.4	2.2	99.0	-11.1	51.0	2.8
Rh-Ni/Ce-Al_2O_3	99.1	**39.1**	**75.3**	1.7	99.5	6.6	**62.8**	2.3	99.7	-17.2	51.6	2.7
Equilibrium	**99.6**	**34.7**	**75.2**	**1.8**	**99.9**	**0.9**	**62.3**	**2.5**	**99.9**	**-22.6**	**53.0**	**3.1**
TR O_2/CH_4=0.50	X_{CH4}	X_{CO2}	H_2 yield	H_2/CO	X_{CH4}	X_{CO2}	H_2 yield	H_2/CO	X_{CH4}	X_{CO2}	H_2 yield	H_2/CO
Commercial	92.4	-5.9	60.1	2.0	92.3	-27.8	49.2	3.0	92.5	-45.4	42.3	3.0
Ni/MgO	99.3	0.2	57.1	1.6	95.4	-29.7	42.7	2.5	94.3	-48.0	41.2	3.2
Ni/Ce-Al_2O_3	98.8	-2.4	63.9	1.9	99.6	-28.1	**54.8**	2.7	99.8	-42.7	45.5	3.5
Ni/Zr-Al_2O_3	99.3	0.9	66.6	2.1	99.8	-37.4	51.9	2.4	98.4	-51.1	46.0	3.3
Ni/Ce-Zr-Al_2O_3	99.1	**30.9**	64.2	1.8	99.1	**3.9**	42.0	1.5	99.5	-22.6	44.2	2.5
Rh-Ni/Ce-Al_2O_3	99.2	5.8	**66.8**	1.9	99.5	-23.2	53.1	2.2	99.5	-38.3	41.2	2.9
Equilibrium	**99.9**	**7.5**	**64.9**	**1.9**	**100.0**	**-21.3**	**53.5**	**2.5**	**100.0**	**-41.3**	**45.5**	**3.1**

Activity results operating at O_2/CH_4=0.25 and 0.50 and at S/C ratios ranging from 1.0 to 3.0 are shown in Table 9. As it can be observed, increasing the S/C ratio, the CO_2 conversion decreased, and as a result, the H_2/CO ratio also increased. When Ni/Ce-Al_2O_3 and Rh-Ni/Ce-Al_2O_3 catalysts were tested the highest hydrogen yields were achieved (75.3% for the Rh-Ni/Ce-Al_2O_3 catalyst).

For these experiments an important behaviour related to the S/C ratio can be appreciated. For example for the Rh-Ni/Ce-Al_2O_3 catalysts, when the S/C ratio was increased, the methane conversion remained constant (see Figure 16). However, CO_2 conversion and hydrogen yield dramatically decreased. This effect could be attributed to the WGS reaction. At S/C=1.0, almost all water reacted with the remaining methane through SMR reaction and the CO_2 was converted through DR reaction. Increasing the S/C ratio, the water excess can react with the CO produced from both SMR and CPO, generating CO_2 and H_2 through WGS reaction. Therefore, this reaction could explain the negative CO_2 conversions measured for some catalysts and the hydrogen yield depletion. In the case of the H_2/CO ratio, it remained more or less constant when S/C was increased from 1.0 to 2.0, due to the possible competence between DR and WGS reactions. Nevertheless, it can be clearly observed that increasing S/C ratio up to 3.0, WGS reaction ended being predominant as proved by negative CO_2 conversions measured for all the catalysts tested and the highest H_2/CO ratios achieved. As commented before, no O_2 was measured so it means that all the fed oxygen reacted with methane through CPO reaction or with the other molecules that can be oxidized.

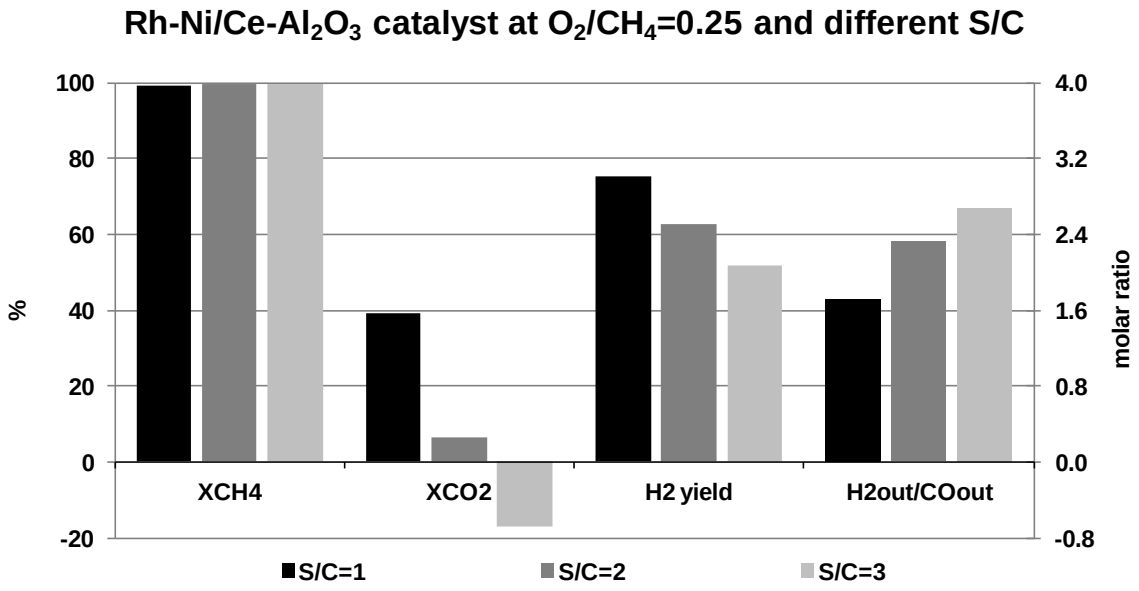

Figure 16: *TR activity results obtained by the Rh-Ni/Ce-Al_2O_3 catalyst operating in the fixed bed reaction system at O_2/CH_4=0.25 and different S/C ratios.*

TR activity results operating at O_2/CH_4=0.50 and different S/C ratios are also summarized in Table 9 for all the catalysts under investigation and in Figure 17 for the Ni/Ce-Zr-Al_2O_3 catalyst. Increasing the O_2/CH_4 ratio up to 0.50, almost equilibrium conversions were also achieved by all tested catalysts. As it was expected by the thermodynamic calculations, lower CO_2 conversions were obtained for all the catalysts and S/C ratios tested. Also under this operation conditions no O_2 was measured by the μ-GC. Firstly, at S/C ratio of 1.0, DR, SMR and CPO reactions occurred. Comparing these results to the ones obtained at O_2/CH_4 ratio of 0.25 and attending to the CO_2 conversion, a lower contribution of the DR was noticed. Operating at O_2/CH_4 ratio of 0.50 more oxygen and nitrogen was fed into the system, so that higher CO concentrations were obtained through CPO reaction. Increasing the S/C ratio, more water was available for WGS reaction so, at S/C=2.0, the carbon dioxide is produced by this reaction and almost no DR reaction took place explaining the negative CO_2 conversions. A similar behaviour was reported at S/C=3.0 reaching the most negative CO_2 conversion values. Consequently, H_2/CO ratio increased due to the consumption of CO through the WGS reaction. For these experiments, the bimetallic catalyst presented the highest hydrogen yield.

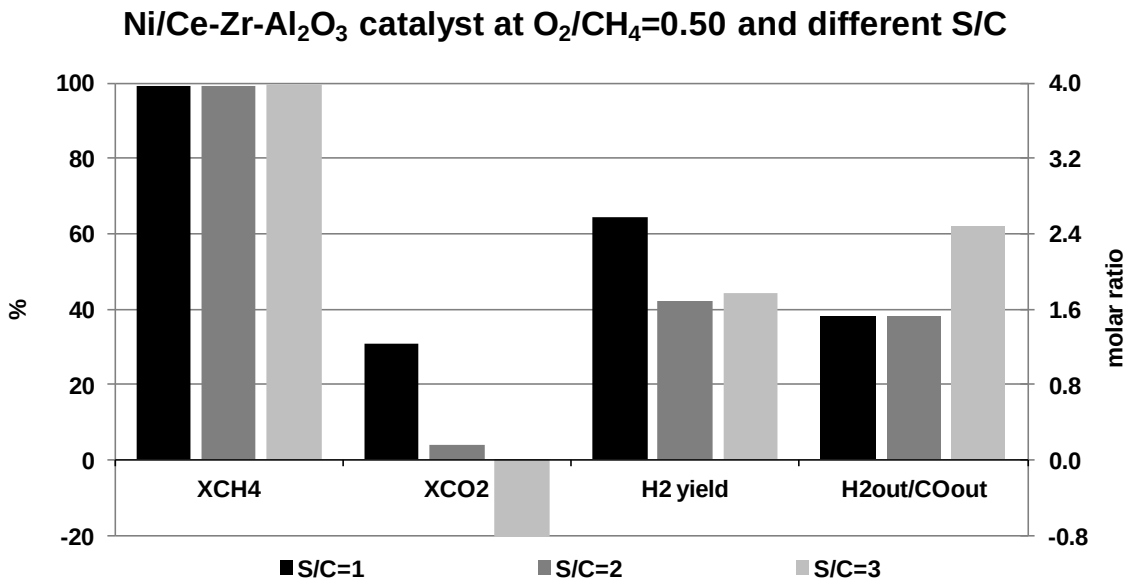

Figure 17: *TR activity results obtained by the Ni/Ce-Zr-Al_2O_3 catalyst operating in the fixed bed reaction system at O_2/CH_4=0.50 and different S/C ratios.*

Comparing the studied TR processes and attending to the O_2/CH_4 ratio, very different carbon dioxide conversions can be appreciated. At O_2/CH_4 ratio of 0.50 and S/C ratio of 1.0, low CO_2 conversions were measured and at higher S/C ratios CO_2 conversions were negative. However, in the case of the O_2/CH_4 ratio of 0.25, the negative CO_2 conversions were only measured for two catalysts, Ni/MgO and Ni/Ce-Al_2O_3, when S/C ratio of 2.0 was used.

For TR processes, the Ni/Ce-Zr-Al_2O_3 catalyst showed a different behaviour achieving the highest CO_2 conversions. These differences can be more clearly observed at higher S/C ratios and they can be attributed to the low selectivity of this catalyst for the WGS reaction.

4.3.5 Results from activity testing using microreactors

Operation with microreactors was carried out for the best conditions considered after operating with a fixed bed reactor system. Thus, attending to the production rates, conversion values and hydrogen yield measured the selection of the best operation conditions for the studied processes were chosen. Then, in order to select the processes to be intensified using microreactors, different aspects were taken into account from the results obtained in the activity tests using a fixed bed reactor.

- From the economical point of view, the energy required for DR and BSR is much higher than the one consumed in the rest of the processes studied, BOR and TR.

- DR and BSR processes are dominated by endothermic reactions and as TR combines the exothermicity of the CPO and WGS reactions, the energy required will be always lower.

- With regards to environmental concern (atmospheric pollutants), DR reaction was the one converting most of the carbon dioxide fed. Nevertheless, low methane conversions were reached and it is also considered an important GHG. On the other hand, in BOR process very high CO_2 conversions (85.4% for the Ni/Ce-Zr-Al_2O_3 catalyst) were also reached and for this process almost full methane conversion (96.3%) was achieved.

- Comparing BOR and BSR processes with regards to their activity, the thermodynamics of BOR process allows reaching higher carbon dioxide conversions which makes possible to obtain higher hydrogen yields. In addition, despite the higher methane conversion predicted by the equilibrium for the BSR process (98.5%), this difference is very low if it is compared with the predicted one for the BOR process (97.3%).

As a consequence, DR and BSR processes were not considered for their study in microreactors. For BOR process, the ratios of O_2/CH_4 0.25 and 0.50 seemed to be the most appropriate ones for being studied using microreactors. In the case of the TR process, the O_2/CH_4 ratio of 0.25 was used to be studied at S/C=1.0 and 2.0.

On the other hand, the catalysts which achieved the highest activities and behaved more stable were impregnated in microreactors to test its performance. These catalysts were the following: Ni/Ce-Al_2O_3, Ni/Ce-Zr-Al_2O_3 and Rh-Ni/Ce-Al_2O_3.

4.3.5.1 Comparison of BOR activity results for both microreactor and fixed bed reactor systems

As it can be observed in Table 10, this innovative reaction system allows an important increase of WHSV and makes them a real alternative for process intensification.

In Table 10, the comparison of the activity results obtained between microreactor and fixed bed reactor for BOR process at O_2/CH_4=0.25 and 0.50 are shown. High methane and carbon dioxide conversions were achieved being close to the equilibrium predicted values. Using the Ni/Ce-Al_2O_3 catalyst the highest conversions values and hydrogen yield were obtained. However, Rh-Ni/Ce-Al_2O_3 catalyst reached the highest H_2/CO ratio values which can be related to the selectivity of this catalyst for WGS reaction.

Table 10: *Comparison between microreactor (Micro) and fixed bed reactor (FBR) activity results in BOR process at O_2/CH_4 ratio of 0.25 and 0.50.*

BOR O_2/CH_4=0.25	**Ni/Ce-Al_2O_3**		**Ni/Ce-Zr-Al_2O_3**		**Rh-Ni/Ce-Al_2O_3**	
	Micro	**FBR**	**Micro**	**FBR**	**Micro**	**FBR**
Catalyst amount (g)	0.0262	0.3402	0.0291	0.3400	0.0240	0.3401
WHSV ($g_{gas}\cdot g_{cat}^{-1}\cdot h^{-1}$)	1710.4	131.8	1539.9	131.7	1867.2	131.8
X_{CH4} (%)	90.2	90.4	85.6	96.3	83.7	95.7
X_{CO2} (%)	85.2	84.3	74.5	85.4	80.6	82.0
H_2 yield (%)	79.7	89.4	75.8	90.9	78.3	90.2
H_{2out}/CO_{out}	1.1	1.2	1.1	1.2	1.1	1.2
BOR O_2/CH_4=0.50	**Ni/Ce-Al_2O_3**		**Ni/Ce-Zr-Al_2O_3**		**Rh-Ni/Ce-Al_2O_3**	
	Micro	**FBR**	**Micro**	**FBR**	**Micro**	**FBR**
Catalyst amount (g)	0.0262	0.3402	0.0291	0.3400	0.0240	0.3401
WHSV ($g_{gas}\cdot g_{cat}^{-1}\cdot h^{-1}$)	2447.5	188.7	2203.6	188.5	2671.9	188.5
X_{CH4} (%)	39.4	97.4	92.6	98.1	96.5	97.6
X_{CO2} (%)	-2.2	46.6	44.4	48.8	55.8	50.0
H_2 yield (%)	10.8	80.7	69.7	81.0	77.8	82.6
H_{2out}/CO_{out}	0.5	1.2	1.1	1.2	1.2	1.2

Another comparison between conventional and advanced reaction systems can be observed in Figure 18. In this case, CH_4 TOF and H_2 PROD values were calculated in order to obtain a better comparison of activity results. Higher TOF and PROD values were obtained for tested microreactors, which it is related with the use of lower catalysts amounts. With regards to the catalytic activity, higher TOF and PROD values were obtained using the Ni/Ce-Al_2O_3 catalyst in all measured cases, due to the lower metal dispersion.

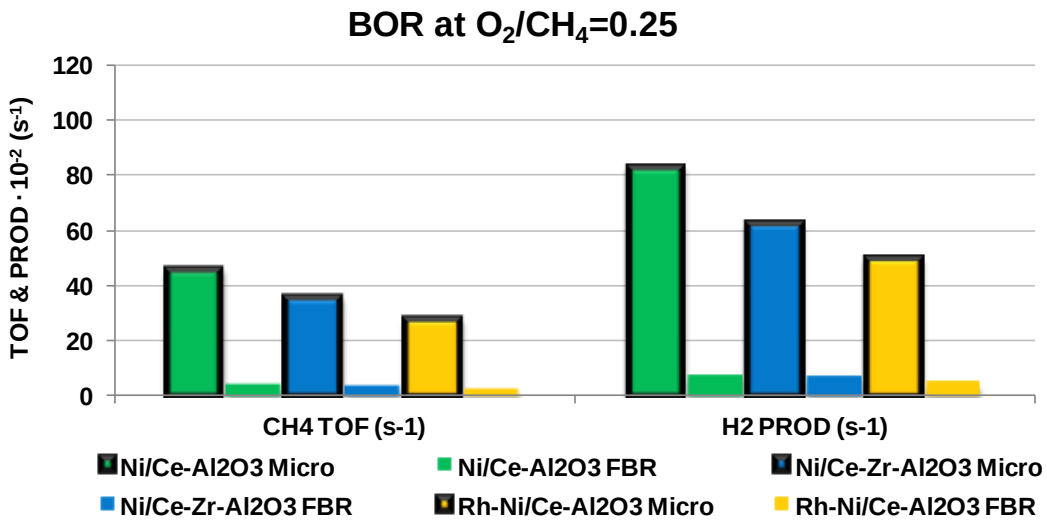

Figure 18: *Comparison between microreactor (Micro) and fixed bed reactor (FBR) TOF and PROD values for BOR process at O_2/CH_4=0.25.*

4.3.5.2 TR activity results

In Table 11, the differences in the WHSV using the microreactor reaction system can be observed again.

Table 11: *Microreactors TR activity results and WHSV values for TR process at O_2/CH_4=0.25 and S/C ratios of 1.0 and 2.0 for both reaction systems.*

TR S/C=1.0, O_2/CH_4=0.25	$Ni/Ce\text{-}Al_2O_3$		$Ni/Ce\text{-}Zr\text{-}Al_2O_3$		$Rh\text{-}Ni/Ce\text{-}Al_2O_3$	
	Micro	FBR	Micro	FBR	Micro	FBR
Catalyst amount (g)	0.0262	0.3402	0.0291	0.3400	0.0240	0.3401
WHSV ($g_{gas}\cdot g_{cat}^{-1}\cdot h^{-1}$)	2097	161	1888	161	2290	161
X_{CH4} (%)	95.0	97.2	93.9	99.0	92.1	99.1
X_{CO2} (%)	42.2	22.3	41.5	34.4	32.8	39.1
H_2 yield (%)	72.0	73.7	**72.8**	67.1	65.5	75.3
H_{2out}/CO_{out}	1.7	2.0	1.8	1.5	1.5	1.7
Biogas TR S/C=2.0, O_2/CH_4=0.25	$Ni/Ce\text{-}Al_2O_3$		$Ni/Ce\text{-}Zr\text{-}Al_2O_3$		$Rh\text{-}Ni/Ce\text{-}Al_2O_3$	
	Micro	FBR	Micro	FBR	Micro	FBR
Catalyst amount (g)	0.0262	0.3402	0.0291	0.3400	0.0240	0.3401
WHSV ($g_{gas}\cdot g_{cat}^{-1}\cdot h^{-1}$)	2483.1	191.3	2235.6	191.2	2710.7	191.2
X_{CH4} (%)	96.6	98.9	96.4	99.4	96.3	99.5
X_{CO2} (%)	11.3	-12.9	6.2	14.4	17.7	6.6
H_2 yield (%)	59.5	61.2	60.4	60.4	**62.1**	62.8
H_{2out}/CO_{out}	2.2	2.6	2.4	2.2	2.6	2.3

Only experiments for TR at O_2/CH_4=0.25 and S/C of 1.0 and 2.0 were carried out in the microreactor system. High methane and carbon dioxide conversions were achieved being them

close from the values predicted by the equilibrium. At S/C=1.0, using the Ni/Ce-Al_2O_3 catalyst the highest conversions were obtained being Ni/Ce-Zr-Al_2O_3 catalyst the one reaching the best hydrogen yield. At S/C=2.0, using the Rh-Ni/Ce-Al_2O_3 catalyst clearly the best activity results were obtained. However, which regards to the CO_2 conversion and hydrogen yield, the same behaviour as for fixed bed reaction system was observed in the microreactors.

In Figure 19 CH_4 TOF and H_2 PROD values were calculated in order to obtain a better comparison of the activity results. Higher TOF and PROD values were obtained using microreactors as lower catalyst amounts were used and similar conversions were reached. All these catalysts were able to achieve equilibrium conversions in both reaction systems, so that the existing TOF and PROD differences are due to the degree of dispersion of the active metal.

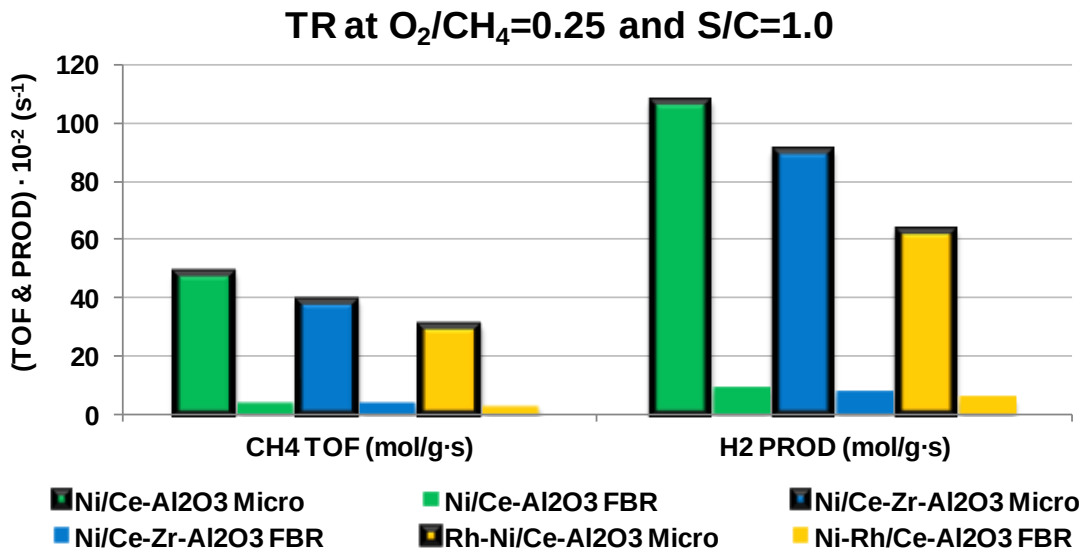

Figure 19: *Comparison between microreactor (Micro) and fixed bed reactor (FBR) for TR process at O_2/CH_4=0.25 and S/C=1.0.*

4.3.6 Tested catalysts characterization results

4.3.6.1 Tested catalysts SEM micrographs

The micrographs for DR reaction, which are shown in Figure 20, were taken from secondary electron detectors in order to study the surface morphology achieving a better observation of carbon filaments in the catalytic surface.

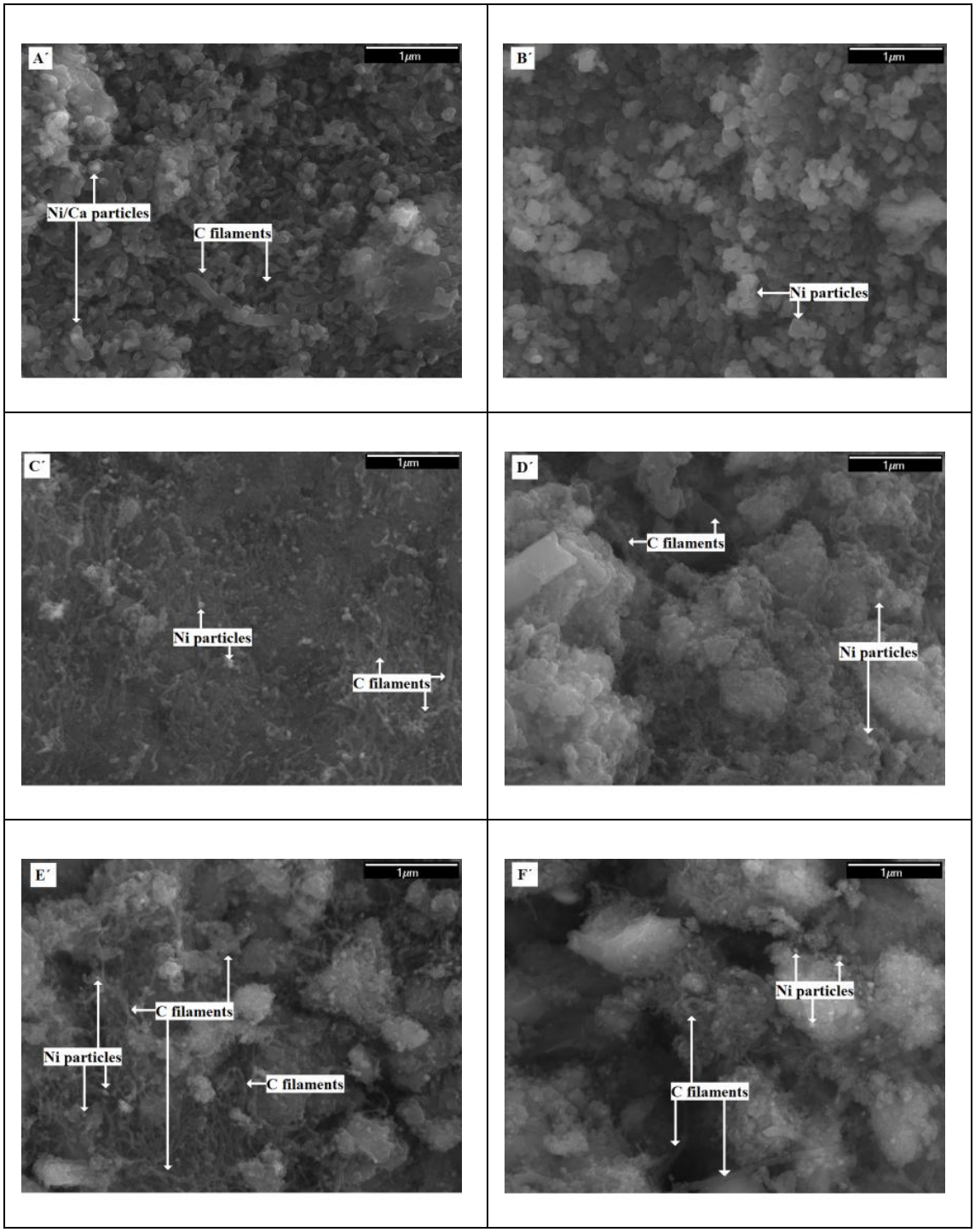

Figure 20: *Tested catalysts surfaces after DR process: Commercial (A´), Ni/MgO (B´), Ni/Ce-Al_2O_3 (C´), Ni/Zr-Al_2O_3 (D´), Ni/Ce-Zr-Al_2O_3 (E´) and Rh-Ni/Ce-Al_2O_3 (F´).*

Most of the micrographs obtained from the catalysts tested after DR reaction showed carbon filaments in the catalytic surface. However, the catalytic surface of the Ni/MgO catalyst appeared apparently free of carbon and this catalyst reached very high CO_2 and CH_4 reforming conversions. In contrast, despite the good reforming conversions reached by the Ni/Ce-Zr-Al_2O_3 and Rh-Ni/Ce-Al_2O_3 catalysts, carbon filaments were observed on their catalytic surfaces. For the commercial, Ni/Ce-Al_2O_3 and Ni/Zr-Al_2O_3 catalysts, little carbon filaments were formed.

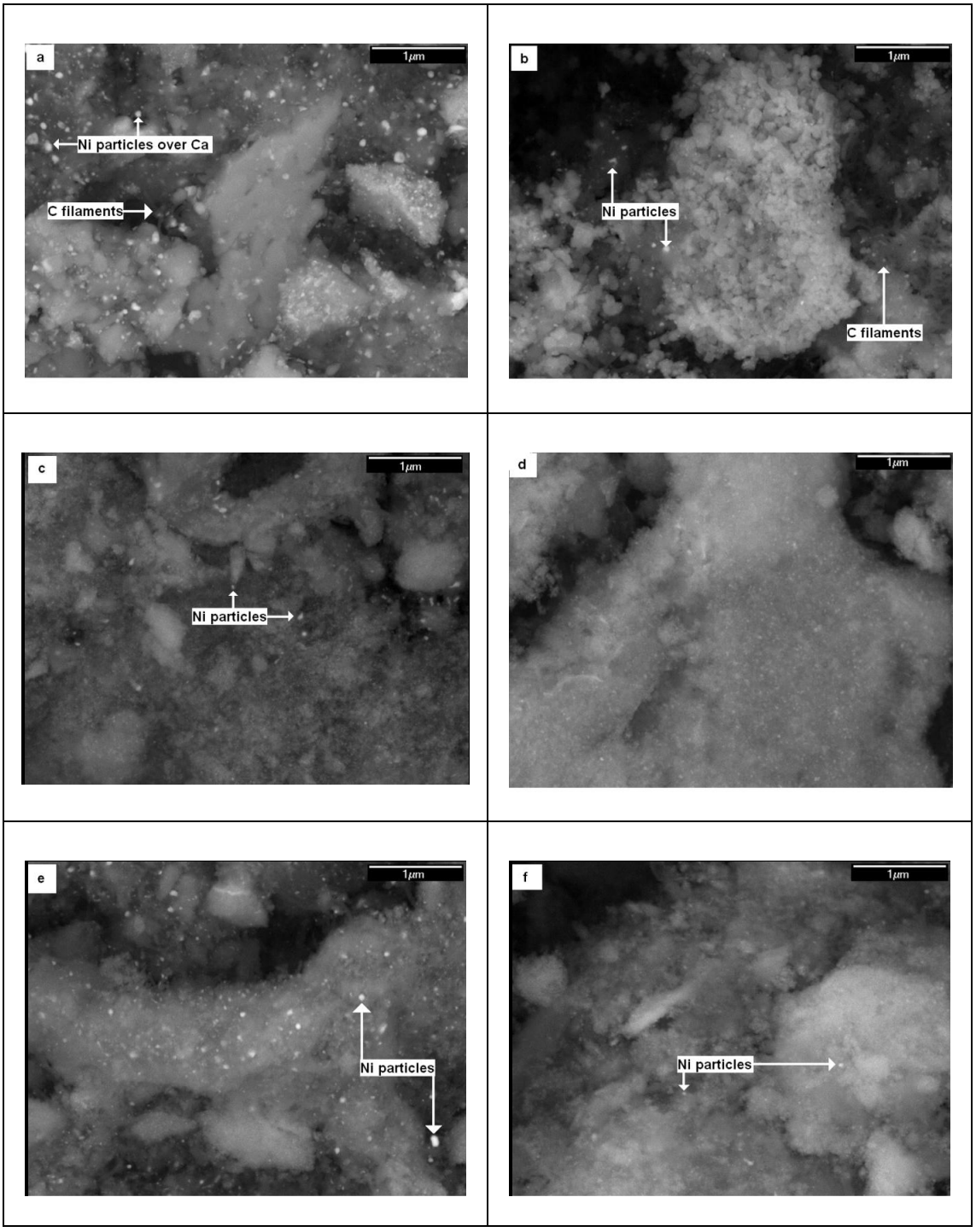

Figure 21: *Tested catalysts surfaces after BOR proceses: Commercial (a), Ni/MgO (b), Ni/Ce-Al_2O_3 (c), Ni/Zr-Al_2O_3 (d), Ni/Ce-Zr-Al_2O_3 (e) and Rh-Ni/Ce-Al_2O_3 (f).*

In Figure 21, catalysts SEM micrographs after BOR process are shown. These images were also taken using backscattered electron imaging technique in order to study the surface composition. The micrographs correspond to the catalysts surface after BOR at O_2/CH_4=0.125. Evidence of nickel aggregates distribution can be seen as well as their small particle size. Comparing with calcined catalysts SEM micrographs, a very similar aggregates size was measured so that apparently no sinterization effect occurred in all analyzed catalysts.

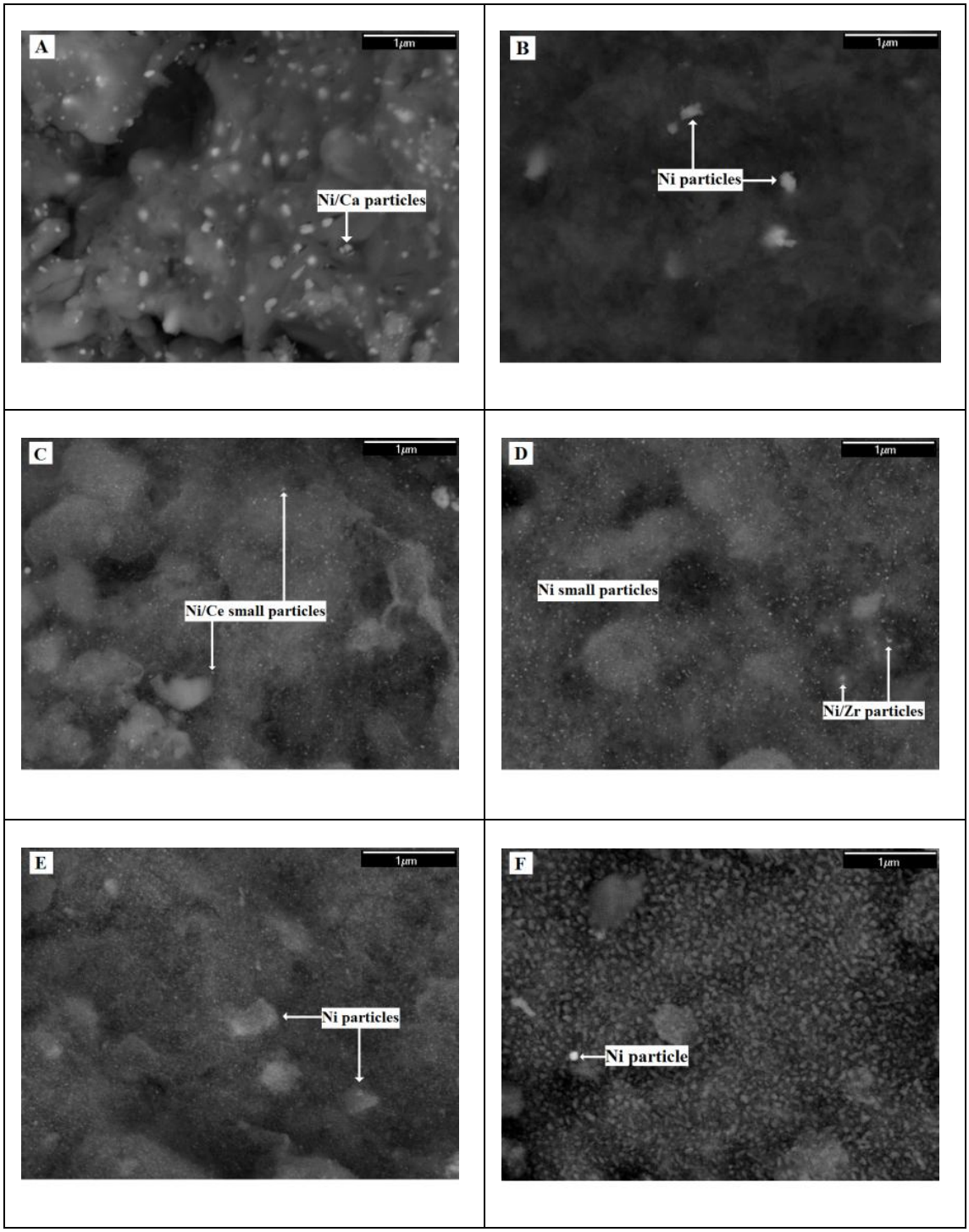

Figure 22: *Tested catalysts surfaces after biogas TR process: Commercial (A), Ni/MgO (B), Ni/Ce-Al_2O_3 (C), Ni/Zr-Al_2O_3 (D), Ni/Ce-Zr-Al_2O_3 (E) and Rh-Ni/Ce-Al_2O_3 (F).*

As commented before, under these conditions DR process is promoted and as a result the presence of carbon filaments could be expected. However, the catalytic surfaces of most of the catalysts appeared apparently free of carbon. This could be due to the presence of oxygen at high temperatures that avoided carbon deposition in the catalytic surfaces. In the case of commercial and Ni/MgO catalysts the presence of small carbon filaments growth was detected.

Finally, in Figure 22 SEM micrographs the spent catalysts in TR process are shown. The micrographs for the catalysts tested in the TR process were also taken using backscattered electron imaging technique. The tested catalysts surfaces appeared cleaner than the ones for used in DR. This could be also due to the oxygen used in the TR feed mixture that avoided carbon deposition at high temperatures. The presence of Ni particles as well as the support modifiers was confirmed in the catalytic surface by backscattered electron imaging.

4.3.6.2 X-ray photoelectron spectroscopy, XPS, study

Figure 23 represents the relationship between the reached hydrogen yield in the BOR process at O_2/CH_4=0.25 and the surface atomic ratios measured by XPS. These ratios were calculated for both fresh reduced catalysts and the used catalysts in the BOR process.

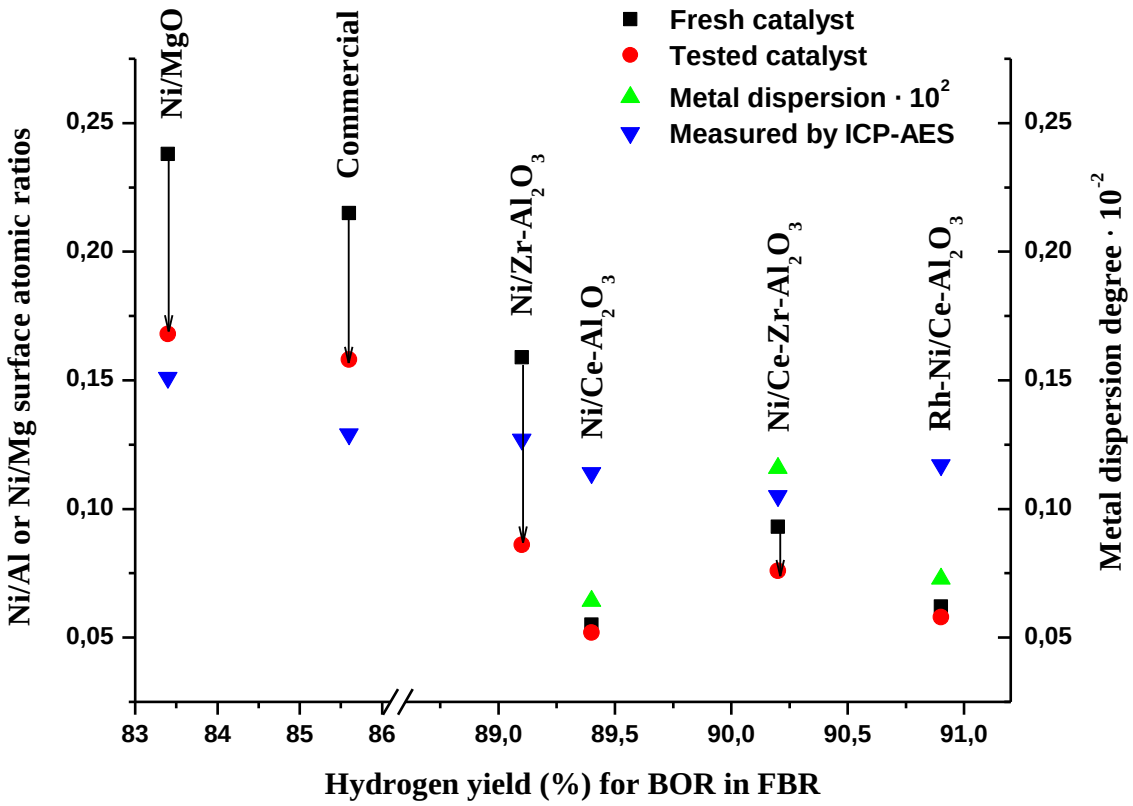

Figure 23: *Results of Ni/Al and Ni/Mg surface atomic ratios measured by XPS and ICP-AES, metal dispersion degree measured by H_2-pulse chemisorptions and hydrogen yields obtained after operation in a FBR for BOR at O_2/CH_4=0.25.*

As it can be observed, the surface atomic ratio of the commercial, Ni/MgO and Ni/Zr-Al_2O_3 catalysts decreased more comparing them with the rest of catalysts. This effect can be attributed to the carbon filaments detected by SEM in the surface of commercial and Ni/MgO catalysts. The carbon is normally deposited in the Ni particles and as a result, the superficial Ni decreased. In addition, in spite of the improvements in the Ni surface dispersion for these three catalysts (compared with the ICP-AES measurements), the lowest hydrogen yield were achieved. For the rest of catalysts, Ni/Ce-Al_2O_3, NiCe-Zr-Al_2O_3 and Rh-Ni/Ce-Al_2O_3 catalysts, although lower surface ratios were measured, higher hydrogen yields were reached. Besides, smaller surface atomic ratios were measured before and after activity tests. Therefore, the XPS analysis confirms the better behavior of these three catalysts in the experiments carried out.

Figure 24 represents the relationship between the hydrogen yield achieved in the biogas TR at O_2/CH_4=0.25 and S/C=1.0 and the surface atomic ratios measured by XPS for fresh and used catalysts. In addition, surface atomic ratios calculated from the ICP-AES data results can be also observed. Furthermore, the hydrogen chemisorption results, metal dispersion degree, for catalysts tested in microreactors are also shown.

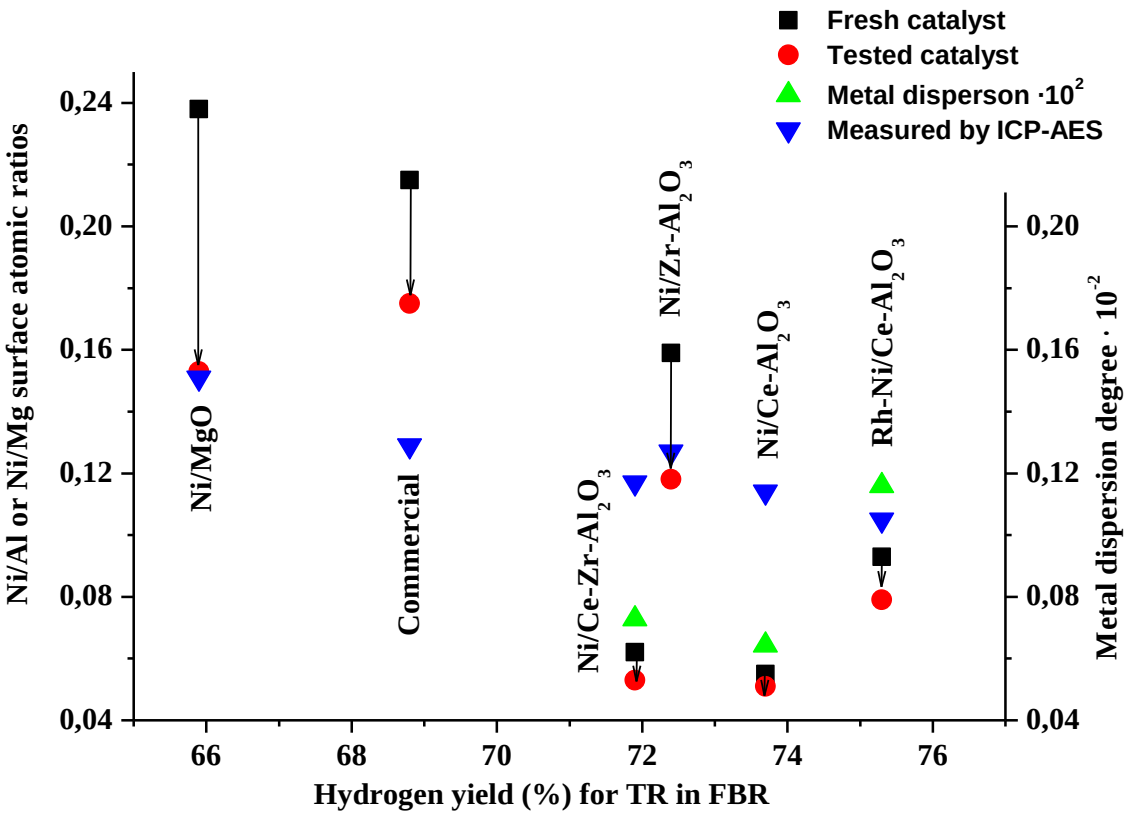

Figure 24: *Results of Ni/Al and Ni/Mg surface atomic ratios measured by XPS and ICP-AES, metal dispersion degree measured by H_2-pulse chemisorptions and hydrogen yields obtained after operation in a FBR for TR at O_2/CH_4=0.25 and S/C=1.0.*

If Ni catalyst contents (ICP-AES) are compared to their surface dispersion (XPS), it can be observed that this active metal was preferentially located on the outer surface of the support particles. For the commercial, Ni/MgO and Ni/Zr-Al_2O_3 catalysts the atomic surface ratios (XPS) suffered important decreases and this could be the reason of the quite low hydrogen yields measured for them. Even any carbon filaments were not detected on their catalytic surfaces, this fact could be explained assuming that carbon deposition in the Ni particles happened, and partially covered Ni sites but this carbon was not filamentous.

Lower Ni surface ratios were measured for the rest of the catalysts (Ni/Ce-Al_2O_3, Ni/Ce-Zr-Al_2O_3 and Rh-Ni/Ce-Al_2O_3) by ICP-AES and XPS. Moreover, if Ni catalysts contents (IPC-AES) are compared to their surface dispersions (XPS), it can be observed that for these catalysts the active metal was not preferentially located on the outer surface of the support particles. However, their catalytic activity was higher and lower decreases in their surface atomic ratios were measured. Hydrogen pulse chemisorption results revealed that the highest metal dispersion was achieved for the Rh-Ni/Ce-Al_2O_3 catalyst. This fact could explain the highest hydrogen yield associated to this catalyst. In the case of Ni/Ce-Al_2O_3 and NiCe-Zr-Al_2O_3 catalysts, a very similar metal dispersion and hydrogen yields were measured.

4.3.7 Conclusions

The main goal of this work is the biogas valorisation for hydrogen production by means of DR, BSR, BOR and TR processes using Ni or Rh-Ni catalysts on promoted alumina. For this purpose, several Ni-based catalysts and a bimetallic Rh-Ni catalyst were used supported on magnesia or modified alumina with CeO_2 and ZrO_2 oxides. In general, high methane and carbon dioxide conversions were reached by all tested catalysts and studied processes in the fixed bed reactor.

High methane and carbon dioxide conversions were reached for DR reaction in the fixed bed reactor system. The Rh-Ni/Ce-Al_2O_3 catalyst achieved the highest hydrogen production yield in DR reaction. However, this process requires huge energy supply and carbon filaments growth was observed by SEM.

For the BSR process, increasing the S/C ratio lower carbon dioxide conversions were measured, which implied a decrease of the hydrogen yield. Consequently, at S/C=1.0 were measured the best results. For this process, the lowest hydrogen yield and H_2^{out}/CO^{out} molar ratio were measured for the bimetallic, Rh-Ni/Ce-Al_2O_3, and Ni/Ce-Zr-Al_2O_3, catalysts although these two catalysts reached the highest methane and carbon dioxide.

In the case of BOR process, the maximum hydrogen yield was obtained at O_2/CH_4=0.25, which corresponds to intermediate values of methane and carbon dioxide conversions. The highest hydrogen yield and H_2out/COout molar ratio were obtained using Rh-Ni/Ce-Al_2O_3 and Ni/Ce-Zr-Al_2O_3 catalysts.

Regarding biogas TR process, different O_2/CH_4 and S/C ratios were tested. For this process, at O_2/CH_4=0.25 and S/C=1.0 the bimetallic catalyst reached the highest carbon dioxide conversions and hydrogen yields.

Thus, Ni/Ce-Al_2O_3, Ni/Ce-Zr-Al_2O_3 and Rh-Ni/Ce-Al_2O_3 catalysts were chosen for their impregnation on microreactors. Only experiments for BOR process at O_2/CH_4=0.25 and 0.50 and for TR at O_2/CH_4=0.25 and S/C=1.0 and 2.0 were carried out in the microreactor systems.

Operating with them, conversions similar to the ones measured using the fixed bed reactor were achieved, being the Ni/Ce-Al_2O_3 catalyst the one producing the highest hydrogen yield when operation under the conditions specified for BOR. By the contrary, the Ni/Ce-Zr-Al_2O_3 catalyst was the one reaching the highest hydrogen production yield for biogas TR at O_2/CH_4=0.25 and S/C=1.0. If TOF and hydrogen productivity values are compared for both BOR and TR processes, operating with a microreactors one order of magnitude higher activity was measured comparing with the achieved one in the fixed bed reactor. According to the characterization

carried out this Ni/Ce-Al_2O_3 catalyst presented the lowest nickel dispersion, and as similar conversions were obtained for all three catalysts, this one achieved the highest TOF results.

4.4 Biogas reforming processes using Zeolites L based catalysts

A published paper:

Title: Ni and Rh-Ni catalysts supported on Zeolites L for hydrogen and syngas production by biogas reforming processes

Authors: U. Izquierdo[1], V.L. Barrio[1], K. Bizkarra[1], A.M. Gutierrez[2], J.R. Arraibi[2], L. Gartzia-Rivero[3], J. Bañuelos[3], I. Lopez-Arbeloa[3], J.F. Cambra[1]

[1] *Dept. of Chemical and Environmental Engineering, School of Engineering, University of the Basque Country UPV/EHU, c/ Alameda Urquijo s/n 48013, Bilbao, Spain*

[2] *Edp Naturgas Energía, c/ General Concha, 20, 48010 Bilbao, Spain*

[3] *Dept. of Chemical Physics, University of the Basque Country UPV/EHU Apartado 644, 48080 Bilbao, Spain*

Journal: International Journal of Hydrogen Energy

Year: 2014

4.4.1 Introduction

The main challenges of catalytic hydrogen and/or syngas production involves the selected process, the processed feed, and the yield of the catalysts used, which is normally measured by the activity, selectivity, and stability. In the present study, biogas was selected as a raw material because it is considered to be a green and renewable feed [8-10,42]. Using a synthetic biogas without contaminants, four different reforming processes were studied: dry reforming, the most conventional; biogas steam reforming, very well known for natural gas; biogas oxidative reforming, and tri-reforming, suitable process for biogas valorization [43]. For the study of these processes, reversible Water Gas-Shift reaction must also be taken into account due to the high temperatures and conversions. All of them were properly described in the previous 4.3 section. Based on that section, in which γ-Al_2O_3 was used as a support for nickel and rhodium-nickel based catalysts [44,45], the following operating conditions were chosen: S/C ratio of 1.0 and 2.0 for BSR, O_2/CH_4 ratio of 0.25 and 0.50 for BOR, and S/C of 1.0 and O_2/CH_4 of 0.25 for TR reactions. In this work, the catalyst support was also tested with the aim to study its influence in the activity of the catalysts for the described processes.

Catalyst support plays an important role because properties like thermal stability, surface area, capacity of maintaining the metal dispersion during the reaction or acidity can be key factors that stand out from the existing ones [46]. For the reactions of the present study, alumina support is most commonly used due to its thermal stability and in the case of γ-Al_2O_3, the high surface area [46-49]. However, considering the previous mentioned properties, Zeolites also offer higher surface areas, specific micropore structure, and affinity to CO_2 [46,50]. Some types of Zeolites were tested as active metal support in the dry reforming of methane, and it was observed that the nature of Zeolite support has a significant influence on the overall performance of the catalyst [51,52]. The Zeolite L prepared in this study is a crystalline aluminosilicate with a hexagonal symmetry and one-dimensional channels (pore aperture around 7.1 Å) running along the crystal. Its morphology and size can be modulated by the synthesis conditions [53]. These three Zeolites were synthesised by Gartzia-Rivero et al. [53] who described all its structural and morphological properties in previous reference. Zeolite L has been experimentally used as a catalyst not only in the hydrodesulfurisation of fluid catalytic cracking (FCC) gasoline [54], dehydrogenation of propane [55] or isobutane [56,57], but also in selective chlorination of toluene [58]. In general, different types of zeolites are being used as catalyst supports in reforming processes, and commonly studied as potential candidates for dry reforming processes [46,50,51,59-65].

Regarding the active phase, among the existing non-noble metals, Nickel is most widely used for reforming reactions because of its availability and relatively low price. However, it is well known that noble metals like Rhodium, Ruthenium, Palladium, etc. are much more active, stable and their use decreases the tendency of coke formation in the catalytic surface at high

temperatures [29,31], especially when Rh and Ru are used [66]. Although the noble metals are much more expensive, it has been reported that adding a small amount of noble metal to a non-noble metal catalyst increases the activity and dispersion of the non-noble metal due to the spill-over effect [27]. We found that the addition of 1 wt.% of Rh to Ni/Al_2O_3 catalyst has a strong influence on the catalytic performance towards the biogas reforming processes under investigation. On this basis, in this study the effect of Ni and Rh addition to a three different Zeolite L´s is reported.

4.4.2 Disc and nano shape Zeolites based catalysts preparation

The zeolite L's herein used were prepared by microwave-assisted hydrothermal synthesis, which provides a good control over the temperature and ensures homogeneous and efficient heating. Crystals of different morphology (from disc to cylinders) and size (from nm to μm) were obtained starting from a fixed gel composition (9.34 K_2O - 1.00 Al_2O_3 - 20.20 SiO_2 - 412.84 H_2O for the nanosize cylinders and 5.40 K_2O - 5.50 Na_2O - 1.00 Al_2O_3 - 30.00 SiO_2 - 416.08 H_2O for the microsize discs) [67], which was optimised to yield each kind of zeolites.

The experimental procedure for each type of zeolite was quite similar, and it has been previously mentioned about the micrometer crystals [53]. Overall, the alumina and silica suspensions were prepared separately under reflux and heating at 120 ºC. Once a clear solution is achieved, the alumina was added to the silica suspension under vigorous mechanical stirring. The obtained gel was transferred to a polytetrafluoroethylene (PTFE) pressure vessel and heated in a microwave oven at 170 ºC for 1 h (nanosize cylinders) and 160 ºC for 8 h (micrometer size discs). Afterwards, the vessel was cooled down to room temperature and the obtained crystals were washed with boiling doubly distilled water and dried at 90ºC for 16 h.

The alumina suspension was prepared by mixing potassium hydroxide (KOH) and metallic aluminium powder in doubly distilled water under argon flow, and the mixture was stirred at low temperature (0ºC) for 15 min. After letting the solution warm up to room temperature, stirring was continued for 1.5 h under the inert atmosphere. This solution was added to a silica suspension (Ludox, supplied by Sigma-Aldrich) with vigorous mechanical stirring. After aging the gel for 3–6 min, it was transferred to a PTFE pressure vessel and heated in a microwave oven at 175ºC for 12 h. Once the crystallisation process was finished, the vessel was cooled down to room temperature. The obtained solid was washed with boiling doubly distilled water until the pH of the supernatant became neutral. Finally, the crystals were dried at 90ºC for 16 h.

Regarding catalyst preparation, first, the Zeolites were calcined at 1073 K for 4 h in order to stabilize de supports. Then, six different catalysts were prepared by incipient wetness impregnation method: three Ni monometallic catalysts and their three homologous Rh-Ni bimetallic catalysts. In case of monometallic catalysts, an aqueous solution of Nickel (II) nitrate hexahydrate (99.99%; Sigma Aldrich) was added to reach an intended load of 13 wt.% of Ni

[44]. The corresponding solutions were stirred for 2 h using a rotatory evaporator and then heated up until all the water was removed. Next, the catalysts were dried and calcined at 1073 K for 4 h in the oven. For the bimetallic catalysts, the same Ni proportion used for monometallic catalysts was incorporated, and after the calcination step, a Rh (III) nitrate hydrate (~36% as Rh; Sigma Aldrich) aqueous solution was added to achieve nominal loading of 1 wt.% of Rh. Once the Rh was incorporated, the bimetallic catalysts were calcined again under the conditions described previously. The calcinations were carried out under an oxidative atmosphere in order to ensure oxidation of the metal species, and remove the salts of the reactants used for their preparation as well as the possible humidity inside the pores. In addition, it has been reported that dispersion increases in the samples that are previously calcined and then activated with hydrogen [60]

4.4.3 Disc and nano shape fresh and calcined catalysts characterization

4.4.3.1 Chemical composition, ICP-AES, and H_2 pulse chemisorption

The catalysts chemical compositions, which were determined by ICP-AES, are shown in Table 12. The metal contents of most of the catalysts are very similar to their nominal ones (1.0 wt.% Rh and 13.0 wt.% Ni).

Table 12: *Calcined catalysts chemical composition and H_2 chemisorption results.*

	Disc		**Cylindrical (1-3 µm)**		**Cylindrical (30-60 nm)**	
	Catalyst		**Catalyst**		**Catalyst**	
	Ni	**Rh - Ni**	**Ni**	**Rh - Ni**	**Ni**	**Rh - Ni**
Composition (wt.%)	11.14	0.88 - 12.36	12.66	1.02 - 14.07	11.92	1.09 - 13.17
Active metal Sa (m^2/g)	3.12	3.51	3.44	3.25	3.75	**9.56**
Metal dispersion (%)	4.21	4.13	3.97	3.36	4.72	**10.48**
Crystallite size (nm)	24.05	24.79	25.49	30.50	21.45	**9.79**

The H_2 pulse chemisorption results for the reduced catalysts are also outlined in Table 12. The active metal proportions used for calculating the parameters were the ones obtained by the ICP technique. Among the obtained results, the measured parameters were quite similar in the case of monometallic catalysts, but not for the bimetallic ones. For the catalysts supported on the Disc Zeolite L, small differences between the monometallic and bimetallic catalysts were detected. In case of Cylindrical (1–3 µm) catalysts, significant differences regarding the crystal sizes were observed, which was similar to the rest of the measured parameters. However, the expected increase of metal dispersion due to the spill-over effect was not noticed for those two catalysts.

For the Cylindrical (30-60 nm) catalysts, the biggest differences were detected; both monometallic and bimetallic catalysts supported on this Zeolite L presented the highest active metal surface area and metal dispersion, these catalysts being the ones with the smallest particle size. Moreover, the bimetallic catalyst experienced increased dispersion when Rh was incorporated. The previously prepared catalysts did not experience the spill-over effect, which could be explained due to the obtained lowest crystal particle size that could incorporate inside the porous structure of this support.

4.4.3.2 Textural properties, BET, of the Zeolites L and the corresponding catalysts

The textural properties of the fresh and calcined Zeolites and calcined catalysts are outlined in Table 13. The measured BET surface area was estimated according to the obtained N_2 absorption-desorption isotherm.

First, the textural properties of all Zeolite L's were measured. After calcination, a significant change of these properties was noticed in terms of the surface area diminution, which can be attributed to the high temperature (1073 K) that was used. The pore volume and the pore radius remained without significant differences. Finally, the fresh and calcined Cylindrical (30–60 nm) samples presented the highest values of total pore volume and pore size. After metal incorporation, as it could be expected, much lower surface areas were measured when catalysts and Zeolites L were compared. Both the monometallic and bimetallic catalyst surface areas decreased, although the catalysts supported on the Cylindrical (30–60 nm) remained with the higher areas.

Attending to the total pore volume, the value of this parameter decreased when Ni and Rh was incorporated. The values of Table 13 correspond to the pore volume measured for the mesopores (calculated through BJH method) and the parentheses values correspond to the micropores (using DR method). For the mono and bimetallic samples the micropores contribution was negligible. For Cylindrical (30–60 nm) catalyst, after metal impregnation the pore volume decreased and the pore size increased for both samples. Indeed taking into account the results obtained by the H_2 pulse chemisorptions, in the case of the monometallic catalyst, small pores could be blocked by metal atoms, and for the bimetallic catalyst, the particles could incorporate in the internal porous structure.

In the case of Disc and Cylindrical (1–3 μm) catalysts, the increase in pore size is five times higher than for the Cylindrical (30–60 nm) catalysts, which are between two to three times higher. However, as the initial pore size value for the Cylindrical (30–60 nm) Zeolite L is bigger than for the Disc and Cylindrical (1–3 μm), they presented higher pore size values. Therefore, for the Cylindrical (30–60 nm) bimetallic catalyst, the characteristics of the support, with a higher pore volume and size, enabled that metal incorporation (with smaller particles as it was measured by H_2 chemisorption) in the internal structure.

Table 13: *Fresh and calcined support and fresh catalysts textural properties, BET (parentheses values: micropores volume contribution).*

	Disc				Cylindrical (1-3 µm)				Cylindrical (30-60 nm)			
	Zeolite L		Catalyst		Zeolite L		Catalyst		Zeolite L		Catalyst	
	Fresh	Calcined	Ni	Rh-Ni	Fresh	Calcined	Ni	Rh-Ni	Fresh	Calcined	Ni	Rh-Ni
Surface area (m^2/g)	258.1	134.4	40.4	41.74	159.9	152.0	22.62	26.18	418.7	335.0	95.32	64.12
Pore volume (cm^3/g)	0.043 (0.123)	0.061 (0.064)	0.095 -	0.117 -	0.048 (0.077)	0.043 (0.072)	0.054 -	0.067 -	0.905 (0.174)	0.933 (0.130)	0.449 -	0.625 -
Pore size (Å)	13.8	17.1	54.0	62.5	13.3	13.3	55.0	57.8	54.3	66.8	95.5	198.0

4.4.3.3 Scanning and transmission electron microscope micrographs, SEM and TEM

Figure 26 illustrates the morphology and size distribution of the synthesised Zeolites L. The smallest Zeolites were characterised by TEM, which reveals crystals with a size of about 30-60 nm, and even resolves the channel structure. Particle-size distribution was unreliable in this case since the nanoparticles tend to agglomerate and self-associate into larger clusters of 80–100 nm. The morphology of the other supports was analysed by SEM. The larger crystals were up to 2 µm in length and around 1 µm in diameter, keeping the same cylindrical morphology. Indeed, Dynamic Light Scattering (DLS) provided just a population centred at 1.5 µm, owing to their similar length and diameter (high aspect ratio). Finally, the disc/coin-shape Zeolites were characterised by a low aspect ratio (thin crystals). In fact, the DLS suggested two main domains; one placed at 0.7–1.0 µm, assigned to the disc diameter, and the other at 0.1–0.2 µm, attributed to the thickness.

Figure 25: *A: TEM image of zeolite L nanocrystals, B: SEM image and DLS size-distribution for the micrometer Cylindrical Zeolite L and C: the same for disc-shape crystals.*

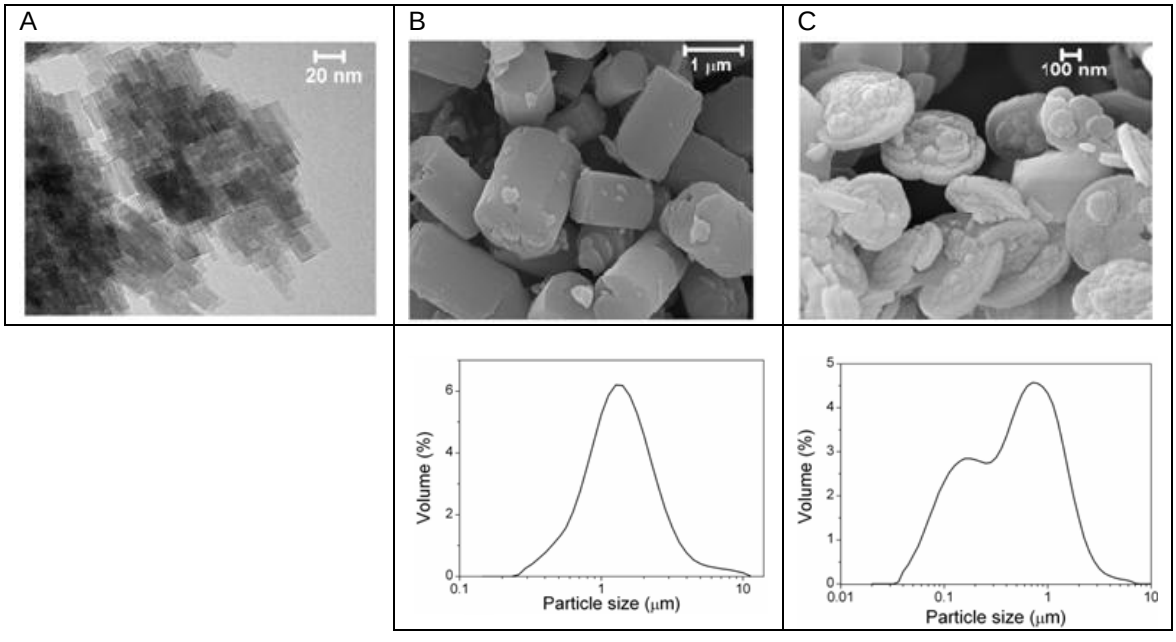

4.4.3.4 Temperature-programmed reduction, TPR

Figure 26 shows all TPR profiles of calcined catalysts. In the case of catalysts based on Cylindrical Zeolite L (1–3 µm), the profiles are very similar. The main peak at around 730 K is attributed to the reduction of NiO with very low interaction with the support [68]. The presence of two other small peaks can be observed at 820 and 1000 K assigned to the reduction of NiO particles with high interaction with the support and to Ni species located on the hexagonal prism, respectively [33,69]. When Rh was incorporated, the profiles differed in: (i) peak at around 450 K attributed to the Rh-Al interaction [70], (ii) higher hydrogen consumption measured for the bimetallic catalyst at 730 K, and (iii) lower reduction temperature required for the Ni species (spill-over effect).

For Disc Zeolite L catalyst profiles, as for the Cylindrical (1–3 µm) Zeolite L, the presence of the three peaks is not very clear due to the proximity between them. After Rh incorporation the reduction peak of NiO gradually shifted to lower temperatures, contributing mainly to the first one.

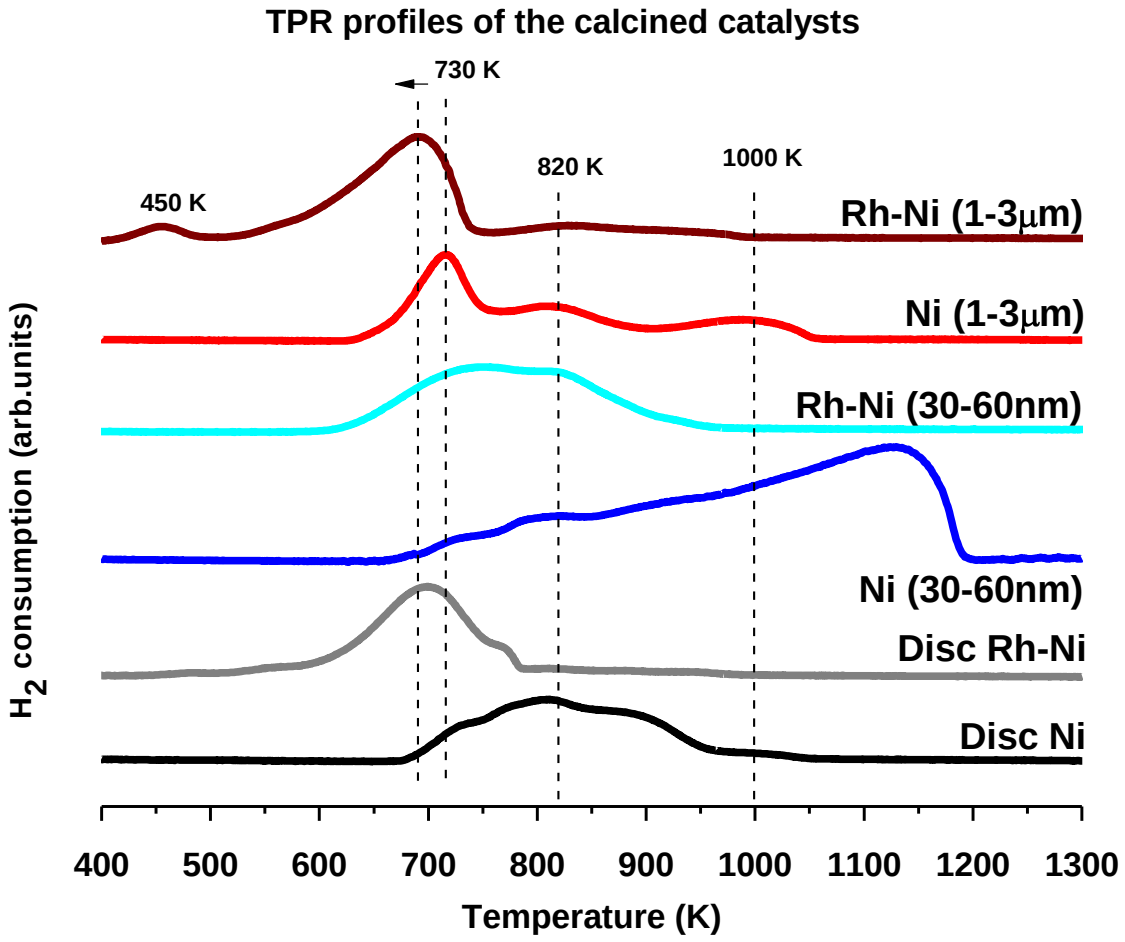

Figure 26: *TPR profiles of calcined catalysts.*

For the Cylindrical (30–60 nm) Zeolite L catalysts, in the case of Ni monometallic catalyst, the main peak appeared at the highest temperature (1150 K). For the bimetallic catalyst, the addition of Rh might contribute to the formation of Rh-Al species at lower temperatures instead of the non-stoichiometric and stoichiometric Ni-spinels formed at high temperatures [71].

4.4.3.5 XRD of the Zeolites L and catalysts

XRD analyses were carried out for all the Zeolites L and catalysts. Figure 27 presents the obtained XRD profiles for Disc Zeolite L and the consequent two catalysts. Disc Zeolite L was perfectly identified by the detected peaks at all the measured 2θ positions (Powder Diffraction File (PDF): 01-080-1580). This profile was used as a reference to compare and identify the contributions of different Ni and Rh species. In the case of Ni catalysts, and comparing its profile to the one obtained for Disc Zeolite L, the peaks that correspond to NiO can be clearly observed (PDF: 00-044-1159) at 2θ = 43.46. Taking into account the NiO contribution, the calculated crystallite size (calculated by Scherrer equation) is around 30 nm. Lastly, a very similar profile to the one obtained by Ni catalyst was measured for Rh-Ni catalysts. Thus, no peaks coming from any Rh interaction (PDF: 00-005-0685) were detected and additionally, the crystallinity of NiO was maintained constant as proved by the same crystal size. In addition, the calculated crystal sizes are very similar to the ones measured by the H_2 chemisorption technique (24.05 nm for monometallic; 24.79 nm for bimetallic catalyst). Besides, no Rh contributions were detected by this technique even after more accurate measurements in the range of 2θ where these peaks should appear (2θ = 80.5 or 89.1). However, the presence of this metal was detected by doing semi-quantitative X ray fluorescence analyses to Rh containing catalysts (See Figure. 5) in addition to the analysis done by ICP-AES. As a result, Rh species must be too small (<4 nm) as it was not possible to be detected by XRD.

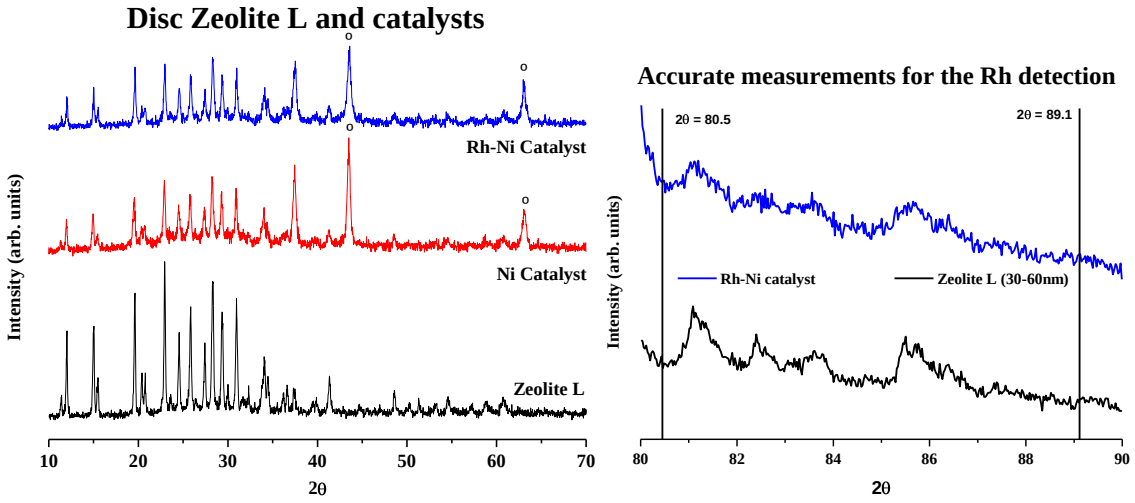

Figure 27: *a) Different XRD spectra for the Disc Zeolite L and the corresponding catalysts. NiO peaks are marked by "o" symbol. b) Accurate measurements for the Rh detection.*

The same analyses were carried out for the Cylindrical (1–3 μm) Zeolite L and corresponding catalysts. The XRD spectra are shown in Figure 28. From the analysis performed on Zeolite L (1–3 μm), the presence of two different types of structures was detected. One of them corresponds to Zeolite L and the other to Merlinoite zeolite (PDF: 01-083-1533) as can be seen in the diffractogram of Figure 28. The contribution of each type of zeolite to the sample was semi-quantitatively calculated, the sample being composed by approximately 75% of Zeolite L and 25% of Merlinoite. Focussing on the spectra of the catalysts, NiO crystals of around 60 nm were detected for the Ni catalyst. In the case of Rh-Ni catalyst, the NiO particles suffered some dispersion as crystals of about 30 nm were found. Moreover, for this catalyst no contribution of any Rh species was measured by this technique, although this metal was detected again by X Ray Fluorescence and in the previously presented ICP-AES analyses.

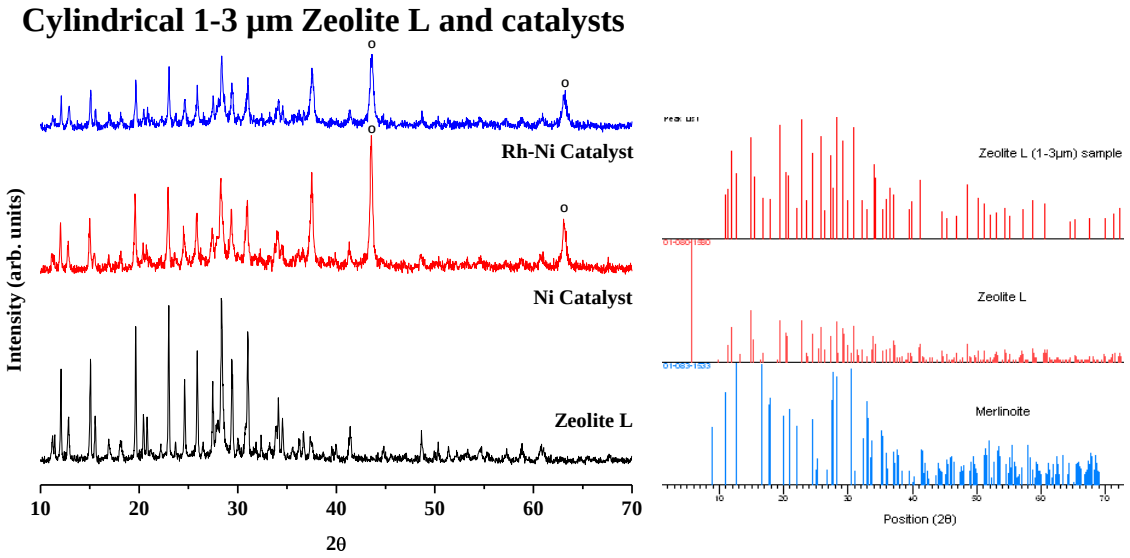

Figure 28: *a) XRD spectra for the Cylindrical (1-3 μm) Zeolite L and catalysts. NiO peaks are marked by "o" symbol. b) XRD diffractogram for the Zeolite L (1-3 μm).*

Lastly, in Figure 29, XRD spectra for Cylindrical (30–60 nm) Zeolite L and the resulting catalysts are shown. In this case, approximately 20 nm NiO crystals were detected for Ni catalysts. In the case of Rh-Ni catalyst, due to the dispersion effect again, NiO crystals of around 5 nm were found. In this case, the measured crystal sizes are very similar to the ones measured by the H_2 chemisorption technique (21.45 nm for monometallic; 9.79 nm for bimetallic catalyst). For this catalyst, no Rh interactions were noticed using this technique, but their presence, as for the rest of Rh containing catalysts, was confirmed by the X Ray Fluorescence and ICP-AES analyses.

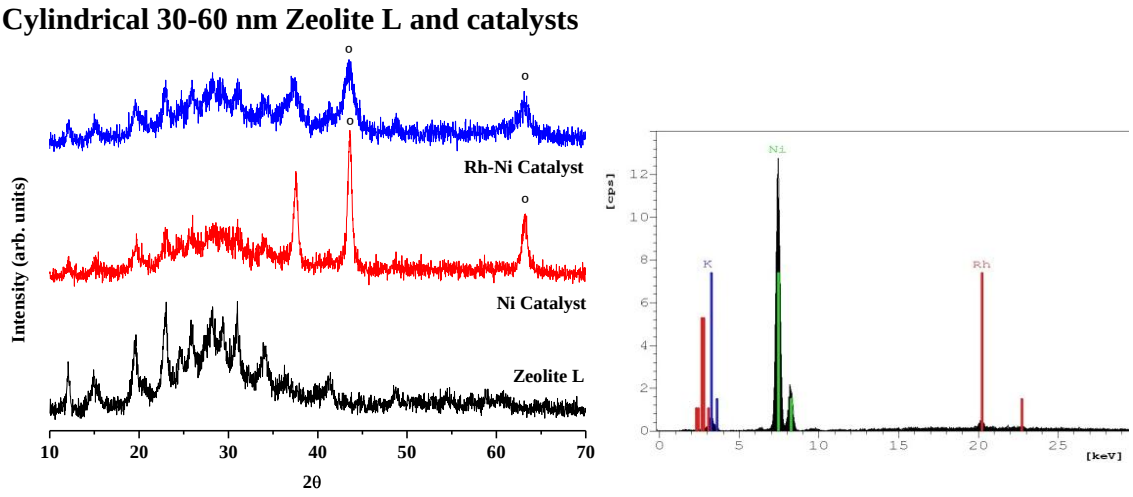

Figure 29: *a) XRD spectra for the Cylindrical (30-60 nm) Zeolite L and catalysts. NiO peaks are marked by "o" symbol. b) X-Ray Fluorescence analysis results for the Rh-Ni Catalyst.*

4.4.3.6 XPS results of the used samples

Information on the Ni state and the surface composition of the used catalysts was obtained by XPS analysis. For all catalysts, the binding energy of Ni $3p_{3/2}$ core level was measured at 856.6 eV and it was attributed to the Ni^{2+} species. The presence of metallic Ni was not observed in none of the samples. In the case of Rh, it was only detected for the Disc sample, suggesting that for the Cylindrical (30-60 nm) and Cylindrical (1-3 μm) the Rh should be incorporated into the porous structure. Deconvolution of the C 1s signal gives a peak at 284.5 eV with a small contribution at 286.6 eV that would be related to graphitic carbon and C=O [72], respectively. The C=O can be assigned to the interaction of CO_2 on the metallic and/or zeolite surface [73]. The presence of carbon species with a strong charge effect at around 282.7 eV was also observed.

Table 14 compiles the relative intensities of the total carbon with respect to the Rh-Ni and Ni catalysts used. The percentage of the C (1s) area coverage for the bimetallic samples is lower ranging from 30.9% to 39.4%. Thus, a higher percentage was measured for the Ni catalysts. Only the Ni catalysts obtained a low percentage that could due to the low activity achieved for this catalyst.

Table 14: *Tested catalysts surface composition obtained by XPS.*

Tested catalysts	Disc		Cylindrical (30-60 nm)		Cylindrical (1-3 μm)	
	Rh-Ni	Ni	Rh-Ni	Ni	Rh-Ni	Ni
Sample Relative intensities (%) of C(1s)	39.4	40.8	32.4	47.9	30.9	36.1

4.4.4 Activity results

All the prepared catalysts were tested for DR, BSR, BOR and TR reactions. The activity results presented in Figures 30 and 31 correspond to the measured parameter for each tested catalyst and studied process. Figure 30 presents the methane conversion results for the tested catalysts and studied processes.

Attending the results obtained for the different processes, in the DR process, the methane conversion reached almost the equilibrium values for the catalysts apart from the Ni and Rh-Ni (1–3 μm) catalysts, which did not reach that value. In the case of Ni Disc catalyst, the value reached was higher than the equilibrium due to the possible presence of hot spots inside the fixed bed reactor. For the BSR process, the effect of water addition by increasing the S/C ratio was not positive as the methane conversion measured did not change or slightly decreased. On the contrary, in the BOR process, the increase of oxygen content was positive for all the catalysts except for Ni and Rh-Ni (1–3 μm) catalysts, which was probably due to the heat being released by the methane oxidation reaction onto the particle surface. For the TR process, in the case of bimetallic catalysts, the methane conversion reached high values similar to the ones for BOR process at O_2/CH_4 = 0.25.

Focussing on the tested catalysts, the Ni and Rh-Ni (1–3 μm) catalysts presented lower values for methane conversion compared to other catalysts. Moreover, when the monometallic Ni (1–3 μm) catalyst was tested for BSR at S/C = 2.0 and TR processes, the measured methane conversion was negative. This fact might be due to the low affinity to water addition of this type of Zeolite L, which could inhibit these processes. The small amount of methane produced (4.9% in BSR and 6.1% in TR process) could be explained through the contribution of the methanation reaction [74], and can be due to the presence of Ni species in the hexagonal prism of Zeolite L.

Both, the Ni and Rh-Ni Disc and Cylindrical (30–60 nm) catalysts achieved higher methane conversions. For these catalysts, Rh incorporation improved the methane conversion reaching values higher than 80% in all the studied processes except DR. Therefore, the Zeolite L catalysts that were made showed that the presence of Rh evidenced a better catalytic activity. Indeed, for these bimetallic systems, for BOR at O_2/CH_4 = 0.50, and the TR processes, similar methane conversion values were achieved; thus, the water addition did not seem to clearly improve methane conversion.

Focussing on the results obtained, for the BOR process at O_2/CH_4 = 0.50, the methane conversion for Rh-Ni Disc catalyst was 97.53% and 95.10% for Cylindrical (30–60 nm) catalysts. In the TR process, the methane conversion for Rh-Ni Disc catalyst was 97.04% and 96.42% for Cylindrical (30–60 nm) catalysts. Therefore, the BOR at O_2/CH_4 = 0.50 and the TR processes using bimetallic Rh-Ni Disc and Cylindrical (30–60 nm) catalysts seemed to be the most appropriate conditions and catalysts to convert almost all the methane fed.

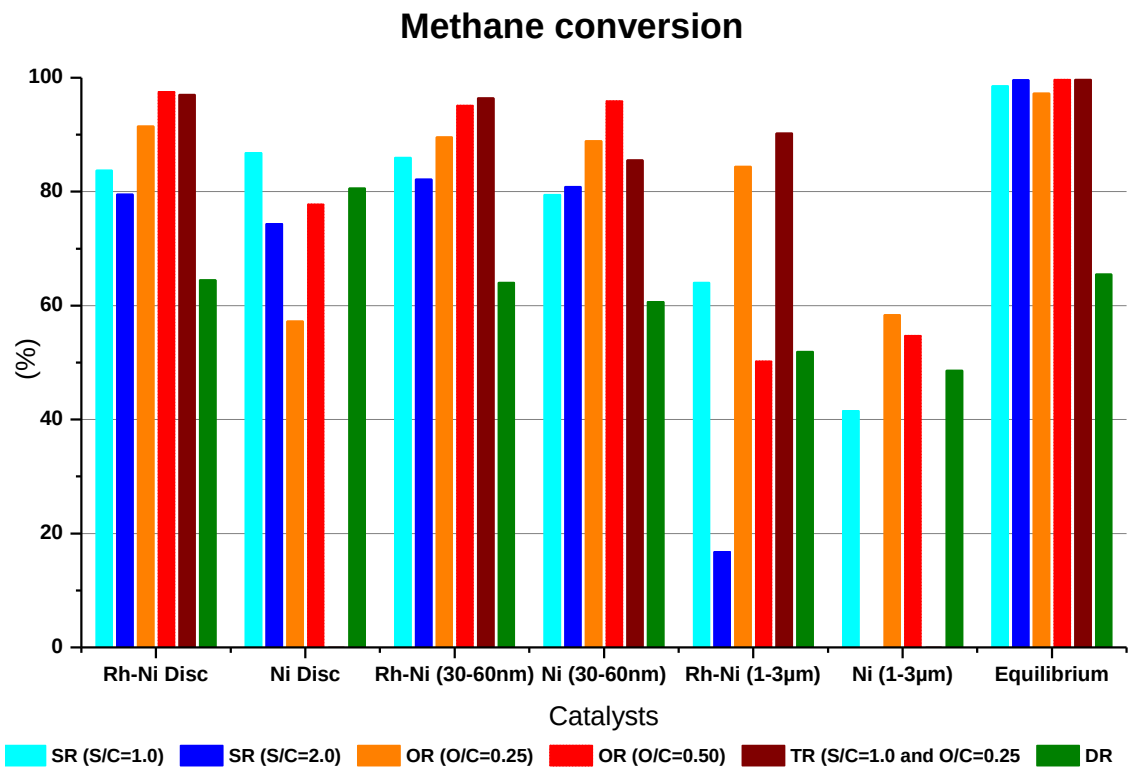

Figure 30: *Methane conversion results of the tested catalysts and studied processes.*

In Figure 31, carbon dioxide conversion activity results are shown for all the tested catalysts and studied processes. Regarding the processes studied, as it happened for the methane conversion, the CO_2 reforming capacity decreased when the S/C ratio was increased from 1.0 to 2.0. On the contrary, the high values for the methane conversion reached in the BOR at O_2/CH_4=0.50 and the TR processes, were not reached for the CO_2 conversion. For the BOR processes, the contrary tendency was followed because higher CO_2 conversions were reached when lower oxygen was introduced in the system. This could be due to the presence of more methane that could react with the CO_2 through the DR reforming reaction. And finally, for the CO_2 conversion, the DR and the BOR at O_2/CH_4=0.25 processes reached the maximum values -very closed to the equilibrium conversion- except for the Ni (1-3 µm) catalyst.

Taking into account all the processes studied, for the bimetallic Rh-Ni Disc and Cylindrical (30-60 nm) catalysts CO_2 equilibrium conversions were almost achieved in all the tested processes. For those two catalysts is evidenced that the presence of Rh metal again increased the CO_2 conversion values in all the tested processes and conditions (Except to the BSR process at S/C=1.0).

Focusing in the results, for Ni Disc catalyst, this catalyst did not show apparent activity when it was tested in the TR process as the CO_2 and CH_4 conversion values demonstrate with a minus 9.2% of CO_2 conversion and minus 11.9% of CH_4 conversion which could be associated to the methanation reaction [74].

Regarding the Ni and Rh-Ni (1-3 µm) catalyst, they showed lower CO_2 conversion capacity if they are compared with the rest of the catalysts, nevertheless the measured values were specially high for the BOR at O_2/CH_4=0.25 and DR processes. For the Ni (1-3 µm) catalyst, the CO_2 conversion was minus 10.5% at S/C=2.0 and minus 7.5% for the TR process.

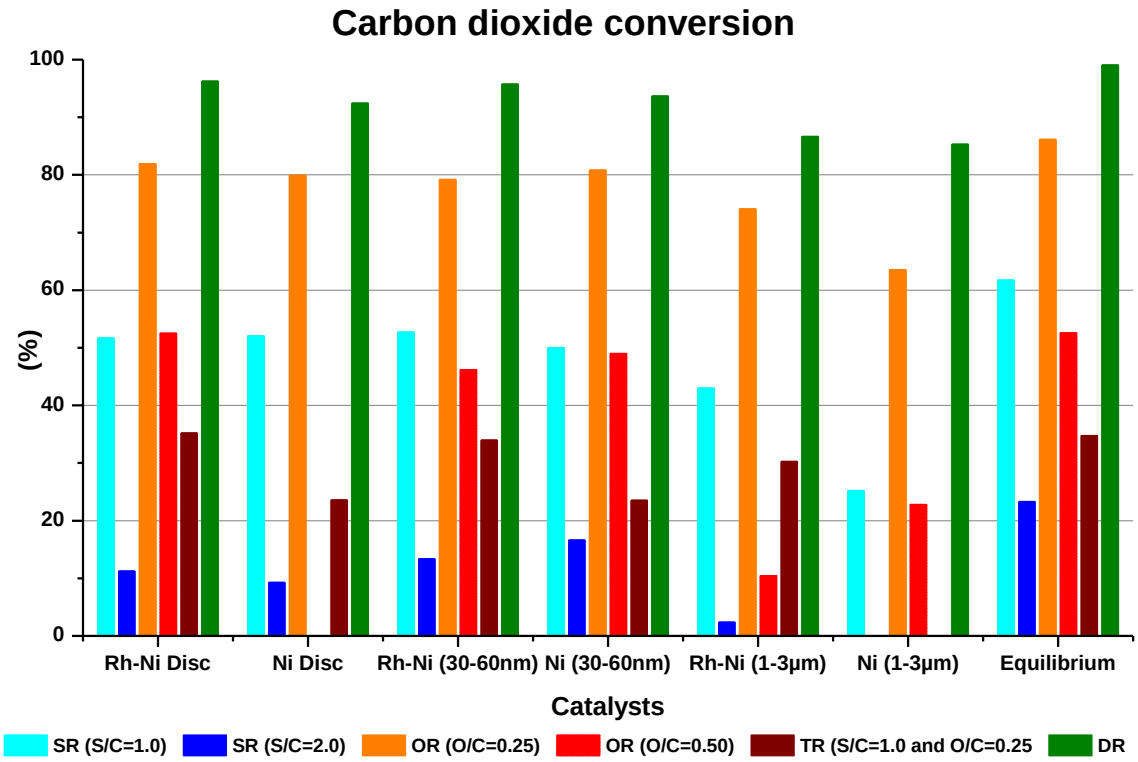

Figure 31: *Carbon dioxide conversion results of the tested catalysts and studied processes.*

In Figure 32 hydrogen production yield results of the tested catalysts and processes are represented. This parameter depends on the hydrogen produced and the methane and water fed to the system (see section 4.2.1 Activity measurements). Thus, the hydrogen production flow-rate depends on the catalysts activity, the methane volumetric flow-rate -that was kept constant in all the studied processes- but in the case of the water content, it was different in the tested processes and for the BOR and DR processes, no water was added to the system. This means that comparisons should be made in a certain process between the tested catalysts.

Attending to the previous considerations, the bimetallic Disc and Cylindrical (30-60 nm) catalysts seemed to be the most appropriate ones for the different studied BSR and BOR processes obtaining the highest hydrogen yield for the BOR process at the O_2/CH_4 ratio of 0.25.

As a consequence of the poor methane and carbon dioxide conversions reached by the Ni and Rh-Ni (1-3 µm) catalysts, the lowest hydrogen production yields were achieved by these catalysts.

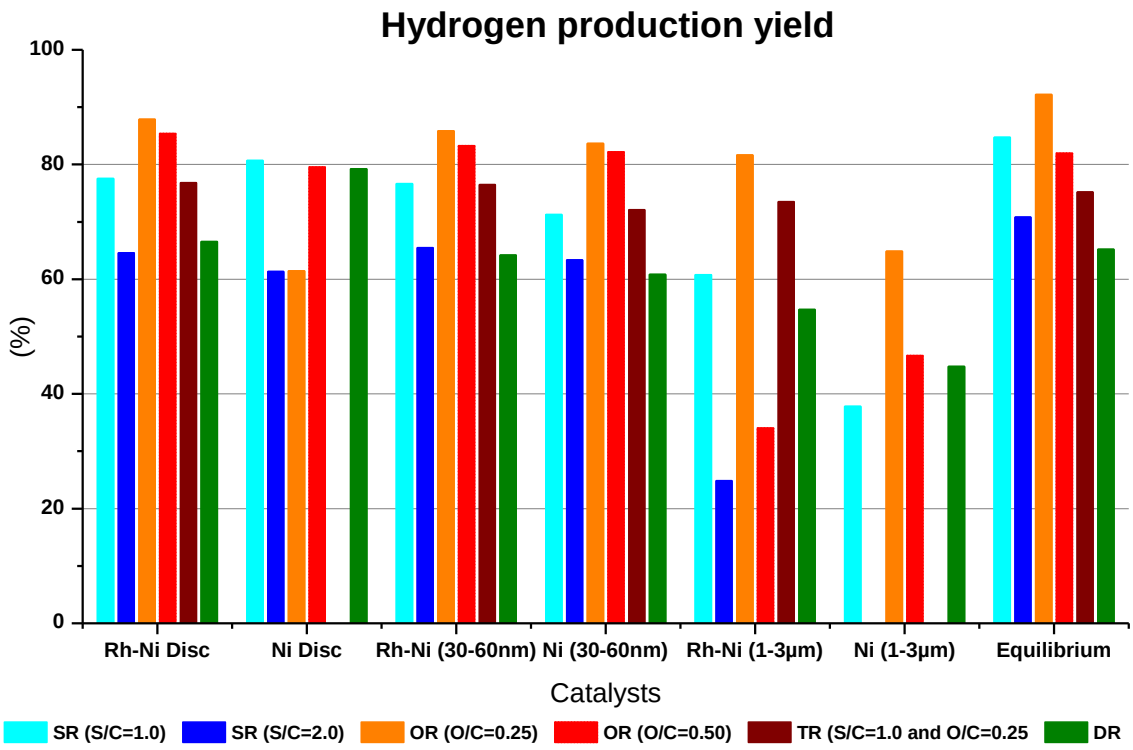

Figure 32: *Hydrogen production yield results of the tested catalysts and studied processes.*

Finally, in Figure 33, the last calculated parameter results are shown, which corresponds to the synthesis gas ratio, H_2/CO. The desired ratio for liquid hydrocarbons production through Fischer-Tropsch synthesis and for the methanol synthesis is close to 2 [11,22,23]. Moreover, a synthesis gas ratio of 1 is needed for the Oxo (also known as hydroformylation), which can be obtained through DR and BOR processes.

Focussing on the equilibrium calculations results, BSR at S/C = 2.0 is the unique process that overcomes this ratio. For the BSR at S/C = 1.0 and TR processes, ratios near to this value can be obtained so that a subsequent step (apart from the purification) should be considered to achieve the desired syngas ratio of 2. Operating in BOR or DR processes conditions, syngas ratios of 1 can be reached. In any case, the most active catalysts would be selected in order to achieve the highest conversion values and the most selective ones in order to facilitate the subsequent purification steps.

With regard to the catalysts' results, for H_2/CO ratio, close values to 2 for were reached for almost all the catalysts as it should be expected for the equilibrium ones. Only Ni (1–3 μm) catalysts did not reach those values.

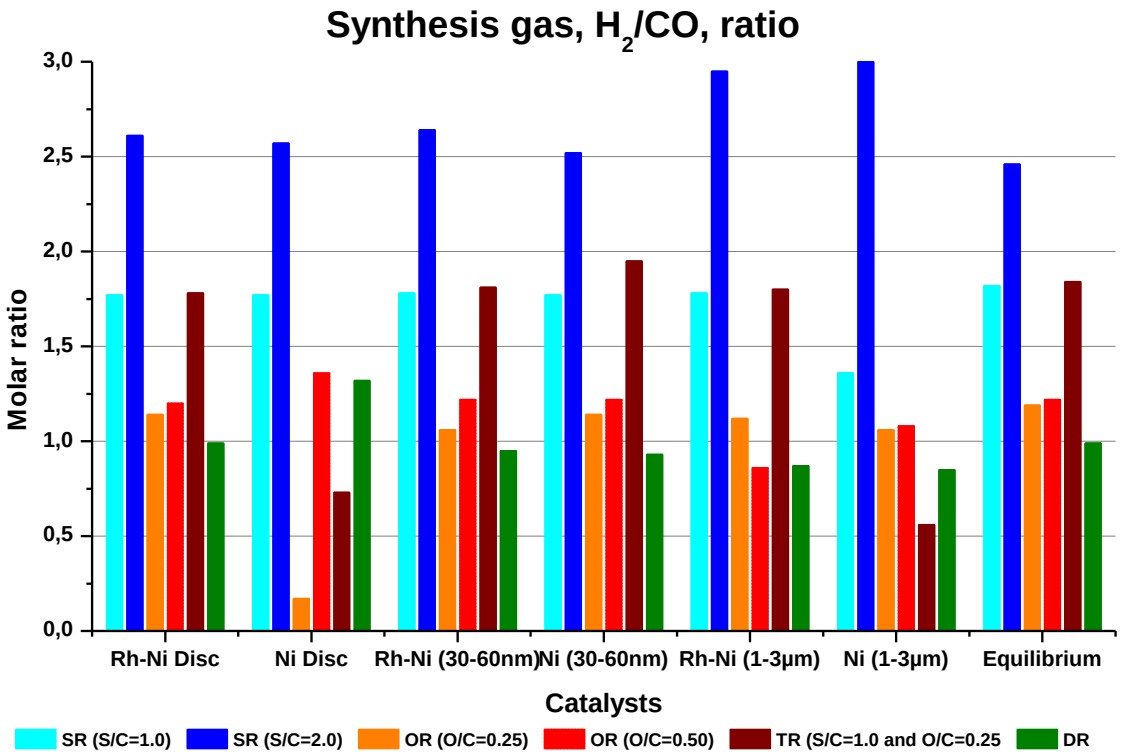

Figure 33: *Synthesis gas, H_2/CO ratio results of the tested catalysts and studied processes.*

In Figure 34, the H_2 yield, metal dispersion and ICP-AES results (as metal content) are represented for Zeolite L studied catalysts and for the γ-Al_2O_3 catalysts [44] in order to compare them. For the Disc and Cylindrical (30-60nm) catalysts higher H_2 yields were reached for similar metals content. This higher production of hydrogen can be attributed to the higher dispersion of the metals incorporated into the Zeolite L measured by H_2 chemisorption. As it was commented before, in Section 3.1.1., in the case of the Cylindrical Zeolite L the metal dispersion achieved for both samples was very high with a very small particles size. Nevertheless, the anchorage of NiO species for the bimetallic sample (as TPR analysis shown) enhanced a higher performance for this catalytic sample. For the Ni Cylindrical (30-60 nm) and bimetallic Rh-Ni Disc and Cylindrical (30-60 nm) catalysts, hydrogen yield higher than 80% was reached. In the case of the bimetallic samples lower carbon was measured by XPS covering the external surface.

Comparing the results with the ones obtained for γ-Al_2O_3 catalysts higher hydrogen yields, for γ-Al_2O_3 catalysts, the maximum hydrogen yield achieved was around 70% while for the Zeolite L catalysts was higher than 80%. Thus, the support had a clear effect improving the hydrogen obtained.

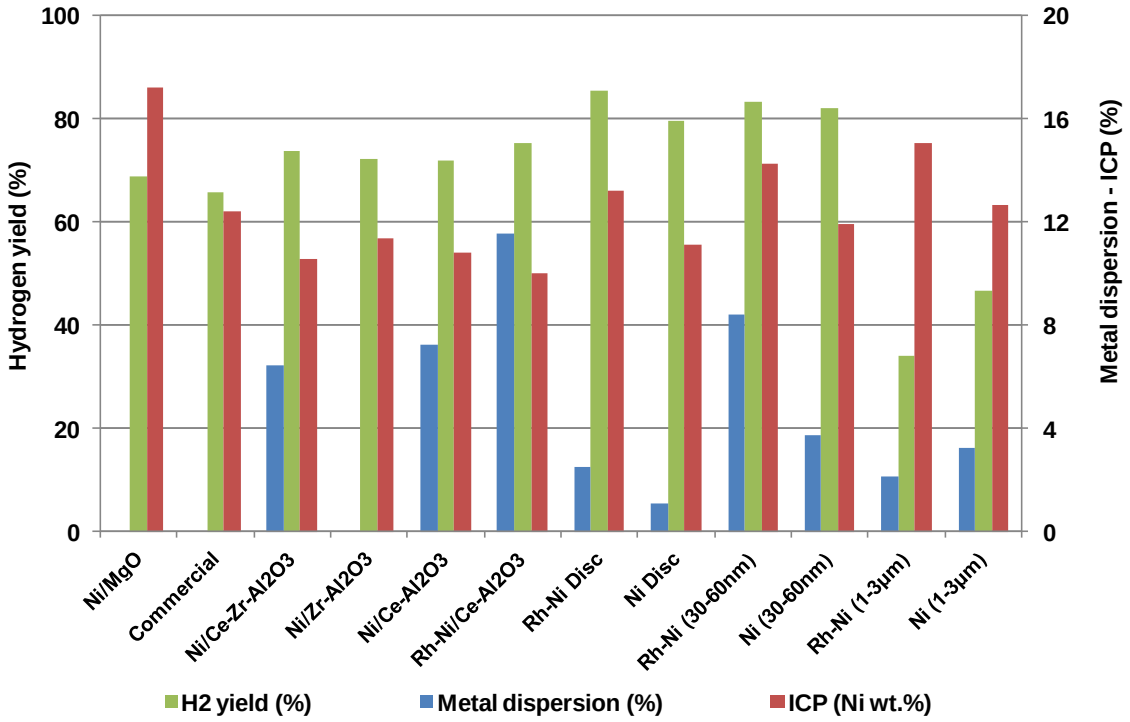

Figure 34: *H_2 yield, metal dispersion and ICP-AES results for the tested catalysts.*

4.4.5 Conclusions

The main objective of this work was to use Zeolite L as a catalyst support based on Ni and Rh-Ni metals for the study of several biogas reforming processes in order to generate renewable energy. In this sense, the hydrogen and/or syngas generated and their possible uses were also analysed.

Taking into account the catalysts' activity and according to the morphological difference between the Disc and Cylindrical (30–60 nm) Zeolites L, different activities were measured. For the BSR processes, the Disc catalysts were more active at the lowest S/C ratio, and the activity decreased when the S/C ratio increased to 2.0. On the contrary, the Cylindrical (30–60 nm) catalysts were more active in BOR at O_2/CH_4 = 0.50 and decreased when the S/C ratio increased to 0.5.

In all the tested processes, Ni and Rh-Ni catalysts based on Cylindrical (1–3 μm) Zeolite L achieved the lowest activity values. This could be associated to: i) the presence of Merlinoite zeolite – detected by XRD – which contributes around 25% of the sample, and ii) the presence of NiO species with low interaction with the support – measured by TPR – that were not active.

With the exception of Ni Disc catalysts for BSR at S/C = 1.0 and DR processes, the bimetallic catalysts showed much better reforming capacities in the tested processes and conditions. Thus, Rh incorporation increased catalytic activity in all the reforming processes tested and obtaining a low carbon deactivation (measured by XPS). The Rh-Ni catalysts based on Disc and specially the Cylindrical (30–60 nm) Zeolite L seemed to be a very promising catalyst due to its very high metallic dispersion (measured by H_2 chemisorption), the presence of NiO species with strong interaction with the support (measured by TPR), and excellent activities. Therefore, the nano Zeolite L, prepared with the lowest size of particle incorporated into Zeolite L, was most active for the biogas reforming reaction.

4.5 Biogas reforming processes using Na^+ and Cs^+ doped Zeolites LTL based catalysts

A published paper:

Title: Microwave synthesis of LTL zeolite with tunable size and morphology: an optimal support for metal-catalyzed hydrogen production from biogas reforming processes

Authors: L. Gartzia-Rivero[1], J. Bañuelos[1], U. Izquierdo[2], V.L. Barrio[2], K. Bizkarra[2], J.F. Cambra[2], I. López-Arbeloa[1]

[1] *Dept. of Chemical Physics, University of the Basque Country UPV/EHU Apartado 644, 48080 Bilbao, Spain*

[2] *Dept. of Chemical and Environmental Engineering, School of Engineering, University of the Basque Country UPV/EHU, c/ Alameda Urquijo s/n 48013, Bilbao, Spain*

Journal: Particle & Particle system characterization

Year: 2013

4.5.1 Introduction

The term `zeolite´ is said to have its origin in the two Greek words *zeo* and *lithos*, meaning `boiling stone´ [75,76]. In general, zeolites are microporous crystalline aluminosilicates with well-defined three-dimensional pore structures, where water and other type of molecules such as co-cations and organic molecules can allocate [77,78]. Among the wide variety of natural and synthetic zeolites, Linde Type L zeolite (LTL) is one of the most interesting and versatile hosts. Its framework is characterized by one-dimensional channels running along the crystal with hexagonal symmetry. The well-arranged pores of around 7.1 Å in diameter make this kind of framework an excellent candidate for shape-selective catalysis, host for several different type of guests (ions, metals, organic molecules...), and for mass transport and/or occlusion [79]. In fact, LTL zeolite has been used in a broad range of fields: catalytic processes [80], ion-exchange and separation [81], antenna materials [53,82], photosensitizers in solar cells or light-emitting diodes, luminescent solar concentrators [83], colour changing media, and is also widely used in bio-medicine [84].

For these nanoscale materials to be competitive it is essential to ensure a good quality of the LTL zeolite crystals, which means homogeneous size distribution of the crystals, defined morphology, and high crystallinity. LTL zeolite is mostly synthesized under hydrothermal conditions using high-pressure vessels and heating with conventional ovens. Gel composition (water content, alkalinity, oxides proportion) as well as the heating conditions (heating rate and temperature) determine crystal size and morphology. LTL zeolites with sizes ranging from nanometers to micrometers and barrel-or disc-shaped morphology have been reported [85-87].

Microwave heating has become a valuable tool in modern organic synthesis and in the production of nanoparticles and nanostructures. It provides an accurate control of the temperature, ensuring temperature uniformity, preventing gradient formation within the oven and samples. Therefore, the heating process is more efficient, chemical reaction times are reduced, and side reactions are avoided in great extent. This means, an improvement in the yield and reproducibility of the process, and hence, a friendlier environmental methodology [88].

For this study, we have extrapolated the optimal conditions described in previous reports on LTL zeolite synthesis using conventional ovens, to microwave heating [67,89]. One of the aims of this work is to improve crystal quality and decrease the reaction time needed for its synthesis, which otherwise takes several days. We have analyzed the effect of the reaction conditions (heating rate, time, temperature, and static/dynamic conditions) on the size, morphology, and chemical properties (acidity, ion-exchange capacity) of the resulting crystals.

These LTL zeolite crystals were then used as catalyst supports due to their high surface area and structural stability, combined with their chemical composition [46,50]. Once the catalysts

were prepared, the biogas valorisation – a renewable resource – for hydrogen production through dry and oxidative reforming (DR and BOR respectively) processes was studied. DR process is being widely studied because methane and carbon dioxide are consumed in the system, both considered the most harmful green house gases. Regarding the active phase of the catalysts, nickel and rhodium metals were used to prepare the corresponding bimetallic catalysts.

The selection of the type of process and the experimental conditions has been carried out on the basis of our previous results; it was reported that a ratio of O_2/CH_4=0.25 was the most appropriate one to reach the highest hydrogen production yield for BOR process [44], and a H_2/CO ratio around 1 was appropriate for the hydroformylation reaction [44,90].

With regard to the active metal species incorporated to these supports, Nickel was chosen because it is widely used for reforming reaction catalysts, mainly due to its high activity, availability and relatively low price. However, it is well known that noble metals like Rhodium (Rh), Ruthenium (Ru), Palladium (Pd), etc. are much more active, stable and their use decreases the tendency to coke formation in the catalytic surface at high temperatures [29,31], especially when Rh and Ru are used [66]. Although the noble metals are much more expensive, their use is recommended because the addition of small amount of noble metal to a non-noble metal catalyst leads to an increase in the activity due to the spill-over effect [27]. Therefore, the synthesized zeolites under microwave heating have been tested as support for the corresponding catalysts. To this end, the parameters to evaluate the methane and carbon dioxide conversion, as well as hydrogen production yield, have been calculated to understand their activity.

4.5.2 Cs^+ and Na^+ doped zeolites catalyst preparation for DR and BOR

The size and morphology of LTL zeolite crystals can be modulated by changing the source of the reactants, the composition of the gel (alkalinity, water content, SiO_2/Al_2O_3 ratio, etc.), the reaction time, the reaction temperature, and the aging time of the gel. We initially used a fixed gel composition (previously optimized) [67] for each type of zeolite (nanocrystals and disc- or coin-shaped crystals) and analyzed the influence of the reaction conditions and gel pre-treatment in the microwave-assisted hydrothermal synthesis. In all cases, this type of heating reduced the synthesis time up to 90% with regard to conventional ovens (days to hours) and enabled a more precise control of the temperature preventing gradient formation within the sample. Therefore, zeolites can be produced in few hours, with the consequent saving in time and energy and improved quality.

4.5.2.1 LTL zeolite nanocrystals

In these small zeolites, diffusion of the guest molecules (i.e., metals) deeper inside the pores of the host is much easier, and, at the same time, they are better supports for adsorption processes because of a larger external surface.

The general hydrothermal synthetic route is detailed in the experimental section. The oxide molar ratio in the gel was fixed at $9.34K_2O:1.00Al_2O_3:20.20SiO_2:412.84H_2O$ [67]. The nanocrystals were successfully obtained after heating at 170 ºC for one hour and straightaway identified by the X-ray diffraction pattern. The corresponding dimensions, ranging from 15 to 50 nm were determined using SEM and TEM images (Figure 35). The particles show a general tendency to agglomerate into larger clusters of 80-100 nm, not allowing a size distribution analysis.

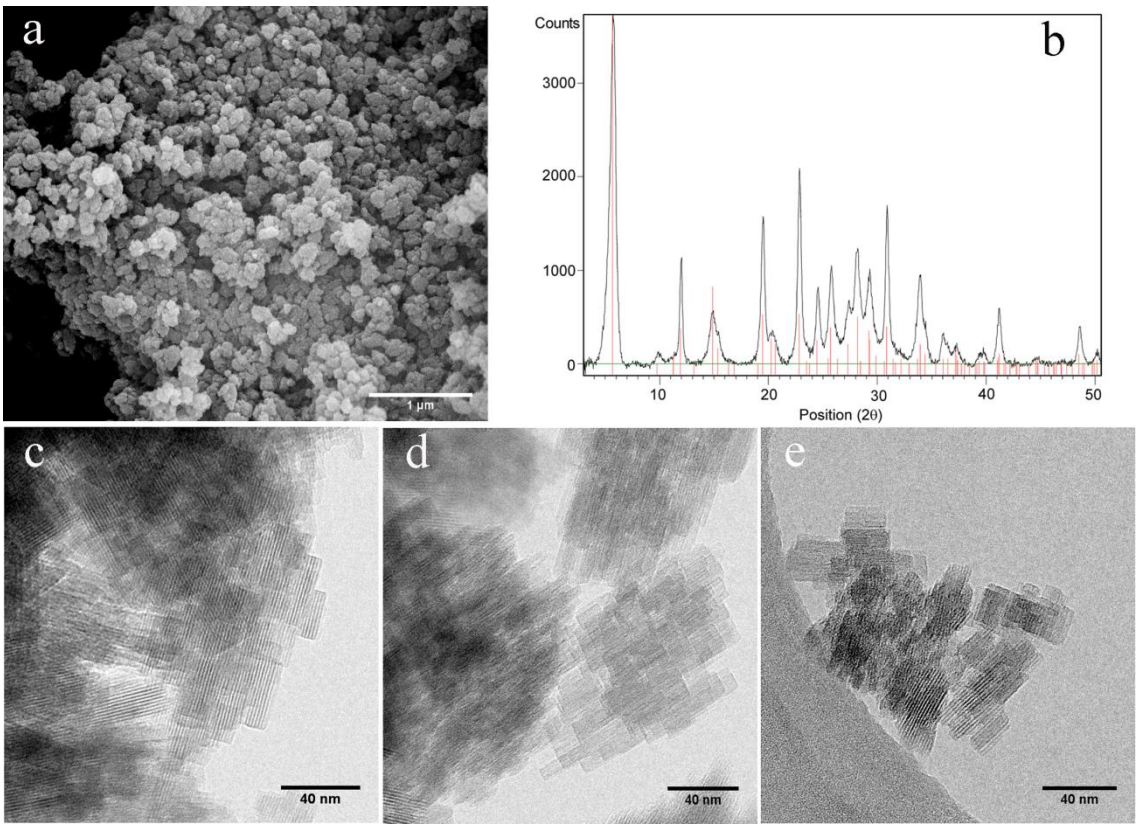

Figure 35: *a) SEM image of LTL zeolite nanocrystals, synthesized with Ludox OX-50, and the corresponding X-ray diffraction pattern (background extracted) (b) for phase identification (PDF from database in red is included for comparison). TEM images of LTL zeolite nanocrystals obtained under static (c) or dynamic conditions (d) and after aging of the synthesis gel (e).*

The growth of crystals can be controlled by several factors such as static/dymamic conditions during synthesis, previous aging of the gel before heating or with different silica sources. Figures 35c and 35d show the TEM images of the nanocrystals obtained under static and

dynamic conditions (stirring during the synthesis). The static crystallization led to crystals with a size of about 40 nm, whereas the dynamic conditions yielded smaller crystals (around 15-20 nm), both keeping the cylindrical morphology (aspect ratio defined as length/diameter, decreased from 3.5 to 2.5). In previous reports using conventional heating, dynamic and static conditions had a negligible impact on the size or morphology of crystals smaller than 1000 nm [67,89,90]. The crystallization process is thermally activated, thus the heating method plays a crucial role in it, particularly the rate and uniformity of the heat applied to the reaction mixture, enhanced when microwave heating is used. Therefore, stirring is recommended for smaller nanoparticles probably because it hampers crystal growing and favours the formation of seeds.

The aging of the gel, before the heating process, also determines the nucleation/growing of the crystals. Figure 36e shows that a 4-hour aging at room temperature allowed obtaining crystals with a length of around 20 nm and an aspect ratio of about 2.5. Thus, comparing with the nanocrystals synthesized in static conditions, the aging of the gel reduces crystal size, because same as with the dynamic conditions, it boosts the formation of more nuclei rather than their growth.

Finally, we also checked the effect of silica source: a water-silica suspension (LUDOX HS-40) or a suspension prepared from silica powder (Aerosil OX-50). Each type of silica contains different impurities exerting different effects on crystal nucleation, thus generating LTL zeolite crystals with characteristic properties in each case. The LTL zeolite nanocrystals obtained using Ludox HS-40 as the silica source and those generated with Aerosil OX-50 are depicted in Figure 35 and Figure 36, respectively. The latter crystals, in Figure 36, seem to be slightly larger. To verify the intuitive results from the TEM images, the average crystal size was estimated (defined as average domain size) by the Scherrer equation:

$$\beta_{hkl} = k \cdot \lambda / L_{hkl} \cdot \cos\theta \qquad (6)$$

where k is a dimensionless shape factor (k=0.9), λ is the X-ray wavelength (λ=1.54 Å), L_{hkl} the line broadening at half maximum intensity (β_{Inst}=0.1°), and θ is the Bragg angle using two. This equation was applied for two different reflection families, such as (00l) and (hkl), from which information related to the length and diameter of the crystals was respectively extracted.

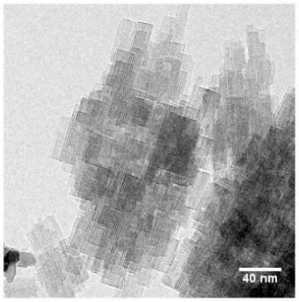

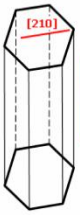

Silica Source	Crystallite Size [nm] (210)	Crystallite Size [nm] (001)
Ludox HS-40	15	50
Aerosil OX-50	9	65

Figure 36: *TEM image of LTL zeolite nanocrystals synthesized using Aerosil OX-50 as silica source. The crystallite sizes (determined by Scherrer formula) are tabulated and classified into the two crystallographic reflections suitable for describing the length (001) and diameter (210), according to the scheme, of LTL zeolite nanocrystals obtained by two different silica sources.*

Results confirmed that the crystals achieved using Aerosil OX-50 were slightly longer. Possibly, the synthesis gel prepared with Aerosil OX-50 needs a much longer crystallization time to yield the same product than when using Ludox HS-40. That is, Ludox HS-40 allows a faster nucleation time and provides more nuclei, which implies a high number of crystals but with a smaller size. Therefore, smaller nanocrystals are obtained using Ludox as the silica source and dynamic conditions for an aged gel.

4.5.2.2 Disc-shaped LTL zeolite crystals

In the previous section, we have shown how crystal size can be adjusted by the synthesis conditions. Nonetheless, the morphology of the crystal can be also controlled. Thus, crystals with disc shape are available (low aspect ratio) where their thickness can be also modified in a controlled way. This type of zeolites are desirable to ease their coupling with external devices (i.e., to obtain uniform and well-organized monolayers or membranes) [91], and to have a high number of one-dimensional pores with short diffusion path lengths (around 100,000 channels in a crystal with diameter of 600 nm) [92].

The synthetic procedure is detailed in the experimental section. Gel composition was set at $5.40K_2O$:$5.50Na_2O$:$1.00Al_2O_3$:$30.00SiO_2$:$416.08H_2O$ oxides molar ratio [67,89], using Ludox as silica suspension. After heating in a microwave oven at 160 ºC, disc-shaped LTL zeolite crystals were achieved. These particles exhibit a homogeneous morphology with an average length of 200 nm, and an average diameter of 1 µm (aspect ratio < 1), which varies upon the heating-rate and reaction time, since both factors control the growing of the crystal. Accordingly, the size distribution of these particles studied by DLS (Figure 37) provided two main populations; one assigned to crystal length and the other one to the diameter, depending on the direction the laser passed in the different surfaces of the crystal. The shoulder at lowest sizes represents the length of the discs, while the peak at higher ones shows the data referred to the diameters.

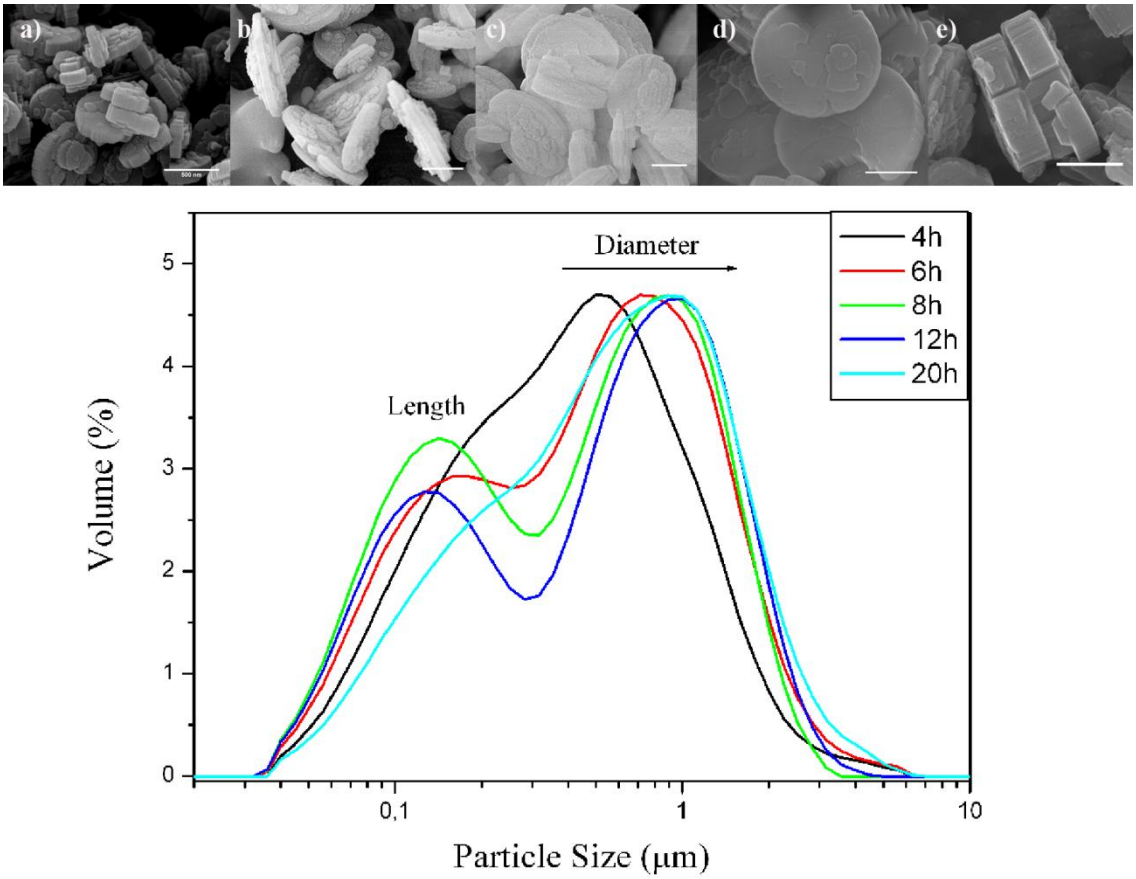

Figure 37: *SEM images of disc/coin-shaped LTL zeolite crystals synthesized under a) 4h, b) 6h, c) 8h, d) 12h and e) 20h of reaction-time together with the corresponding particle size distribution for each crystal by DLS. All the scale bars indicated the same distance (500 nm).*

The high quality of the herein reported LTL zeolite obtained by microwave is not only evident by their narrow size-distribution and homogeneous morphology, but also by their purity and crystallinity. The X-ray full-profile refinement allowed the comparison between experimental and calculated profiles, and the determination of compound unit cell parameters (a,b=18.35, c=7.52Å). Figure 38 highlights the nice agreement (Y_{obs}-Y_{calc} values, blue line) of our homemade LTL zeolite crystals, without sign of crystalline impurities. The low line broadening in the XRD pattern confirms their high crystalline grade. Indeed, the crystalline size (calculated by the Scherrer formula, Table S1 in Supporting Information) indicates that a unique particle contains few crystalline domains, indicating the high quality of the synthesized particles.

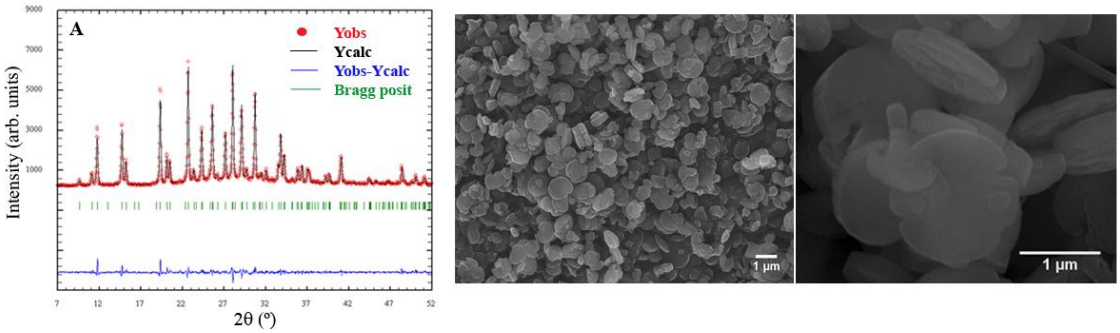

Figure 38: *X-ray full-profile refinement of LTL zeolite synthesized by microwave fitted by the Fullprof program without structural model. SEM images at different magnifications are also enclosed.*

The reaction time is a crucial parameter since it determines the nucleation and growing processes, and hence the size and morphology of the LTL zeolite crystals. We have carried out several independent hydrothermal syntheses just changing the reaction time from 4 to 20 hours. The increase of the reaction time to 12 h led to bigger (longer diameters, from 0.6 to 1.2 µm), but thinner crystals (lower length, from 180-130 nm), as shown in Figure 38. From this point on, the crystal stopped growing in diameter, only increasing in length, which means thicker discs (180 nm length). Therefore, we can obtain thin (coins) or thick discs by only adjusting the reaction time in the microwave oven. In fact, in cases in which the length of the crystals was similar to the diameter (reaction time of 4 and 20 hours), the peak corresponding to the lowest sizes could not be properly distinguished due to the proximity between them. Furthermore, enlarged synthesis times led to smooth crystal surfaces (Figure 37). Therefore, crystals with aspect ratio between 0.3 (discs) and 0.12 (coins) can be generated by only changing the reaction time in few hours. This implies that the number of pore openings per total external surface of the crystals can be controlled, as well as the diffusion path length, which is expected to have an impact on reaction rates.

In contrast to conventional ovens, microwave ovens allow controlling the heating-rate, which greatly improves the heat-up speed and prevents temperature gradients. Thus, we analyzed the time needed to reach the synthesis temperature (from 10 min to 1 h) maintaining the same reaction time and temperature. Figure 39 shows that a faster heating-rate led to a predominantly amorphous phase, whereas the slower one yielded a more crystalline phase, without signs of amorphous population. It seems that a heating-rate that is too fast prevents the formation of the nuclei necessary for the crystallization of LTL zeolite, while a slower heating rate promotes the formation of abundant nuclei.

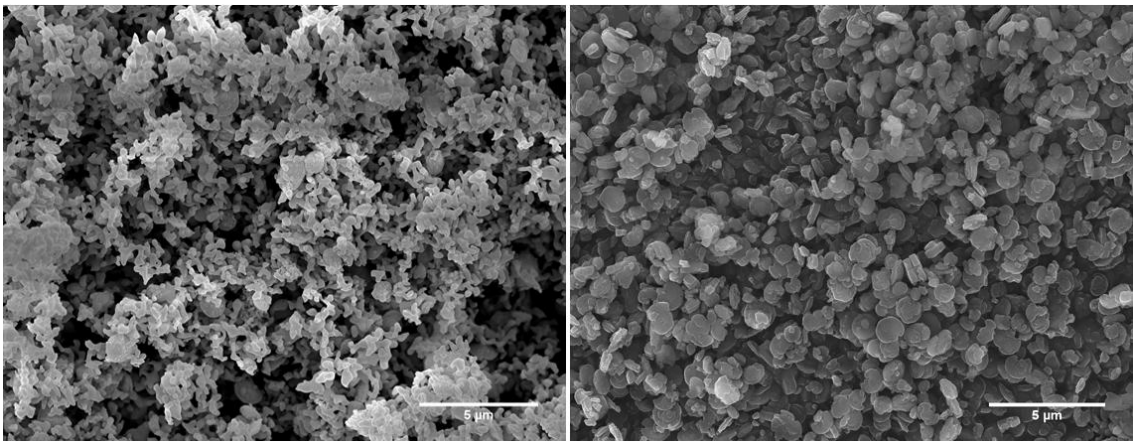

Figure 39: *SEM pictures of LTL zeolite crystals after 4 h of crystallization and different heating-rates: a) 10 min, b) 1 h.*

Summarizing, highly crystalline discs with a controlled thickness can be obtained by just fixing the reaction time at a slow enough heating rate.

4.5.2.3 Zeolites sysnthesis and catalysts preparation

Synthesis of LTL zeolite: The amount of oxide reactants was set to obtain an optimal gel composition for each type of zeolite, either nanosized or disc-shaped. The alumina and silica suspensions required for the gel were prepared separately. The alumina suspension was prepared mixing potassium hydroxide and aluminium hydroxide in bidistilled water and the solution refluxed in an oil bath at 120ºC until a clear solution was obtained. On the other hand, potassium hydroxide dissolved in bidistilled water was added to a silica suspension (Ludox HS-40, supplied by Sigma-Aldrich or Aerosil OX-50 by Evonik Industries) and refluxed for 14 hours in an oil bath at 120ºC.

After cooling the suspension to room temperature, the potassium aluminate solution was added to the potassium silica suspension under vigorous stirring. The obtained gel was transferred to a PTFE pressure vessel and heated in a microwave oven (Ethos1, Milestone) at 160ºC or 170ºC for nanosized and disc-shaped zeolites, respectively. Once the crystallization process was finished, the vessel was cooled to room temperature. The obtained product was washed with boiling bidistilled water until the pH of the supernatant was neutral. Finally, the powder was dried at 90ºC for 16h.

Next, the LTL zeolite was exchange with Na^+ and Cs^+ to adjust the pH inside the channels. In order to achieve this, the LTL zeolite was suspended in water and exchanged with an excess of NaCl or CsCl under reflux and stirring for 45 minutes at 80ºC [93]. The cation-exchanged zeolites were then washed and dried in the oven.

Catalyst preparation: First, the zeolites were calcined at 1073 K for 4 h in order to stabilize the supports. Then, through the wetness impregnation method, the six Rh-Ni bimetallic catalysts were prepared. To this end, an aqueous solution that consisted on Nickel (II) nitrate hexahydrate (99.99%; Sigma Aldrich) and Rh (III) nitrate hydrate (~36% as Rh; Sigma Aldrich) was added to reach an intended load of 13 wt.% of Ni and 1wt.% of Rh respectively. The corresponding solutions were stirred for 2 h using a rotatory evaporator and then heated up until all the water was removed. Next, the catalysts were dried and calcined at 1073 K for 4 h in the oven. The calcinations were carried out under an oxidative atmosphere in order to ensure oxidation of the metal species, and remove the salts of the reactants used for their preparation as well as the possible humidity inside the pores.

4.5.3 Na^+ and Cs^+ doped zeolites fresh and calcined catalysts characterization

4.5.3.1 Textural properties

Table 15 summarizes the textural properties measured for the calcined zeolites and catalysts in which high surface areas are observed, especially for the Nano (N) calcined zeolites. The mentioned calcination process affects directly to the LTL zeolite surface area, as was reported in our previous work, by decreasing their surface area and the total pore volume [94]. In addition, the micropore region is also significantly affected. However, this process is essential to stabilize the support and remove the salts incorporated during the catalyst preparation process.

Table 15: *Textural properties of the calcined supports and catalysts.*

	BET (m^2/g)	Pore volume (cm^3/g)	Micro Pore volume (cm^3/g)	Pore size (Radius, A)
D-Na^+	0.4	0.0058	0	263.9
Rh-Ni/D-Na^+	3.1	0.0042	0	250.9
D-Cs^+	12.7	0.0757	0.0020	121.6
Rh-Ni/D-Cs^+	17.1	0.1313	0.0009	155.0
Disc	59.0	0.0690	0.0223	30.48
Rh-Ni/D	38.1	0.1261	0.0115	71.96
N-Na^+	143.5	0.7436	0.0225	105.9
Rh-Ni/N-Na^+	42.9	0.1653	0.0044	77.0
N-Cs^+	96.3	0.6473	0.0097	135.6
Rh-Ni/N-Cs^+	36.5	0.1544	0.0024	84.8
N	210.4	0.7851	0.0493	78.61
Rh-Ni/N	68.4	0.1935	0.0093	58.87

Comparing the Disc (D) and N zeolites, higher areas were obtained for the N zeolites, especially for the pure one (210.4m^2/g). Moreover, as it was expected, in general lower areas were measured after metal incorporation.

In the case of D zeolites, for the D-Na^+ and its homologous catalyst, a very low surface area was measured. This effect could be a consequence of the calcination process where a strong sintering of this support was observed, while the rest of the catalysts maintained their particle size distribution. This could explain the low BET area measured. In the case of the other two Disc zeolites and catalysts, lower areas were measured for the D-Cs^+ zeolite and catalyst in comparison with the D ones. An unexpected higher are for the catalyst than for the support was measured for the D-Cs^+ zeolite.

Attending to the N zeolites, the Na^+ and Cs^+ incorporation decreased the surface area and pore volume, while the pore size increased. The incorporation of Cs^+ reduced in a greater extent the surface area than for the Na^+.

When metal atoms were incorporated to the N catalysts the pore volume decreased, which may be due to the incorporation of the metal particles into the pores. In contrast, the observed increase of such parameter for the D catalysts might be due to structural changes in the LTL zeolite framework.

4.5.3.2 TPR profiles

In the Figure 40 the TPR profiles for the fresh calcined catalysts are shown. It is well known that the temperature reduction of particles depends on the location and the type of interaction of the metal with the support [95]. The catalysts supported on the Disc-shaped zeolites started the reduction at lower temperature probably due to a weaker metal-support interaction.

In addition to the TPR profiles, the deconvolution of the peaks for the Rh-Ni/D and Rh-Ni/N catalysts was carried out in order to explain the contribution to the peaks formed by the different Ni and Rh interactions with the support. For the N catalysts two main peaks were detected at 470 and 565ºC respectively. According to the literature, the peak at 470ºC is attributed to the reduction of the NiO species [95]. The presence of the peak at higher temperature could suggest a strong interaction between Ni and support. Even more, for these catalysts no Rh species reduction peaks at low temperature were observed. However, for the D catalysts a rhodium oxide reduction peak at low temperatures, around 185ºC, was detected [96]. For these catalysts lower temperatures were needed to reduce all the metal species. In addition, for the D catalysts the presence of an additional reduction peak was observed, which could be attributed to some other interaction of the metal atoms with the support.

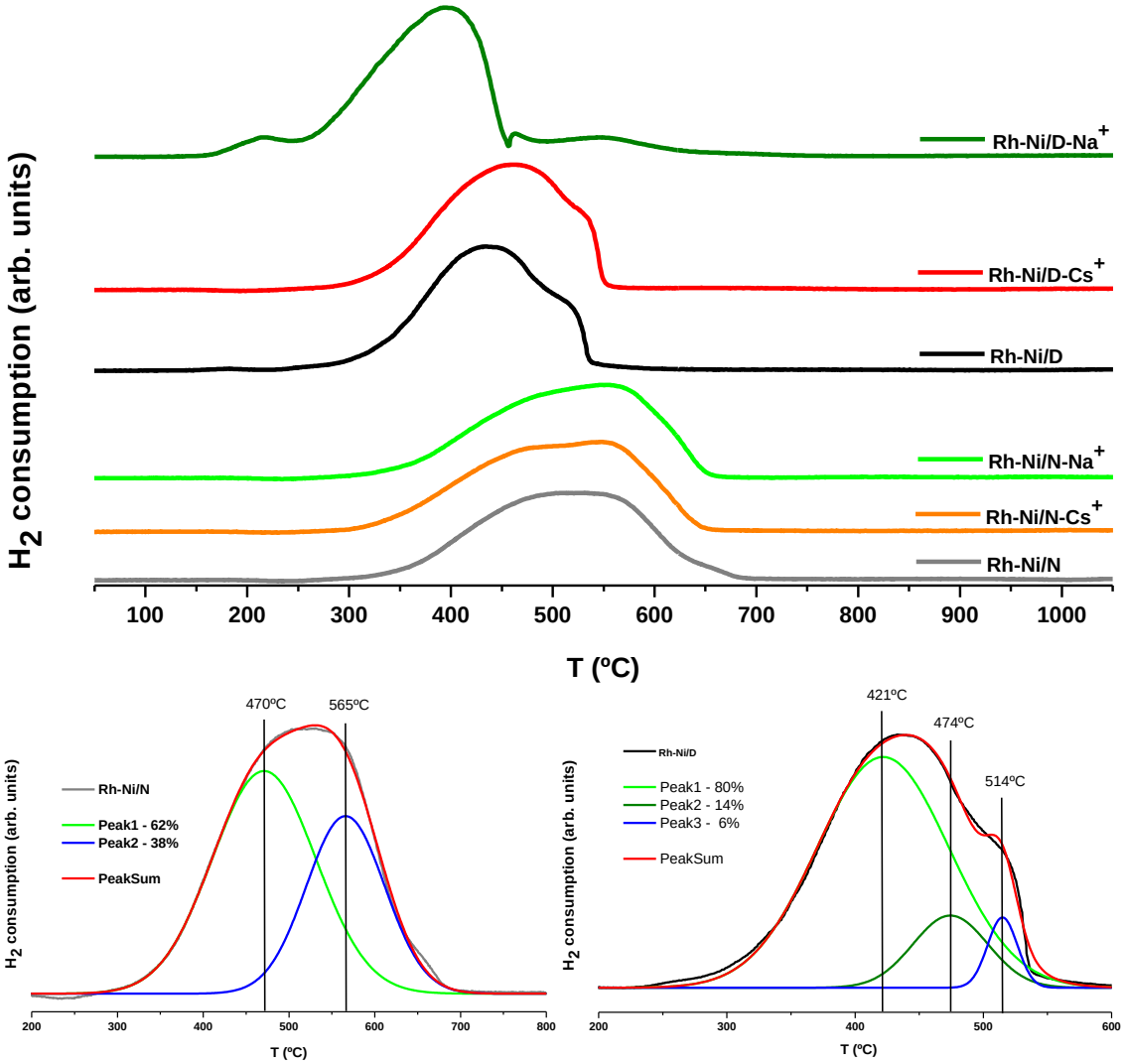

Figure 40: *TPR profiles of the fresh calcined catalysts. Deconvolution of the Rh-Ni/N and Rh-Ni/D profiles.*

4.5.3.3 X-ray diffraction, XRD, measurements

XRD analyses were carried out for all the reduced catalysts, being their profiles represented in Figure 41. The structure of the LTL zeolite was perfectly identified by all the peaks detected at the measured 2θ positions from 5 to 42 (PDF: 01-080-1580). However, in the case of the Rh-Ni/Disc-Na^+ catalyst the LTL zeolite structure disappeared because only NaCl, as an impurity (PDF: 01-077-2064), and Ni crystals were detected. This result is in good agreement with the textural properties, measured by means of N_2 absorption-desorption for this catalyst, and low BET surface area and porosity, which could be associated with the possible sintering process commented above.

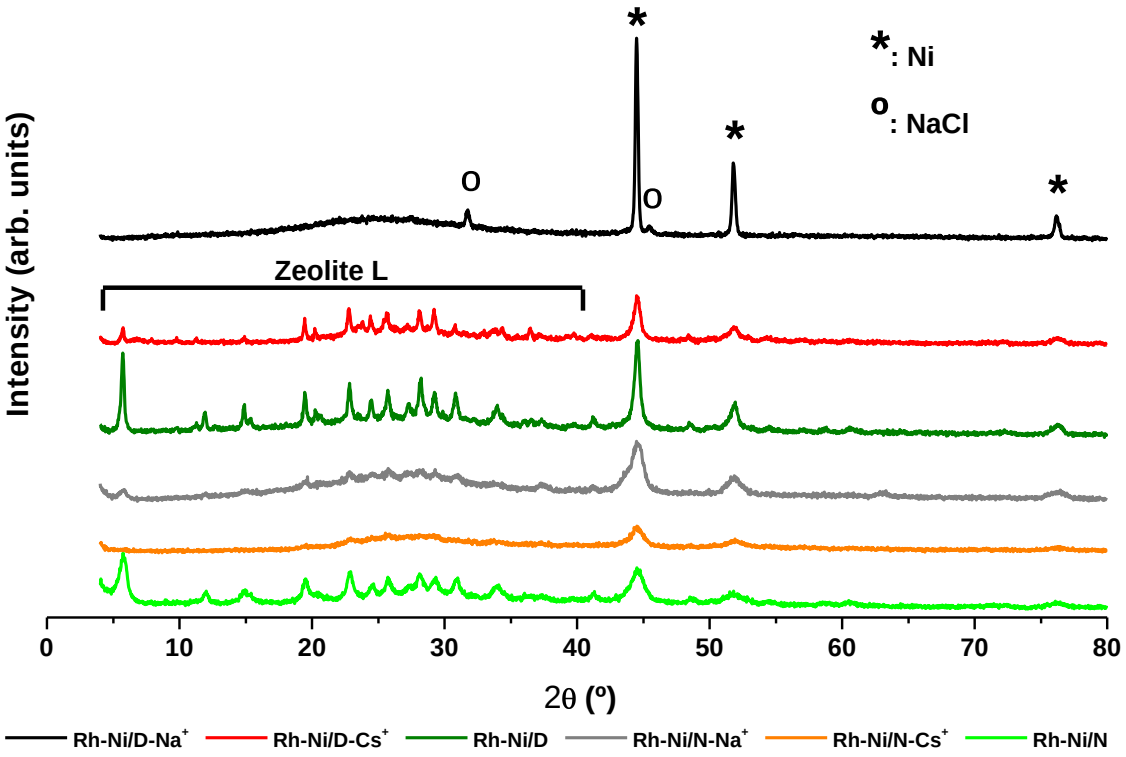

Figure 41: *Fresh reduced catalysts XRD spectra.*

The peaks corresponding to the metallic Ni were identified at 2θ values of around 44.5, 53.9 and 76.3º (PDF: 01-087-0712). Taking into account the stronger Ni contribution, 2θ=44.5º, the crystallite sizes calculated by the Scherrer equation for the catalysts under investigation are summarized in the Table 16.

Table 16: *Ni crystal sizes calculated by Scherrer equation.*

Catalyst	Position [°2θ]	Ni Crystallite size [nm]	Catalyst	Position [°2θ]	Ni Crystallite size [nm]
Rh-Ni/D-Na$^+$	44.48	~100	**Rh-Ni/N-Na$^+$**	44.46	
Rh-Ni/D–Cs$^+$	44.48	~20	**Rh-Ni/N–Cs$^+$**	44.49	~10
Rh-Ni/D	44.49	~25	**Rh-Ni/N**	44.50	~10

Unfortunately, no Rh contributions were detected by this technique. Thus, this effect can be assigned to the formation of small particles which could not be detected by this technique (crystal size<4 nm). Nevertheless, the presence of this metal was confirmed by TEM-EDX, ICP-AES and XPS.

4.5.3.4 Transmission electron microscope, TEM, images

In Figure 42 TEM micrographs for the fresh reduced catalysts are depicted. High densities of well dispersed particles are observed for all the catalysts prepared. Although the dispersion was not measured by this technique, it seems to be high due to the small particle size achieved. However, for the Rh-Ni/D-Na^+ catalyst higher particles are appreciated. The obtained micrographs by TEM and the calculated Ni particle sizes by XRD are in good agreement. On the one hand, particles around 100nm were measured by XRD for the Rh-Ni/D-Na^+ catalyst. On the other hand, in general bigger particles were estimated for the D catalysts than for the N catalysts by XRD, which is also appreciable in the TEM micrographs.

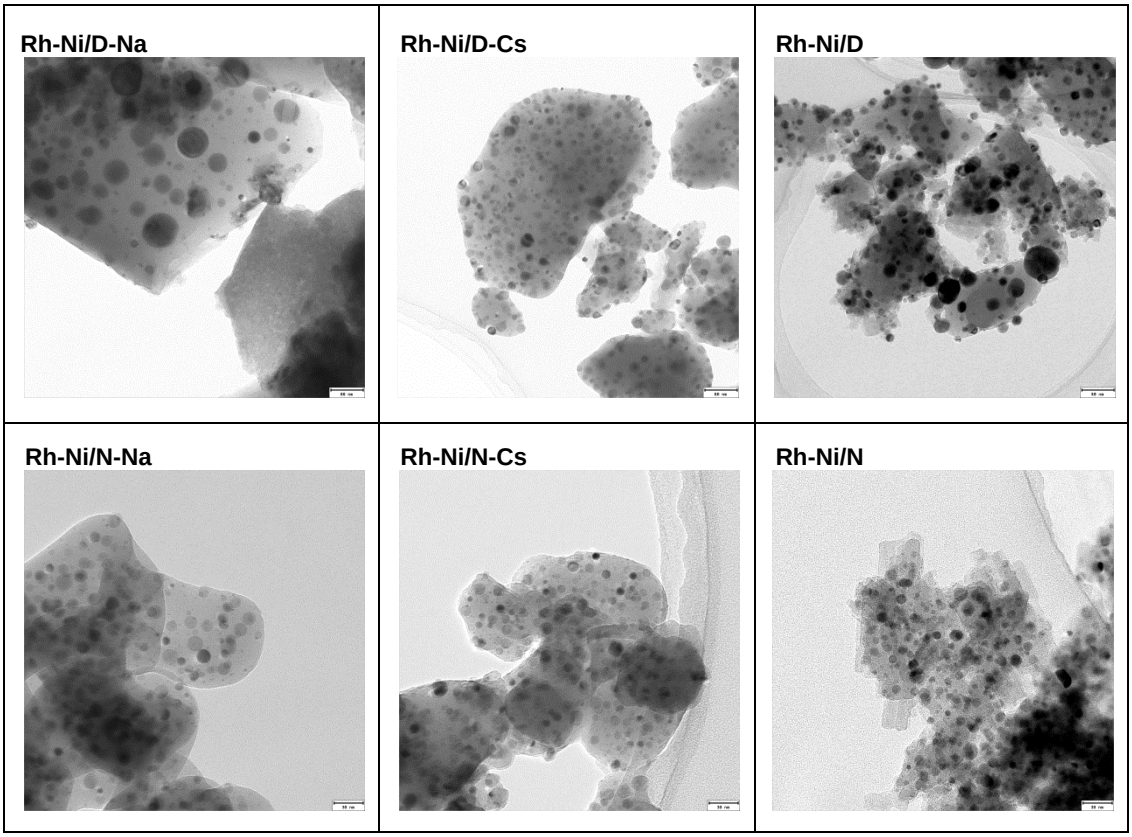

Figure 42: *TEM micrographs of the calcined catalysts. Scale size for the Disc and Nano catalysts of 80nm and 30nm respectively.*

4.5.3.5 ICP-AES and XPS characterization results

Finally, ICP-AES and XPS results are summarized in the Table 17. The catalysts chemical composition obtained from ICP-AES revealed Ni and Rh real compositions close to their intended ones (13.0 and 1.0 wt.% respectively). In addition, this technique enables the calculation of a Ni/zeolite atomic ratio to compare it with the ones obtained from XPS analyses. The measured Ni/zeolite atomic ratios by ICP-AES, as the metal and zeolite proportions correspond to the bulk catalysts, are lower than the calculated from the XPS results, as the latter correspond to the external catalyst surface. Thus, higher atomic ratios will be always expected from the XPS measurements.

Table 17: *ICP-AES measured metal compositions. Ni and Rh atomic ratios calculated for ICP-AES and XPS results.*

Catalysts	Composition (ICP, wt.%)		Atomic % (ICP)		Atomic % (XPS)	
	Ni	Rh	Ni	Rh	Ni	Rh
Rh-Ni/D-Na$^+$	11.57	0.84	0.252	0.0083	5.174	-
Rh-Ni/D-Cs$^+$	12.44	0.78	0.242	0.0076	5.605	1.058
Rh-Ni/D	12.90	0.85	0.223	0.0082	3.098	0.892
Rh-Ni/N-Na$^+$	11.58	0.86	0.272	0.0091	1.805	-
Rh-Ni/N-Cs$^+$	13.27	0.82	0.261	0.0079	2.026	0.438
Rh-Ni/N	13.75	0.93	0.223	0.0083	0.470	0.286

Among the prepared catalysts, XPS measurements revealed again differences between D and N catalysts. Attending to the Ni atomic concentration, values obtained for the D catalysts are very high compared to the ones for the N catalysts. This is in good agreement with the particle sizes observed in the TEM micrographs and measured by XRD. This high difference could be justified again because the Ni atoms were preferentially located in the outer part of the D catalysts, whereas in the N catalysts are placed mainly in the inner part of the pores. When N and D catalysts are separately compared, the lower ratios were always calculated for the non doped supports and the highest ones for the Cs^+ doped supports. Accordingly, it is stated that the presence of Na^+ and Cs^+ hinders the metal incorporation into the pores, in agreement with the BET results commented above. The same behavior was noticed for the Rh atomic ratio. It was not possible to detect it by this technique, due to the presence of Na in the samples.

4.5.4 Catalytic activity results

The previously characterized catalysts were tested in DR and BOR processes. With regard to the results for the DR process (Figure 43), high conversion values were obtained by all N catalysts but not for all the D ones. Among the N catalysts, no significant differences are observed in their activity. For the three catalysts, carbon dioxide conversion values around 90% and methane conversions around 45% were reached. In contrast, despite the Rh-Ni/D catalyst showed a very similar activity, worse results were measured for the Rh-Ni/D-Cs^+ catalyst. Finally, as it was expected, no activity was measured by the Rh-Ni/D-Na^+ catalyst in the DR process.

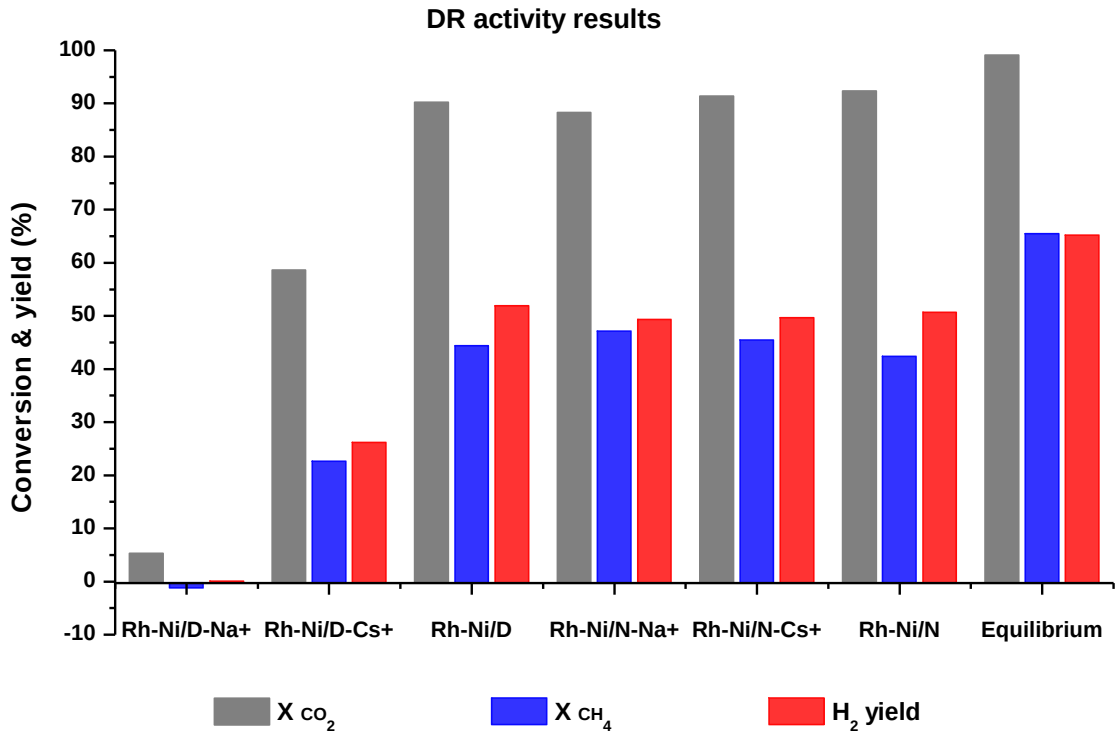

Figure 43: *DR catalytic activity results.*

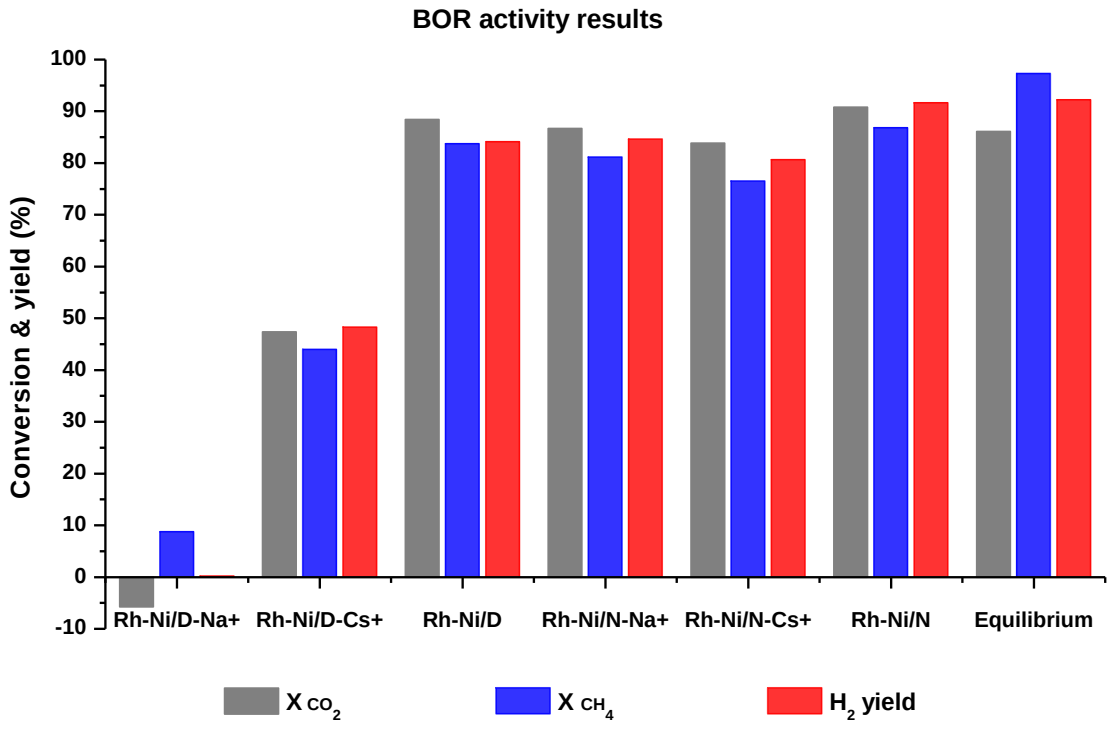

Figure 44: *BOR catalytic activity results.*

In the case of BOR process also high methane and carbon dioxide conversion values were reached (Figure 44). In addition, the catalysts activity behaviour was very similar to the one observed in the DR process. All the N catalysts showed a good catalytic activity as well as the

Rh-Ni/D catalyst. The Rh-Ni/D-Cs^+ catalyst conversion values were lower, and as a consequence, the obtained hydrogen yield too. Finally, the Rh-Ni/D-Na^+ catalyst was also not active for the BOR process. For this process the catalytic activity measured was closer to the calculated equilibrium conversion values.

Attending to DR and BOR catalytic activity, for the fresh calcined LTL zeolites a concordance between catalysts characterization and their catalytic activity is noticed. For the Rh-Ni/D-Na^+ catalyst low BET areas were measured and big Ni particles were observed by TEM, and measured by XRD. As a consequence, no activity was measured by both DR and BOR processes. In addition, for the Rh-Ni/D-Cs^+ catalyst lower BET areas were measured if they are compared with the more active catalysts. Besides, for this catalyst the highest Ni atomic concentration was measured by XPS. Focusing on the rest of the prepared catalysts, better characterization results were reported (higher surface areas, better metal surface dispersion, lower atomic concentrations, and lower particle size) and as a consequence, higher hydrogen yields were obtained.

Finally, comparing the catalysts tested with previous studies of the authors [94], worst results were obtained under DR conditions by the catalysts tested in the present study but almost the same results were achieved operating under BOR conditions.

4.5.5 Conclusions

High-quality LTL zeolite crystals with tunable size and morphology are achieved by hydrothermal synthesis assisted by microwave-heating, just adjusting a few reaction conditions (stirring, aging of the gel, time, and heating rate), and selecting the appropriate silica source. Thus, crystals of different length (from nm to μm) and shape (from cylinders to discs with different thickness) can be obtained straightforwardly.

The catalytic activities of the catalysts prepared from the not doped LTL zeolites, Rh-Ni/D and Rh-Ni/N, were higher than the corresponding to the Na^+ and Cs^+ exchanged supports, being not significant the differences between them. In addition, the Na^+ and Cs^+ incorporation affected mainly to the D catalysts, owing to the special morphology of these supports.

4.6 References

[1] C.J. Winter, Hydrogen energy - Abundant, efficient, clean: A debate over the energy-system-of-change, Int J Hydrogen Energy. 34 (2009) S1.

[2] I. Dincer, Green methods for hydrogen production, Int J Hydrogen Energy. 37 (2012) 1954.

[3] J. Xu, W. Zhou, Z. Li, J. Wang, J. Ma, Biogas reforming for hydrogen production over nickel and cobalt bimetallic catalysts, Int J Hydrogen Energy. 34 (2009) 6646.

[4] D.B. Levin, R. Chahine, Challenges for renewable hydrogen production from biomass, Int J Hydrogen Energy. 35 (2010) 4962.

[5] G. Kolb, J. Schürer, D. Tiemann, M. Wichert, R. Zapf, V. Hessel, Fuel processing in integrated micro-structured heat-exchanger reactors, J Power Sources. 171 (2007) 198.

[6] D. Deublein, A. Steinhauser, Biogas from waste and renewable resources: an introduction, Ed. Wiley. 2nd Edition (2011).

[7] W. Soetaert, E.J. Vandamme, Biofuels, Ed. Wiley. (2009).

[8] S. Rasi, A. Veijanen, J. Rintala, Trace compounds of biogas from different biogas production plants, Energy. 32 (2007) 1375.

[9] P. Börjesson, M. Berglund, Environmental systems analysis of biogas systems - Part I: Fuel-cycle emissions, Biomass Bioenergy. 30 (2006) 469.

[10] P. Kolbitsch, C. Pfeifer, H. Hofbauer, Catalytic steam reforming of model biogas, Fuel. 87 (2007) 701.

[11] D.P. Antonio, P. Nathaniel, Estudios de viabilidad de sistemas de purificación y aprovechamiento de biogas. Capítulo 5: Nuevos usos del biogas, Ministerio de ciencia e Innovación. PS120000 (2010) 2007.

[12] S.L. Lakhapatri, M.A. Abraham, Deactivation due to sulfur poisoning and carbon deposition on Rh-Ni/Al_2O_3 catalyst during steam reforming of sulfur-doped-n-hexadecane, Appl Catal A-Gen. 364 (2009) 113.

[13] C.S. Lau, A. Tsolakis, M.L. Wyszynski, Biogas upgrade to syn-gas (H_2-CO) via dry and oxidative reforming, Int J Hydrogen Energy. 36 (2011) 397.

[14] A. Effendi, Z.G. Zhang, K. Hellgardt, K. Honda, T. Yoshida, Steam reforming of a clean model biogas over Ni/Al_2O_3 in fluidized- and fixed-bed reactors, Catal Today. 77 (2002) 181.

[15] L.E. Briand, W.E. Farneth, I.E. Wachs, Quantitative determination of the number of active surface sites and the turnover frequencies for methanol oxidation over metal oxide catalysts I. Fundamentals of the methanol chemisorption technique and application to monolayer supported molybdenum oxide catalysts, Catal Today. 62 (2000) 21.

[16] J. Chen, C. Yao, Y. Zhao, P. Jia, Synthesis gas production from dry reforming of methane over Ce0.75Zr0.25O_2-supported Ru catalysts, Int J Hydrogen Energy. 35 (2010) 1630.

[17] Y. Li, X. Wang, C. Xie, C. Song, Influence of ceria and nickel addition to alumina-supported Rh catalyst for propane steam reforming at low temperatures, Appl Catal, A. 357 (2009) 213.

[18] H. Scott Fogler, Elements of chemical reaction engineering, Englewood Cliffs: Prentice-Hall PTR. 3rd ed (1999).

[19] J. Thormann, P. Pfeifer, K. Schubert, U. Kunz, Reforming of diesel fuel in a micro reactor for APU systems, Chem Eng J. 135 (2008) S74.

[20] J. Huang, J. Weinstein, R.S. Besser, Particle loading in a catalyst-trap microreactor: Experiment vs. simulation, Chem Eng J. 155 (2009) 388.

[21] V. Hessel, H. Löwe, A. Müller, G. Kolb, Chemical Micro Process Engineering, KGaA: Weinheim. 1st ed (2005).

[22] A.E. Castro Luna, M.E. Iriarte, Carbon dioxide reforming of methane over a metal modified Ni-Al_2O_3 catalyst, Appl Catal A-Gen. 343 (2008) 10.

[23] S.T. Sie, R. Krishna, Fundamentals and selection of advanced Fischer–Tropsch reactors, Appl Catal A-Gen. 186 (1999) 55.

[24] C. Kwak, J.J. Lee, J.S. Bae, S.H. Moon, Poisoning effect of nitrogen compounds on the performance of CoMoS/Al_2O_3 catalyst in the hydrodesulfurization of dibenzothiophene, 4-methyldibenzothiophene, and 4,6-dimethyldibenzothiophene, Appl Catal B-Environ. 35 (2001) 59.

[25] M. Wisniewski, A. Boréave, P. Gélin, Catalytic CO_2 reforming of methane over Ir/$Ce_{0.9}Gd_{0.1}O_{2-x}$, Catal Commun. 6 (2005) 596.

[26] E.X. Verykios, Mechanistic aspects of the reaction of CO_2 reforming of methane over Rh/Al_2O_3 catalyst, Appl Catal A-Gen. 255 (2003) 101.

[27] D. San-José-Alonso, J. Juan-Juan, M.J. Illán-Gómez, M.C. Román-Martínez, Ni, Co and bimetallic Ni–Co catalysts for the dry reforming of methane, Appl Catal A-Gen. 371 (2009) 54.

[28] K. Tomishige, M. Nurunnabi, K. Maruyama, K. Kunimori, Effect of oxygen addition to steam and dry reforming of methane on bed temperature profile over Pt and Ni catalysts, Fuel Proc Technol. 85 (2004) 1103.

[29] M. García-Diéguez, I.S. Pieta, M.C. Herrera, M.A. Larrubia, L.J. Alemany, Nanostructured Pt- and Ni-based catalysts for CO_2-reforming of methane, J Catal. 270 (2010) 136.

[30] V.A. Tsipouriari, A.M. Efstathiou, Z.L. Zhang, X.E. Verykios, Reforming of methane with carbon dioxide to synthesis gas over supported Rh catalysts, Catal Today. 21 (1994) 579.

[31] C. Yang-guang, K. Tomishige, K. Yokoyama, K. Fujimoto, Promoting effect of Pt, Pd and Rh noble metals to the Ni0.03Mg0.97O solid solution catalysts for the reforming of CH_4 with CO_2, Appl Catal A-Gen. 165 (1997) 335.

[32] A. Iriondo, J.F. Cambra, M.B. Güemez, V.L. Barrio, J. Requies, M.C. Sánchez-Sánchez, Effect of ZrO_2 addition on Ni/Al_2O_3 catalyst to produce H_2 from glycerol, Int J Hydrogen Energy. 37 (2012) 7084.

[33] N. Laosiripojana, W. Sutthisripok, S. Assabumrungrat, Synthesis gas production from dry reforming of methane over CeO_2 doped Ni/Al_2O_3: Influence of the doping ceria on the resistance toward carbon formation, Chem Eng J. 112 (2005) 13.

[34] S. Therdthianwong, C. Siangchin, A. Therdthianwong, Improvement of coke resistance of Ni/Al_2O_3 catalyst in CH_4/CO_2 reforming by ZrO_2 addition, Fuel Process Technol. 89 (2008) 160.

[35] E. Acha, J. Requies, V.L. Barrio, J.F. Cambra, M.B. Güemez, P.L. Arias, Water effect in hydrogen production from methane, Int J Hydrogen Energy. 38 (2013) 7659.

[36] A.P. Packer, D. Larivière, C. Li, M. Chen, A. Fawcett, K. Nielsen, Validation of an inductively coupled plasma mass spectrometry (ICP-MS) method for the determination of cerium, strontium, and titanium in ceramic materials used in radiological dispersal devices (RDDs), Anal Chim Acta. 588 (2007) 166.

[37] J. Requies, M.A. Cabrero, V.L. Barrio, M.B. Güemez, J.F. Cambra, P.L. Arias, Partial oxidation of methane to syngas over Ni/MgO and Ni/La_2O_3 catalysts, App Catal, A. 289 (2005) 214.

[38] M.C. Sánchez-Sánchez, R.M. Navarro, J.L.G. Fierro, Ethanol steam reforming over $Ni/M_xO_y\_Al_2O_3$ (M=Ce, La, Zr and Mg) catalysts: Influence of support on the hydrogen production, Int J Hydrogen Energy. 32 (2007) 1462.

[39] M.E. Davis, R.J. Davis, Fundamentals of chemical reaction engineering, McGraw-Hill Professional. (2003).

[40] A. Iriondo, V.L. Barrio, J.F. Cambra, P.L. Arias, M.B. Guemez, M.C. Sanchez-Sanchez, Glycerol steam reforming over Ni catalysts supported on ceria and ceria-promoted alumina, Int J Hydrogen Energy. 35 (2010) 11622.

[41] K. Polychronopoulou, J.L.G. Fierro, A.M. Efstathiou, The phenol steam reforming reaction over MgO-based supported Rh catalysts, J Catal. 228 (2004) 417.

[42] W. Qiao, X. Yan, J. Ye, Y. Sun, W. Wang, Z. Zhang, Evaluation of biogas production from different biomass wastes with/without hydrothermal pretreatment, Renew Energ. 36 (2011) 3313.

[43] H.J. Alves, C.B. Junior, R.R. Niklevicz, E.P. Frigo, M.S. Frigo, C.H. Coimbra-Araujo, Overview of hydrogen production technologies from biogas and the applications in fuel cells, Int J Hydrogen Energy. 38 (2013) 5215.

[44] U. Izquierdo, V.L. Barrio, N. Lago, J. Requies, J.F. Cambra, M.B. Güemez, P.L. Arias, Biogas steam and oxidative reforming processes for hydrogen production in conventional and microreactor reaction systems, Int J Hydrogen Energy. 37 (2012) 13829.

[45] U. Izquierdo, V.L. Barrio, J. Requies, J.F. Cambra, M.B. Güemez, P.L. Arias, Tri-reforming: A new biogas process for synthesis gas and hydrogen production, Int J Hydrogen Energy. 38 (2013) 7623.

[46] P. Frontera, A. Macario, A. Aloise, F. Crea, P.L. Antonucci, J.B. Nagy, Catalytic dry-reforming onCatalytic dry-reforming on Ni–zeolite supported catalyst, Catal Today. 179 (2012) 5.

[47] O.A. Bereketidou, M.A. Goula, Biogas reforming for syngas production over nickel supported on ceria–alumina catalysts, Catal Today. 195 (2012) 93.

[48] S. Damyanova, B. Pawelec, K. Arishtirova, J.L.G. Fierro, Biogas reforming over bimetallic PdNi catalysts supported on phosphorus-modified alumina, Int J Hydrogen Energy. 36 (2011) 10635.

[49] X. Junke, Z. Wei, L. Zhaojing, W. Jihui, M. Jianxin, Biogas reforming for hydrogen production over a Ni–Co bimetallic catalyst: Effect of operating conditions, Int J Hydrogen Energy. 35 (2010) 13013.

[50] A.H. Fakeeha, W.U. Khan, A.S. Al-Fatesh, A.E. Abasaeed, Stabilities of zeolite-supported Ni catalysts for dry reforming of methane, Chinese J Catalysis. 34 (2013) 764.

[51] A. Kaengsilalai, A. Luengnaruemitchai, S. Jitkarnka, S. Wongkasemjit, Potential of Ni supported on KH zeolite catalysts for carbon dioxide reforming of methane, J. Power Sources. 165 (2007) 347.

[52] W. Nimwattanakul, A. Luengnaruemitchai, S. Jitkarnka, Potential of Ni supported on clinoptilolite catalysts for carbon dioxide reforming of methane, Int. J. Hydrogen Energy. 31 (2006) 93.

[53] L. Gartzia-Rivero, J. Bañuelos-Prieto, V. Martínez-Martínez, I. López Arbeloa, Versatile Photoactive Materials Based on Zeolite L Doped with Laser Dyes, ChemPlusChem. 77 (2012) 61.

[54] Q. Huo, T. Dou, Z. Zhao, H. Pan, Synthesis and Application of a Novel Mesoporous Zeolite L in the Catalyst for the HDS of FCC Gasoline, Appl Catal A Gen. 381 (2010) 101.

[55] K.G. Azzam, G. Jacobs, W.D. Shafer, B.H. Davis, Dehydrogenation of propane over Pt/KL catalyst: Investigating the role of L-zeolite structure on catalyst performance using isotope labeling, Appl Catal A Gen. 20 (2010) 264.

[56] J.M. Hill, R.D. Cortright, J.A. Dumesic, Silica- and L-zeolite-supported Pt, Pt/Sn and Pt/Sn/K catalysts for isobutane dehydrogenation, Appl Catal A Gen. 168 (1998) 9.

[57] R.D. Cortright, J.A. Dumesic, L-zeolite-supported platinum and platinum/tin catalysts for isobutane dehydrogenation, Appl Catal A Gen. 129 (1995) 101.

[58] A.P. Singh, S.B. Kumar, Para selective chlorination of toluene with an L-zeolite catalyst, Appl Catal A Gen. 126 (1995) 27.

[59] J.S. Chang, S.E. Park, H. Chon, Catalytic activity and coke resistance in the carbon dioxide reforming of methane to synthesis gas over zeolite-supported Ni catalysts, Appl Catal A Gen. 145 (1996) 111.

[60] U.L. Portugal, A.C.S.F. Santos, S. Damyanova, C.M.P. Marques, J.M.C. Bueno, CO_2 reforming of CH_4 over Rh-containing catalysts, J Mol Catal A-Chem. 184 (2002) 311.

[61] U.L. Portugal, C.M.P. Marques, E.C.C. Araujo, E.V. Morales, M.V. Giotto, J.M.C. Bueno, CO_2 reforming of methane over zeolite-Y supported ruthenium catalysts, Appl Catal A-Gen. 193 (2000) 173.

[62] C. Crisafulli, S. Scirè, S. Minicò, L. Solarino, Ni–Ru bimetallic catalysts for the CO_2 reforming of methane, Appl Catal A-Gen. 225 (2002) 1.

[63] D. Halliche, O. Cherifi, A. Auroux, Microcalorimetric studies and methane reforming by CO_2 on Ni-based zeolite catalysts, Thermochim Acta. 434 (2005) 125.

[64] S.M. Gheno, S. Damyanova, B.A. Riguetto, C.M.P. Marques, C.A.P. Leite, J.M.C. Bueno, CO_2 reforming of CH_4 over Ru/zeolite catalysts modified with Ti, J Mol Catal A-Chem. 198 (2003) 263.

[65] A.N. Pinheiro, A. Valentini, J.M. Sasaki, A.C. Oliveira, Highly stable dealuminated zeolite support for the production of hydrogen by dry reforming of methane, Appl Catal A Gen. 355 (2009) 156.

[66] J.R. Rostrup-Nielsen, Aspects of CO_2-reforming of Methane, Stud Surf Sci Catal. 81 (1994) 25.

[67] A. Zabala Ruiz, D. Bruhwiler, T. Bau, G. Calzaferri, Synthesis of Zeolite L. Tuning Size and Morphology, Monatsh Chem. 136 (2005) 77.

[68] A.M. Diskin, R.H. Cunningham, R.M. Ormerod, The oxidative chemistry of methane over supported nickel catalysts, Catal Today. 46 (1998) 147.

[69] A. Luengnaruemitchai, A. Kaengsilalai, Activity of different zeolite-supported Ni catalysts for methane reforming with carbon dioxide, Chem Eng J. 144(1) (2008) 96.

[70] J.J. Strohm, J. Zheng, C. Song, Low-temperature steam reforming of jet fuel in the absence and presence of sulfur over Rh and Rh–Ni catalysts for fuel cells, J Catalysis. 238 (2006) 309.

[71] M. El Doukkali, A. Iriondo, J.F. Cambra, L. Jalowiecki-Duhamel, A.S. Mamede, F. Dumeignil, Pt monometallic and bimetallic catalysts prepared by acid sol-gel method for liquid phase reforming of bioglycerol, J Mol Catal A Chem. 368–369 (2013) 125.

[72] S. Rakass, H. Oudghiri-Hassani, P. Rowntree, N. Abatzoglou, Steam reforming of methane over unsupported nickel catalysts, J Power Sources. 158 (2006) 485.

[73] B. Pawelec, S. Damyanova, K. Arishtirova, J.L.G. Fierro, L. Petrov, Structural and surface features of PtNi catalysts for reforming of methane with CO_2, Appl Catal A. 323 (2007) 188.

[74] M.P. Lai, W.H. Lai, R.F. Horng, C.Y. Chen, W.C. Chiu, S.S. Su, Experimental study on the performance of oxidative dry reforming from simulated biogas, Energy Procedia. 29 (2012) 225.

[75] A. Damour, ZSM-5 type zeolites: Synthesis and use in gasphase reactions with ammonia, Ann Mines. 17 (1840) 191.

[76] A.F. Cronsted, M.L. Occelli, H. . Robson, Molecular Sieves, Translation ed., Van Nostrand Reinhold, New York, 1992.

[77] H. Manzano, L. Gartzia-Rivero, J. Bañuelos, I. López-Arbeloa, Ultraviolet Visible Dual Absorption by Single BODIPY Dye Confined in LTL Zeolite Nanochannels, J Phys Chem C. 117 (2013) 13331.

[78] M. Veiga-Gutiérrez, M. Woerdemann, E. Prasetyanto, C. Denz, L. De Cola, Tweezers Assembly-Line for the Construction of Complex Functional Zeolite L Structures, Adv Mater. 24 (2012) 5199.

[79] A. Mech, A. Monguzzi, F. Meinardi, J. Mezyk, G. Macchi, R. Tubino, Sensitized NIR erbium(III) emission in confined geometries: a new strategy for light emitters in telecom applications, J Am Chem Soc. 132 (2010) 4574.

[80] A. Corma, F. Rey, J. Rins, M.J. Sabater, S. Valencia, Supramolecular self-assembled molecules as organic directing agent for synthesis of zeolites, Nature. 431 (2004) 287.

[81] T.P. Lee, B. Saad, E.P. Ng, B. Salleh, Zeolite Linde Type L as micro-solid phase extraction sorbent for the high performance liquid chromatography determination of ochratoxin A in coffee and cereal, J Chromatogr A. 1237 (2012) 46.

[82] G. Calzaferri, K. Lutkouskaya, Light harvesting by a periodic mesoporous organosilica chromophore, Photochem Photobiol Sci. 7 (2008) 879.

[83] J.S. Batchelder, A.H. Zewail, T. Cole, Luminescent solar concentrators 1: Theory of operation and techniques for performance evaluation, Appl Optics. 18 (1979) 3090.

[84] J. El-Gindi, K. Benson, L. De Cola, H.J. Galla, N.S. Kehr, Cell Adhesion Behavior on Enantiomerically Functionalized Zeolite L Monolayers, Chem Int Ed. 51 (2012) 1.

[85] R. Szostak, Molecular Sieves: Principles of Synthesis and Identification, Blackie Academic & Professional, London. (1998).

[86] D.W. Breck, N.A. Acara, Union Carbide Corporation, U. S Patent 909264. (1962).

[87] A.I. Lupulescu, M. Kumar, D.J. Rimer, A Facile Strategy To Design Zeolite L Crystals with Tunable Morphology and Surface Architecture, J Am Chem Soc. 135 (2013) 6608.

[88] I. Bilecka, M. Niederberger, Microwave chemistry for inorganic nanomaterials synthesis, Nanoscale. 2 (2010) 1358.

[89] G. Schulz-Ekloff, D. Wöhrle, B. van Duffel, R.A. Schoonheydt, Chromophores in porous silicas and minerals: preparation and optical properties, Micropor Mesopor Mater. 51 (2002) 91.

[90] N. Sudheesh, S.K. Sharma, R.S. Shukla, R.V. Jasra, $HRh(CO)(PPh_3)_3$ encapsulated mesopores of hexagonal mesoporous silica (HMS) acting as nanophase reactors for effective catalytic hydroformylation of olefins, J Mol Catal A Chem. 296 (2008) 61.

[91] A. Zabala Ruiz, H. Li, G. Calzaferri, Orienting zeolite L microcrystals with a functional linker, Angew Int Ed. 45 (2006) 5282.

[92] G. Calzaferri, Nanochannels: Hosts for the supramolecular organization of molecules and complexes, Langmuir. 28 (2012) 6216.

[93] R.Q. Albuquerque, G. Calzaferri, Proton activity inside the channels of zeolite L, Chem Eur J. 13 (2007) 8939.

[94] U. Izquierdo, V.L. Barrio, K. Bizkarra, A.M. Gutierrez, J.R. Arraibi, L. Gartzia, Ni and Rh-Ni catalysts supported on Zeolites L for hydrogen and syngas production by biogas reforming processes, Chem Eng J. (2013).

[95] A.M. Garrido Pedrosa, M.J.B. Souza, A.O.S. Silva, D.M.A. Melo, A.S. Araujo, Fischer-Tropsch synthesis and the generation of DME in situ, Catal Comm. ,7 (2006) 791.

[96] M. Ocsachoque, F. Pompeo, G. Gonzalez, New and Future Developments in Catalysis: Catalysis by Nanoparticles, Catal Today. 172 (2011) 226.

CHAPTER 5

Ethylene glycol steam and oxidative reforming

Articles available online:

Title: Sustainable syngas production from ethylene glycol reforming processes using Rh based catalysts in microreactors

Authors: U. Izquierdo, M. Wichert, V.L. Barrio, G. Kolb

Title: Microreactor hydrogen production from ethylene glycol reforming using Rh catalysts supported on CeO_2 and La_2O_3 promoted α-Al_2O_3

Authors: U. Izquierdo, M. Wichert, V.L. Barrio, G. Kolb, P.L. Arias, J.F. Cambra, R. Zapf, A. Ziogas, S. Neuberg

Table of contents

List of figures

List of tables

5.1 Introduction

Hydrogen production from renewable sources and its utilization as a fuel for fuel cells is a promising way to minimize the actual dependence on fossil fuels. This dependence should be gradually reduced not only due to the fossil fuels depletion, but also owing to the environmental problems that entail their utilization. The challenge lays in the development of the most efficient, economical and environmentally friendly hydrogen production route. Thus, the energy conversion should be based on sustainable energy carriers in order to solve the concerns of environmental pollution and to ensure availability. In this context, the use of bio-renewable organic sources such as polyalcohols, in an intensified process through the use of a microstructured reactor seems to be a promising alternative [1,2].

The reforming of biomass-derived oxygenates such as ethanol or glycerol has been deeply studied. However, in the case of ethylene glycol, few studies have been addressed most of them focusing on aqueous phase reforming (APR). Ethylene glycol can be produced directly and efficiently via catalytic hydrogenation of cellulose or cellulosic biomass derived oxygenated compounds [3]. Cellulose, as the most abundant component of biomass (accounting for 35-50%), is being considered as a promising alternative to fossil resources [4]. In addition, EG is the most abundant molecule of compounds derived from the catalytic conversion of cellulose, accounting for more than 70% of cellulose derivatives, thus making EG a renewable and available energy carrier [5,6]. The group led by Prof. Dr. Tao Zhang reached full cellulose conversion and 61.0% EG yield by using a carbon supported tungsten carbide catalyst loaded with 2% of nickel [7,8] and lower conversions and yields by using other type of catalysts [9].

Therefore, the renewable and non-volatile nature makes EG an attractive feedstock for hydrogen production via steam reforming. Steam reforming is the preferred route for the conversion of biomass-derived oxygenates because the water is present in the feed already as described above and because steam reforming promises high efficiency in terms of higher hydrogen production yields [10,11]. The operation under SR conditions requires energy supply in order to achieve the reaction temperature and to feed the endothermic reaction. However, this fact is counterbalanced by the possibility to operate at atmospheric pressure which makes this process more attractive, easier and safer than APR [12].

The most important reactions that involve the EG steam reforming and oxidative steam reforming processes under investigation are the following:

EG SR:	$C_2H_6O_2 + 2\ H_2O = 2\ CO_2 + 5\ H_2$	$\Delta H^o = 91\ kJ{\cdot}mol^{-1}$	(1)
EG OSR	$C_2H_6O_2 + 1/2O_2 + H_2O = 2\ CO_2 + 4\ H_2$	$\Delta H^o = -150\ kJ{\cdot}mol^{-1}$	(2)
EG decomposition:	$C_2H_6O_2 = 2\ CO + 3\ H_2$	$\Delta H^o = 168\ kJ{\cdot}mol^{-1}$	(3)
r-WGS:	$CO_2 + H_2 = CO + H_2O$	$\Delta H^o = 41\ kJ{\cdot}mol^{-1}$	(4)

By-products formation: $CO + 3\ H_2 = CH_4 + H_2O$ (5)

$C_2H_6O_2 + H_2 = C_2H_4 + 2\ H_2O$ (6)

$C_2H_6O_2 = C_2H_4O + H_2O$ (7)

$C_2H_6O_2 + 2\ H_2 = C_2H_6 + 2\ H_2O$ (8)

Apart from the reactions that produce hydrogen (1-3) and the r-WGS reaction, the main possible routes through which different by-products can be formed are listed (5-8). [13].

Regarding the catalysts used, nickel [14,15], noble metal [10,16,17] and bimetallic catalysts [12,18] were studied in the APR process. In the case of the gas phase EG reforming, few investigations were found in the literature [3,7] which applied Ni based catalysts, inert sand (SiO_2) or natural olivine. However, in the open literature to our knowledge, only Davda et al. [15] used Rh supported on SiO_2 for APR. However, Rh is known to be an excellent catalyst for steam reforming of all kind of fuels [2,10]. In this work catalysts supported by α-alumina were designed based upon two different preparation methods in order to compare their activity; namely a common wash-coating procedure with subsequent impregnation [19] (named as conventional method, xRh-cm) and nanoparticle catalysts prepared according to a method described by Ashida et al. (named as nanoparticle catalysts, xRh-np). Through this method, Rh nanoparticles are supposed to be obtained by doing a liquid phase reduction of the Rh^{3+} ion in ethanol solvent with Polyvinylpyrrolidone (PVP) of the various molecular weights [20]. Finally, the support was chosen such that it had minimum acidity to reduce the risk of carbon formation of the catalyst.

These catalysts were tested under conditions of gas phase steam reforming of EG using microstructured reactors. It is well established that heat and mass transfer limitations are reduced when operating with microreactors and this fact makes them the most appropriate system to be used when fast and highly exothermic or endothermic reactions are studied [21]. Additionally, the operation with microreactores also allows reaching much higher Volume Hourly Space Velocities owing to the improved mass transport in comparison with the conventional fixed bed reactors and this makes possible to intensify the process [22]. In a microchannel heat-exchanger the heat supply is possible in a much more efficient way compared to conventional technology.

According to the results obtained from the experiments with the catalysts mentioned before, the catalyst that obtained the best results was selected and its support was modified to design new catalytic formulations (Section 5.4). Then, this new catalysts were tested under the same operating conditions in order to improve their activity and stability and reduce the by-product formation. With this aim, and basing on the previous experiments, 2.5 wt.% Rh on α-alumina (named 2.5Rh) was used as a reference which was modified by using CeO_2 and La_2O_3 promoters.

The used of CeO_2 as additive was decided owing to the unique features attributed to this oxide when it is incorporated into the catalytic support. On one hand, under reductive atmosphere Ce^{4+} ions can be reduced to Ce^{3+} forming Ce_2O_3 and as a consequence, the corresponding oxygen vacancy [23]. In addition the ceria-based catalysts may enhance the active metal phase dispersion into the support surface, increasing the reforming capacity [24-26]. Furthermore, the ceria is a well-suited material to suppress coke formation in reforming reactions [27]. Regarding the use of lanthana oxide, it has also been applied to improve the resistance against coke formation of reforming catalysts [28]. Additionally, it has been reported that La_2O_3 reduces the acidity of the alumina, prevents metal sintering and avoids catalyst deactivation [29].

5.2 Experimental procedure

5.2.1 Catalyst preparation and impregnation

For the preparation of the conventional catalysts, Rh ($RhCl_3 \cdot xH_2O$, Alfa Aesar, Johnson Matthey Company) was dissolved in distilled water in order to achieve the intended loadings of 1.0, 2.5 and 5.0 wt.% of Rh. Then, the α-alumina was added and after subsequent stirring, the mixture was left for three hours without stirring at room temperature. These samples are named below as 1.0 Rh-cm, 2.5 Rh-cm and 5.0 Rh-cm respectively.

The nanoparticle catalysts were prepared by mixing distilled water and ethanol as a first step. Then, PVP ($(C_6H_9NO)_x$, Sigma Aldrich Chemie) and the corresponding amount of Rh were added in order to achieve the same metal content, 1.0, 2.5 and 5.0 wt.% of Rh, as for the conventional catalysts. The resulting mixture was refluxed at 80ºC for 3 hours. After cooling the mixture under continuous stirring overnight, a rotary evaporator was used to remove the ethanol. Finally, the α-alumina was added to the obtained solution and after successive stirring, the mixture was left for three hours without stirring at room temperature. These samples are named below as 1.0 Rh-np, 2.5 Rh-np and 5.0 Rh-np respectively.

In the case of the Rh catalysts supported on modified α-alumina they were designed based on a common wash-coating procedure with subsequent impregnation [2]. The corresponding Rh amount to achieve the intended metal load of 2.5 wt.% was dissolved in distilled water. Then, certain amounts of α-alumina and modifiers were added in order to achieve the intended load of 10 wt% (2.5 Rh-10Ce) and 20 wt% (2.5 Rh-20Ce) of CeO_2 ($Ce(NO_3)_3$ * 6 H_2O, Alfa Aesar) and 5 wt% (2.5 Rh-5La) and 10 wt% (2.5 Rh-10La)of La_2O_3 ($La(NO_3)_3$ * 6 H_2O, FLUKA). After several minutes of subsequent stirring, the mixtures were left for three hours without stirring at room temperature.

After the preparation described above, all catalysts were calcined at 450ºC for 6 hours. The catalysts coatings were performed applying a procedure described by Zapf et al. [19] in which polyvinyl alcohol (PVA), distilled water and acetic acid were added to the previously calcined catalysts.

Sandwich-type reactors were applied for the activity tests. Two platelets carrying 14 channels each with 500 µm width and 250 µm depth introduced by wet chemical etching, which have been described in previous studies [21,22]. After an initial calcination of the plates the catalyst suspension was coated onto the plates by distributing manually some suspension drops along the plate's channels and removing any excess suspension from the completely filled channels. Subsequently, calcination at 600ºC for 2 hours was carried out. The described coating and calcinations step was repeated twice. In addition, a certain amount of suspension was also calcined in order to characterize the resulting catalysts powder with same properties as the coated samples.

After calcination the reactors including inlet and outlet capillaries were sealed by laser welding. They were put into a stainless steel block equipped with thermocouples and heating cartridges to adjust the desired reaction temperature as described previously [30].

5.2.2 Activity measurements

A lab scale set up was applied for the activity tests (see Figure 1). A mixture of water and ethylene glycol with a S/C ratio of 4.0 was used for experiments conducted under conditions of SR. In the case of OSR experiments a synthetic air stream composed of 21% O_2 and 79% N_2 (vol.) was introduced to reach the targeted atomic O/C ratio of 0.15. The liquid feed mixture was placed in a tank under N_2 pressure as driving force for feeding a liquid mass flow controller (LMFC). Before starting the experiments, the reactor was by-passed until a stable feed composition was measured and the desired reactor temperature was reached. The desired conditions were normally achieved approximately after 30 min. by-passing the reactor.

The obtained product composition was analyzed using an online Mass Spectrometer (MS) equipped with two heated inlet systems (20-200°C), an Electron Ion Source, a Quadrupole analyzer, a Faraday and a secondary electron multiplier detector. Then, the effluent stream was cooled down, water and organic liquids were removed and permanent gases were analyzed by an online µ-GC (Varian CP-4900 Micro-GC) equipped with a heated sample line (30-110°C) consisting of 4-channel modules with four independent injectors and capillary columns connected with TCD detectors.

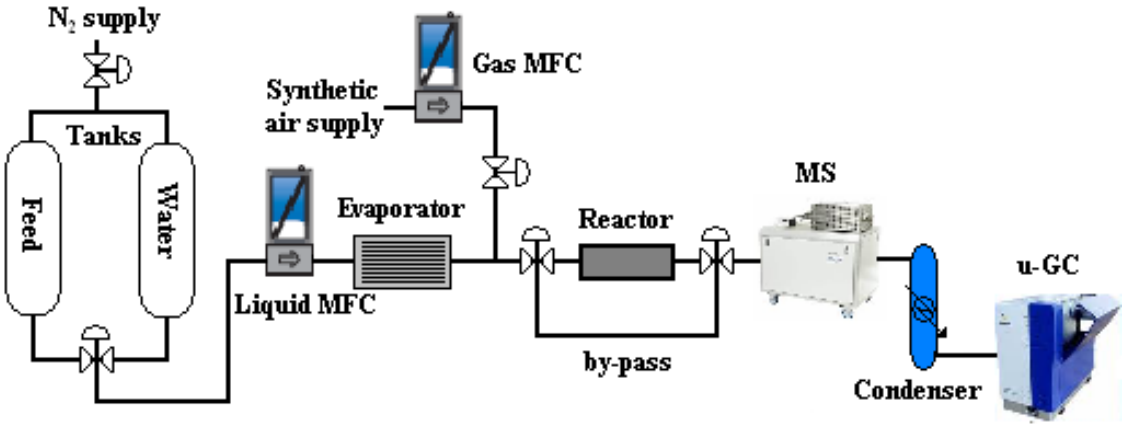

Figure 1: *Scheme of the experimental set up.*

All the catalysts were tested at atmospheric pressure. For SR experiments the effect of temperature was studied at 625, 675 and 725°C at a VHSV of 200 NL/h·g_{cat}. Then, at a constant temperature of 675 °C, the VHSV was modified to 100 and 300 NL/h·g_{cat}. In the case of OSR experiments, the effect of the VHSV was studied at a temperature of 675°C. Each experimental condition was investigated for 1 hour duration. Thus, the tests performed for each catalyst can be summarized as shown in Table 1.

Table 1: *Experimental conditions of the carried out activity tests.*

Process	**SR**					**OR**		
Time progress (h)	1	2	3	4	5	6	7	8
Temperature (ºC)	725	675	625	675		675		
VHSV (NL/ h ·g_{cat})	200			300	100	100	200	300

The conversion of $C_2H_6O_2$ and the selectivity towards different carbon containing species $C_iH_jO_k$ were calculated from the following equations:

$$X_{C_2H_6O_2} = \frac{c_{0,C_2H_6O_2} - c_{1,C_2H_6O_2}}{c_{0,C_2H_6O_2}} \times 100[\%] \quad (1)$$

$$S_{C_iH_jO_k} = \frac{i}{2}\frac{c_{1,C_iH_jO_k}}{c_{0,C_2H_6O_2} - c_{1,C_2H_6O_2}} \times 100[\%] \quad (2)$$

where C_0 and C_1 are the concentration of the species at the reactor inlet (as determined by bypass measurements) and outlet respectively, which were determined taking into account the volume changes of the reaction.

5.3 xRh-cm and xRh-np catalysts for ethylene glycol reforming

Article available online:

Title: Sustainable syngas production from ethylene glycol reforming processes using Rh based catalysts in microreactors

Authors: U. Izquierdo[1], M. Wichert[2], V.L. Barrio[1], G. Kolb[2]

[1] *Dept. of Chemical and Environmental Engineering, School of Engineering, University of the Basque Country UPV/EHU, c/ Alameda Urquijo s/n 48013, Bilbao, Spain*

[2] *Institut fur Mikrotechnik Mainz GmbH, IMM, Carl-Zeiss-Str. 18-20, 55129 Mainz, Germany*

Journal: Applied catalyst B: Environmental

Year: 2014

5.3.1 Fresh catalysts characterizations results

5.3.1.1 Textural properties, BET

The textural properties of fresh calcined catalysts are shown in Table 2. Taking into account that a surface area of 10.6 m^2/g was measured for the bare α-alumina, the rest of the catalysts showed increased surface area due to the Rh incorporation. Comparing among the catalysts, higher surface areas were obtained for the samples prepared by the nanoparticle method. A similar increase of the catalysts surface area was also reported in [31,32]. As far as the other measured parameters are concerned, increased pore size and pore volume were observed.

Table 2: *Catalysts textural properties, BET surface area, S_{BET}, Pore volume, Pv, and Pore radius, Pr.*

Catalyst	S_{BET} (m^2/g)	Pv (cm^3/g)	Pr (Å)
α-Al_2O_3	10.6	0.013	49
1.0Rh-np	10.4	0.073	140
2.5Rh-np	12.1	0.085	141
5.0Rh-np	15.1	0.113	150
1.0Rh-cm	10.3	0.083	161
2.5Rh-cm	11.4	0.067	118
5.0Rh-cm	12.3	0.080	130

5.3.1.2 Temperature programmed reduction, TPR

TPR profiles of the fresh calcined catalysts are shown in the Figure 2. For each TPR analysis, the same amount of catalyst was used in order to compare their reduction peaks. Therefore, as it can be observed in the figure, the size of the reduction peaks, proportional to the H_2 required for the species reduction, increased with the Rh metal load for both types of prepared catalysts. However, a considerably higher reduction peak was measured for the 5.0Rh-cm catalysts, which can be related to the higher amount of reducible species (This is confirmed by the XPS analyses carried out. See Table 3).

The main reduction peaks, appear between 158 and 167ºC. In addition, smaller reduction peaks were detected at lower reduction temperatures (between 84 and 96ºC). For the 2.5Rh-cm catalyst, the peak at the low temperature is the highest. It has been reported that these peaks correspond to a three-dimensional RhOx phase (large particles) and two-dimensional surface RhOx phase species at low and high temperatures respectively [32,33]. The low temperature peaks are assigned to the reduction of RhOx species over the alumina surface and the other one, at higher temperature, to the RhOx species placed in the interface metal-support [34]. If the deconvolution of the peaks is carried out, for all the catalysts, except to the 2.5Rh-cm, a

better reducibility of the RhOx species placed in the interface metal-support is observed. In the case of the 2.5Rh-cm catalysts, as the highest reduction peak is located at 94ºC, a major reduction of the RhOx species over the alumina surface occurred. Attending to the activity results described in section 5.3.2, for this catalyst stable conditions and good activity results were achieved.

Apart from the described peaks, smaller interactions were detected at temperatures between 553 and 576ºC. These peaks can correspond to the interaction between the Rh and the α-alumina [20]. Finally, a different behavior was noticed for the 2.5Rh-np catalyst when a small peak at around 210ºC was detected. In addition, for this catalyst no peak was detected at the lowest temperature.

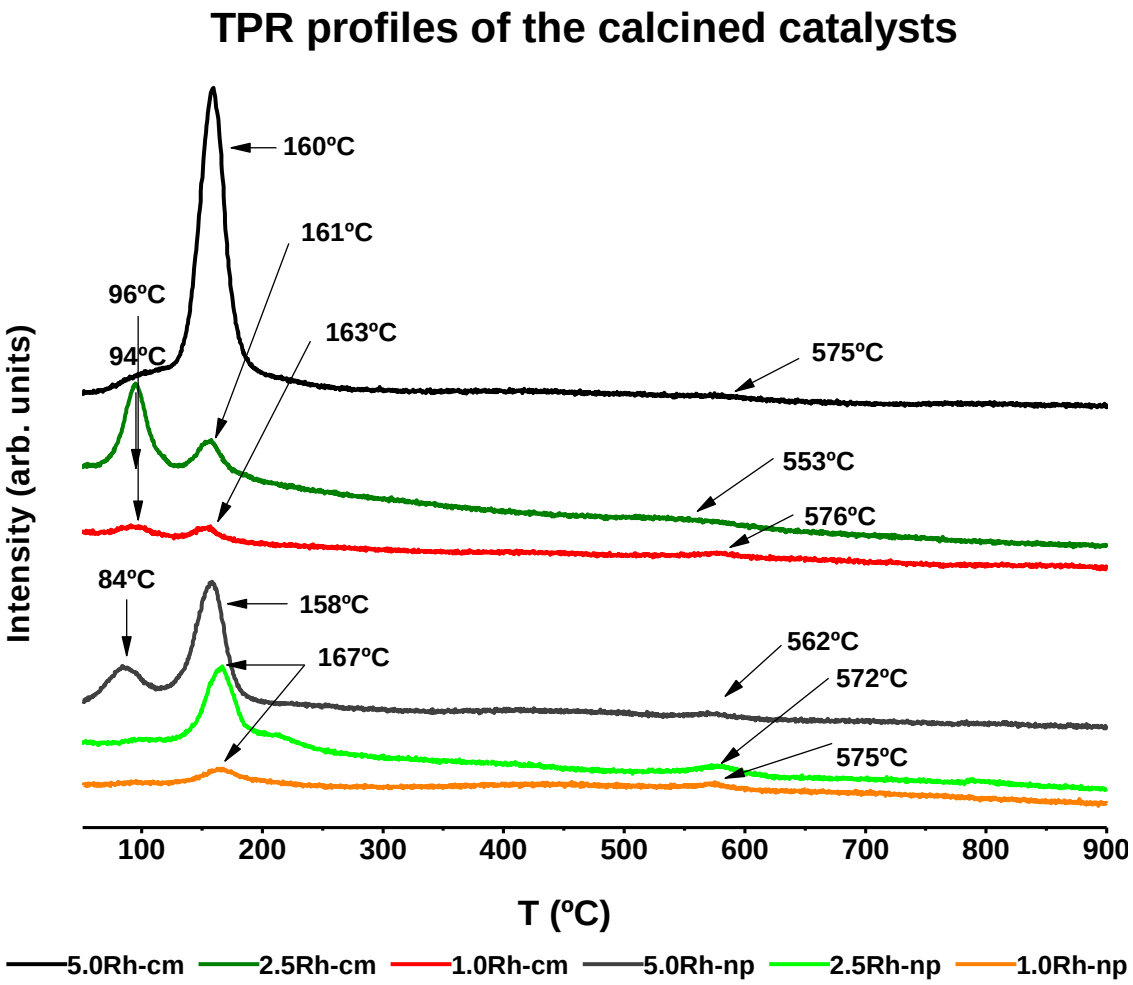

Figure 2: *TPR profiles of the calcined catalysts.*

5.3.1.3 Transmission electron microscope, TEM

In the Figure 3, the obtained TEM micrographs are collected. Using this technique, the particle sizes and dispersion differences between the two types of catalysts were observed.

According to the obtained micrographs, particle aggregates were observed for the 5.0Rh-np catalyst. When independent particles sizes were measured for this catalyst, most of them ranged between 4 and 6 nm and also few ranged from 10 to 15 nm. In the case of its homologous 5.0Rh-cm catalyst, a better dispersion of the particles and more homogeneous size distribution was observed. However, more particles in the size range of 10-15 nm were measured in the micrograph of the latter catalyst.

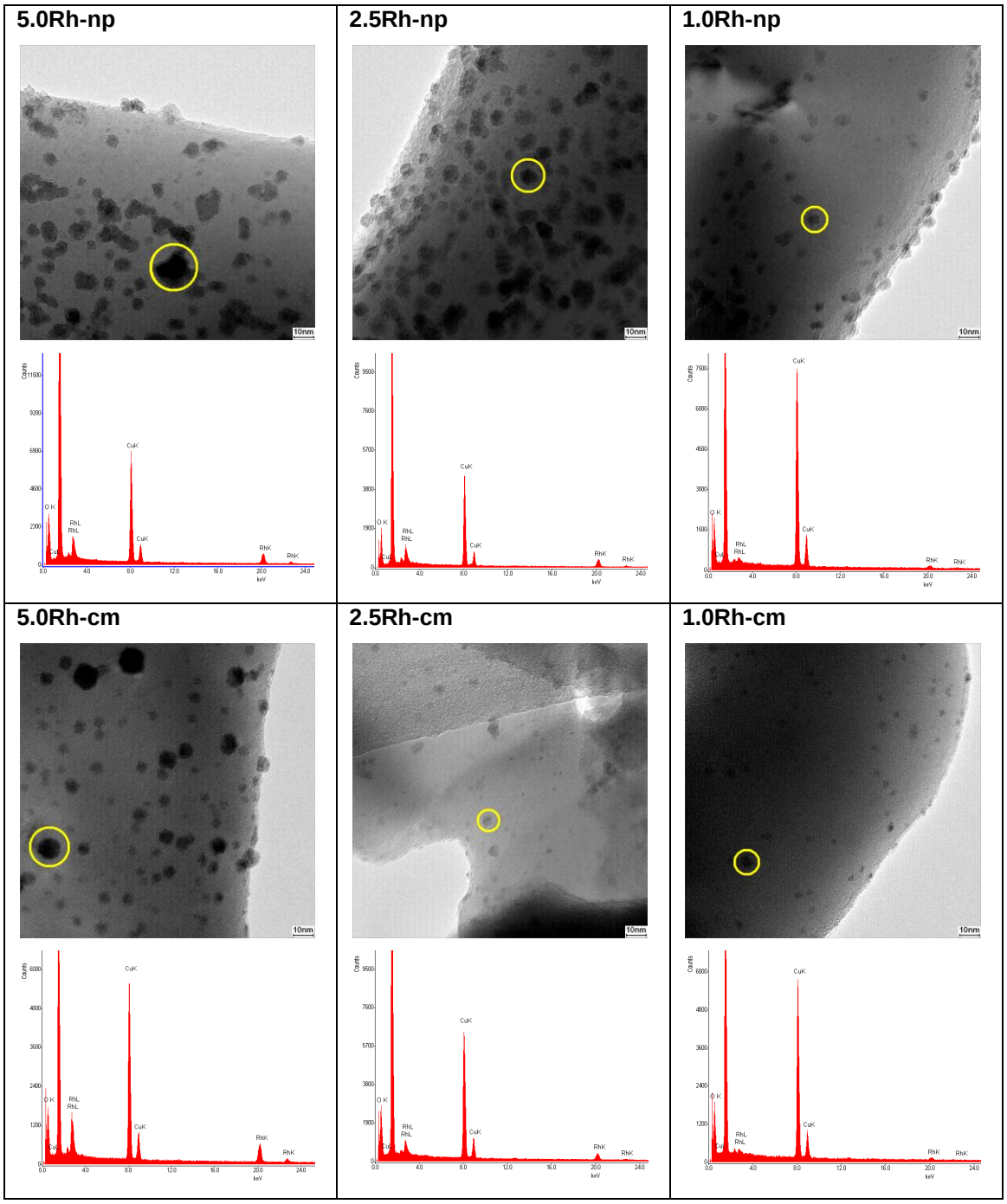

Figure 3: *TEM micrographs of the calcined catalysts. Scale bar=10 nm.*

For the 2.5Rh-np catalyst a lower density of particles was observed with a majority between 4-6 nm, but also few between 10-15 nm. For this catalyst no particle aggregates were observed. In the case of its counterpart prepared by impregnation, the 2.5Rh-cm catalyst, an even lower particle density was observed and all particles were smaller than 5 nm. Finally, for the 1.0Rh catalysts the lowest particles density was observed. Comparing both catalysts, bigger particles were measured for the 1.0Rh-np catalyst, ranging between 3-6 nm than for the 1.0Rh-cm, for which all the observed particles were smaller than 4 nm. Thus, although the dispersion has not been analytically measured by H_2 pulse chemisorptions, a good dispersion of small noble metal particles is observed especially for the samples prepared by the impregnation method.

5.3.1.4 X-ray diffraction, XRD

The obtained XRD spectra for the fresh calcined catalysts are shown in the Figure 4. The α-Al_2O_3 was perfectly indentified (marked by the + symbol in the figure) by the corresponding peaks among the measured 2θ positions (Corundum, PDF: 01-075-0783). In the case of Rh species, the rhodium oxide contributions (Distinguished by the º symbol in the figure) should appear at 48.97 and 53.89º (PDF: 01-071-2084) in the measured 2θ region. However, only very small peaks were detected.

Accurate measurements were carried out to distinguish the peaks that correspond to the rhodium oxide, in order to calculate the particles size by the Scherrer equation. Therefore, in the right side of the Figure 4, magnified spectra obtained for the 5.0Rh-cm and 5.0Rh-np catalysts are shown. With these spectra, rhodium oxide contributions at 48.49 and 48.91º, respectively, were detected. As a result, rhodium oxide particles sizes of 15 nm for the 5.0Rh-cm and 10 nm for the 5.0Rh-np catalyst were estimated using the Scherrer equation. These results are in good agreement with the particle sizes observed in the TEM micrograph, taking into account that also smaller particles were observed. For the samples with lower Rh content, no peaks were detected. This only could be explained due to the limitations of the technique regarding the crystalline particles sizes (a particle size below 5 nm cannot be detected) which is also in good agreement with the micrographs obtained by TEM. In addition, the technique is also limited by the amount of the metal in the catalysts, which is low in the case of the 1.0Rh and 2.5Rh catalyst.

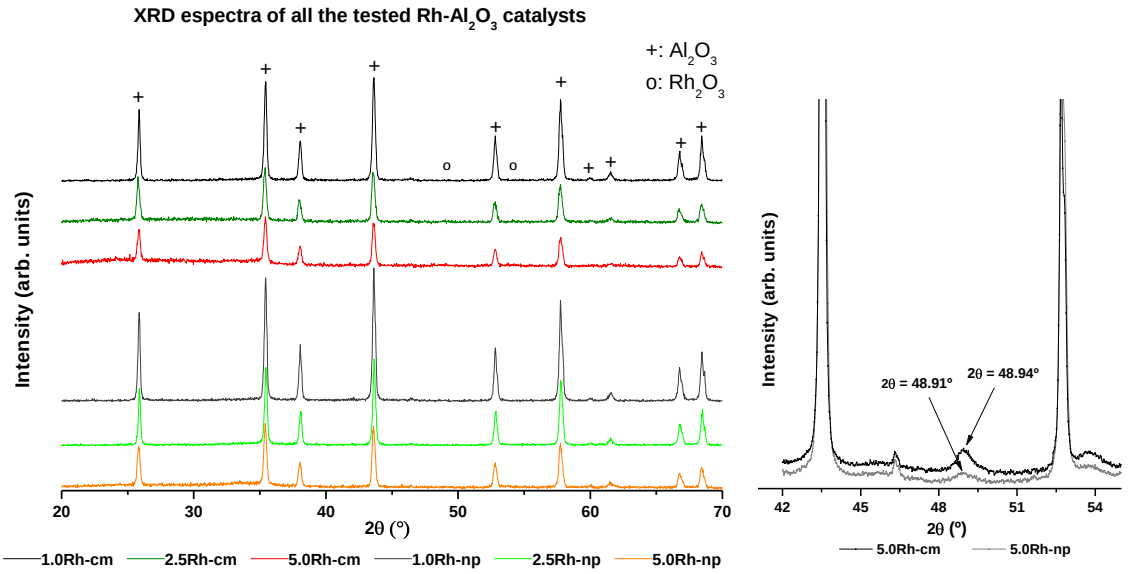

Figure 4: *XRD spectra of the Rh catalysts (left); Magnified XRD spectra for the 5Rh-cm and np catalysts (right).*

5.3.1.5 X-ray Photoelectron Spectroscopy, XPS

XPS analysis was carried out to determine the chemical composition of the catalysts surface and to better understand the nature of interaction between the dispersed metal species and the support. The results of the fresh calcined and tested catalysts are summarized in Table 3. In the case of the tested catalysts, the measurements were carried out after the conditions specified in the Table 3.

Table 3: *Fresh calcined and tested catalysts, binding energies of Al 2p and Rh $3d_{5/2}$ core levels, atomic concentrations and Rh^o and Rh^{3+} proportions (in parenthesis). Theoretical, fresh and tested catalysts surface atomic.*

Catalyst	Fresh catalysts				Tested catalysts					Atomic ratios		
	Al 2p [eV, (%)]	Rh 3d [%]	Rh^{3+} [eV, (%)]	Rh^o [eV, (%)]	C [%]	Al 2p [eV, (%)]	Rh 3d [%]	Rh^{3+} [eV,(%)]	Rh^o [eV, (%)]	Rh/Al Theor	Rh/Al Fresh	Rh/Al Tested
1.0Rh-cm	72.9 (32.5)	0.94	308.9 (81.2)	307.3 (18.8)	86.2	74.2 (2.9)	0.76	308.8 (20.9)	307.4 (41.4)	0.005	0.03	0.06
2.5Rh-cm	73.0 (33.1)	1.98	308.5 (78.8)	307.2 (31.2)	59.0	74.3 (13.6)	0.83	308.5 (21.4)	307.5 (37.4)	0.013	0.06	0.06
5.0Rh-cm	73.4 (30.6)	2.75	308.5 (84.4)	307.4 (15.6)	60.1	74.2 (10.1)	0.63	308.8 (35.7)	307.6 (28.2)	0.026	0.09	0.26
1.0Rh-np	73.5 (35.1)	1.51	308.9 (63.2)	307.2 (36.8)	72.5	74.4 (6.8)	0.44	308.7 (27.8)	307.4 (34.2)	0.005	0.04	0.06
2.5Rh-np	72.8 (30.5)	3.15	308.3 (67.8)	307.2 (32.2)	83.2	76.1 (5.9)	0.74	308.8 (41.8)	307.4 (12.7)	0.013	0.10	0.12
5.0Rh-np	73.3 (26.9)	4.89	308.2 (62.6)	307.2 (37.4)	86.7	74.7 (4.6)	0.59	n.d	n.d.	0.026	0.18	0.13

For the XPS results interpretation, the peak that corresponds to C_{1s} was used in order to standardize all the spectra obtained for both fresh reduced and spend catalysts. Focusing on the results obtained for the fresh reduced catalysts, two main differences can be observed if cm

and np catalysts are compared; the total Rh atomic concentration (Rh_{3d}) and the metallic Rh atomic concentration (Rh^o) were both higher for the np-catalysts than for their homologous cm ones. For both type of catalysts the Rh_{3d} increased with the Rh theoretical amount, but in the case of the Rh^o, no clear tendency was observed. Thus, more active sites were supposed to be available for the np fresh reduced catalysts.

Attending to the columns that correspond to the catalysts tested, the results obtained were not expected when compared with those obtained for the fresh calcined samples, but they agree with the activity results obtained (see section “3.2 Results from activity testing”). For all the np-catalysts very high carbon atomic concentration was measured. Due to this fact, the Rh_{3d} detected for these catalysts was very low and as a consequence, Rh^{3+} or Rh^o could not to be detected for the 5Rh-np catalysts by this technique. In the case of the rest of np-catalysts, although a high carbon atomic concentration, Rh^{3+} and Rh^o species were detected as specified in the table. For the cm-catalysts, higher Rh_{3d} were measured due to the apparently lower carbon deposition. For the 2.5Rh-cm catalyst was measured the highest Rh_{3d} and also the highest Rh^o.

According to the activity results obtained, the 5.0Rh-cm and 2.5Rh-cm catalysts showed the best performance. In addition, for all the tested catalysts a doublet at higher binding energies was detected, at 310.4 and 315.0eV respectively. According to those binding energies, the doublet could be attributed to the Rh but this has not been reported in the literature neither in any data base. Finally, higher Rh/Al ratios were measured for the fresh np-catalysts than for the cm catalysts, as expected. Each catalyst showed higher Rh/Al ratio after testing, apart from the 5Rh-np catalysts, which could originate from the preferential carbon deposition on the alumina surface.

5.3.2 Results from activity testing

Figure 5 shows the conversion of EG as obtained over the catalysts under investigation at different reaction temperature and under conditions of SR. It is obvious that cm-catalysts show much higher activity. Apart from the sample 1.0Rh-cm, full conversion was always achieved while the np-catalysts showed much lower activity. While 1.0Rh-np sample Rh showed lower activity compared to the sample 2.5Rh-np as expected, the activity of the 5.0Rh-np sample is even lower, which is not explained by the catalyst characterization described above.

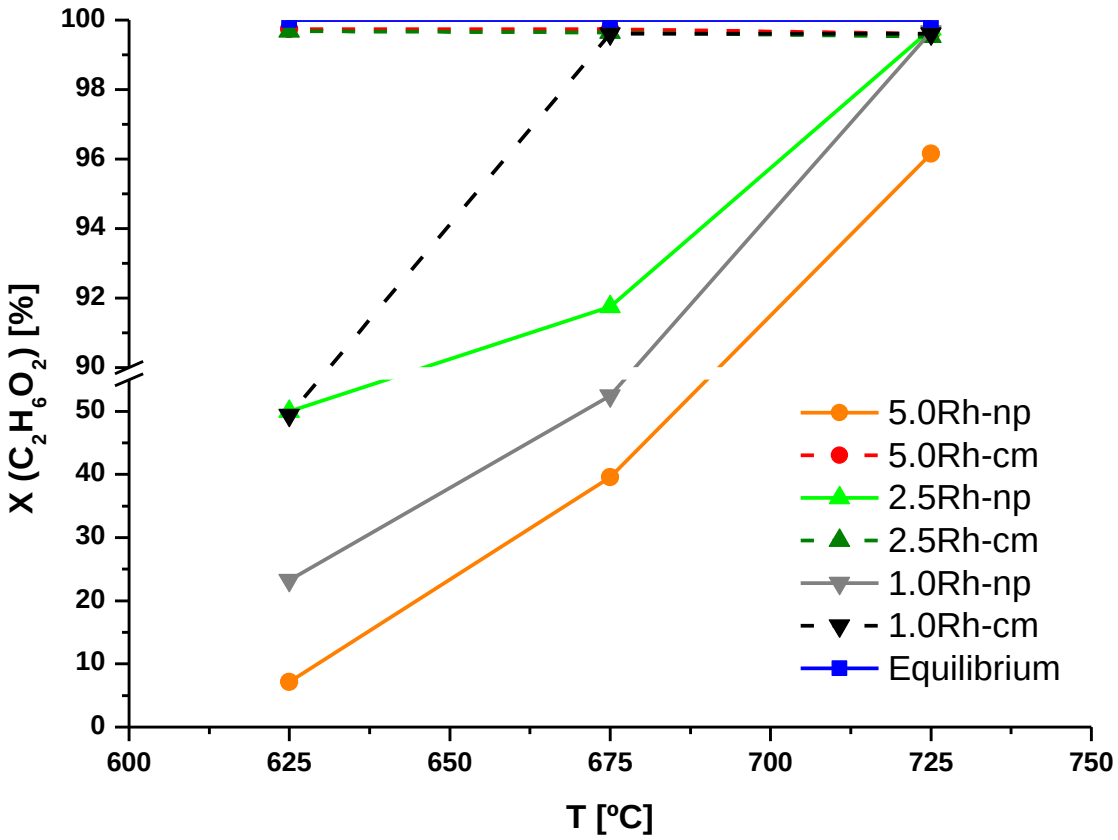

Figure 5: *Conversion vs. reaction temperature as obtained for all catalysts under investigation under conditions of SR.*

For the cm samples, the selectivity towards the by-products is compared in Figure 6. While the selectivity towards CO (see Figure 6a) and CO_2 (see Figure 6b) is close to the thermodynamic equilibrium for the samples 2.5Rh-cm and 5.0Rh-cm, the 1.0 Rh-cm sample shows higher selectivity towards CO (the primary product of steam reforming) and lower selectivity towards CO_2, because the water-gas shift activity of the catalyst is insufficient. The selectivity towards CH_4 (see Figure 6c) shows a more complicated pattern. The 5.0Rh-cm sample shows values close to the thermodynamic equilibrium of the methanation reaction. For the 2.5Rh-cm sample the values are lower than those expected from thermodynamics, which is attributed to a low methanation activity of the catalyst. As the result, no CO is converted to methane. The 1.0Rh-cm sample obviously released methane as a result of incomplete conversion of EG during

steam reforming and has likely no methanation activity at all. Acetaldehyde is formed as by-product mostly over the 2.5Rh-cm and 5.0Rh-cm samples (see Figure 6d).

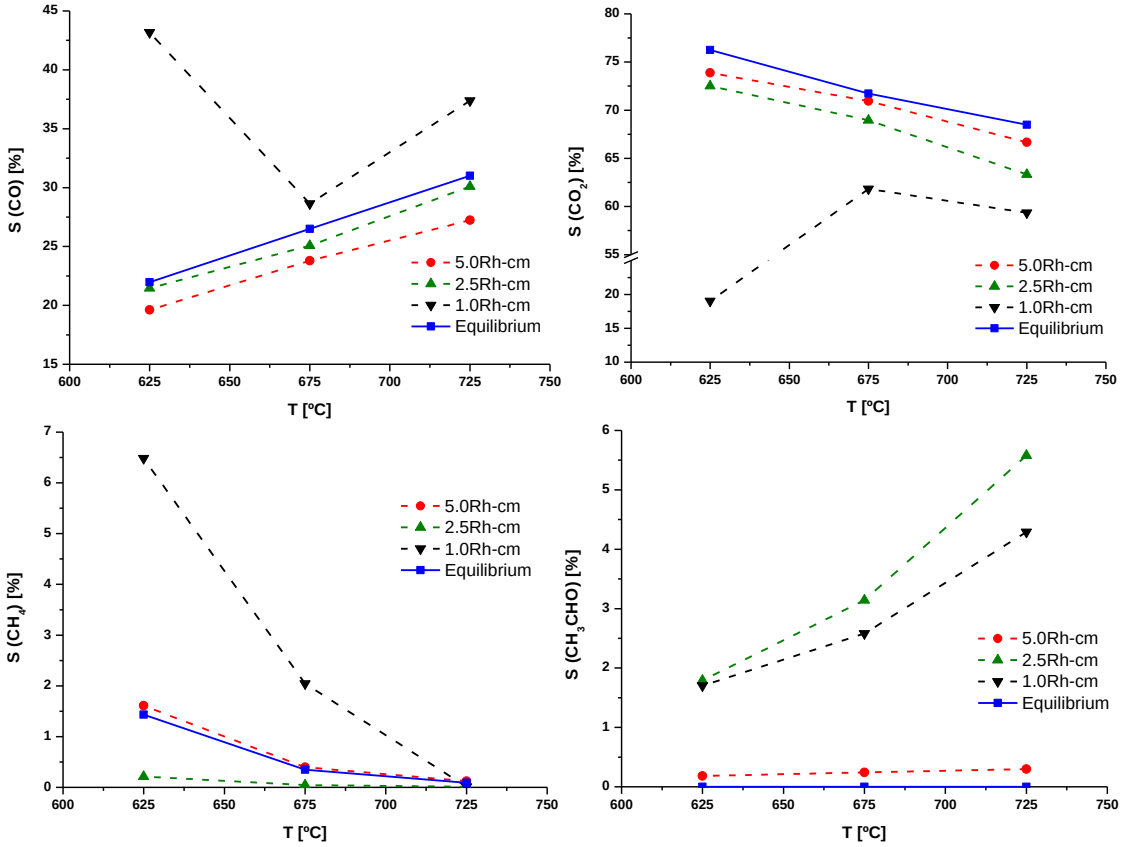

Figure 6: *Selectivities vs. reaction temperature as obtained for the catalysts prepared according to the conventional method (cm) under conditions of SR; (a) top left: CO selectivity; (b) top right: CO_2 selectivity; (c) bottom left: CH_4 selectivity; (d) bottom right: CH_3CHO selectivity; the values as calculated for the thermodynamic equilibrium of the reaction mixture are included.*

Figure 7 shows a comparison of the samples contaning 2.5 % Rh prepared by the cm and np methods (2.5Rh-cm and 2.5Rh-np). The np catalyst shows a much higher CO selectivity, lower CO_2 selectivity and also higher acetaldehyde selectivity (see Figure 7a). The methane selectivity of the np catalyst is higher as well as its selectivity towards other undesired by-products, namely higher hydrocarbons such as ethylene and ethane, which proves once more the inferior performance of this catalyst type (see Figure 7b).

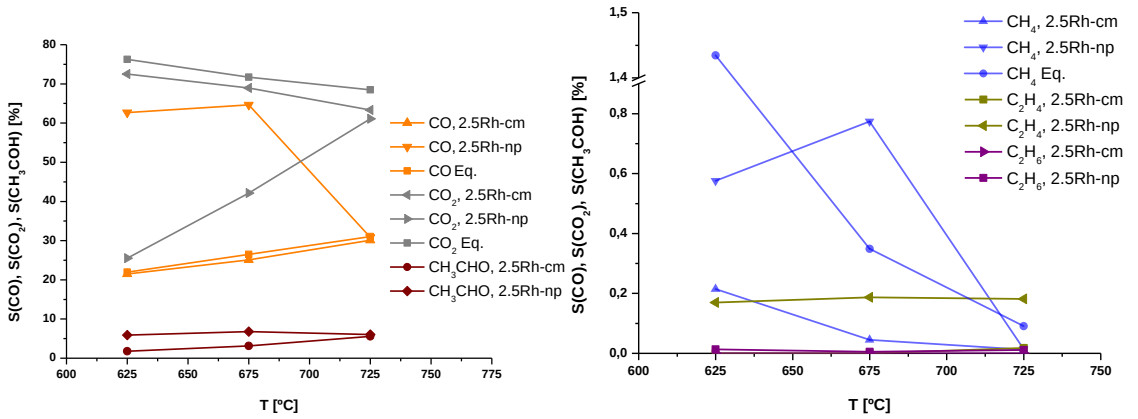

Figure 7: *Selectivities vs. reaction temperature as obtained for the catalysts containing 2.5 wt.% Rh prepared according to the conventional method (cm) and the nanoparticle method (np) under conditions of SR; (a) left: CO, CO_2 and CH_3CHO selectivity; for CO and CO_2 the values as calculated for the thermodynamic equilibrium of the reaction mixture; (b) right: CH_4, C_2H_4,C_2H_6 selectivity; for CH_4 the values as calculated for the thermodynamic equilibrium of the reaction mixture.*

Figure 8 shows a comparison of the conversion as obtained for all catalysts at different space velocities, which documents the inferior performance of the np catalysts, showing dramatically lower conversion at higher feed flow rates.

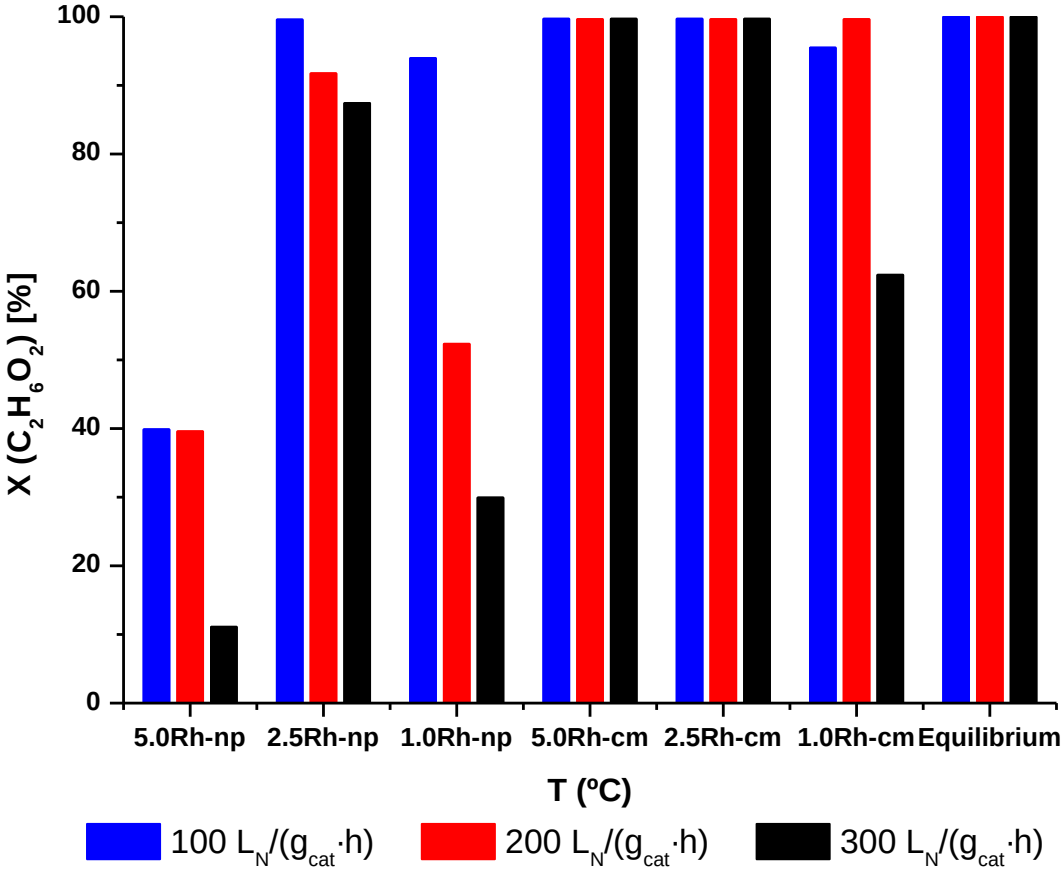

Figure 8: *Conversion as obtained for all catalysts under investigation at a reaction temperature of 675°C under conditions of SR at different VHSV.*

Figure 9 shows the selectivities towards methane, ethylene and acetaldehyde as determined under conditions of SR and OSR at all samples under investigation. The methane formation is lowest for the cm samples containing 2.5% Rh and more. It is suppressed by lower space velocity and oxygen addition in most cases (see Figure 9a and 9b). Similar observations were made with respect to ethylene, while no ethylene was formed at the cm samples containing 2.5% and 5% Rh (see Figure 9c and 9d). The results are less straight-forward for acetaldehyde (see Figure 9e and 9f). No clear effect of increased feed flow rate could be observed, while the oxygen addition obviously increased the acetaldehyde formation unexpectedly.

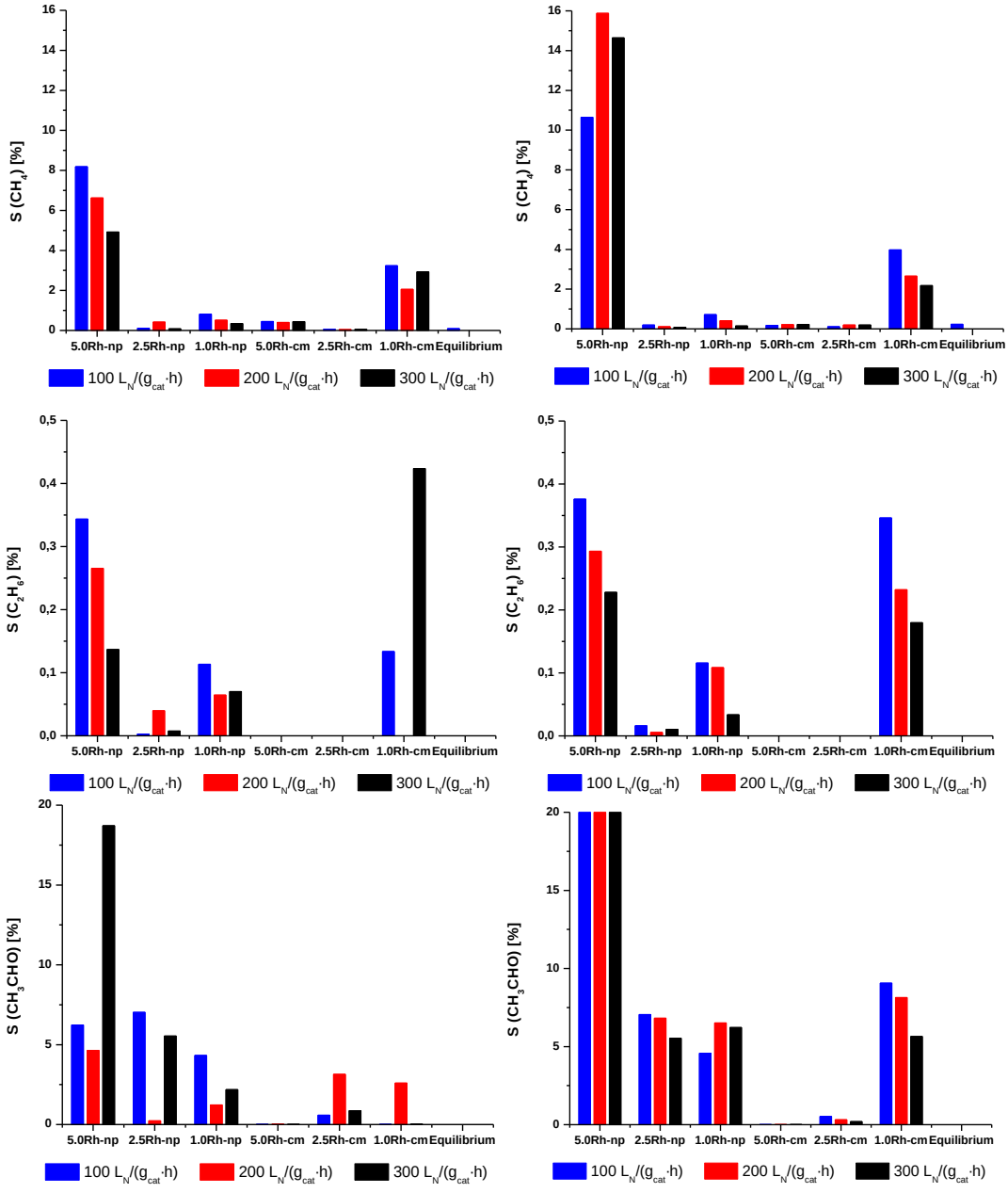

Figure 9: *Selectivities at different VHSV as obtained for all catalysts at 675°C reaction temperature under conditions of SR and OSR; (a) top left: CH_4 selectivity (SR); (b) top right: CH_4 selectivity (OSR) (c) center left: C_2H_6 selectivity (SR); (d) center righ: C_2H_6 selectivity (OSR); (e) bottom left: CH_3CHO selectivity (SR); (f) bottom right: CH_3CHO selectivity (OSR).*

Figure 10 shows the hydrogen molar composition measured for the SR process carried out at different temperatures. Higher hydrogen molar concentrations were measured at higher temperatures for the np samples. In the case of both 2.5Rh-cm and 5.0Rh-cm samples, the hydrogen composition measured followed the equilibrium predictions. However, for the samples with lower metal content, the measured hydrogen composition was lower at the lowest temperature.

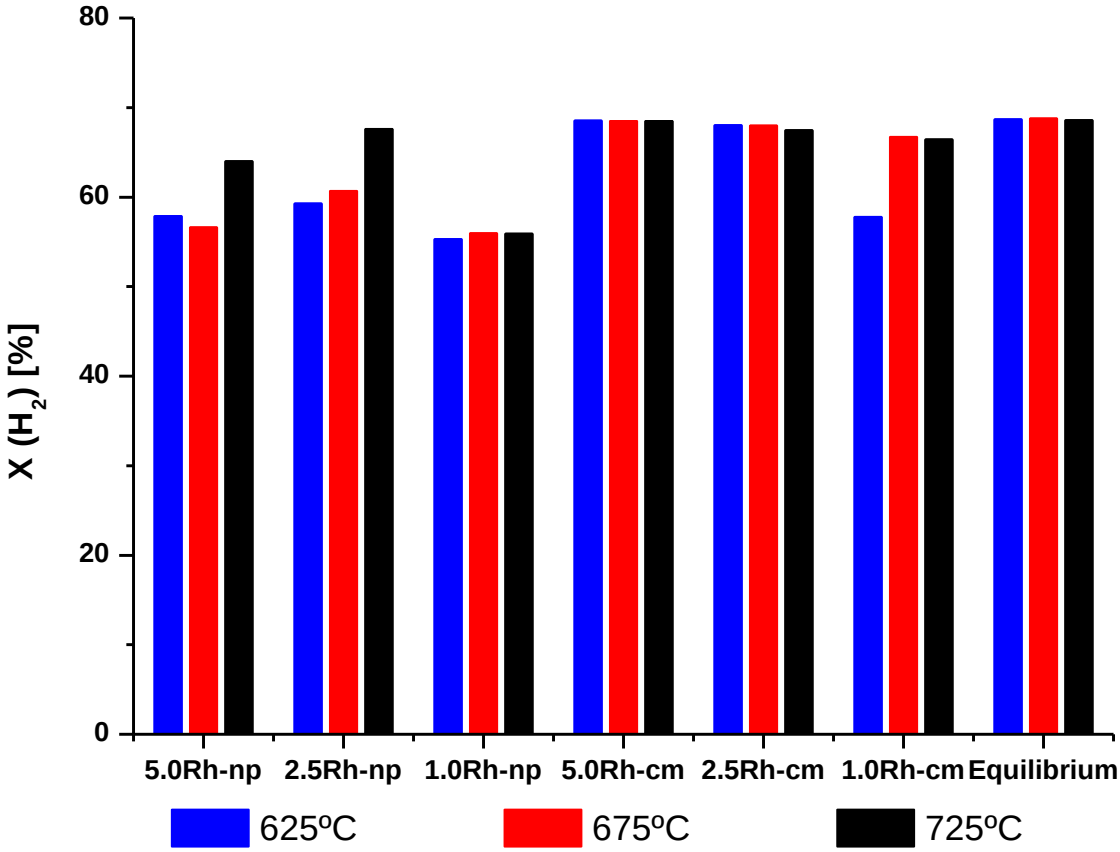

Figure 10: *Measured hydrogen molar compositions under SR at different T (Dry basis).*

In Table 4 the calculated hydrogen production rates are shown for the different experimental condition studied. As expected after the results presented, the 2.5Rh-cm catalyst reached the highest hydrogen production rates under all the conditions tested with the exception of SR at 725ºC, and surprisingly the 5.0Rh-np sample the lowest.

Table 4: *Hydrogen production rates at the tested conditions.*

Catalyst: amount	$C_2H_6O_2$ SR				$C_2H_6O_2$ OSR	
	VHSV=200 NL/ h g_{cat}		T=675ºC		T=675ºC	
	T (ºC)	H_2 flow ($L/g_{cat}h$)	VHSV ($L/g_{cat}h$)	H_2 flow ($L/g_{cat}h$)	VHSV ($L/g_{cat}h$)	H_2 flow ($L/g_{cat}h$)
1.0Rh-np: 0.0166 g	725	75.4			300	51.5
	675	43.6	300	40.6	200	34.4
	625	20.9	100	32.7	100	41.4
2.5Rh-np: 0.0161 g	725	95.8			300	79.2
	675	77.8	300	96.4	200	61.8
	625	46.4	100	38.8	100	41.7
5.0Rh-np: 0.0145 g	725	81.0			300	20.3
	675	29.0	300	15.4	200	15.0
	625	7.2	100	12.5	100	10.4
1.0Rh-cm: 0.0160 g	725	91.5			300	50.0
	675	91.8	300	6.8	200	34.3
	625	38.9	100	3.2	100	24.4
2.5Rh-cm: 0.0171 g	725	94.9			300	**146.6**
	675	**99.9**	300	**150.69**	200	**119.4**
	625	**101.7**	100	**50.83**	100	**48.9**
5.0Rh-cm: 0.0164 g	725	**97.7**			300	133.3
	675	98.9	300	148.4	200	82.7
	625	98.7	100	49.5	100	36.7

5.3.3 Conclusions

Rh containing catalysts were prepared by different preparation methods and tested for their activity in steam reforming and oxidative steam reforming of ethylene glycol. While the samples prepared by a conventional impregnation method showed generally higher activity compared to catalysts prepared from Rh nanoparticles, all samples suffered from by-product formation of species such as acetaldehyde, ethane and ethylene regardless if oxygen was added to the feed or not.

In future investigations how the catalyst activity can be further improved and by-product formation can be suppressed by addition of ceria or lanthana to the catalyst formulation will be investigated. In addition, the catalysts stability will be investigated through long term experiments.

5.4 2.5Rh-cm catalyst support modification with CeO_2 and La_2O_3

Article available online:

Title: Microreactor hydrogen production from ethylene glycol reforming using Rh catalysts supported on CeO_2 and La_2O_3 promoted α-Al_2O_3

Authors: U. Izquierdo[1], M. Wichert[2], V.L. Barrio[1], G. Kolb[2], P.L. Arias[1], J.F. Cambra[1], R. Zapf[2], A. Ziogas[2], S. Neuberg[2]

[1] *Dept. of Chemical and Environmental Engineering, School of Engineering, University of the Basque Country UPV/EHU, c/ Alameda Urquijo s/n 48013, Bilbao, Spain*

[2] *Institut fur Mikrotechnik Mainz GmbH, IMM, Carl-Zeiss-Str. 18-20, 55129 Mainz, Germany*

Journal: International Journal of hydrogen energy

Year: 2014

5.4.1 Fresh catalysts characterization

5.4.1.1 Textural properties, BET

Textural properties of the fresh calcined catalysts are also summarized in Table 5. Taking into account that a surface area (SA) of 10.6 m^2/g was measured for the bare α-alumina, this SA increased when Rh was incorporated. In addition, higher SA was measured when support modifiers were added to the corresponding catalysts. These textural property changes could be due to the interactions between Rh and modifiers with the alumina [31,32]. Comparing the catalysts containing ceria and lanthana additives, the incorporation of CeO_2 contributed more than La_2O_3 to the surface area increase. Regarding the total pore volume (PV) with respect to the catalysts with modified support, higher total PV was measured for the CeO_2 containing catalysts than for the La_2O_3 ones, and all of them reached higher values than 2.5Rh catalyst. This could be explained by the larger SA measured in the other catalysts prepared. The average pore size radius (PR) was measured. While pores of 11.8 nm were measured for the 2.5Rh catalyst, the CeO_2 containing samples showed similar PR in the range of 10 nm, while the La_2O_3 containing samples showed PR in the range of 15 nm both independent of the corresponding content of CeO_2 and La_2O_3.

Table 5: *Catalysts textural properties: BET surface area, SA, pore volume, PV, and pore radius, PR.*

Catalyst	Surface area SA (m^2/g)	Pore volume PV (cm^3/g)	Pore radius PR (Å)
2.5Rh	11.4	0.067	118
2.5Rh-10Ce	19.9	0.097	98
2.5Rh-20Ce	30.1	0.149	99
2.5Rh-5La	11.7	0.093	158
2.5Rh-10La	12.4	0.089	145

5.4.1.2 Temperature programmed reduction, TPR

In Figure 11, TPR profiles of the fresh calcined catalysts are represented. For the 2.5Rh catalyst, three main peaks were observed with maximums at 94, 161 and around 570ºC. The peaks at 94 and 161ºC are assigned to the reduction of isolated RhO_x species, corresponding to a three-dimensional RhOx phase (large particles) and two-dimensional surface RhOx phase species at low and high temperatures, respectively [32,33]. In the case of the peak at higher temperature, it has been reported that it corresponds to the reduction of the formed Rh-support strong interactions [35]. Finally, in spite of rhodium aluminates species formation being reported at very high temperatures, 800-1000ºC [35], they were not detected for this catalyst.

As far as the remaining catalysts are concerned, a significant change in the reducibility of the formed species was observed. For the CeO_2 containing catalysts, a unique reduction peak appeared at low temperature centered at 102ºC, which is wider than the peak measured for the 2.5Rh catalyst at similar temperature (see Table 6), but covered almost the same temperature range, from 60ºC to 200ºC, approximately. A new peak appeared at very high temperature, with maximum between 885 and 903ºC. Comparing the CeO_2 containing catalysts with the 2.5Rh catalyst, this peak cannot be attributed to a rhodium aluminates species. Therefore, this peak could be assigned to surface and bulk reduction of Ce^{4+}-Ce^{3+} species [25,36]. For both CeO_2 containing catalysts, the small peak assigned to a rhodium-support interaction detected at intermediate temperature, between 460-570ºC, remained.

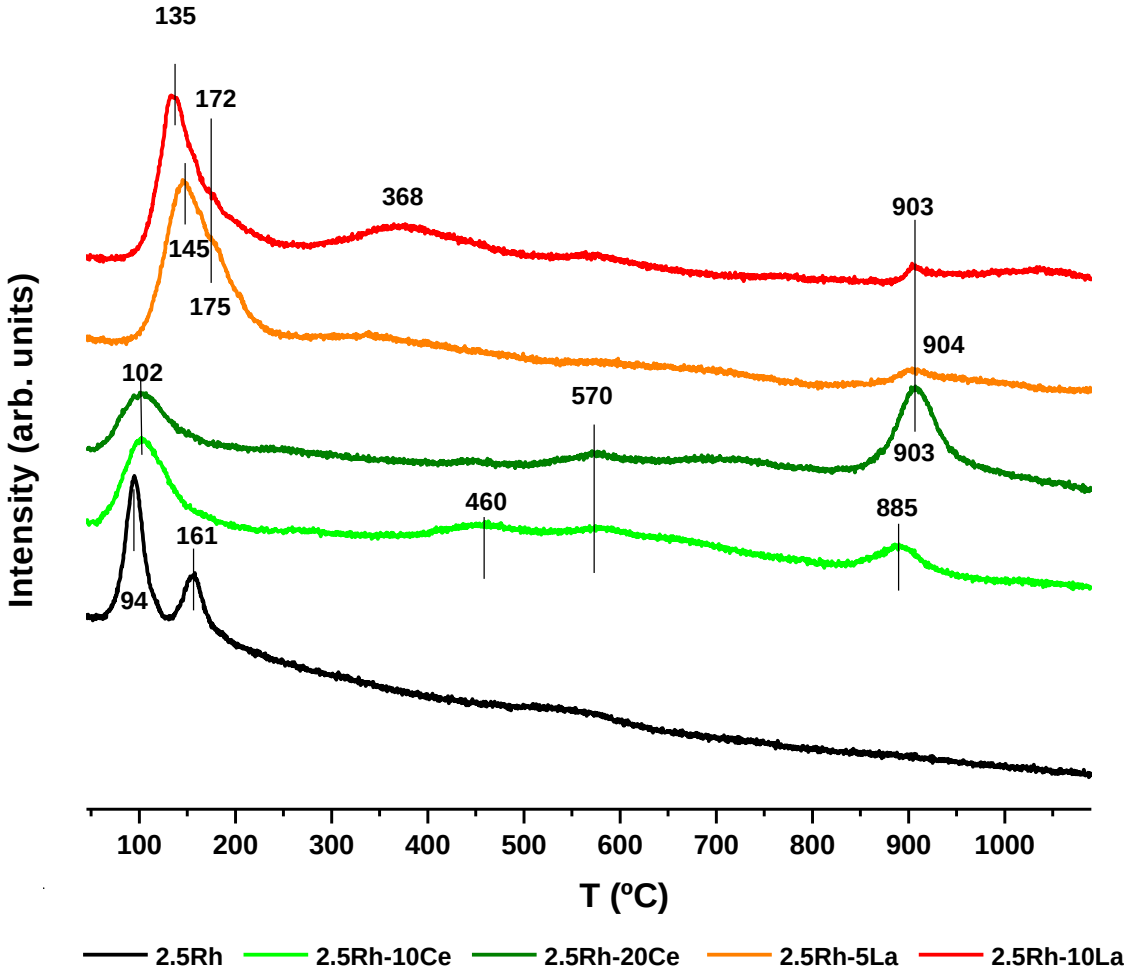

Figure 11: *TPR profiles of the calcined catalysts.*

In the case of the La_2O_3 doped catalysts, similar reduction profiles as for the CeO_2 doped samples were obtained, but the reduction of the RhOx species occurred at higher temperatures. In addition, the detected broad peak is clearly formed by the contribution of two smaller ones, with maxima at 135ºC and 175ºC. Regarding the peaks formed at intermediate temperature, (between 368 and 570ºC) they were also detected for the La_2O_3 containing catalysts for which the highest contribution was measured at 368ºC. Finally, the peaks observed at the highest temperatures are smaller, lower area, compared with the CeO_2 containing samples.

Table 6: *Deconvolution of the peaks detected by TPR.*

Catalyst	Peaks (ºC)	Area	Width
2.5Rh	95	443.4	20.5
	161	238.8	27.2
	550	115.0	87.5
º2.5Rh-10Ce	102	538.7	42.7
	460	156.8	82.7
	570	84.2	58.3
	885	149.3	42.0
2.5Rh-20Ce	102	338.2	46.7
	460	65.9	82.3
	570	119.4	76.0
	903	566.4	44.9
2.5Rh-5La	145	399.4	30.2
	175	923.9	59.6
	904	136.7	68.5
2.5Rh-10La	135	497.2	27.1
	172	585.7	60.9
	903	60.1	31.1

5.4.1.3 Transmission electron microscope, TEM

In Figure 12 the TEM micrographs for the fresh catalysts are shown. In general, the Rh particles are well dispersed and independent and no aggregates can be observed. Small particles can clearly be observed for all CeO_2 and La_2O_3 containing samples. For the 2.5Rh-10Ce catalyst all the Rh particles observed are smaller than 3 nm and they are very well dispersed. In addition, CeO_2 small particles can also be observed, which are larger, between 4-6 nm, than the Rh particles. In the case of the 2.5Rh-20Ce catalyst, similar Rh particles were detected. However, bigger CeO_2 particles were formed in this catalyst, bigger than 5 nm, which might be due to the higher amount of additive [18]. Regarding the La_2O_3 containing catalysts, apart from the Rh particles no any La structure was observed for the 2.5Rh-5La catalyst. However, big crystals were detected for the 2.5Rh-10La catalyst, around 10 nm, which some authors identified possible different lanthanum oxide species [37-39]. However, as the samples were only calcined, the La_2O_3 structure seems to be one most likely present, despite it could not be identified. For both La_2O_3 containing catalysts well dispersed Rh particles with a particle sizes smaller than 4 nm were observed.

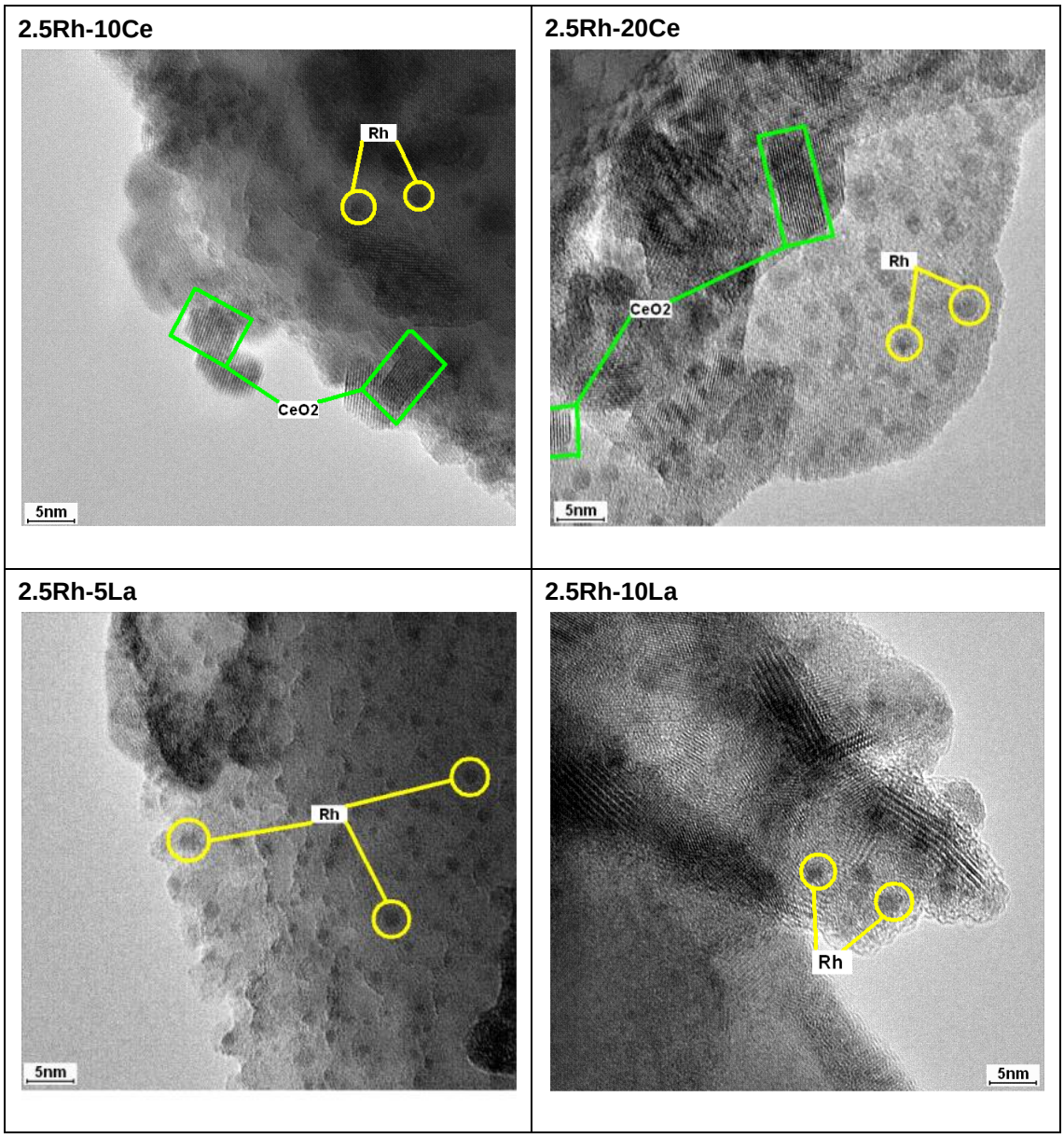

Figure 12: *TEM micrographs of the calcined catalysts. Scale bar of the 2.5Rh =40nm. Rest of micrographs scale bar=5nm.*

5.4.1.4 X-ray diffraction, XRD

XRD spectra of the fresh calcined catalysts are shown in the Figure 13. In those spectra the α-Al_2O_3 was perfectly indentified (Marked by the symbol + in the figure) by the corresponding peaks among the measured *2θ* positions of 34.46, 38.05, 43.62, 52.89, 57.76, 61.57, 66.74 and 68.44º (Corundum, Powder Diffraction File (*PDF*): 01-075-1862). In the case of Rh species, the rhodium oxide contributions were supposed to appear at least at 48.97 and 53.89º (PDF: 01-071-2084) in the measured *2θ* region. However, no peaks were detected. This only could be explained due to the limitations of the technique regarding the crystal sizes and the low amount of this compound in the sample. Regarding the CeO_2 (marked by the asterisk symbol in the figure), peaks were detected in both catalysts at *2θ*=28.76, 33.52, 47.66 and 56.65º, identified

according to the 00-004-0593 PDF. Finally, in the case of the La_2O_3 containing catalysts, the peaks contributions should be detected at least at 2θ= 30.81, 40.64 and 46.36º but no peaks appeared as it also happened for the Rh crystals.

Through this technique, the crystal sizes calculated according to the Scherrer equation were calculated. For the CeO_2 containing catalysts, these results agreed with the ones obtained by TEM; even though the minimum of 200 TEM images would be needed in order to obtain a good particle size distribution, similar conclusions can be obtained; smaller CeO_2 particles were detected for the 2.5Rh-10Ce catalyst than for the 2.5Rh-20Ce one (4 and 7 nm respectively). Regarding the Rh, particles were detected by TEM but not crystals by XRD which could be due to the small size and the concentration present in the catalysts. Regarding the lanthanum oxide species, as big particles were observed by TEM, around 10nm, the reason for which they were not detected by XRD could be related with the amorphous structure formed.

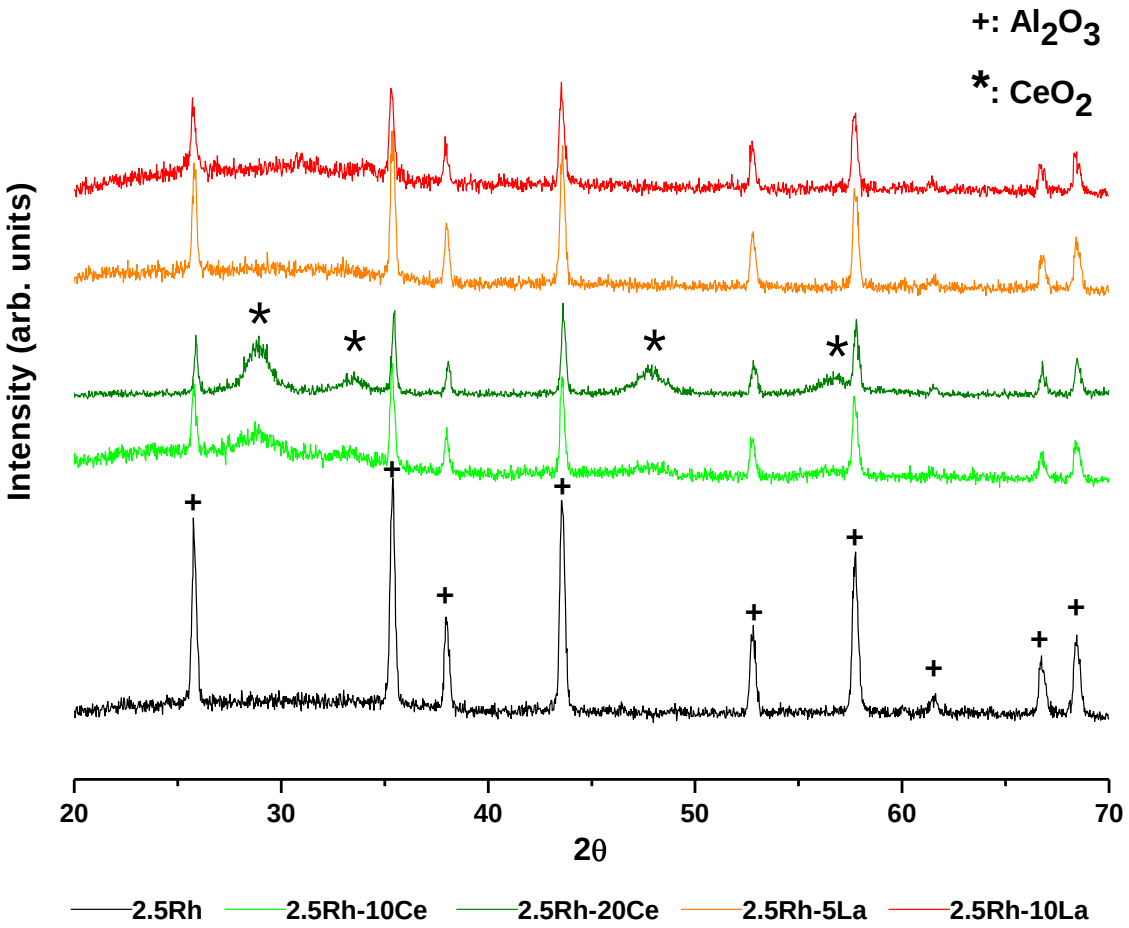

Figure 13: *XRD spectra of the Rh catalysts.*

5.4.1.5 X-ray Photoelectron Spectroscopy, XPS

XPS results of the fresh calcined catalysts summarized in Table 7 have been analyzed in order to determine the chemical composition of the catalyst surface. Comparing the obtained results, higher metallic Rh was detected for the 2.5Rh catalyst but the total Rh_{3d} proportion was the

lowest. This means that the Rh could be preferentially located in the pores. In the case of the CeO_2 containing catalysts, the metallic Rh proportion was lower, but the total Rh_{3d} proportion higher. Finally, for the La_2O_3 containing catalysts the total Rh_{3d} amount increased even more, but the measured metallic Rh was the lowest one. Thus, for the samples containing additives the Rh could be preferentially located in the surface and the modifiers addition could oxidize the initial metallic Rh. In addition, these results agreed with the textural properties presented in Table 5 due to the larger surface areas and higher total pore volumes measured for the samples containing additives. Regarding the detected surface proportions for the additives and their atomic concentrations, the obtained results revealed that they also were preferably located on the surface of the catalysts. Finally, atomic ratios of the most relevant species were calculated in order to confirm their enrichment on the surface. As expected, higher proportions were measured by XPS, and all the calculated Ce/Al and La/Al proportions increased with the amount used for the catalysts preparation. In the case of Rh/Al proportion, it increased due to the lower Al content used in the catalysts containing modifiers.

Table 7: *Fresh calcined catalysts binding energies (BE) of Al 2p, Rh $3d_{5/2}$, Ce $3d_{5/2}$, La $3d_{5/2}$ core levels, atomic concentrations (AC) and Rh^0 and Rh^{3+} proportions. Theoretical and fresh catalysts surface atomic ratios (AR).*

Catalyst	BE and AC [eV, (%)]			Rh 3d	BE and prop. [eV, (%)]		Rh/Al AR		Ce/Al AR		La/Al AR	
	Al 2p	Ce $3d_{5/2}$	La $3d_{5/2}$	[%]	Rh^0	Rh^{3+}	Theor.	Fresh	Theor.	Fresh	Theor.	Fresh
2.5Rh	73.0 (33.1)	-	-	1.98	307.2 (31.2)	308.5 (78.8)	0.013	0.060	-	-	-	-
2.5Rh-10Ce	73.2 (22.0)	882.6 (10.2)	-	2.76	307.2 (8.0)	308.7 (91.9)	0.014	0.125	0.057	0.462	-	-
2.5Rh-20Ce	73.0 (17.8)	883.1 (14.9)	-	2.89	307.2 (17.5)	308.9 (82.5)	0.016	0.162	0.129	0.837	-	-
2.5Rh-5La	72.9 (27.4)	-	835.2 (6.7)	2.90	307.2 (4.1)	308.9 (95.9)	0.013	0.106	-	-	0.054	0.244
2.5Rh-10La	73.0 (21.0)	-	835.0 (11.0)	3.74	307.2 (4.0)	308.9 (96.0)	0.014	0.178	-	-	0.114	0.525

5.4.2 Results from activity testing

The results presented in Figures 14 and 15 correspond to the test carried out at different temperatures and a constant VHSV of 200$L_N/(g_{cat}h)$. In the case of Figure 4, SR activity results obtained for the catalysts under investigation are shown in terms of EG conversion (left) and hydrogen yield (right). Almost full conversion was achieved by all tested catalysts and only the 2.5Rh-10Ce catalyst obtained slightly lower conversion at the temperature of 725ºC. Attending to the hydrogen selectivity plot, the 2.5Rh catalyst obtained lower values at the highest temperature which can be related to the byproducts formation as shown in Figure 5. As far as the remaining catalysts are concerned, very similar hydrogen selectivity values were measured.

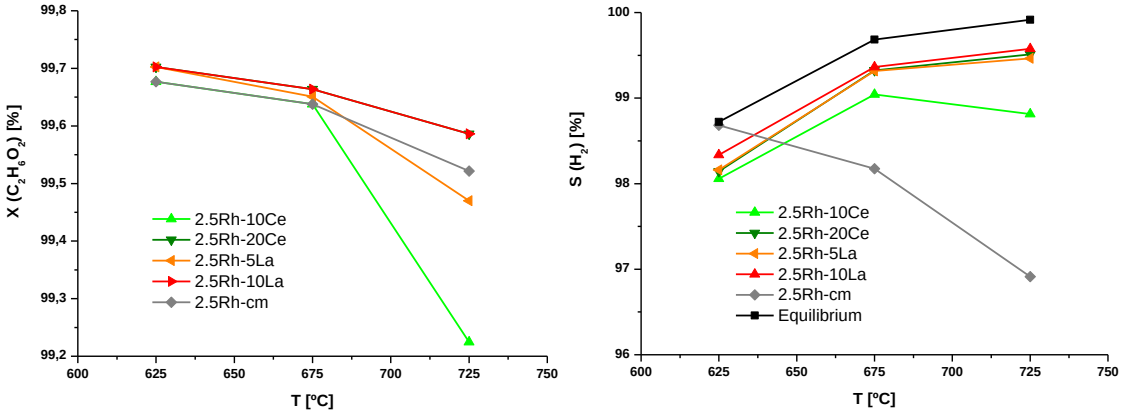

Figure 14: *Ethylene glycol conversion (left) and hydrogen selectivity (right) vs. reaction temperature as obtained for all catalysts investigated under conditions of SR; VHSV of 200L/(g_{cat}h).*

The selectivity towards the main by-products formed is represented in Figure 15. The measured by-products are CO, CO_2, CH_4 and CH_3CHO (Fig. 15a, b, c and d respectively). The catalysts did not show any selectivity towards C_2H_4 or C_2H_6. In general, all the catalysts containing additives behaved similarly. The only difference observed between them referred to the increase CH_3CHO selectivity observed for the CeO_2 containing catalysts, which increased with the temperature. However, the 2.5Rh catalyst showed different results; the CO selectivity was closer to equilibrium conversion and the CO_2 selectivity much lower than the equilibrium conversion. On the other hand, attending to the CH_4 selectivity results (Fig. 15c), this catalyst showed very low selectivity towards CH_4. This effect might increase the calculated H_2 selectivity but it did not, because the high CH_3CHO selectivity (See Fig. 15d) consumed the hydrogen.

In Figures 16 the results obtained during operation conditions of OSR at a reaction temperature of 675ºC and different VHSV are presented in terms of the EG conversion (left) and hydrogen yield (right). As observed before, almost full ethylene glycol conversion was achieved by all tested catalysts under OSR process. Attending the existing small differences, the 2.5Rh catalyst achieved a bit lower conversion, and quite small differences can be observed among the

catalysts containing additives. In addition, only the 2.5Rh catalyst was smoothly affected by the VHSV increase.

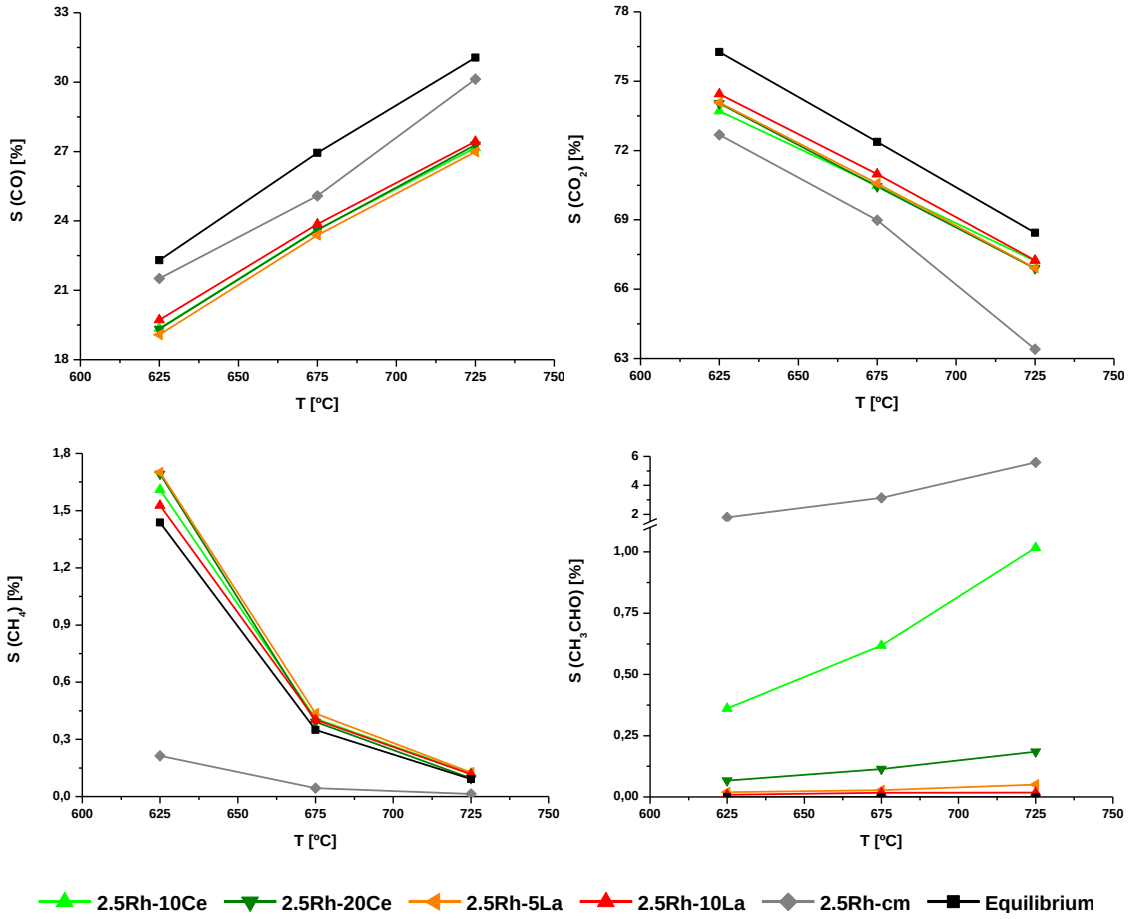

Figure 15: *Selectivities vs. reaction temperature as obtained for the studied catalysts under conditions of SR; (a) top left: CO selectivity; (b) top right: CO_2 selectivity; (c) bottom left: CH_4 selectivity; (d) bottom right: CH_3CHO selectivity; the values as calculated for the thermodynamic equilibrium of the reaction mixture are included VHSV of 200L/(g_{cat}h).*

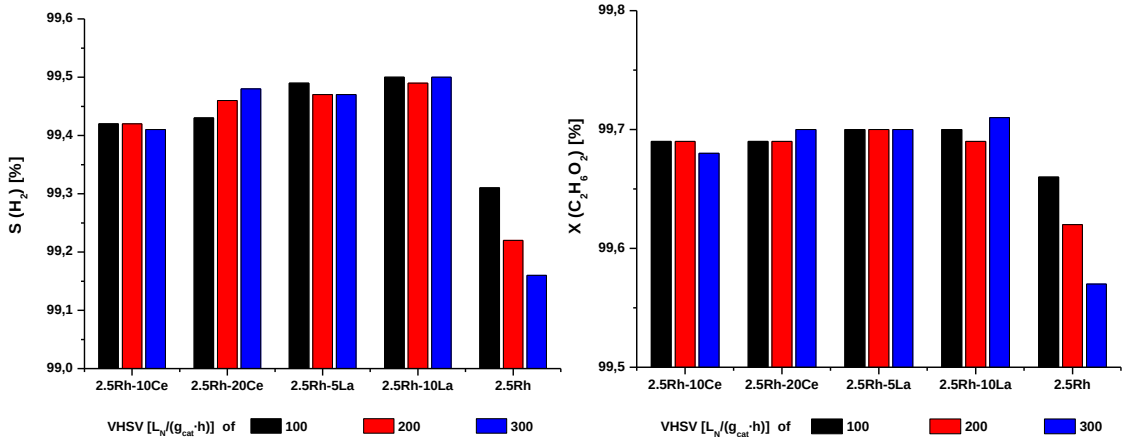

Figure 16: *Ethylene glycol conversion and hydrogen selectivity vs. space velocity as obtained for all catalysts under investigation under conditions of OSR.*

In Figure 17 a comparison between the main by-product formation at different VHSV for both SR and OSR processes are presented. In general, higher CH_4 and CH_3CHO selectivity was measured operating under SR conditions. However, although higher CH_4 selectivity was measured for the 2.5Rh catalyst under OSR conditions, this catalyst showed the lowest CH_4 selectivity of all samples tested. Regarding the CH_3CHO selectivity, it was negligible for all catalysts except to the 2.5Rh sample. For this catalyst were obtained the highest concentrations of this by-product, especially under SR conditions at the VHSV of 200 $L_N/(g_{cat}h)$. Thus, in spite of the small differences between CeO_2 and La_2O_3 containing catalysts regarding the methanation reaction, higher CH_3CHO selectivity was measured for the sample containing less CeO_2, while the addition of lanthana suppressed the CH_3CHO selectivity almost completely.

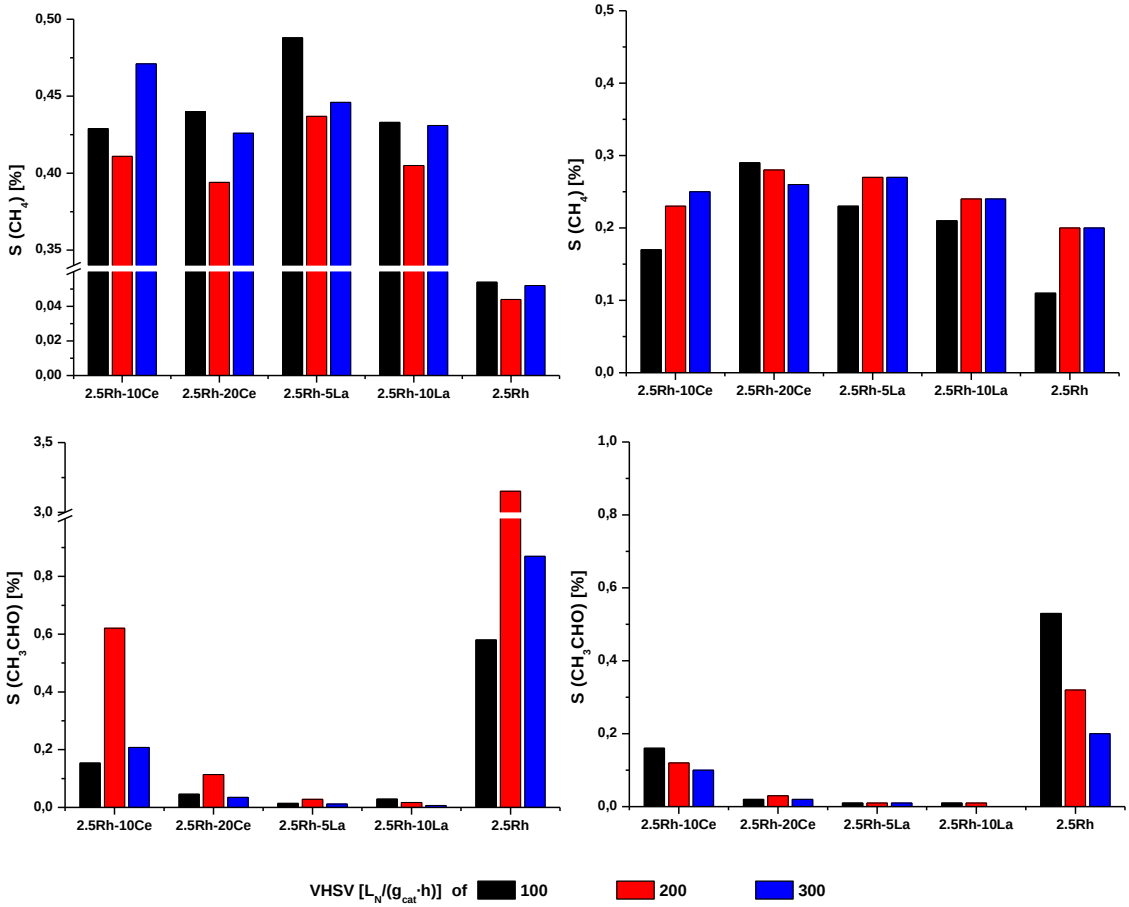

Figure 17: *Selectivities at different VHSV as obtained for all catalysts at 675°C reaction temperature under conditions of SR and OSR; (a) top left: CH_4 selectivity (SR); (b) top right: CH_4 selectivity (OSR); (c) bottom left: CH_3CHO selectivity (SR); (d) bottom right: CH_3CHO selectivity (OSR).*

In Table 8 the hydrogen production rates measured at the different conditions tested are summarized. The 2.5Rh catalyst obtained the highest hydrogen production rates at the lowest temperatures under SR conditions. This effect could be due to the higher selectivity of this catalyst to the r-WGS reaction, which it is explained with the low CO_2 selectivity measured (Fig.

15b). In the case of the OSR process, the 2.5Rh catalyst reached the highest hydrogen production at low VHSV tested but the 2.5Rh-5La catalyst was the one obtaining the highest production rates at the highest VHSV.

Table 8: *Hydrogen production rates at the tested conditions.*

Catalyst: amount	$C_2H_6O_2$ SR				$C_2H_6O_2$ OSR	
	VHSV=200 NL/ h g_{cat}		T=675ºC		T=675ºC	
	T (ºC)	H_2 flow ($L/g_{cat}h$)	VHSV ($L/g_{cat}h$)	H_2 flow ($L/g_{cat}h$)	VHSV ($L/g_{cat}h$)	H_2 flow ($L/g_{cat}h$)
2.5Rh: 0.0171	725	94.93			300	146.63
	675	**99.91**	300	**150.69**	200	**119.38**
	625	**101.68**	100	**50.83**	100	**48.92**
2.5Rh-10Ce: 0.0190	725	96.99			300	105.79
	675	98.59	300	148.47	200	87.71
	625	98.53	100	49.50	100	48.06
2.5Rh-20Ce: 0.0189	725	97.63			300	141.15
	675	98.91	300	148.69	200	90.72
	625	98.61	100	49.50	100	48.06
2.5Rh-5La: 0.0172	725	**97.68**			300	**148.79**
	675	98.98	300	148.86	200	95.37
	625	98.71	100	49.58	100	42.88
2.5Rh-10La: 0.0173	725	93.45			300	139.33
	675	98.93	300	148.71	200	85.59
	625	98.85	100	49.53	100	**49.61**

Finally, a long term experiment was conducted under SR conditions, at a VHSV of 200 $L_N/(g_{cat}h)$ and the lowest reaction temperature of 625ºC. For this experiment the 2.5Rh-20Ce catalyst was selected. The results, presented in the Figure 8, showed complete conversion (>99.9%), and a constant and stable process during 115h, though the hydrogen concentration declined slightly. However, in this case a low amount of C_2H_4 was observed (below 0.1%), which was not measured at the same operation conditions in the previous experiments. In the case of CH_3CHO, the highest concentration measured by the µ-GC was 0.05927% (vol.).

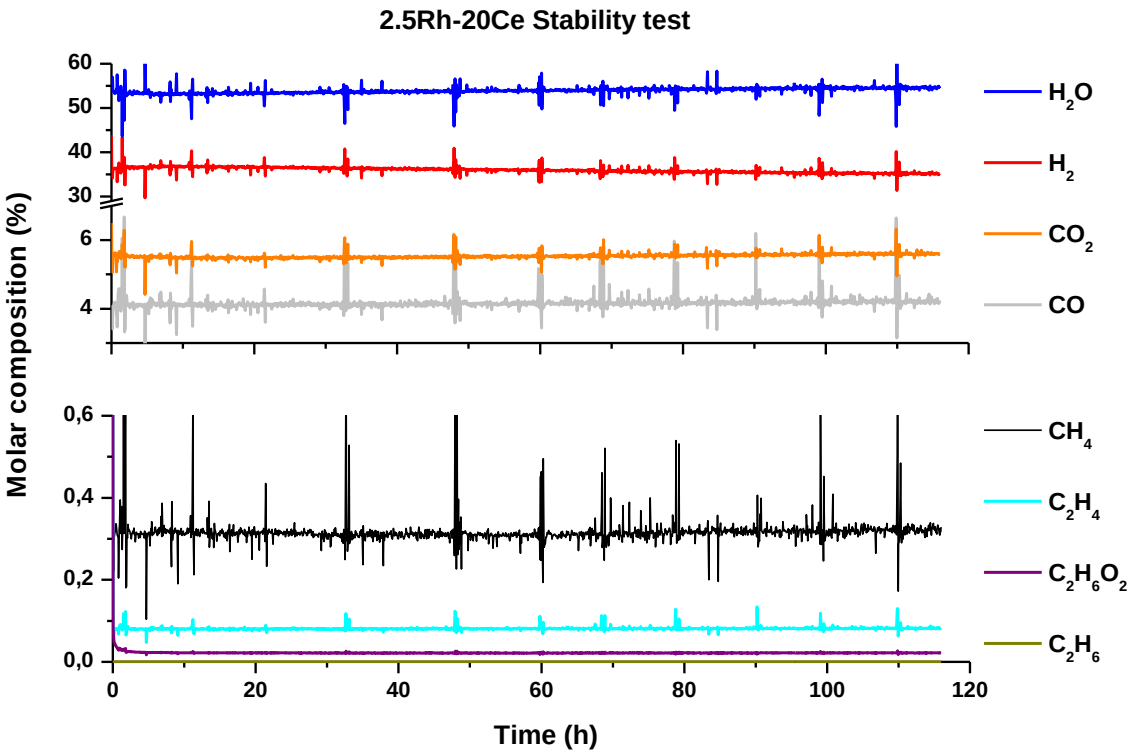

Figure 18: *Obtained product composition for the 2.5Rh-20Ce catalyst stability test carried out at 625ºC and VHSV of 200 LN/(g_{cat}h).*

5.4.3 Conclusions

The valorization of ethylene glycol as a raw material for syngas production using Rh based catalysts supported on α-Al_2O_3 modified with La_2O_3 or CeO_2 oxides was the main objective of this work focusing on stable catalyst performance and suppression of the formation of by-products such as acetaldehyde.

While the samples prepared by a conventional impregnation method showed generally higher activity compared to catalysts prepared from Rh nanoparticles, all samples suffered from by-product formation of species such as acetaldehyde, ethane and ethylene regardless if oxygen was added to the feed or not.

The 2.5Rh-20Ce catalyst showed the highest surface area and pore volume. In addition, the reduction peaks measured for this catalyst were the highest at the highest temperatures. This can be due to stronger metal-modifier and support-modifier interactions. The XRD analyses revealed well dispersed rhodium oxide particles with a size lower than 4 nm for all the prepared catalysts. In the case of XPS results, they confirmed an enrichment of the active species on the catalyst surface although initially (after calcination) the proportion of Rh in a metallic state was lower for the catalysts with the modified support.

Regarding the activity results, complete conversion and selectivities close to the equilibrium were achieved by all catalysts containing additives for both SR and OSR processes. In addition, for these catalysts C_2H_4 and C_2H_6 by-products were only detected in minor amounts during the long-term stability test and the concentrations of the measured by-products, CH_4 and CH_3CHO, were very low. The 2.5Rh catalyst showed the lowest CH_4 selectivity but the highest towards CH_3CHO. Thus, the measured hydrogen selectivity for this catalyst was the lowest in both SR and OSR processes. The addition of La_2O_3 and CeO_2 suppressed the formation of acetaldehyde, which is harmful for downstream processing such as water-gas shift catalysts and PEM fuel cells, while this is not the case for methane. However, due to a high selectivity observed for this catalyst to the r-WGS reaction, it reached the highest hydrogen production rate at low temperatures for SR. A long term experiment was conducted using the 2.5Rh-20Ce catalyst which lasted more than 115 hours showing almost stable behavior.

5.5 References

[1] D.J.M. De Vlieger, A.G. Chakinala, L. Lefferts, S.R.A. Kersten, K. Seshan, D.W.F. Brilman, Hydrogen from ethylene glycol by supercritical water reforming using noble and base metal catalysts, Appl Catal B Environ. 111 (2012) 536.

[2] G. Kolb, Review: Microstructured reactors for distributed and renewable production of fuels and electrical energy, Chem Eng Proc. 65 (2013) 1.

[3] S. Li, C. Zhang, P. Zhang, G. Wu, X. Ma, J. Gong, On the origin of reactivity of steam reforming of ethylene glycol on supported Ni catalysts, Phys Chem Chem Phys. 14 (2012) 4066.

[4] Y. Zhang, A. Wang, T. Zhang, A new 3D mesoporous carbon replicated from commercial silica as a catalyst support for direct conversion of cellulose into ethylene glycol, Chem Commun. 46 (2010) 862.

[5] H.D. Kim, T.W. Kim, H.J. Park, K.E. Jeong, H.J. Chae, S.Y. Jeong, Hydrogen production via the aqueous phase reforming of ethylene glycol over platinum-supported ordered mesoporous carbon catalysts: Effect of structure and framework-configuration, Int J Hydrogen Energy. 37 (2012) 12187.

[6] H.Y. Law, M.C. Kung, H.H. Kung, Low temperature NOx removal from diesel exhaust by coupling ethylene glycol reforming with SCR, Catal Today. 136 (2008) 40.

[7] N. Ji, T. Zhang, M. Zhang, A. Wang, H. Wang, X. Wang, Direct catalytic conversion of cellulose into ethylene glycol using nickel-promoted tungsten carbide catalysts, Chem Int Ed. 47 (2008) 8510.

[8] N. Ji, T. Zhang, M. Zhang, A. Wang, H. Wang, X. Wang, Catalytic conversion of cellulose into ethylene glycol over supported carbide catalysts, Catal Today. 147 (2009) 77.

[9] G. Zhao, M. Zhang, A. Wang, T. Ahang, Catalytic conversion of cellulose to ethylene glycol over tungsten phosphide catalyst, Chin J Catal. 31 (2010) 928.

[10] P.N. Kechagiopoulos, S.S. Voutetakis, A.A. Lemonidou, I.A. Vasalos, Hydrogen production via steam reforming of the aqueous phase of bio-oil in a fixed bed reactor, Catal Today. 127 (2007) 246.

[11] G. Kolb, Fuel Processing for Fuel Cells, 1st edition ed., Wiley-VCH, Weinheim, 2008.

[12] G.W. Huber, J.W. Shabaker, S.T. Evans, J.A. Dumesic, Aqueous-phase reforming of ethylene glycol over supported Pt and Pd bimetallic catalysts Appl Catal B Environ. 62 (2006) 226.

[13] P.J. Dauenhauer, Millisecond autothermal Catalytic reforming of carbohydrates for synthetic fuels by reactive flash volatilization. University of Minnesota. (2008).

[14] F. Xie, X. Chu, H. Hu, M. Qiao, S. Yan, Y. Zhu, Characterization and catalytic properties of Sn-modified rapidly quenched skeletal Ni catalysts in aqueous-phase reforming of ethylene glycol, J Catal. 241 (2006) 211.

[15] R.R. Davda, J.W. Shabaker, G.W. Huber, R.D. Cortright, J.A. Dumesic, Aqueous-phase reforming of ethylene glycol on silica-supported metal catalysts, Appl Catal B Environ. 43 (2003) 13.

[16] J.W. Shabaker, R.R. Davda, G.W. Huber, R.D. Cortright, J.A. Dumesic, Aqueous-phase reforming of methanol and ethylene glycol over alumina-supported platinum catalysts, J Catal. 215 (2003) 344.

[17] J. Liu, B. Sun, J. Hu, Y. Pei, H. Li, M. Qiao, Aqueous-phase reforming of ethylene glycol to hydrogen on Pd/Fe_3O_4 catalyst prepared by co-precipitation: Metal–support interaction and excellent intrinsic activity, J Catal. 274 (2010) 287.

[18] O. Skoplyak, M.A. Barteau, J.G. Chen, Ethanol and ethylene glycol on Ni/Pt(1 1 1) bimetallic surfaces: A DFT and HREELS study, J Phys Chem B. 110 (2006) 1686.

[19] R. Zapf, C. Becker-Willinger, K. Berresheim, H. Bolz, H. Gnaser, V. Hessel, Detailed Characterization of Various Porous Alumina-Based Catalyst Coatings Within Microchannels and Their Testing for Methanol Steam Reforming, Chem Eng Res Des. 81 (2003) 721.

[20] T. Ashida, K. Miura, T. Nomoto, S. Yagi, H. Sumida, G. Kutluk, Synthesis and characterization of Rh(PVP) nanoparticles studied by XPS and NEXAFS, Surf Sci. 60 (2007) 3898.

[21] M. O'Connell, G. Kolb, R. Zapf, Y. Men, V. Hessel, Bimetallic catalysts for the catalytic combustion of methane using microreactor technology, Catal Today. 144 (2009) 306.

[22] U. Izquierdo, V.L. Barrio, J.F. Cambra, J. Requies, M.B. Güemez, P.L. Arias, Hydrogen production from methane and natural gas steam reforming in conventional and microreactor reaction systems, Int J Hydrogen Energy. 37 (2012) 7026.

[23] A. Yee, S.J. Morrison, H. Idriss, A Study of Ethanol Reactions over Pt/CeO by Temperature-Programmed Desorption and in Situ FT-IR Spectroscopy: Evidence of Benzene Formation, J Catalysis. 191 (2000) 30.

[24] G. Kim, Ceria-promoted three-way catalysts for auto exhaust emission control, Ind Eng Chem Prod Res Dev. 21 (1982) 267.

[25] H.C. Yao, Y.F.Y. Yao, Ceria in automotive exhaust catalysts, J Catalysis. 86 (1984) 254.

[26] D.M. Gu, Y.Y. Chu, Z.B. Wang, Z.Z. Jiang, G.P. Yin, Y. Liu, Methanol oxidation on Pt/CeO_2–C electrocatalyst prepared by microwave-assisted ethylene glycol process, Appl Catal B-Environ. 102 (2011) 9.

[27] K.H. Lin, C.Y. Tsai, A.C.C. Chang, Preparation of High Surface Area Mesoporous $Ni_{2x}Ce_{1-x}O_2$ (x = 0, 0.05, 0.13, 0.2) and Its Applications in Methane Steam Reforming, Modern Research in Catalysis. 2 (2013) 42.

[28] Y. Chen, H. Xu, X. Jin, G. Xiong, Integration of gasoline prereforming into autothermal reforming for hydrogen production, Catal Today. 116(3) (2006) 334.

[29] A. Iriondo, V.L. Barrio, J.F. Cambra, P.L. Arias, M.B. Güemez, R.M. Navarro, Influence of La_2O_3 modified support and Ni and Pt active phases on glycerol steam reforming to produce hydrogen, Catal Commun. 10 (2009) 1275.

[30] G. Kolb, R. Zapf, V. Hessel, H. Löwe, Propane steam reforming in micro-channels—results from catalyst screening and optimization, Appl Catal A. 277 (2004) 155.

[31] M. Ghelamallah, P. Granger, Impact of barium and lanthanum incorporation to supported Pt and Rh on α-Al_2O_3 in the dry reforming of methane, Fuel. 97 (2012) 269.

[32] M. Ocsachoque, M. Pompeo, G. Gonzalez, Rh–Ni/CeO_2–Al_2O_3 catalysts for methane dry reforming, Catal Today. 172 (2011) 226.

[33] Y. Li, X. Wang, C. Xie, C. Song, Influence of ceria and nickel addition to alumina-supported Rh catalyst for propane steam reforming at low temperatures, Appl Catal A Gen. 357 (2009) 213.

[34] I. Cuauhtémoc, G. Del Angel, G. Torres, C. Angeles-Chavez, J. Navarrete, J.M. Padilla, Enhancement of catalytic wet air oxidation of tert-amyl methyl ether by the addition of Sn and CeO_2 to Rh/Al_2O_3 catalysts, Catal Today. 166 (2011) 180.

[35] X. Karatzas, J. Dawody, A. Grant, E.E. Svensson, L.J. Pettersson, Zone-coated Rh-based monolithic catalyst for autothermal reforming of diesel, Appl Catal B-Environ. 101 (2011) 226.

[36] D. Terribile, A. Trovarelli, C. Leitenburg, A. Primavera, G. Dolcetti, The synthesis and characterization of mesoporous high-surface area ceria prepared using a hybrid organic/inorganic route, Catal Today. 47 (1999) 133.

[37] D.A. Constantinou, M.C. Álvarez-Galván, J.L.G. Fierro, A.M. Efstathiou, Low-temperature conversion of phenol into CO, CO_2 and H_2 by steam reforming over La-containing supported Rh catalysts, Appl Catal B-Environ. 117-118 (2012) 81.

[38] H. Chen, H. Yu, F. Peng, H. Wang, J. Yang, M. Pan, Efficient and stable oxidative steam reforming of ethanol for hydrogen production: Effect of in situ dispersion of Ir over Ir/La_2O_3, J Catal. 269 (2010) 281.

[39] M.E. Rivas, J.L.C. Fierro, M.R. Goldwasser, E. Pietri, J.M. Pérez-Zurita, A. Griboval-Constant, Structural features and performance of $LaNi_{1-x}Rh_xO_3$ system for the dryreforming of methane, Appl Catal A-Gen. 344 (2008) 10.

CHAPTER 6

Conclusions

This Thesis work focuses on the **development of new reforming catalysts and advanced reaction systems for hydrogen production**. Therefore, the use and comparison between two different reaction systems, FBR and microreactor, for hydrogen production was studied. Besides, the work carried out also includes the use of different renewable feedstocks for their conversion to hydrogen throughout the study of new catalytic processes. Then, this Thesis work provides valuable information for the scientific community because of the reaction systems and the feedstocks studied and the active, selective and stable new catalytic formulations designed. All this has allowed the publications of seven articles in specialized peer-reviewed scientific journals. Therefore, this PhD Thesis offers new ideas for green and decentralized hydrogen production and proves that it is possible and viable the use of microreactor reaction systems. Thus, it can be considered as a departing point for the design of an entire module for hydrogen production.

The conclusions in this Chapter 6 will be divided, according to the different feedstocks studied, in three main sections.

Methane and natural gas reforming

Hydrogen production from methane and NG steam reforming processes was studied in the FBR and microreactor reaction systems operating at the same WHSV. The effect of increasing temperatures, from 973 to 1073 K, and S/C ratios, from 1.0 to 2.0, was also investigated using Ni/Al_2O_3, Ni/MgO, Pd/Al_2O_3 and Pt/Al_2O_3 catalysts.

The study of methane and natural gas reforming for hydrogen production in the FBR and microreactor systems evidenced that **the microreactor is the appropriate reactor system for operating at high WHSV**. Higher methane and natural gas conversions were reached at higher temperatures but they it did not improve significantly operating at higher S/C ratios. Although **the highest methane conversion (72.9%) was achieved using the Ni/Al_2O_3 catalyst** operating under SMR at S/C=1.0, it suffered from deactivation when operated under NG reforming conditions. By the contrary, even if a slightly lower methane conversion was measured for the Ni/MgO catalyst, it showed high activity and good stability for both methane and NG reforming processes. The noble metal-based catalysts suffered a quick deactivation which was attributed to the carbon deposition observed by SEM. The conversion results measured operating in the FBR were insignificant because of the very high WHSV used.

Biogas reforming processes

Biogas valorisation for hydrogen production by means of DR, BSR, BOR and TR processes using Ni/MgO, $Ni/Ce\text{-}Al_2O_3$, $Ni/Zr\text{-}Al_2O_3$, $Ni/Ce\text{-}Zr\text{-}Al_2O_3$, $Rh\text{-}Ni/Ce\text{-}Al_2O_3$ and $\gamma\text{-}Al_2O_3$-based commercial catalyst was studied. For the processes under investigation a process variable optimization was carried out by increasing the S/C ratio for BSR process, from 1.0 to 3.0, the

O_2/CH_4 ratio for BOR process, from 0.125 to 0.50, and their possible combinations for TR, at the temperature of 800ºC and atmospheric pressure in the FBR. Afterwards, the most interesting processes were tested in the microreactor system in order to study their possible intensification using the catalysts considered as the best ones.

The study of the process variables optimization carried out using the FBR concluded that **the S/C ratio of 1.0 for BSR, the O_2/CH_4 ratio of 0.25 for BOR and the combination between the S/C of 1.0 and the O_2/CH_4 of 0.25 ratios for TR were the most appropriate conditions for hydrogen production**. At these experimental conditions all catalysts reached very high biogas conversions but the CeO_2 containing ones were especially active. In addition the characterization carried out by XPS showed that the decrease in the Ni/Al ratio during the reaction test measured for these catalysts was the lowest. Therefore, **Rh-Ni/Ce-Al_2O_3, Ni/Ce-Zr-Al_2O_3 and Ni/Ce-Al_2O_3 catalysts were coated onto microreactors**. When microreactors were used, although the experiments were carried out at higher WHSV, the measured biogas conversion values were similar than the ones measured in the FBR. The highest hydrogen production yields were also obtained operating under O_2/CH_4 ratio of 0.25 for BOR and the combination between the S/C of 1.0 and the O_2/CH_4 of 0.25 ratios for TR. Comparing the catalytic activity through the TOF and PROD parameters, **activity values one order of magnitude higher were calculated for the microreactor system**. Regarding the catalytic systems employed, **the Ni/Ce-Al_2O_3 catalyst was the most active one**.

Then, the use of zeolites, with different morphology and size, as catalyst support based on Ni and Rh-Ni metals for the study of the biogas reforming processes was considered. Apart from the study of the process variable optimization, the influence of the zeolite morphology and the Rh addition was also studied with the FBR.

The results obtained allow reaching exactly the same conclusions as for the Al_2O_3 and MgO-based catalysts. **For zeolite-based catalysts the morphology and size of the support plays an important role in the catalytic behavior**. Then, while the Cylindrical (1–3 μm) catalysts achieved the lowest activity values, the Disc catalysts showed better activities and the Cylindrical (30–60 nm) catalysts the highest ones. In general, the bimetallic catalysts showed better performance and in particular the **bimetallic Cylindrical (30–60 nm) catalyst seemed to be the most promising one** due to its very high metallic dispersion degree, small particle size and excellent activities.

Finally, Na^+ and Cs^+ doped zeolites-based bimetallic catalysts were prepared in order to be tested under DR and BOR at the O_2/CH_4 ratio of 0.25 with the FBR. In the case of Na^+ and Cs^+ doped zeolites-based catalysts **their activities were lower than the ones measured using non-doped zeolites as catalyst support, Rh-Ni/D and Rh-Ni/N**. In addition, **Na^+ and Cs^+ incorporation affected mainly to the Disc catalysts**.

Ethylene glycol steam and oxidative reforming

EG as feed for syngas production by SR and OSR was studied using microchannel testing reactors. The product composition was determined at a S/C of 4.0, reaction temperatures between 625°C and 725°C, atmospheric pressure and VHSV between 100 and 300 NL/(g_{cat}h). Initially, catalysts with different Rh loading, from 1.0 to 5.0 wt.%, and supported on α-Al_2O_3 were prepared by two different preparation methods. Then, the support of the catalyst showing the best performance was modified with different contents of CeO_2 or La_2O_3 oxides in order to reduce by-products formation.

Through the experiments carried out, it can be concluded that **the samples prepared by a conventional impregnation method showed generally higher activity** compared to catalysts prepared from Rh nanoparticles method. However, all the samples suffered from by-product formation of species such as acetaldehyde, ethane and ethylene regardless oxygen was added to the feed or not. **The 2.5Rh-cm catalyst reached the highest hydrogen production rates at all the tested experimental conditions**, but not under SR at 725ºC and VHSV of 200 L/g_{cat}h. **α-Al_2O_3 support modification by CeO_2 and La_2O_3 oxides diminished the by-products formation** and total conversion and selectivities close to the equilibrium predicted ones were achieved by these catalysts for both SR and OSR processes. **A long term experiment conducted using the 2.5Rh-20Ce catalyst lasted more than 115 hours** showing almost completely stable behavior at 625ºC, VHSV of 200 L_N/g_{cat}h and under SR conditions.